# Characterisation of the terminal enzymes of haem biosynthesis from *Staphylococcus aureus*

**Charlie Hobbs**

**A thesis submitted to the University of Kent at Canterbury for the degree of PhD in Biochemistry in the Faculty of Sciences**

**Department of Biosciences**

**2016**

# Declaration:

No part of the thesis has been submitted in the support of an application for any degree or other qualification of the University of Kent, or any other University or Institution of learning.

Charlie Hobbs

# Acknowledgements:

Firstly I would like to thank my supervisor, Dr Mark Shepherd, for giving me the opportunity to perform this study, for all of his advice, training and support during the course of the project, especially during the transfer from the Research Masters programme to the PhD programme.

I would also like to thank Dr Ian Blomfield and all the members of the Shepherd and Blomfield lab groups and during my time in the lab for their insights, advice and support at various points during my research.

Many thanks also to the Warren, Rossman and Geeves research groups and Kevin Howland for the use of various pieces of equipment that have been fundamental in being able to perform experiments or obtain the data required during this project.

I would also like to thank Dr Jim Reid from the University of Sheffield for allowing me to visit his lab to gain experience in performing a series of ferrochelatase assays that were proving to be problematic in the early stages. His advice and insights into parts of the project have also been invaluable.

Finally I would like to thank all of friends and family for their support and encouragement over the last four years. In particular I would like to thank: my karate club for giving me a refreshing break from research life and the confidence in myself that has proved essential during presentations that I have made at conferences and departmental events. My fiancée Aga has been a constant source of support throughout my research, helping me with various problems that have arisen and generally putting up with me during this time, especially as she was carrying out her own PhD degree at the same time.

Last, but by no means least, I would like to thank my parents for everything that they have done for me. Without them and their constant support throughout my life, I would not have been able to achieve anything that I have been able to achieve in life. Without their aid and funding, I would not have been able to carry out any of the work that is contained herein.

# Abstract:

Haem is an essential molecule that is required for a wide variety of functions in all forms of life. This molecule is required for oxygen transport in humans as a prosthetic group of haemoglobin and myoglobin and is also an integral component of various cytochromes as well as being a cofactor for peroxidases and catalases. Until very recently it was generally accepted that the haem biosynthetic pathway was a conserved process in most organisms that synthesise haem. This dogma has changed with the discovery of two new pathways by which haem can be synthesised. The most recently discovered of these pathways, known as the coproporphyrin-dependent pathway, is utilised by many actinobacteria and firmicutes (including *Staphylococcus aureus*) and is now thought to be an ancestral pathway to the now more widely distributed classical pathway. In light of this discovery, the current work seeks to examine the biochemical and kinetic properties of the enzymes involved in the terminal stages of haem synthesis in *S. aureus* (HemY, HemH and HemQ).

HemY from *S. aureus*, which is classically known as a protoporphyrinogen IX oxidase, catalyses the antepenultimate step in a coproporphyrinogen-dependant pathway *in vivo* was shown for the first time to catalyse the oxidation of coproporphyrinogen III as well as protoporphyrinogen IX, demonstrating that this enzyme can catalyse steps in both classical and coproporphyrin-dependant haem biosynthesis *in vitro*. Kinetic analyses revealed that the previously-observed stimulation of HemY activity by the terminal pathway enzyme HemQ (a coprohaem decarboxylase) occurred via a peroxidase-mediated mechanism resulting in the generation of superoxide, although this stimulation was not observable when HemY is utilising the native coproporphyrinogen III substrate. This generation of toxic free radicals could explain why HemQ enzymes have not been identified in organisms that synthesise haem via the classical protoporphyrin IX pathway.

The HemH enzyme, also known as ferrochelatase, has also been further characterised with its *in vivo* substrates ($Fe^{2+}$ and coproporphyrin III), where activity was shown to be diminished by a regulatory metal binding site. The activity of this enzyme with a variety of alternative metal substrates was also assessed, with the enzyme being able to insert metals that are commonly inserted by other ferrochelatases.

Kinetic constants for HemQ, a coprohaem decarboxylase, were determined for the first time and HemQ was further assessed for an ability to bind other tetrapyrroles: non-metallated porphyrins were found to bind much tighter than the metalloporphyrins that are the *in vivo* substrate and product for this enzyme.

Together, these intriguing observations have implications for the divergent evolution of haem biosynthesis in ancestral microorganisms and provides new insights into the flux of intermediates through the terminal stages of haem biosynthesis in *S. aureus*.

# Abbreviations:

| | | |
|---|---|---|
| **AdoCbl** | - | 5'-deoxyadenosylcobalamin |
| **ALA/5-ALA** | - | (δ/5)-aminolaevulinic acid |
| **ATP** | - | Adenosine triphosphate |
| **BLAST** | - | Basic Local Alignment Search Tool |
| **BSA** | - | Bovine Serum Albumin |
| **C'gen$_{III}$** | - | Coproporphyrinogen III |
| **C$_{III}$** | - | Coproporphyrin III |
| **CoA** | - | Coenzyme A |
| **dAdo** | - | 5'-deoxyadenosyl (radical) |
| **DDSH** | - | 12, 18-didecarboxysirohaem |
| **DMSO** | - | Dimethyl Sulfoxide |
| **DNA** | - | Deoxyribonucleic acid |
| **DTT** | - | Dithiothreitol |
| **EDTA** | - | Ethylenediaminetetraacetic acid |
| **EPR** | - | Electron Paramagnetic Resonance |
| **FAD** | - | Flavin Adenine Dinucleotide |
| **FMN** | - | Flavin Mononucleotide |
| **HMB** | - | Hydroxymethylbilane |
| **HPLC** | - | High Performance Liquid Chromatography |
| **HRP** | - | Horseradish Peroxidase |
| **INH** | - | 4-bromo-3-(50-carboxy-40-chloro-20-fluoro-phenyl) -1-methyl-5-trifluoromethyl-pyrazo |
| **IPTG** | - | Isopropyl β-D-1-thiogalactopyranoside |
| **MeCbl** | - | Methylcobalamin |

| | | |
|---|---|---|
| **M'gen$_{IX}$** | - | Mesoporphyrinogen IX |
| **M$_{IX}$** | - | Mesoporphyrin IX |
| **MOPS** | - | 3-(*N*-morpholino)propanesulfonic acid |
| **NATA** | - | N-acetyl-tryptophanamide |
| **NCBI** | - | National Center for Biotechnology Information |
| **NEB** | - | New England Biolabs |
| **P'gen$_{IX}$** | - | Protoporphyrinogen IX |
| **PBG** | - | Porphobilinogen |
| **PCR** | - | Polymerase Chain Reaction |
| **PDB** | - | Protein Databank |
| **P$_{IX}$** | - | Protoporphyrin IX |
| **PPO** | - | Protoporphyrinogen IX Oxidase |
| **RNA** | - | Ribonucleic acid |
| **ROS** | - | Reactive Oxygen Species |
| **SAM** | - | S-adenosyl-L-methionine |
| **SDS-PAGE** | - | Sodium Dodecylsulphate-Polyacrylamide Gel Electrophoresis |
| **SOD** | - | Superoxise Dismutase |
| **TAE** | - | Tris/Acetic acid/EDTA |
| **Temed** | - | Tetramethylethylenediamine |
| **TFA** | - | Trifluoroacetic acid |
| **U'gen$_{III}$** | - | Uroporphyrinogen III |

# Table of Contents:

Chapter I

# Introduction

# 1.1 – Structure and function of tetrapyrroles

Tetrapyrroles are organic molecules that can perform a variety of functions and are essential for many forms of life. These molecules can perform a wide variety of functions depending on their overall structure, the proteins that they are associated with and if they have a metal associated with them. They can exist as either linear or cyclic molecules, and are usually strongly coloured due to the conjugated ring system contained within tetrapyrroles.

Linear tetrapyrroles such as phytochromobilin mainly appear in plants and have important light sensing capabilities used by the photoreceptor phytochrome (Terry & Lagariass 1991; Terry et al. 1993; Han et al. 2010). Other linear tetrapyrroles such as biliverdin, which is also a precursor molecule to phytochromobilin (Franklin et al. 2003), and bilirubin commonly arise as degradation product of cyclic tetrapyrroles, notably from haem, in other organisms (Bulmer et al. 2008; Minetti et al. 1998). Biliverdin and bilirubin have rather similar structures and have been shown to have beneficial antioxidant capabilities (Minetti et al. 1998). Bilirubin can also be toxic if it is present in high enough concentrations, caused by conditions such as neonatal hyperbilirubinemia in children, which can lead to acute or chronic neurological disorders (Bulmer et al. 2008).

Cyclic tetrapyrroles are derived from a common precursor, Uroporphyrinogen III, which is processed via a series of enzyme-catalysed reactions to yield the end products haem (or heme), chlorophyll, cobalamin, sirohaem (or siroheme), and Factor $F_{430}$ (Martins et al. 2001). These molecules have different metals associated with the centre of the porphyrin ring and possess various side chain modifications present. These modifications can range from small vinyl and propionic acid side chains, as found in haem, or complex additions and alterations to the structure, as seen with chlorophyll and vitamin $B_{12}$, which give rise to varying spectral features and colours. These tetrapyrroles, shown in Figure 1.1, are occasionally called the "pigments of life" because of the differences in colour and how essential they are to life (Battersby 2000).

## 1.1.1 – Haem

The main distinguishing feature of haem is the presence of a ferrous ion ($Fe^{2+}$) in the centre of the tetrapyrrole ring. Haem is required for many different functions, ranging from the transport of oxygen and carbon dioxide in multicellular organisms as part of the proteins haemoglobin and myoglobin, to being an integral component of the electron transport chain as a cofactor for various cytochromes. In addition, other enzymes such as peroxidases, catalases and cytochrome P450s also utilise haem as a cofactor. There are many forms of haem present in nature, with the most common form being haem *b*, also known as protohaem IX, which is the form of haem mostly associated with the functions mentioned above. Haem *b* is also used as the starting point for the synthesis of other forms of haem such as haem *o*, haem *a* and haem *c* (Brown et al. 2002; Kranz et al. 2009). These haem forms are utilised in various different proteins related to cytochromes, with the "*c*" form being an integral part of cytochrome *c* (Kranz et al. 2009) and the "*o*" and "*a*" forms being cofactors for cytochrome respiratory oxidases (Brown et al. 2002)

Haem is a versatile co-factor, with many different functions available depending on the protein it is bound to. Whilst it is well known for oxygen and carbon dioxide transport, the ability to bind these diatomic gasses is also utilised by many organisms as gas sensors, being able to also bind carbon monoxide and nitric oxide in this capacity and able to initiate the biochemical response of the organism to the change in the availability of the gas ligand (Kobayashi et al. 2010; Rodgers 1999). There are three such proteins that have been characterised; the NO sensing soluble guanylate cyclase, FixL which is a bacterial $O_2$ sensor-kinase and a bacterial CO sensor CooA. Binding of gasses to the haem in these proteins induces conformational changes which initiates their functions (Rodgers 1999). The binding of haem can also act as a redox-sensor with various proteins containing haem regulatory motifs that cause a change based on haem being present, such as the redox sensor protein PpsR from the photosynthetic bacterium *Rhodobacter sphaeroides* which binds haem as part of its light/dark cycle (Girvan & Munro 2013).

Substrate binding and interactions is also a major factor in the catalytic cycle of cytochrome P450s, with the iron centre being involved in co-ordination of substrates and being heavily involved in the required reaction, which varies depending on the type of cytochrome P450 (Meunier et al. 2004). The ferric ($Fe^{3+}$) state of the central iron in haem is also well known to be able to react very effectively with hydrogen peroxide, with the iron forming a reaction where the O-O bond is cleaved forming a strongly oxidising oxene intermediate, that quickly reacts with the heme molecule to form Compound I, an oxyferryl species [Fe(IV)=O], and water. Compound I is subsequently reduced back to the ferric iron state either by reacting with another oxyferryl group (Compound II, [Fe(IV)=OH]) or by a direct two-electron reduction (Vlasits et al. 2010). The central iron also has the ability to form reactive oxygen species in the presence of hydrogen peroxide, as has been witnessed in haem-binding proteins that are not dedicated peroxidases or catalases, highlighting the ease at which this reaction can take place (Shepherd & Dailey 2009; Mayfield et al. 2013). These reactive oxygen species can cause damage to the cell, which shows how this essential molecule can also be cytotoxic to cells if left unregulated and reach concentrations above 1 µM of unbound, free, haem (Girvan & Munro 2013).

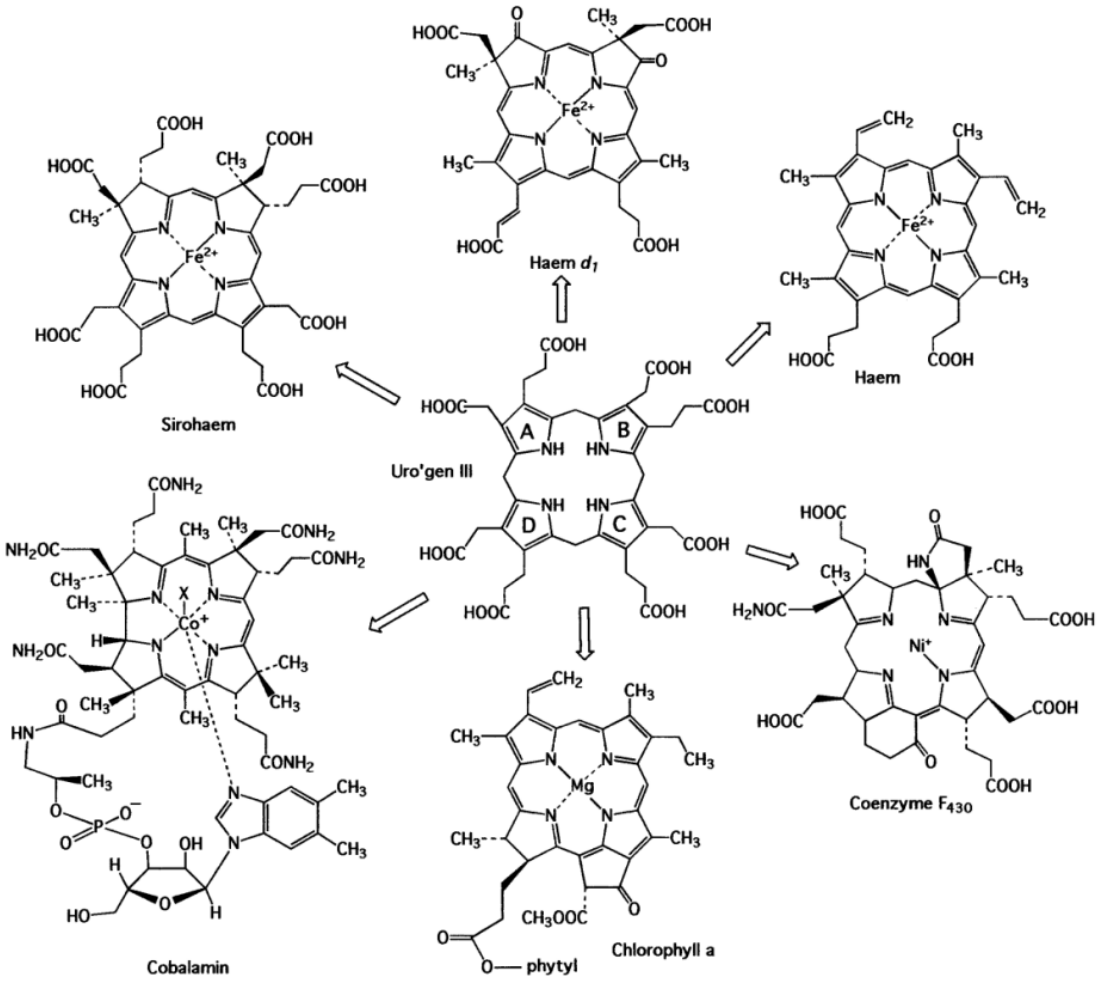


**Figure 1.1** – The cyclic tetrapyrroles. Uroporphyrinogen III (centre) and the different modified tetrapyrroles that it can form (Raux et al. 2000). In the synthesis of these modified tetrapyrroles, uroporphyrinogen III is the final common molecule to each pathway, causing it to be known as the common tetrapyrrole precursor.

## 1.1.2 – Chlorophyll

Chlorophylls have a central magnesium ion and are found in plants and cyanobacteria, and photosynthetic bacteria possess a very similar pigment called bacteriochlorophyll. These pigments are required to absorb solar energy to be used in photosynthesis. The synthesis of this molecule shares the majority of steps with the classical haem biosynthetic pathway, with dedicated chlorophyll synthesis occurring after magnesium insertion into protoporphyrin IX before major modifications to the side chains on the outside of the porphyrin ring (Masuda 2008).

## 1.1.3 – Cobalamin

Cobalamin, also known as vitamin $B_{12}$, has a central cobalt ion and can only be synthesised by bacteria and archaea. There are two biologically active forms of this compound, methylcobalamin (MeCbl) and 5'-deoxyadenosylcobalamin (AdoCbl), which are used as cofactors in methyltransferase and isomerase enzyme families, respectively. These forms differ with respect to the groups that coordinate the cobalt ion; MeCbl has a methyl group bound whilst AdoCbl has a deoxyadenosyl side chain (Gherasim et al. 2013).

## 1.1.4 – Sirohaem

Sirohaem, which like haem also has a central iron atom, is required for the six-electron reduction of sulphite to sulphide as a cofactor for several sulphite reductases (Murphy et al. 1974) in bacteria, archaea and fungi. This process is also part of the sulphur assimilation pathway in plants. Sirohaem is also required as a cofactor of ferredoxin-nitrite reductase, reducing nitrite to ammonia (Murphy et al. 1974).

## 1.1.5 – Factor $F_{430}$

Coenzyme $F_{430}$, which has an associated nickel ion, is used in the enzyme methyl-coenzyme M reductase as the final part of methanogenesis, and is only found in archaea (Thauer 1998).

# 1.2 – Haem Biosynthesis

The haem biosynthetic pathway was until recently thought to be highly conserved throughout nature, although recent research has revealed a number of new pathways for haem biosynthesis. There are now three known routes that haem synthesis follows; the classical pathway, the alternative haem biosynthesis pathway that proceeds via the production of sirohaem, and the coproporphyrin-dependant pathway that is proposed to be an ancestral pathway to the classical pathway and does not utilise protoporphyrin IX intermediates (Dailey et al. 2015). These pathways are currently not known to co-exist in the same organism.

All three pathways, which are described below, stem from the same tetrapyrrole precursor uroporphyrinogen III, which is believed to be synthesised from δ-aminolaevulinic acid via the same order of intermediates. Defects in haem biosynthesis can seriously inhibit growth of organisms or result in a shift to fermentative growth for survival (Mayfield et al. 2013; Dailey et al. 2010). In humans, defects give rise to a class of disease states known as porphyrias which can elicit symptoms ranging from photosensitivity to abdominal pains or life threatening neurological attacks (Poblete-Gutiérrez et al. 2006).

## 1.2.1 - Making the Macrocycle: Uroporphyrinogen III

### 1.2.1.1 – Synthesis of δ-aminolaevulinic acid

The two basic components for tetrapyrrole production in most eukaryotic cells are glycine and succinyl-CoA, which are substrates for the enzyme δ-aminolaevulinic acid synthase (Beale et al. 1975) that produces δ-aminolaevulinic acid (ALA, also known as 5-ALA) in the first dedicated step of tetrapyrrole biosynthesis. Plants and most prokaryotes (not including α- proteobacteria) use glutamate, α-ketoglutarate or glutamine in different pathways utilising a tRNA-dependent five-carbon pathway (Beale 1990), as opposed to the four-carbon pathway (Kresge et al. 2006) that animals use for 5-ALA production (Figure 1.2).

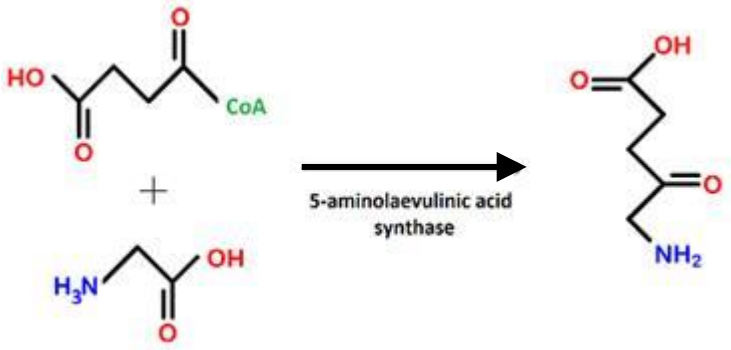


**Figure 1.2:** Synthesis of δ-aminolaevulinic acid (ALA) from succinyl CoA and glycine via the C-4 pathway.

### 1.2.1.2 – Porphobilinogen synthase

The synthesis of ALA is the first dedicated step in haem biosynthesis, with the next step being the formation of a pyrrole ring from two molecules of 5-ALA. This reaction requires the enzyme porphobilinogen synthase (PBG synthase), which links the amino group on the first ALA with the carboxyl group on the second ALA (Figure 1.3). This results in the production of water and the formation of porphobilinogen (PBG), which contains a pyrrole ring.

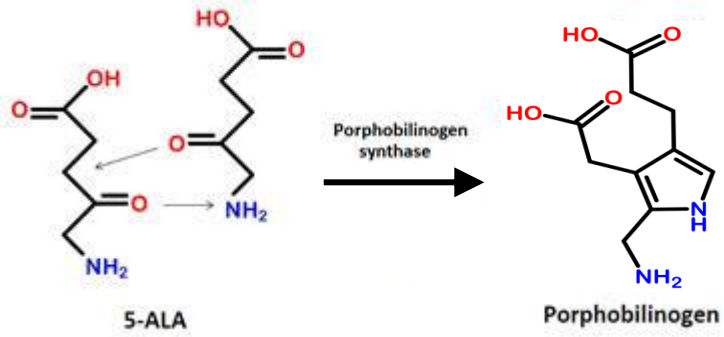


**Figure 1.3** – Formation of porphobilinogen from the hydrolysis of two molecules of δ-aminolaevulinic acid by PBG synthase.

### 1.2.1.3 – Porphobilinogen deaminase

PBG molecules are deaminated by porphobilinogen deaminase to produce the tetrapyrrole hydroxymethylbilane, the first tetrapyrrole/porphyrin ring in the pathway. This enzyme, also known as HemC (Panek & O'Brian 2002), acts by binding a dipyrromethane cofactor (made up of two molecules of PBG) that acts as a primer for the oligomerisation of four PBG molecules resulting in the formation of a protein-bound linear hexapyrrole (Layer et al. 2010). The formation of the hexapyrrole results in the formation of ammonia, as the amino groups are cleaved from the PBG molecules to form the macromolecule. This is then cleaved to produce hydroxymethylbilane (HMB), a linear tetrapyrrole, and the dipyrromethane cofactor is recycled.

### 1.2.1.4 – Uroporphyrinogen synthase

Hydroxymethylbilane is cyclised by uroporphyrinogen III synthase, which also inverts one of the end pyrrole rings, which is normally referred to as the D ring, before joining it to the pyrrole ring at the other end of the chain (the A ring) to form uroporphyrinogen III (Figure 1.4). Uroporphyrinogen III synthase works by first removing the hydroxyl group on the "A" ring to form an azafulvene intermediate.

This intermediate reacts with the substituted α-position of the "D" ring to form a spirocyclic pyrrolenine, where the "A" and "C" rings are linked to the "D" ring by the same carbon atom. The final step is the rearrangement of the "D" ring involving inversion and deprotonation resulting in bond formation between the "A" and "D" rings (Layer et al. 2010).

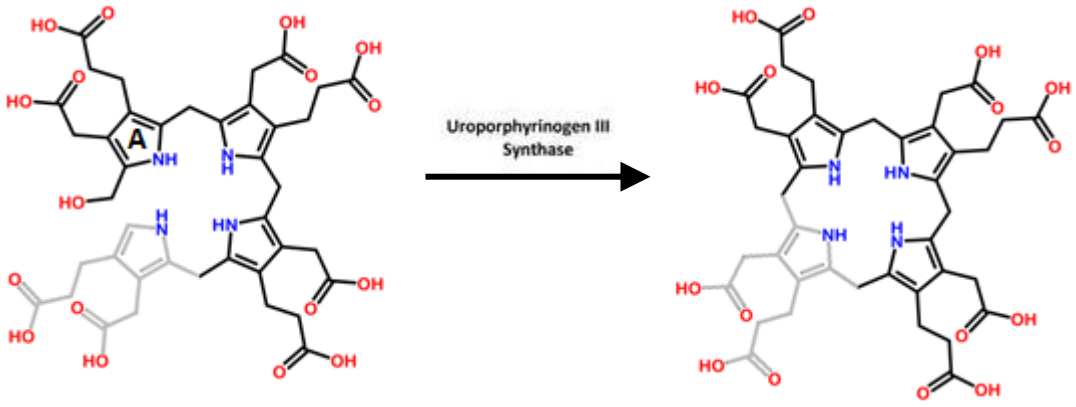


**Figure 1.4 –** Formation of uroporphyrinogen III by uroporphyrinogen III synthase. The "D" ring (coloured in grey) is inverted prior to forming a bond that links the "A" and "D" rings.

This reaction is the final step that is common to all modified tetrapyrroles that occur in nature. From this point uroporphyrinogen III (U'gen$_{III}$) can proceed down several different pathways to form any of the final products illustrated in Figure 1.1.

## 1.2.2 – Classical Haem Synthesis Pathway

Until very recently it was believed that most haem producing organisms synthesised haem using the same pathway. This pathway, now referred to as the classical pathway, proceeds from uroporphyrinogen III with two rounds of modifications to the side chains on the exterior of the macrocycle to form protoporphyrinogen IX before oxidation of the ring and finally insertion of iron to form haem. This metal chelation step is very important in photosynthetic organisms, as the chlorophyll biosynthesis branches from this pathway at this point where a $Mg^{2+}$ ion is inserted into protoporphyrin IX by magnesium chelatase instead of a $Fe^{2+}$ ion by ferrochelatase (Walker & Weinstein 1991).

### 1.2.2.1 – Uroporphyrinogen decarboxylase

Uroporphyrinogen III is an important molecule in modified tetrapyrrole synthesis. As mentioned in Section 1.1, it is the common precursor for the biosynthesis of all modified tetrapyrroles that are used in nature (Figure 1.1). In the haem biosynthetic pathway, uroporphyrinogen III is processed by uroporphyrinogen III decarboxylase, which removes the carboxyl groups on the acetyl side chains in a stepwise manner (Bushnell et al. 2011), leaving methyl side chains. The mechanism for this reaction has not been fully elucidated, but is widely regarded to begin with the decarboxylation of the D ring of uroporphyrinogen III in what has been determined to be a fast reaction followed by the other three rings in a much slower set of reactions (Barnard & Akhtar 1979).

Uroporphjyrinogen decarboxylase exists as a homodimer in both humans (Whitby et al. 1998) and in *Nicotiana tabacum* (Martins et al. 2001) based on their crystal structures, with proposals for the reaction mechanism involving the shuttling of intermediates between subunits (Heinemann et al. 2008). Later research suggests that each subunit can work independently for this reaction, with single chain proteins still able to fully convert uroporphyrinogen III to coproporphyrinogen III ($C'gen_{III}$) when one active site is mutated (Phillips et al. 2009). Further experiments on the bovine enzyme yielded a Hill coefficient of approximately 1, suggesting a non-cooperative relationship between the two active sites (Straka & Kushner 1983).

### 1.2.2.2 – Coproporphyrinogen oxidase

Coproporphyrinogen III is oxidised by coproporphyrinogen III oxidase to protoporphyrinogen IX ($P'gen_{IX}$) in a reaction that removes carboxyl groups from the propionates on rings A and B leaving vinyl substituents (Figure 1.5). This step is the final modification of the main side chains of the tetrapyrrole ring.

There are two alternative enzymes that can catalyse this process, HemF and HemN, creating a branch in the pathway. The reaction involving HemF is oxygen-dependent, with molecular oxygen being used as the final electron acceptor. This form of coproporphyrinogen oxidase is mainly found in eukaryotic organisms with there being very few bacteria that encode this enzyme, with examples being *Salmonella typhimurium* and *Rhodobacter sphaeroides* (Xu & Elliott 1993; Zeilstra-Ryalls & Schornberg 2006). In addition to $CO_2$, this reaction releases hydrogen peroxide ($H_2O_2$), where the protons react with the electron accepting oxygen molecule. The HemN enzyme that is expressed in most bacteria is oxygen-independent, with an unknown electron acceptor being utilised (Layer et al. 2010).

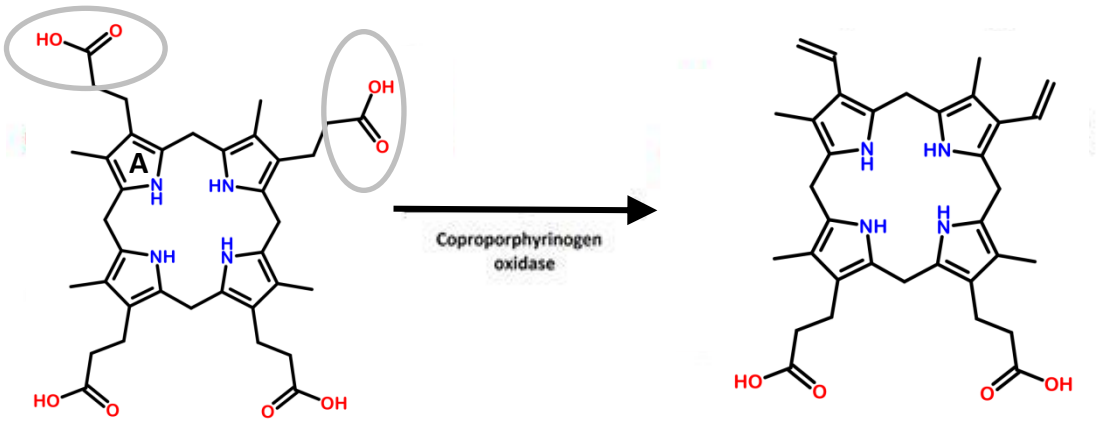


**Figure 1.5 –** Conversion of coproporphyrinogen III to protoporphyrinogen IX by coproporphyrinogen oxidase. Grey rings indicate carboxyl groups that are removed by the enzyme.

### 1.2.2.3 – Protoporphyrinogen oxidase

The penultimate step in the synthesis of haem *via* the classical pathway is the oxidation of protoporphyrinogen IX to protoporphyrin IX by protoporphyrinogen IX oxidase (also known as PPO). This enzyme catalyses the six-electron oxidation of protoporphyrinogen IX, altering the pattern of the double bonds of the ring to produce a highly absorbent and fluorescent product and allowing for insertion of a variety of metal ions. As with the coproporphyrinogen oxidase reaction there are multiple forms of protoporphyrinogen oxidase, the oxygen-dependent HemY (T. A. Dailey et al. 1994), the oxygen-independent HemG (Nishimura et al. 1995; Boynton et al. 2009) and finally HemJ, which is proposed to use molecular oxygen as an electron acceptor, but the true mechanism is not fully understood (Kato et al. 2010; Kobayashi et al. 2014; Boynton et al. 2011). The presence of multiple enzymes creates the same kind of pathway branching as the alternative coproporphyrinogen oxidases and allows for use of this pathway under a range of environmental conditions.

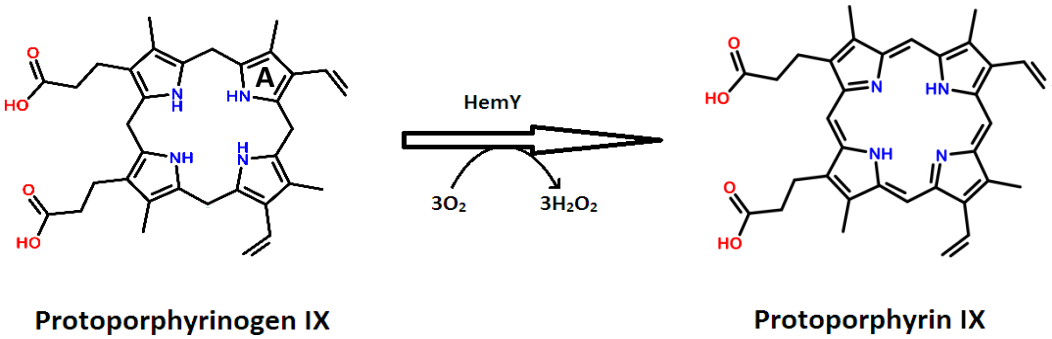


**Figure 1.6 –** Overview of conversion of protoporphyrinogen IX to protoporphyrin IX by the oxygen-dependent HemY.

The oxygen-dependent reaction that is catalysed by the HemY enzyme (Figure 1.6) uses oxygen as the electron acceptor. This enzyme is the most commonly studied protoporphyrinogen oxidase and is mostly found in eukaryotic organisms, however it is also found in a number of bacterial species (Kobayashi et al. 2014). This protein has been purified and assayed in a large number of organisms including plants (e.g. barley (Jacobs & Jacobs 1987)), mammals (e.g. murine (Dailey & Karr 1987), bovine (Siepker et al. 1987), human (Dailey & Dailey 1996)), fungi (e.g. *Saccharomyces cerevisiae* (Poulson & Polglase 1975) and bacteria (e.g. *Bacillus subtilis* (Hansson & Hederstedt 1992)).

This form of protoporphyrinogen oxidase uses a flavin adenine dinucleotide (FAD) cofactor, which gives the protein a characteristic yellow appearance. This cofactor is responsible for initially receiving the electrons from the protoporphyrinogen molecule before transferring them to the molecular oxygen acceptor. The FAD can only transfer two electrons at a time, which reduces to $FADH_2$, suggesting that the six electron oxidation occurs in three stages and progresses via two intermediates (tetrahydro- and dihydro- porphyrinogens).

While a tautomerisation mechanism has been proposed whereby the tetrapyrrole remains bound to the enzyme during oxidation (Jordan 1991; Koch et al. 2004), it is currently unknown if partially oxidised intermediates dissociate from the enzyme during the course of the reaction. This reaction has also been shown to be stimulated by peroxidase-derived reactive oxygen species produced by enzymes such as cytochrome *c* (Shepherd & Dailey 2009), which is particularly relevant in mammalian systems where HemY and cytochrome *c* are co-localised to the mitochrondrial intermembrane space. Intriguingly, a similar stimulation of bacterial HemY has been observed by the terminal enzyme of the coproporphyrin-dependent pathway, HemQ (Dailey et al. 2010).

The oxygen independent reaction, catalysed by the HemG enzyme, follows a different path. HemG shuttles electrons into the electron transport chain and uses compounds such as nitrate or fumarate as the terminal electron recipients (Jacobs & Jacobs 1976). The HemG protein from *E. coli* has been recently characterised and this protein was shown to bind flavodoxin and uses menaquinone as an electron acceptor (Boynton et al. 2009).

The HemJ enzyme has been discovered very recently in organisms that have no homologues of *hemG* nor *hemY* yet still produce haem (Kato et al. 2010). This protein has been shown to function in an aerobic environment, and seems to be distantly related to a subunit of respiratory complex I (Kato et al. 2010). However, attempts to complement a *hemG* mutant of *E. coli* with *hemJ* were unsuccessful (Boynton et al. 2011).

The formation of protoporphyrin IX is the final step that is common to both the classical haem biosynthesis pathway and the chlorophyll biosynthesis pathway in organisms that contain both pathways. Following the formation of protoporphyrin IX, the porphyrin can either have an iron ion inserted by ferrochelatase, as outlined below, or have a magnesium ion inserted by magnesium chelatase, which is the first dedicated step towards the synthesis of chlorophylls and bacteriochlorophylls (Jensen et al. 1998).

### 1.2.2.4 – Ferrochelatase

The final reaction in the classical haem synthesis pathway involves the insertion of an iron (II) ion ($Fe^{2+}$) into protoporphyrin IX by the terminal enzyme in the pathway, ferrochelatase. Ferrochelatases have been shown to act on a range of porphyrins (Dailey et al. 1983; Dailey & Lascelles 1974), inserting a series of different metal ions *in vitro* (Karlberg et al. 2002; Lecerof et al. 2003; Hansson et al. 2006). However, their role in the biosynthesis of haem is to insert a ferrous ion into the middle of the porphyrin ring (Layer et al. 2010). This is achieved by distorting the planar porphyrin molecule into a 'saddle' conformation before allowing a metal ion to be inserted into the ring, which is coordinated by the nitrogen atoms on the pyrrole rings (Layer et al. 2010).

While there is no oxygen-dependent nor independent isoforms, there are membrane-associated and soluble ferrochelatases. Besides solubility there are other differences between amongst ferrochelatases, with the majority of membrane-associated enzymes containing a [2Fe-2S] iron sulphur cluster of unknown function, with the exception of *Saccharomyces cerevisiae* (Karlberg et al. 2002). A class of soluble [2Fe-2S]-containing bacterial ferrochelatases has also been identified that coordinates the cluster via three cysteine residues located in the centre of the primary sequence, rather than via three cysteine residues at the C-terminus as in mammalian ferrochelatases (Shepherd et al. 2006). Another functional variation can be found at the C-terminus, where membrane-associated forms have a longer sequence that is believed to be a factor involved in dimerisation of the enzyme (Wu et al. 2001; Karlberg et al. 2002). It is also in this region where *S. cerevisiae* has slight differences that do not allow for the formation of a [2Fe-2S] iron-sulphur cluster, but still allows for stable dimers to be formed (Karlberg et al. 2002).

Both soluble and membrane-bound forms of ferrochelatases have been shown to utilise protoporphyrin, mesoporphyrin and deuteroporphyrin as substrates as well as a variety of divalent metals, including zinc, copper and cobalt among the main metals tested (Dailey et al. 1983; Lecerof et al. 2003; Hansson et al. 2011). Zinc in particular has been used as a common alternative to iron in experiments as it has been shown to be more stable in an aerobic environment and also allows for fluorescence-based assays to be performed (Camadro et al. 1984).

## 1.2.3 – The Alternative Haem Biosynthetic Pathway

An alternative pathway for haem biosynthesis was discovered very recently that produces haem *via* a very different pathway to the classical pathway (Buchenau et al. 2006). This pathway, which has currently been observed in sulphate-reducing bacteria and methanogenic archaea (Bali et al. 2011; Lobo et al. 2014; Palmer et al. 2014) , produces haem from sirohaem in a series of reactions that modify the side chains present on the exterior of the porphyrin ring.

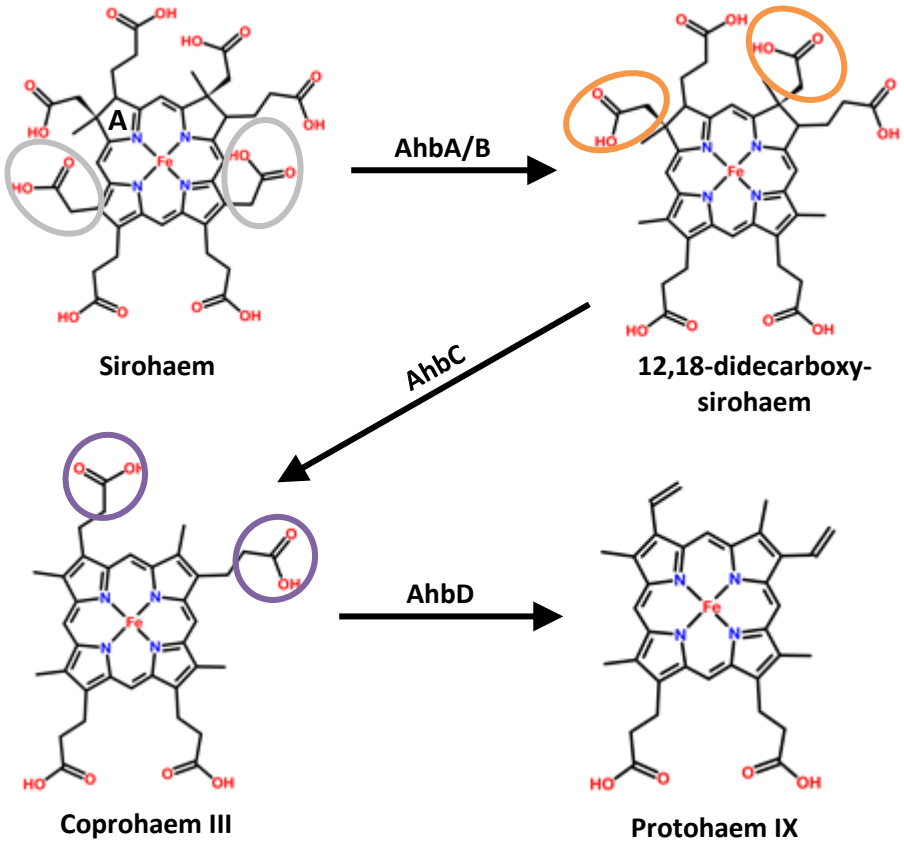


**Figure 1.7** – Overview of the alternative haem biosynthetic pathway starting from sirohaem. Sirohaem is first decarboxylated at the C12 and C18 positions (grey) by sirohaem decarboxylase (AhbA/B complex) before acetic acid residues are cleaved at positions C2 and C7 (orange) by a radical SAM enzyme (AhbC) and finally decarboxylation of the side chains at positions C3 and C8 (purple) by haem-*b* synthase (AhbD) to form protohaem IX.

### 1.2.3.1 – Sirohaem Decarboxylase

The first dedicated step along the alternative pathway is the double decarboxylation of sirohaem by sirohaem decarboxylase to form 12, 18-didecarboxysirohaem carried out by the dimeric complex AhbA/AhbB (Palmer et al. 2014). This reaction is believed to occur in two steps, with the substrate leaving the protein following a single decarboxylation and entering in a different orientation to perform the second. This reaction modifies the side chains located on C12 and C18 of sirohaem, located on rings C and D respectively, leaving methyl groups at these positions (Palmer et al. 2014).

### 1.2.3.2 – Transformation to coprohaem III

Following decarboxylation of sirohaem on rings C and D, the acetic acid groups on rings A and B are cleaved off by AhbC (Bali et al. 2011). This reaction is proposed to be performed by a radical SAM enzyme, using radicals to cleave the acetate groups from C2 and C7 (Kuhner et al. 2014; Bali et al. 2011).

### 1.2.3.3 – Haem *b* Synthase

The final reaction in the alternative haem biosynthetic pathway is the decarboxylation of coprohaem III to protohaem IX, aka haem *b*. This reaction is catalysed by AhbD, also known as haem *b* synthase, in this system, which is also a radical SAM enzyme (Bali et al. 2011). This protein, which has been shown to have two 4Fe-4S clusters, uses the deoxyadenosyl radical, dAdo, to cleave the propionate groups on rings A and B and transform them into vinyl groups, producing protohaem IX (Lobo et al. 2014).

## 1.2.4 – The coproporphyrin-dependent pathway

A third branch to synthesise haem has been discovered even more recently than the alternative haem biosynthetic pathway and this progresses via coproporphyrin III rather than protoporphyrin IX (Dailey et al. 2015). The pathway (Figure 1.8), which has mostly been found in Gram-positive organisms of the Actinobacteria and Firmicutes, is ancestral to the classical pathway (Dailey et al. 2015).

Whilst this pathway is the most recent to be discovered, clues as to its existence have been available for a number of years. The first clue occurred in experiments where coproporphyrinogen was being monitored for conversion to protoporphyrin in cell extracts. Cell extracts from organisms such as *Staphylococcus aureus* and *Micrococcus lysodeikticus* failed to produce protoporphyrin IX, but did accumulate coproporphyrin III (Jacobs et al. 1971). It was later discovered that HemY proteins from *B. subtilis* could oxidise coproporphyrinogen III as well as protoporphyrinogen IX (Hansson et al. 1997), which is the branch point where the coproporphyrin-dependent pathway begins.

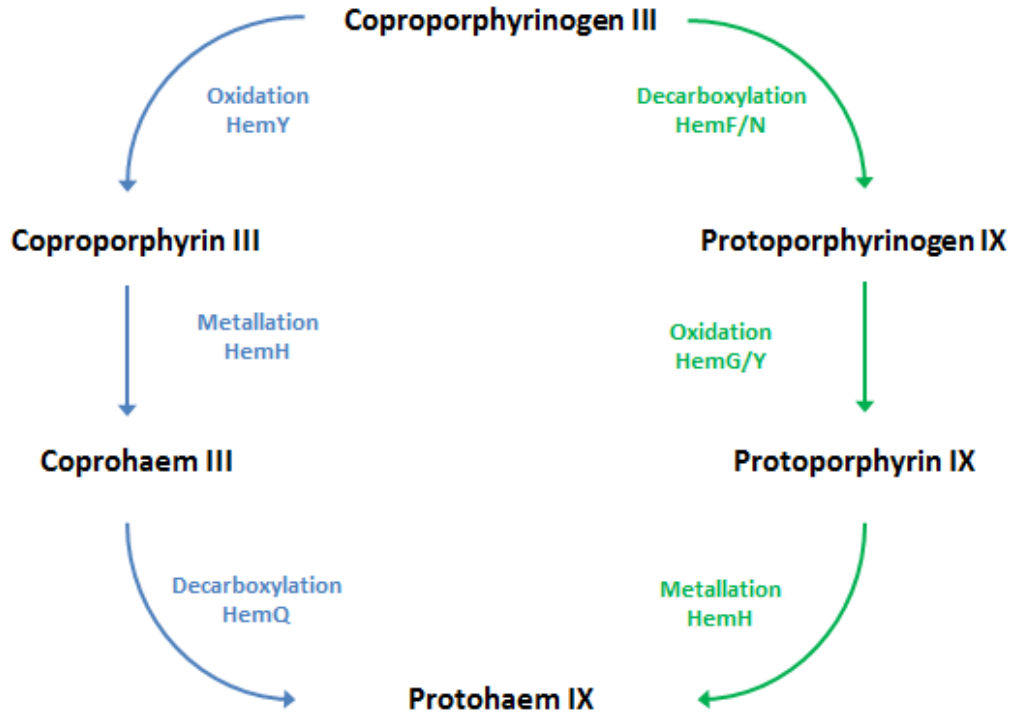


**Figure 1.8 –** Comparison between the classical pathway (green) and the coproporphyrin-based pathway (blue). Starting with C'gen$_{III}$ the main difference in reaction orders is the decarboxylation step, which occurs first in the classical pathway (catalysed by HemF or HemN) and last in the coproporphyrin-dependent pathway (catalysed by HemQ).

### 1.2.4.1 – Oxidation of coproporphyrinogen III

The first step in this pathway branch is oxidation of coproporphyrinogen III to coproporphyrin III, rather than the conversion to protoporphyrinogen IX that is seen in the classical pathway. This reaction is catalysed by HemY enzymes and the reaction is similar to the oxygen-dependent protoporphyrinogen oxidase reactions performed by HemY proteins in the classical pathway (mentioned in section 1.2.2.3 and expanded on in chapter III). Indeed, the HemY enzyme from *B. subtilis* has been shown to oxidise both coproporphyrinogen III and protoporphyrinogen IX (T. A. Dailey et al. 1994; Hansson & Hederstedt 1994), which has implications for the evolution of the classical pathway from the ancestral coproporphyrinogen pathway (Dailey et al. 2015).

### 1.2.4.2 – Coproporphyrin III ferrochelatase

As with the classical pathway, insertion of a ferrous iron atom into the tetrapyrrole ring follows oxidation of the macrocycle. This reaction is catalysed by enzymes annotated as HemH (as in the classical pathway), This reaction, inserting $Fe^{2+}$ into coproporphyrin III, appears to occur in the same way as the classical reaction but produces coprohaem III as a product (Dailey et al. 2015; Lobo et al. 2015). Intriguingly, HemH ferrochelatases from Gram-positives have previously been shown to insert iron into both coproporphyrin III and protoporphyrin IX (Dailey et al. 2015).

### 1.2.4.3 – Coprohaem III decarboxylation

The final reaction in the coproporphyrin-dependent pathway is the decarboxylation of coprohaem III to form haem. This reaction is very similar to the reaction catalysed by AhbD of the alternative pathway, in that it is proposed to utilise radicals to cleave the propionate side chains on rings A and B (Celis et al. 2015). However, the HemQ enzyme that catalyses this reaction is not a radical SAM enzyme (Dailey et al. 2010) and is likely to rely upon a porphyrin or aromatic derived radical to activate the propionate carbon atoms (Celis et al. 2015). HemQ is unique to organisms that synthesise haem *via* the coproporphyrin-dependent pathway and can utilise peroxides to initiate a radical-based oxidative decarboxylation reaction (Dailey et al. 2015; Lobo et al. 2015; Celis et al. 2015).

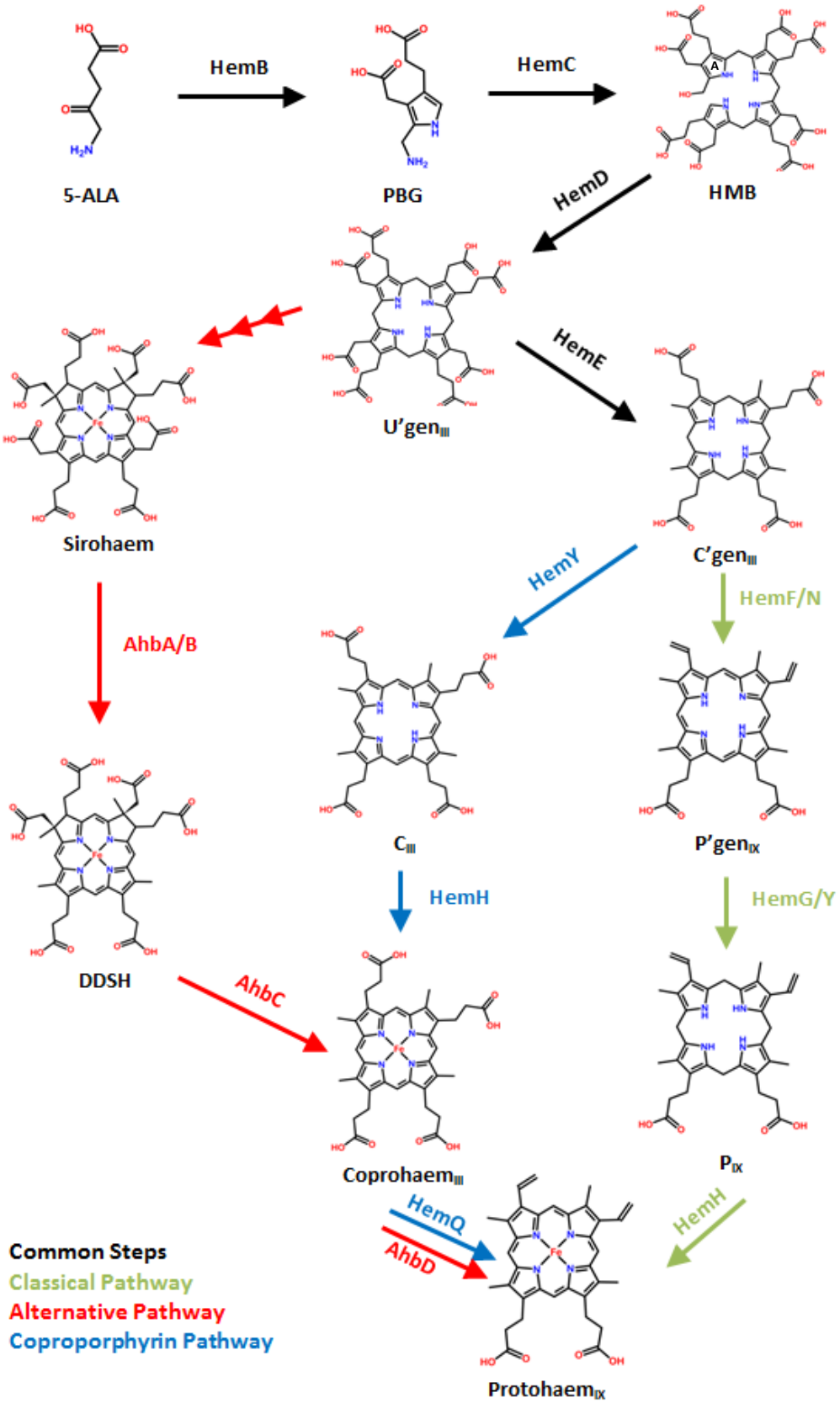


**Figure 1.9** – Overview of haem biosynthesis *via* the three discovered pathways: The classical pathway (green), commonly utilised by Gram-negative bacteria and eukaryotic organisms, the Alternative Pathway (red), primarily utilised by sulphate reducing bacteria and methanogenic archaea, and the coproporphyrin-dependent pathway (blue), currently only discovered in Gram-positive organisms such as *S. aureus* and *B. subtilis*. Reactions utilised by more than one pathway are shown in black

# 1.3 – The importance of *Staphylococcus aureus*

Discovered in 1880, *Staphylococcus aureus* is a Gram positive organism that can cause minor skin infections and post-operative wound infections (Deurenberg & Stobberingh 2008). This organism occurs as a commensal organism in a significant proportion of the human population (Wertheim et al. 2005; Casey et al. 2007) and is most commonly found inhabiting the anterior nasal passage or skin (Williams 1963) although it has been discovered colonising the gastrointestinal tract, vagina, oral cavity and axillae (Williams 1963; Guinan et al. 1982; Koukos et al. 2015). Whilst this organism can co-exist with humans without incident, *S. aureus* infections can range in severity from skin conditions such as impetigo bullosa, to more serious, life threatening conditions such as bacteremia (Archer 1998). This pathogen can be very dangerous to children and those with an impaired immune system with conditions such as staphylococcal scalded skin syndrome (Grama et al. 2016). *S. aureus* has also reacted quickly to penicillin based antibiotics, quickly acquiring resistance mechanisms to β-lactam antibiotics soon after widespread introduction (Deurenberg & Stobberingh 2008) with methicillin resistant *S. aureus* strains (MRSA) also being able to carry resistance genes to other classes of antimicrobials (Smith & Jarvis 1999; Deurenberg & Stobberingh 2008).

## 1.3.1 - Discovery and characteristics of *S. aureus*

As mentioned above, *S. aureus* was discovered in 1880 by the surgeon Sir Alexander Ogston whilst viewing stained preparations of pus from patients with post-operative wound suppuration or abscesses under a microscope (Ogston 1882). Among the bacteria that were discovered was a coccus shaped bacterium, which was given the name *Staphylococcus* due to the grape-like clusters that they formed (Ogston 1882). A sample of this bacterial strain was later isolated and grown and were finally given the name *Staphylococcus aureus* due to the golden appearance of the colonies that were formed (van Belkum et al. 2009). This organism has a genome size of approximately 2.8 - 2.9 mega base pairs (Lowy 1998; Kim et al. 2014) with virulence and antimicrobial resistance genes being found both in the chromosomal and extra chromosomal elements of the genome (Lowy 1998).

For many years, identification of *S. aureus* relied on using a coagulase agglutination assay, where the protein coagulase converts fibrinogen (contained in plasma) to fibrin, which gives rise to a clumping effect in comparison with a saline control. This clumping used to be regarded as a positive result for *S. aureus* (Turutoglu et al. 2005), which at the time was the only coagulase-positive *Staphylococcus* species that had been discovered, with other *Staphylococcus* species (e.g. *Staphylococcus epidermidis*) being classified as coagulase-negative *Staphylococcus* species (Casey et al. 2007). There are reports of other species of *Staphylococcus* that have been found to be coagulase-positive, such as *Staphylococcus shleiferi* subspecies *coagulans* (Thibodeau et al. 2012), which could render classical identification practices inaccurate, however there are now modernised molecular techniques that give more accurate identifications. An example of these techniques is pulsed-field gel electrophoresis which is now considered the gold-standard test for detecting *S. aureus* in clinical settings (Deurenberg & Stobberingh 2008).

*S. aureus* belongs to the Firmicute phylum of bacteria, a phylum that has a low G+C content in its genome (Charneski et al. 2011) when compared with other phyla such as actinobacteria, that can have a G+C content as high as 70% (Ventura et al. 2007). In general, *Staphylococci* belong to the staphylococcaceae family, of the bacilliales order from the bacilli class of firmicutes. This family is one of the major branch points where the *coccus* shape of the bacterium begins to form, as opposed to rod-shaped bacteria such as *Bacillus subtilis* (which also belongs to the bacillales order).

## 1.3.2 - Clinical importance and antibiotic resistance

Since its discovery in the 1880's, *S. aureus* has been recognised as a pathogen that has been very likely to cause infections of wounded tissues (Ogston 1882) and even in the 1990s, it remained the most common organism that was isolated from wound and soft-tissue infections (Smith & Jarvis 1999). Infections by this pathogen usually originate following colonisation, which occurs in approximately 30% of healthy individuals (Archer 1998), before potentially causing a range of infections. Common infections mostly include superficial conditions (e.g. carbuncles, cellulitis and impetigo) whilst less common afflictions can include pneumonia, endocarditis and bacteremia (Smith & Jarvis 1999).

Should an infection progresses to the bacteremia stage, *S. aureus* can spread to peripheral sites in distant organs which increases the potential for septic shock to occur, which has a high mortality rate if not treated (Archer 1998). Other serious conditions that can arise from *S. aureus* infections include staphylococcal scalded skin syndrome, which mostly affects children due to their lack of immunity (Grama et al. 2016), toxic shock syndrome and food-borne gastroenteritis (Archer 1998).

Antimicrobial resistance of *S. aureus* has become as big problem in the clinical setting, as it has quickly adapted to new forms of penicillin based antimicrobials to form resistant strains. In 1942 the first penicillin resistant isolate of *S. aureus* was observed, 2 years after the widespread use of penicillin for medical use, and by 1960 around 80% of strains were penicillin resistant (Deurenberg & Stobberingh 2008). The gene responsible for this resistance, producing β-lactamase, has been discovered on transmissible genetic elements, most commonly plasmids, with the form expressed by *S. aureus* being stable for over 50 years (Medeiros 1997). A similar pattern was seen after the introduction of methicillin, a penicillinase resistant form of penicillin, where resistant strains had been detected 2 years after introduction. This was later found to be due to acquisition of a 2.1 kb gene called *mecA* (Deurenberg & Stobberingh 2008), which produces an altered penicillin binding protein (PBP2'/PBP2a) and is believed to have originated in a coagulase-negative strain *Staphylococcus sciuri* (Smith & Jarvis 1999).

Methicillin-resistant *S. aureus* (MRSA) strains also tend to multi-drug resistant, as the plasmid-borne transposon can also carry resistance genes for many other antimicrobials, including erythromycin and tetracycline (Smith & Jarvis 1999). These resistance genes appear to be collected on a mobile genomic island called the staphylococcal cassette chromosome *mec* (SSC*mec*), of which seven types have been recognised ranging from 20.9 kb to 66.9 kb in size (Deurenberg & Stobberingh 2008). Of these seven cassette types, only types II and III (53.0 kb and 66.9 kb in size respectively) contain genes responsible for multiple classes of antibiotics. The emergence of these resistant strains is currently contributing the impending antimicrobial resistance crisis, which will eventually see epidemics break out for which there are few effective treatments without the discovery of novel ways of combatting pathogenic organisms (Michael et al. 2014).

## 1.3.3 - Iron acquisition and haem metabolism

*S. aureus* has the ability to uptake haem from the environment, which is its main source of iron. The acquisition of this nutrient is essential for the survival the majority of pathogens in their host organism, without it pathogens will be unable to grow efficiently and will be eliminated by host defences (Ratledge & Dover 2000). The presence of iron in host organisms is very tightly regulated, with iron being sequestered to the carrier proteins (such as ferritins, transferrin and lactoferrin) or bound to protoporphyrin as haem in hemoproteins, leaving virtually no free iron in the host (Wandersman & Delepelaire 2004).

Faced with the scarce amounts of iron available in hosts, pathogens such as *S. aureus* have developed mechanisms to acquire iron from these sources. Previous studies on *S. aureus* has shown that the preferred iron source for acquisition is haem, which is the most abundant form of iron in the body (localised to haemoglobin and myoglobin) (Skaar, Humayun, et al. 2004). Gram-positive bacteria intake haem using cell wall anchored proteins to relay haem from host proteins to an ABC transporter system, which delivers the metalloporphyrin to the cytoplasm (Cavallaro et al. 2008). In *S. aureus*, this system is made up of nine different proteins, forming the well-characterised Isd system. This system involves three different stages to acquire and degrade the haem molecule. The first stage involves the transfer of haem across the cell wall, performed by the haem-binding IsdA, IsdB, IsdC and IsdH proteins (Grigg et al. 2007; Maresso & Schneewind 2006; Pluym et al. 2008). The second process is the transport of haem across the cell membrane, performed by the IsdDEF complex before finally being degraded by the haem oxygenases IsdG and IsdI (Maresso & Schneewind 2006). Gram-negative organisms have to transport haem across two separate membranes, with these two actions being performed using two different systems. To transport iron-siderophore complexes across the outer membrane, Gram-negative organisms (such as *E. coli*) use the TonD-dependent energy transduction system which is composed of the proteins: TonB, ExbB, ExbD and FepA (Higgs et al. 2002). Transport across the inner membrane involves different families of ABC transporters, resembling the Gram-positive system, that appear to vary according to specific organisms (Cavallaro et al. 2008).

Once inside the cell, haem is degraded by haem monoxygenases, in a reaction that appears to be conserved throughout mammals and bacterial speces that contain them, producing biliverdin, carbon monoxide and releasing the iron contained within the porphyrin ring (Maresso & Schneewind 2006). As of 2006, two types of haem oxygenase systems have been described in Gram-positive pathogens: the HmuO system characterised in *Corynebacterium diphtheria*e, which is homologous to the human haem oxygenase enzyme (Wandersman & Delepelaire 2004) and the IsdG/IsdI system that has been characterised from *S. aureus*, which has a lack of amino acid sequence identity to other bacterial haem-degrading enzymes and has homologues in *Listeria monocytogenes, Bacillus anthracis* and *Staphylococcus epidermidis* (Skaar, Gaspar, et al. 2004). Following haem breakdown, the iron is stored by the pathogen in ferritins and haem-containing bacterioferritins (the latter of which is unique to prokaryotes) before being used. The iron can also be re-formed into haem via the biosynthetic pathway, where it is then used as a co-factor in enzymes or binds to HemA to regulate its own synthesis (Wandersman & Delepelaire 2004).

# 1.4 – Aims of the Project

The overarching aim of this project was to increase the understanding of how haem is synthesised in the cutaneous pathogen *Staphylococcus aureus*. At the start of the project, the two recently discovered branches to the haem biosynthetic pathway had not been reported, and it was thought that the role of HemQ was to facilitate HemY-mediated oxidation of protoporphyrin IX in the classical pathway (Dailey et al. 2010) rather than catalysing the terminal step of the coproporphyrin-dependent pathway. Hence, the initial aims of the current project were to:

- Measure the impact of *S. aureus* HemQ upon HemY kinetics.
- Determine whether the mechanistic basis for HemQ-mediated stimulation of HemY relies upon the generation of reactive oxygen species.
- Determine whether HemQ required bound haem for stimulation of HemY to occur.
- Measure the affinities of different tetrapyrroles for HemQ.

Following the discovery of the pathway branches outlined in sections 1.2.3 and 1.2.4, the research aims switched to the *bona fide in vivo* reactions for the HemY, HemH and HemQ enzymes:

- Determine if HemQ-mediated stimulation of HemY occurs when coproporphyrinogen III is used as a substrate.
- Isolate recombinant purified *S. aureus* HemH and perform kinetic characterisation.
- Investigate how structural features of HemY, HemH, and HemQ are adapted to their *in vivo* function.

This thesis is set out in a logical order that follows the coproporphyrin-dependent pathway (i.e. HemY, HemH, HemQ), and the data are discussed in terms of how substrate specificities and interactions between pathway enzymes may have influenced the evolution of the classical haem synthesis from the ancestral coproporphyrin-dependent pathway.

Chapter II

# Materials & Methods

# 2.1 – Strains List

The following strains (Table 2.1) were either made during the project or acquired from the laboratories of Prof. Martin Warren (University of Kent) or Prof. Harry Dailey (University of Georgia). Bacterial strains were grown as outlined in Section 2.3 before purifying the relevant proteins as described in Section 2.4.

**Table 2.1 -** *E. coli* strains used during this study with their purposes, origins and antibiotic resistances

| Internal Strain Number | *E. coli* Strain | Plasmid(s) | Usage | Antibiotic Resistance | Origin |
|---|---|---|---|---|---|
| MS82 | BL21 STAR DE3 | pET14b-*S. aureus hemY*, pLysS | *S. aureus* HemY expression | Kanamycin Chloramphenicol | Warren Lab |
| MS8 | BL21 | pLysS | Transformation with a *hemQ*-containing plasmid | Chloramphenicol | - |
| MS51 | JM109 | - | Transformation with a HemQ containing plasmid | - | - |
| MS122 | BL21 | pET14b-*S. aureus hemQ*, pLysS | *S. aureus* HemQ expression | Ampicillin Chloramphenicol | This Work |
| MS73 | JM109 | pTrcHis-Human *hemY* | Human HemY expression | Ampicillin | Dailey Lab |
| MS76 | JM109 | pTrcHis-*P. acnes hemY* | *P. acnes* HemY expression | Ampicillin | Dailey Lab |
| MS4 | TOP10 | - | Competent cells used in cloning experiments | - | - |
| MS83 | BL21 STAR DE3 | pET14b-Human *hemE*, pLysS | Expression of Human HemE | Ampicillin Chloramphenicol | Warren Lab |
| MS84 | BL21 DE3 | pET14b-*M. thermautotrophicus hemB* - *B. megaterium hemC hemD* | Expression of haem synthesis proteins: HemB, HemC and HemD | Ampicillin Chloramphenicol | Warren Lab |
| MS117 | JM109 | pTrcHis-*M. tuberculosis hemQ* | Plasmid recovery for *S. aureus hemH* cloning | Ampicillin | Dailey Lab |
| MS41 | JM109 | pTrcHis-*B. subtilis hemH* | Plasmid recovery for *S. aureus hemH* cloning<br>*B. subtilis* HemH expression | Ampicillin | Dailey Lab |

| | | | | | |
|---|---|---|---|---|---|
| MS116 | JM109 | pTrcHis-*P. acnes hemHQ* | Plasmid recovery for *S. aureus hemH* cloning / *P. acnes* HemHQ expression | Ampicillin | Dailey Lab |
| MS368 | JM109 | pTrcHis-*S. aureus hemH* | Expression of *S. aureus* HemH | Ampicillin | This Work |

## 2.2 – Plasmids

The following plasmids were either made during the project or acquired from the laboratories of Prof. Martin Warren (University of Kent) or Prof. Harry Dailey (University of Georgia). Plasmid stocks were transformed into chemically-competent *E. coli* cells as outlined in Section 2.11. Plasmids that were to be used as the vector for the cloning of *S. aureus hemH* were extracted from *E. coli* overnight starter cultures as outlined in Section 2.10.2.

**Table 2.2 -** Bacterial plasmids used during this study with their purposes and origins

| Plasmid | Gene | Organism | Usage | Origin |
|---|---|---|---|---|
| pET-28a-*S. aureus hemY* | *hemY* | *S. aureus* | Overexpression of *S. aureus* HemY | Warren Lab |
| pET-14b-*S. aureus hemQ* | *hemQ* | *S. aureus* | Overexpression of *S. aureus* HemQ | Warren Lab |
| pTrcHis-Human PPO | *hemY* | Human | Expression of Human HemY | Dailey Lab |
| pTrcHis-*P. acnes hemY* | *hemY* | *P. acnes* | Expression of *P. acnes* HemY<br>Cloning of *S. aureus hemH* | Dailey Lab |
| pTrcHis-*B. subtilis hemH* | *hemH* | *B. subtilis* | Expression of *B. subtilis* Ferrochelatase<br>Cloning of *S. aureus hemH* | Dailey Lab |
| pTrcHis-*M. tuberculosis hemQ* | *hemQ* | *M. tuberculosis* | Cloning of *S. aureus hemH* | Dailey Lab |
| pTrcHis-*S. aureus hemH* | *hemH* | *S. aureus* | Expression of *S. aureus* HemH | This work |
| pET-14b-Human *hemE* | *hemE* | Human | Expression of Human HemE | Warren Lab |
| pET-14b-*hemB-D* | *hemB*<br>*hemC*<br>*hemD* | *M. thermautotrophicus*<br>*B. megaterium*<br>*B. megaterium* | Expression of haem synthesis enzymes:<br>HemB, HemC and HemD | Warren Lab |

# 2.3 – Bacterial Growth

## 2.3.1 - Starter cultures

Strains were streaked out on agar plates containing the appropriate antibiotics (working concentrations are detailed in Table 2.3 below). Single colonies were used to inoculate 10 mL of LB media (10g/L NaCl, 10g/L Tryptone, 5g/L Yeast Extract) in sterile falcon tubes (50 mL). These were then placed in a Innova 3100 shaking waterbath (New Brunswick Scientific, USA) at 37 ˚C and 180 rpm for approximately 16 h (overnight).

**Table 2.3 –** Stock and working concentrations of antibiotics used during this study

| Antibiotic | Stock Concentration (mg/mL) | Working Concentration (mg/mL) |
|---|---|---|
| Ampicillin | 125 | 0.125 |
| Chloramphenicol | 34 | 0.034 |
| Kanamycin | 50 | 0.05 |

## 2.3.2 – Protein overexpression

A starter culture of the desired strain was grown as described above, with appropriate antibiotics. This was then transferred to a 2L baffled flask containing 1L of sterile LB, for strains containing pET-based plasmids, or 1L of sterile Circlegrow medium (MP Biomedicals, USA), for strains containing pTrcHis plasmids, and was incubated at 37˚C and 160rpm. Flasks containing LB were monitored via optical density at 600nm ($OD_{600}$), with Isopropyl β-D-1-thiogalactopyranoside (IPTG) being added (final concentration = 400mM) when cells reached an $OD_{600}$ of 0.6. Flasks were then incubated at 19°C and 160 rpm for 16 h. Flasks containing cells that overexpressed *S. aureus* HemY also had riboflavin added at this point to promote FAD cofactor incorporation (final concentration = 0.75 µg/mL). Flasks containing Circlegrow were grown for 24 h at 37°C and 160 rpm without any extra growth supplements. Cells were then harvested by centrifugation in a Beckman Coulter Avanti J series centrifuge (Rotor: JLA 9.1 (Beckman Coulter), 4000 rpm, 4 ˚C, 20 min) and the cell pellets collected and placed in a sterile 50 mL falcon tube. Cells were stored at -20˚C if they were not to be immediately used.

## 2.4 – Protein purification

All proteins purified contained a $His_6$-tag for affinity chromatography. Cell pellets from 1L cultures of cells overexpressing HemY or HemQ were re-suspended in 30 mL of protein storage buffer containing 50mM Tris/ 3-(*N*-morpholino)propanesulfonic acid (MOPS) pH 8.0, 100mM KCl, 0.2% (v/v) Tween 20. Cultures (1L) overexpressing HemH were re-suspended in 30 mL of protein storage buffer containing 50mM Tris/MOPS pH 8.0, 100mM KCl, 1% (w/v) sodium cholate. Cell suspensions were sonicated in a Soniprep150 Sonicator (MSE, UK) for 6 x 30 s bursts on ice at an amplitude of 10 microns, with a 30 s interval between bursts, to break open the cells. The suspension was then centrifuged (Rotor: JA 25.50 (Beckman Coulter), 18,000rpm, 4˚C, 20 mins) to remove insoluble cell debris. The supernatant was applied to a column containing Talon metal affinity resin (Clontech Laboratories Inc., USA) with a 2.5 mL column volume, which had been pre-equilibrated with 5 column volumes of protein storage buffer (12.5 mL). 50 mL of protein storage buffer was then passed through the column to remove any unbound proteins from the column. 10 mL of wash buffer (protein storage buffer including 15 mM imidazole) was then added to the column to remove any weakly-bound protein. The solution that was eluted from the column at this stage was collected to be concentrated (this sample will later be referred to as the "Wash" sample). 10 mL of elution buffer (protein storage buffer including 300 mM imidazole) was then added to the column to elute the protein of interest (this sample will later be referred to as the "Elution" sample). 10 mL of protein storage buffer including 1M imidazole was then added to remove any remaining protein from the column. 12.5 mL of protein storage buffer was then added to re-equilibrate the column for storage. The 10 mL wash and elution samples were placed in 10 kDa cut-off spin concentrators (Millipore, USA) and centrifuged at 5,000 x g to concentrate the samples down to a volume between 0.5 mL and 1 mL. The samples were then passed through PD10 de-salting columns (GE Healthcare, UK), equilibrated with protein storage buffer, and transferred into fresh protein storage buffer to remove any imidazole from the buffer. Samples (50 µL) were collected throughout all steps for subsequent analysis by Sodium Dodecylsulphate-Polyacrylamide Gel Electrophoresis (SDS-PAGE).

# 2.5 – SDS-PAGE

Sodium Dodecylsulphate-Polyacrylamide Gel Electrophoresis (SDS-PAGE) was used to assess the purity of protein samples. SDS-PAGE gels were cast freshly before use using a BIORAD mini-protean gel system (BIO-RAD Laboratories, USA). The gels utilised for this work were cast with a 12% (v/v acrylamide) resolving gel and a 4% (v/v) stacking gel prepared according to the following recipe for 10 mL of gel solution:

**Table 2.4 –** Recipes for manufacturing 10 mL of 4% (v/v) and 12% (v/v) acrylamide gels for SDS-PAGE.

| **Chemical** | **Volume Required (mL)** | |
|---|---|---|
| | **4%** | **12%** |
| Water | 6.3 | 4.3 |
| 40% (v/v) Acrylamide | 1 | 3 |
| 1.5M Tris pH8.8 | 2.5 | 2.5 |
| 10% (w/v) SDS | 0.1 | 0.1 |
| 10% (w/v) APS | 0.1 | 0.1 |
| Temed | 0.01 | 0.004 |

Cast gels were transferred to the gel tank and filled with a running buffer (250mM glycine, 25mM Tris, 0.1% (w/v) SDS, pH 8.3). Protein samples were then diluted 1:1 with loading dye (50mM Tris, 2% (w/v) SDS, 0.5% (w/v) Bromophenol Blue, 10% (v/v) Glycerol, 100mM dithiothreitol (DTT) [added just before use]) and applied to the wells. Sample volumes used in the wells were 5 µL for samples direct from the purification column, with concentrated samples added in different volumes (up to 20 µL). 5 µL of a size marker (NEB Colour Protein Standard Broad Range, New England Biolabs, USA) was also included in a separate lane. The gels were run at 150V until the loading dye had reached the bottom of the gel (≈ 45 min) before being stained for 1 h in a solution containing 50% (v/v) methanol, 10% (v/v) acetic acid, 2.5g/L coomassie brilliant blue. Gels were then de-stained (in 10% (v/v) methanol, 10% (v/v) acetic acid) until the gel matrix became colourless.

## 2.6 – Markwell Assay

Protein solutions were quantified using a Markwell assay as previously described (Markwell et al. 1978). Markwell reagents A (20g/L $Na_2CO_3$, 4g/L NaOH, 1.6g/L Sodium tartrate, 10g/L SDS) and B (4% (w/v) $CuSO_4.5H_2O$) were mixed in a 49:1 ratio to form reagent C. 1 mL of reagent C was then added to test tubes containing 0.25 mL of either diluted protein sample or bovine serum albumin (BSA) standards of known concentrations (diluted in distilled $H_2O$). Samples were vortexed and then left on the bench top for 60 min. 75 µL of a diluted Folin & Ciocalteu's phenol reagent (Sigma, USA) solution (1:1 in $dH_2O$) was then added and vortexed to mix before a 45 min incubation at room temperature. Samples were then inverted and the appearance of blue chromophore (Figure 2.1) was measured at 660 nm, with $dH_2O$ used as to blank the spectrophotometer (Cary 60 UV/Vis, Agilent Technologies, USA).

The absorbance of the BSA standards was plotted on a standard curve (Figure 2.2) which was used to convert the absorbance values for test samples into µg/mL concentrations by comparing to the linear regression fit for the standards. The concentration was then converted to molar concentrations using the protein's molecular mass and corrected for dilution. Unknown samples were measured in triplicate and the concentrations averaged to provide a measure of reproducibility, with BSA standards being single repeats which were performed alongside each assay sample set that was assessed.

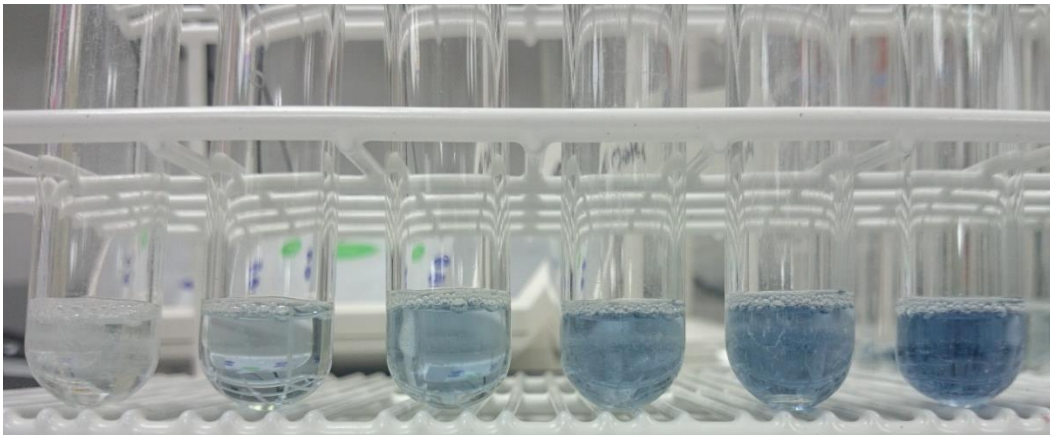

**Figure 2.1 –** Example of a set of BSA standards (0-250µg/mL left-right) used during each Markwell assay. A blue chromophore develops during the assay which was detected using UV/Vis spectroscopy at 660 nm, producing the standard curve shown in Figure 2.2.

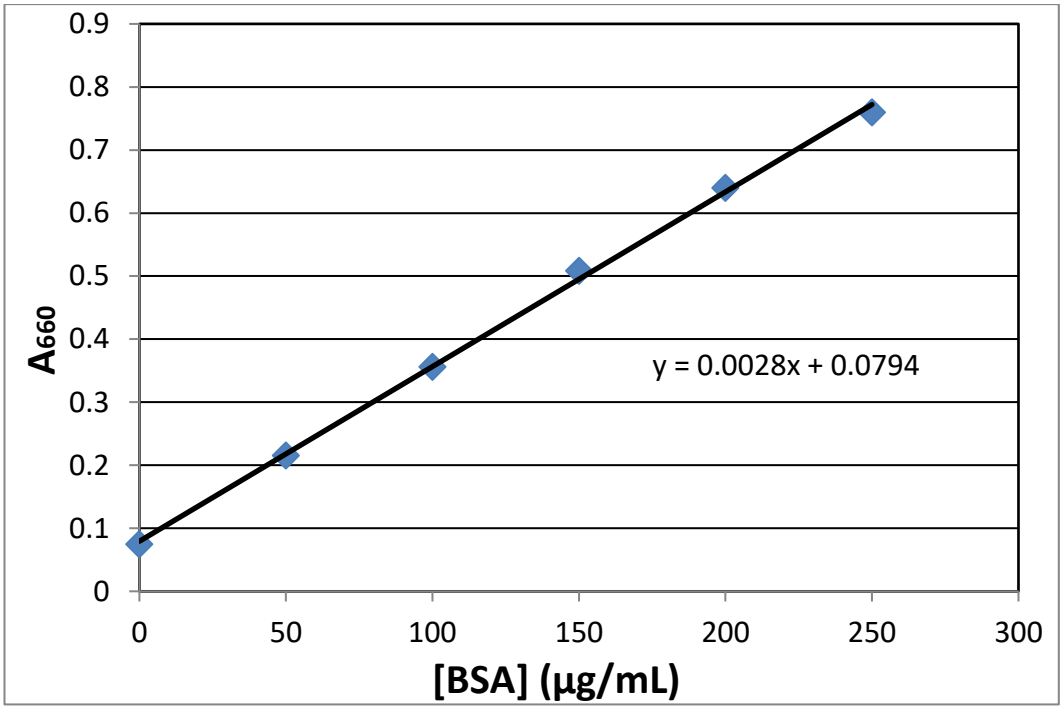


**Figure 2.2 –** Example of a BSA standard curve produced from a Markwell assay. Linear regression parameters (shown in the equation) were used to convert test sample absorbance values for this dataset by re-arranging the formula to find a value for the *x* variable using a known *y* value. Standard curves were produced for every individual Markwell assay dataset that was collected.

# 2.7 – Reducing porphyrins to porphyrinogens

Protoporphyrin IX and coproporphyrin III powders (Frontier Scientific, USA) were reduced to protoporphyrinogen IX and coproporphyrinogen III respectively using potassium hydroxide and sodium amalgam.

## 2.7.1 – Preparation of sodium amalgam

Sodium amalgam was produced under nitrogen from elemental sodium (Sigma) and mercury (Sigma). 1.17g of dried and scored sodium was added to 25g of mercury in a side-arm, round bottom flask under a constant stream of nitrogen and gently mixed until the metals reacted. A stainless steel spatula was quickly used to further mix the amalgam and prevent large chunks of amalgam from forming. The amalgam was then crushed using a mortar and pestle. The amount of amalgam produced was sufficient for reduction of one sample of porphyrin to porphyrinogen. Mercury was recovered by dissolving amalgam in 25% (v/v) acetic acid, followed by washing with large volumes of water to remove any impurities.

## 2.7.2 – Reduction of porphyrins

3 mg of porphyrin powder was solubilised in a few drops of ammonium hydroxide and then added to 3 mL of a solution containing 10 mM KOH and 20% (v/v) ethanol. A further 3 mL of 10 mM KOH solution was then added prior to being transferred to a conical flask covered with foil. The amalgam was the added to the flask, which was promptly stoppered and vigorously shaken to allow for reduction to occur, with the stopper gently released periodically allowing for gaseous release. The reaction was allowed to proceed until no gas could be detected leaving the flask.

Following the reaction, the mixture was transferred to a 10 mL syringe with a small amount of glass wool placed at the bottom to filter out the amalgam from the mixture. The solution was collected in a covered glass flask and adjusted to pH 8.0 with a 4 M MOPS solution that had been degassed with nitrogen to remove oxygen. The solution was then stored for 30 mins under nitrogen before use. Following use, the stock solution was left overnight open to oxygen to allow the porphyrinogen to fully oxidise for quantification (see Section 2.9). The solution was stored in the dark during this time to prevent light-induced breakdown of the porphyrin.

## 2.8 – HemY activity assays

HemY was assayed for activity with both protoporphyrinogen IX and coproporphyrinogen III using a continuous fluorimetric method, essentially as previously described (Shepherd & Dailey 2005). Reactions were performed in clear, flat bottomed 96-well plates with a total reaction volume of 100 µL comprising assay buffer (50mM $NaH_2PO_4$, 0.2% (v/v) Tween 20, pH 8.0), 0.5 µM HemY, 0 – 30 µL of porphyrinogen substrate, and $dH_2O$ to bring the reaction volume up to 100 µL.

The porphyrinogen substrate was added in low light levels just before placing the plate into a FLUOstar OPTIMA plate reader (BMG Labtech, Germany) to prevent auto oxidation as much as possible due to its sensitivity to light and oxygen. Reactions were performed with measurements every 30 seconds using an excitation wavelength of 520 nm and emission detected at 620 nm.

4 measurements were taken for each sample, with nonenzymatic auto-oxidation controls for each reaction condition also being recorded for subsequent background subtractions. HemY assays also containing other proteins (e.g. HemQ, horseradish peroxidase (HRP), catalase etc.) were performed using 1 µM of the second protein, unless otherwise stated.

# 2.9 – Spectroscopic quantification of tetrapyrroles

## 2.9.1 – Protoporphyrin IX and Coproporphyrin III

Protoporphyrin IX stock solutions were diluted and quantified in 2.7 M HCl spectrophotometrically using an extinction coefficient of $\varepsilon_{408}$ = 262 $mM^{-1}cm^{-1}$. (Smith 1975). Coproporphyrin III stock solutions were diluted in 0.1 M HCl and quantified spectrophotometrically using an extinction coefficient of $\varepsilon_{399.5}$ = 489 $mM^{-1}cm^{-1}$ (Smith 1975).

## 2.9.2 – Haem

Protohaem IX was quantified using a pyridine haemochrome assay. Protohaem IX solutions were prepared by solubilising haemin powder (Sigma) in dimethyl sulfoxide (DMSO, Fluka [*via* Sigma]) followed by dilution with $dH_2O$. Protohaem IX solutions were mixed in a 1:1 ratio with a solution containing 4.2 M pyridine (Sigma) and 0.4 M NaOH. The resultant solution was then pipetted into two cuvettes with one containing a few grains of sodium dithionite and the other containing a few grains of potassium ferricyanide, for reduction and oxidation of the samples, respectively. Absorption spectra were recorded between 500 nm and 600 nm, with the oxidised sample being used to blank the spectrophotometer so that a reduced-oxidised spectrum was obtained. The difference between the peak at 557nm and the trough at 541nm was used as the absorbance reading with an extinction coefficient of $\varepsilon_{557\text{-}541}$ = 20.7 $mM^{-1}cm^{-1}$ being used for quantitation (Smith 1975).

Coprohaem III stocks were made to a required concentration by re-suspending a known quantity of coprohaem III powder (Frontier Scientific) DMSO and diluting to the required stock concentration with $dH_2O$.

# 2.10 – Cloning of *S. aureus hemH*

## 2.10.1 – Amplification of *hemH* fragment

The *hemH* gene was amplified from *S. aureus* USA300 genomic DNA using the polymerase chain reaction (PCR) and DNA primers that contained restriction sites for NheI and HindIII (forward and reverse primers, respectively). Reactions contained 25 µL of 2x Q5 master mix (NEB), 300 nM of each primer (1.5 µL of 10 µM stocks), 0.5 µL *S. aureus* genomic DNA and 21.5 µL of MilliQ-$H_2O$. The following program was used in the thermal cycler:

**Table 2.5 –** PCR program used for amplifying *S. aureus hemH* from genomic DNA and plasmid preparations.

| **Step** | **Temperature (°C)** | **Time (s)** |
|---|---|---|
| Initial DNA denaturation | 95 | 120 |
| **40 cycles of:** | | |
| DNA denaturation | 95 | 30 |
| Primer annealing | 55 | 30 |
| DNA elongation | 72 | 60 |
| **Final stage and sample storage** | | |
| Final elongation | 72 | 300 |
| Sample storage | 4 | ∞ |

5 µL of the PCR reaction was then analysed on a 1% (w/v) agarose gel, produced using a tris/acetic acid/EDTA buffer (TAE) alongside a 1kb DNA marker (Promega, USA) to check the fragment size. PCR products were purified using a PCR purification kit (Qiagen, Germany) and analysed on a 1% (w/v) agarose TAE gel alongside a 1kb Hyperladder (Bioline, UK) for quantification. Once quantified, samples were stored at -20°C until use. Samples were digested with NheI and HindIII prior to ligation into the plasmid vector, procedures outlined in sections 2.10.2 and 2.10.3, respectively.

## 2.10.2 – Plasmid vector preparation and restriction digests

A pTrcHis plasmid containing *M. tuberculosis hemQ* in the NheI and HindIII restriction sites was recovered from a 10 mL overnight *E. coli* starter culture (strain MS117) using a Qiagen spin miniprep kit and was digested by NheI and HindIII. Conditions used for digests were (for a 10 µL digestion):

- 3 µL plasmid DNA sample
- 1 µL 10x NEBuffer 2 (1 mM DTT, pH 7.9 [NEB])
- 5 Units NheI (NEB) (0.5 µL volume)
- 5 Units HindIII (Promega) (0.5 µL volume)
- 5 µL sterile MilliQ-$H_2O$

Reactions were placed in a 37°C incubator for 3 hours

For whole miniprep sample digestion, reagents were scaled up, but using no more than 1 µL of each restriction enzyme, and left on the bench at room temperature overnight.

Following digestion of whole miniprep samples, the digested fragments were cleaned using a PCR purification kit (Qiagen) and run on a 1% (w/v) agarose TAE gel alongside a 1kb Hyperladder (Bioline) to quantify the amount of plasmid vector DNA present. Samples were stored at -20°C when not being used immediately.

## 2.10.3 – Ligation of the *S. aureus hemH* fragment

Ligation of the DNA fragment was adapted from usual protocols, where there would usually only be one type of vector and one fragment for insertion, due to potential chemical contamination of samples following agarose gel extraction of the DNA which inhibited the activity of the T4 DNA Ligase that was used. Two potential fragments, the original *M. tuberculosis hemQ* fragment and desired *S. aureus hemH* fragment, were present in the ligation, with the *hemH* fragment being in a higher quantity in an attempt to out-compete the original the *hemQ* fragment.
Conditions for the ligations were (for a 20 µL reaction):

- 2 µL 10x T4 ligation buffer (Roche)
- 1 Unit T4 Ligase (Roche, Switzerland) (1 µL volume)
- 50 ng plasmid vector DNA (roughly 3 µL)
- ≈ 100 ng fragment DNA (for a 10:1 fragment : vector ratio)
- nuclease free water to make up to 20 µL (if required)

Reactions were left on the bench top at room temperature overnight, and stored at -20°C if not immediately needed. Ligation mixtures were subsequently transformed into chemically competent *E. coli* cells as outlined in Section 2.11.

## 2.11 – Competent cells and transformation of plasmids

BL21 and TOP10 *E. coli* cells were made chemically competent to allow for transformation of plasmids from stocks or ligation mixtures into cells.

Cells were made chemically competent by taking a 10 mL overnight starter culture and centrifuging at 1789 x g, 4°C for 10 minutes. The resulting cell pellet was re-suspended in 7.5 mL of sterile 15% (v/v) glycerol and put on ice for 10 minutes, before being centrifuged (2795 x g, 4°C for 30 mins). The pellet was then gently re-suspended in 25 mL of a buffer containing 100 mM $MgCl_2$, 15% (v/v) glycerol and centrifuged again (2795 x g, 4°C, 30 mins). The pellet was finally gently re-suspended in 25 mL of a buffer containing 75mM $CaCl_2$, 6 mM $MgCl_2$, 15% (v/v) glycerol before being stored at -80°C in 100 µL aliquots.

For transformations, 100 µL of competent cells were incubated on ice with either 0.5 µL plasmid DNA or 1-2 µL of ligation product for 30 mins before heat shocking the cells at 42°C for 30 seconds. Following heat shock, 1 mL of LB media was added to the cells, followed by incubation with shaking at 37°C for 1 hour to allow the cells to recover. 100 µL of cells were then spread onto a fresh LB plate containing appropriate antibiotics and incubated at 37°C overnight. The remaining cells were then centrifuged (5,000 x g, 5 min) and re-suspended in 100 µL of fresh LB media, before being spread onto another LB plate and incubated at 37°C. Any colonies that formed were struck out onto fresh LB plates (with appropriate antibiotics) to further check for resistance before being grown in liquid media to an $OD_{600}$ of 1.5 and stored in a 1:1 ratio with sterile 50% (v/v) glycerol (final 25% (v/v)) at -80°C.

Colonies were screened for the pTrcHis-*S. aureus hemH* plasmid using colony PCR, where a bacterial colony was suspended in 50 µL of $dH_2O$ and 1 µL of this was added to the PCR mixture instead of a DNA template (as in section 2.10.1). This was performed using primers that anneal to the plasmid vector 100bp either side of the hemH insert, and the amplification of the *hemH* gene was detected using agarose gel electrophoresis. Positive colonies were further verified for the correct insert DNA sequence by Sanger sequencing (Beckman Coulter Genomics, UK), to ensure that

the protein produced would not contain any mutations. Plasmid DNA was extracted from 10 mL starter culture using a Qiagen spin miniprep kit and sent with a series of sequencing primers starting 100bp upstream of the 5' end of the *hemH* gene and spaced 200bp apart. A map of these primer locations is shown in Figure 2.3, with the sequences of these primers available in Appendix 1.

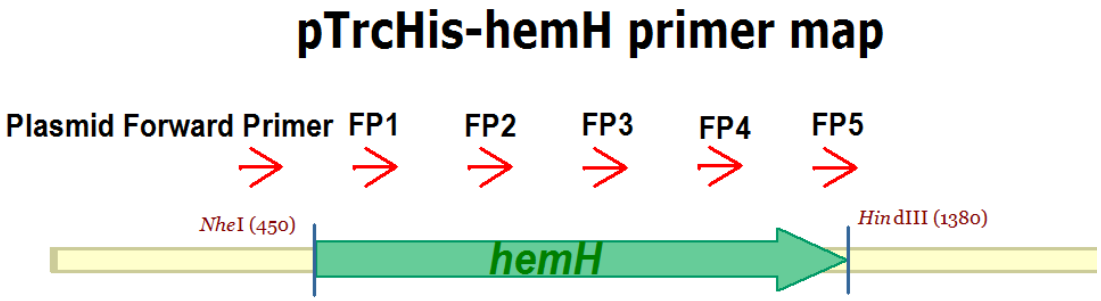


**Figure 2.3 –** Map of sequencing primer locations on the pTrcHis-*hemH* plasmid. Primers (red arrows) are spaced 200 bp apart covering the *hemH* gene.

## 2.12 – Enzymatic production of coproporphyrin III

Coproporphyrin III was synthesised from δ-aminolaevulinic acid (Sigma) using a series of haem synthesis proteins from different organisms (*M. thermautotrophicus* HemB, *B. megaterium* HemC + HemD, Human HemE and *S. aureus* HemY) recombinantly produced and purified from *E. coli*. The reaction, a 10 mL total volume, contained 50 µL of a HemB/HemC/HemD combined solution (giving a final concentration of 120 µg/mL in the reaction) as well as 1 µM of HemE and 1 µM of HemY. The reaction was performed in a buffer consisting of 50 mM Tris/HCl pH 8.0, 150 mM NaCl, 20% (v/v) glycerol, 5 mM DTT, 0.2% (v/v) Tween 20, and 1.5 mM 5-ALA (100 µL of a 150 mM stock). Reactions were incubated overnight at 37°C in a 30 mL glass bell jar covered with foil, with a magnetic stirrer gently mixing the reaction.

Synthesised coproporphyrin was then extracted into an equal volume of diethyl ether (10 mL) and shaken vigorously to allow for transfer of the porphyrin into the ether phase (Figure 2.4). The aqueous and ether phases were then allowed to settle before freezing the aqueous phase at -20°C and recovery of the ether phase into a 15 mL falcon tube. The ether solution was then transferred, in small amounts, to a microcentrifuge tube and placed in a fume hood in the dark to evaporate the ether to leave a precipitate of coproporphyrin III. The precipitate was re-suspended and quantified as described in sections 2.7.2 and 2.9.1. Solutions were stored at 4 °C until use.

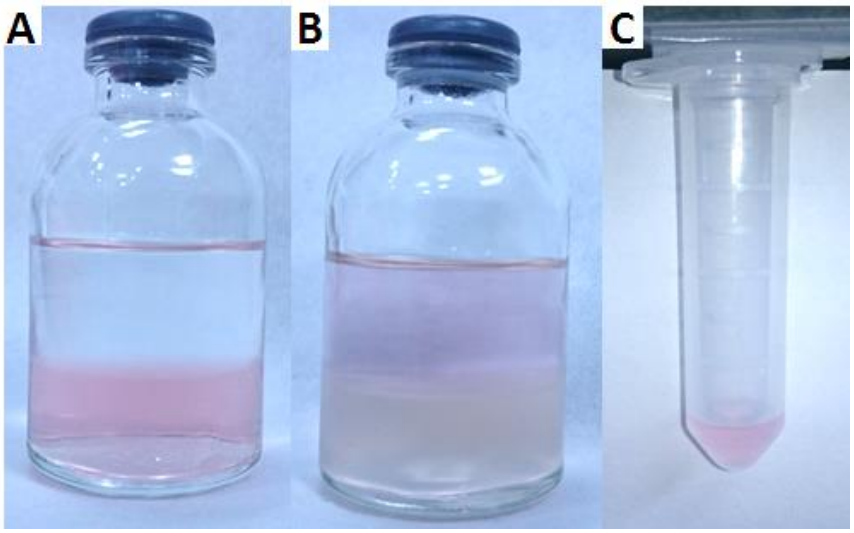


**Figure 2.4 –** Enzymatically synthesised coproporphyrin III before (A) and after (B) extraction into diethyl ether and (C) following solubilising in ammonium hydroxide.

## 2.13 – Ferrochelatase activity assays

HemH was assayed with a porphyrin substrate (either coproporphyrin III or protoporphyrin IX) and a divalent metal ($Fe^{2+}$, $Zn^{2+}$, $Co^{2+}$, $Cu^{2+}$ or $Ni^{2+}$) using a spectrophyotometric assay. Porphyrin solutions were quantified as described in section 2.9.1. Iron solutions, containing ascorbic acid to maintain the reduced state, were quantified spectroscopically using a small amount of ferrozine solution and an extinction co-efficient of $\varepsilon_{562}$ = 27.9 $mM^{-1}cm^{-1}$ (Berlett et al. 2001). Other metal solutions were diluted down from 0.1M stocks made from commercially available powders for ammonium nickel (II) sulphate (Sigma), cobalt (II) chloride (Aldrich, USA), copper (II) chloride (Aldrich) and zinc sulphate (Sigma).

HemH (50 nM) was assayed in a 1 mL cuvette in a ferrochelatase assay buffer (0.1M Tris-HCl pH 8.1, 0.5% (w/v) sodium cholate, 0.5% (v/v) Tween 20, 1mM β-mercaptoethanol) with up to 10 µL of concentrated metal solution and porphyrin solution (volume dependent on the concentration of stock solutions). Reactions were performed at 30°C in a Cary 60 UV/Vis spectrophotometer (Agilent Technologies) and were started by the addition of metal solution and inversion of the cuvette. Absorbance at 392 nm was recorded to monitor kinetic parameters for iron insertion into coproporphyrin III, looking at the change in absorbance at this wavelength using an extinction coefficient of $\Delta A_{392}$ = 115 $mM^{-1}cm^{-1}$ (Lobo et al. 2015) to determine the kinetics for this enzyme. Other metals and protoporphyrin IX were observed for insertion by taking a scan between 375 nm and 600 nm every 6 s. Samples to be analysed by High-Performance Liquid Chromatography (HPLC) were quenched to stop enzymatic activity by diluting 1 in 10 in a solution of 80% (v/v) acetone, 0.02% (v/v) Trifluoroacetic acid (TFA).

## 2.14 – High Performance Liquid Chromatography (HPLC)

HPLC analysis of porphyrins from HemH and HemQ activity assays were performed on an Agilent Technologies 1100 series HPLC system connected to a TELOS C-18 column. Buffers used for this process were A: 0.1% (v/v) TFA and B: Acetonitrile. The column was initially equilibrated in a combination of 80% buffer A and 20% buffer B, with the percentage increasing to 100% B using a linear gradient over 30 min following injection of the sample. The buffer levels remained at 100% B for 10 min before returning to 20% B to re-equilibrate the column. 5 µL of samples or 5 µL of a 5 µM porphyrin standard solution (containing one of: coproporphyrin III, coprohaem III, protoporphyrin IX or protohaem IX) were injected onto the column and porphyrin products were detected using absorbance spectroscopy at 400 nm.

A haem standard curve, for HemQ assays, was generated by analysing several haem concentrations from 0 – 5 µM and plotting the concentration against the peak magnitudes and can be seen in Appendix 4.

## 2.15 – HemQ activity assays

HemQ (50 nM) was assayed for activity with varying concentrations of coprohaem III and $H_2O_2$ in the same reaction buffer as was used for HemH reactions (0.1 M Tris-HCl pH 8.1, 0.5% (w/v) sodium cholate, 0.5% (v/v) Tween 20, 1 mM β-mercaptoethanol). Assays were performed in microcentrifuge tubes at 30°C and started by the addition of protein and mixing by inversion of the tube. 50 µL samples of the reaction were quenched in 450 µL of quenching solution (80% (v/v) acetone, 0.02% (v/v) TFA) at 5, 10 and 15 seconds before being analysed for haem formation by HPLC (section 2.14).

## 2.16 – Fluorescence quenching titrations for HemQ

Fluorescence titrations were performed using a Perkin-Elmer LS50B Luminescence spectrometer (Perkin-Elmer, USA) using 3 mL of 75 nM unloaded HemQ protein (diluted in protein storage buffer) in a 4 mL quartz fluorescence cuvette (Helma Analytics, Germany). Porphyrin and haem stocks were prepared and quantified as described in section 2.9, with protoporphyrin IX and coproporphyrin III stocks diluted (in protein storage buffer) to concentrations of 2.5 µM and 13 µM, respectively. The protein was scanned for fluorescence over a wavelength range of 310 – 400 nm with an excitation wavelength of 280 nm for an initial fluorescence reading. The protein solution was then titrated with small volumes of the ligand of interest (10 µL aliquots), followed by gentle mixing by pipetting. Fluorescence emission scans were recorded between successive additions of ligand. Ligand was added until there was no apparent change in fluorescence. The titration was then repeated using the same amounts of ligand from the same stocks and the fluorescent compound N-acetyl-tryptophanamide (NATA, Sigma) as a control reaction to account for inner filter effects resulting from absorbance of the tetrapyrrole ligands. The NATA was added until the fluorescence at 340 nm was equal to that of the original protein before adding the same quantities of ligand as before. The fluorescence intensities at 340 nm were obtained for both sets of titrations, and the corrected results were plotted using Sigmaplot 9 (Systat Software Inc., USA) for nonlinear regression analysis and estimation of binding constants.

# Chapter III

# Structure/function analyses of the HemY coproporphyrinogen oxidase

# Summary

Haem is synthesised via a series of tetrapyrrole intermediates including non-metallated porphyrins such as protoporphyrin IX, which is well-known to generate reactive oxygen species (ROS) in the presence of light and oxygen. *S. aureus* has an ancient haem biosynthetic pathway that proceeds via the formation of coproporphyrin III, a less reactive porphyrin. Herein, it is reported for the first time that HemY of *S. aureus* is able to generate both protoporphyrin IX and coproporphyrin III, and structural modelling confirms that the tetrapyrrole binding pocket is capable of binding both tetrapyrrole products. In addition, the terminal enzyme of this pathway, HemQ, is shown to stimulate the generation of protoporphyrin IX (but not coproporphyrin III). Assays with hydrogen peroxide, horseradish peroxidase, superoxide dismutase, and catalase confirm that this stimulatory effect is mediated by superoxide, suggesting Fenton chemistry as a likely route for the superoxide-mediated stimulation of protoporphyrinogen IX oxidase activity of HemY. This generation of toxic free radicals could explain why HemQ enzymes have not been identified in organisms that synthesise haem via the classical protoporphyrin IX pathway. This work has implications for the divergent evolution of haem biosynthesis in ancestral microorganisms.

# 3.1 – Introduction

The HemY protein is one of three proteins (along with HemG and HemJ) that can catalyse the penultimate reaction in haem synthesis: oxidation of protoporphyrinogen IX to protoporphyrin IX. These proteins are oxygen-dependent; requiring molecular oxygen to function as the terminal electron acceptor and are not present in organisms that encode the HemG protein, which use nitrate or fumarate as electron acceptors. HemY proteins appear to have different structures, being either membrane-associated or soluble, with the soluble structures being able to oxidise extra substrates (T. A. Dailey et al. 1994; Hansson et al. 1997). The membrane-associated form, found mainly in eukaryotic organisms such as Humans and *Nicotiana tabacum* and also in some Gram-negative bacteria such as *Myxococcus xanthus*, has been shown to follow the classical haem-synthesis pathway. The soluble form, found in Gram-positive bacteria, has been shown to be able to follow the classical pathway and oxidise protoporphyrinogen IX (Hansson & Hederstedt 1994; Dailey et al. 2010) as well as having the ability to oxidise coproporphyrinogen III and mesoporphyrinogen IX (T. A. Dailey et al. 1994). The discovery of the coproporphyrin-dependent pathway of haem synthesis (Dailey et al. 2015) has shown that the soluble HemY proteins utilise coproporphyrinogen III as its primary substrate instead of protoporphyrinogen IX, making this subset of proteins coproporphyrinogen oxidases instead of protoporphyrinogen oxidases. This pathway (Figure 3.1, blue route) has been reported to be more widely distributed and older than the classical protoporphyrin IX pathway (Figure 3.1, red route), pre-dating oxygenic photosynthesis (Dailey et al. 2015).

It has long been known that certain Gram-positives such as *S. aureus* accumulate coproporphyrin III and not protoporphyrin IX (Jacobs et al. 1971) . Interestingly the enzyme HemY from *Bacillus subtilis* has been shown to oxidise both coproporphyrinogen III and protoporphyrinogen IX (Hansson et al. 1997). Further studies reported that a haem-binding protein HemQ that is required for the terminal steps of haem synthesis in species of Actinobacteria and Firmicutes had peroxidase and catalase activity and could stimulate the oxidation of protoporphyrinogen IX by HemY (Dailey et al. 2010; Mayfield et al. 2013). *S. aureus hemQ* mutants were then shown to accumulate coproporphyrin III and the HemQ enzyme was reported to lyse

haem in the presence of peroxide/chlorite (Mayfield et al. 2013). Structural analyses then confirmed the HemQ family of proteins to be distinct from the original assignment to the family of chlorite dismutase enzymes (Celis & DuBois 2015), these differences defined by variations in conserved proximal/distal pocket residues (Hofbauer et al. 2016). However, an overlay of chlorite dismutase coordinates with the crystal structure of apo-HemQ from *Listeria monocytogenes* revealed the chlorite dismutase haem docks neatly in the HemQ active site cleft (Hofbauer et al. 2015). The true *in vivo* role for HemQ was revealed in 2015 when HemQ was confirmed to catalyse the decarboxylation of coprohaem for the noncanonical coproporphyrin-dependent pathway (Dailey et al. 2015; Lobo et al. 2015). Bona fide coproporphyrinogen oxidases were shown to be absent in Actinobacteria and Firmicutes explaining the lack of protoporphyrin IX in these organisms observed over four decades earlier (Jacobs et al. 1971). The lack of a functional coproporphyrinogen oxidase in *S. aureus* was then validated by report of a lack of activity for the purified HemN protein (Lobo et al. 2015), which appears to have been mis-annotated (Dailey et al. 2015). Finally, the HemQ reaction was later shown to proceed via an unusual peroxide-dependent reaction via a harderohaem III intermediate (Celis et al. 2015), and flavin mononucleotide (FMN) has also been shown to be an effective electron acceptor (Dailey et al. 2015).

The current study seeks to investigate mechanisms that have driven the evolution of the classical protoporphyrin IX-dependent pathway present in proteobacteria and eukaryotes. Since the HemQ component of the coproprophyrin pathway has been identified in evolutionarily early-branching (Acidobacteria and Planctomyces) and transitional (Deinococcus-Thermus group) diderm phyla (Dailey et al. 2015; Gupta 1998; Gupta 2011), it is highly likely that this pathway is an evolutionary precursor to the classical protoporphyrin IX pathway. However, the presence of non-functional HemN homologues in the vast majority of Firmicutes/Actinobacteria (Dailey et al. 2015), the identification of *hemF* genes in a small proportion of these families (Dailey et al. 2015), and demonstrations that Gram-positive HemY enzymes can oxidise both protoporphyrinogen IX and coproporphyrinogen III (Dailey et al. 2015; T. A. Dailey et al. 1994; Hansson & Hederstedt 1994), all suggest that ancestral species of Firmicutes/Actinobacteria may have once produced both coproporphyrin III and protoporphyrin IX intermediates. The reported lack of protoporphyrin IX in

Actinobacteria and Firmicutes (Jacobs et al. 1971) indicates that HemQ cannot convert coproporphyrin III to protoporphyrin IX, which is consistent with the requirement for a metallated porphyrin to participate in the peroxide-dependent HemQ mechanism (Celis et al. 2015).

Hence, one plausible route for the protoporphyrin-dependent pathway to have evolved is: i) the necessary appearance of HemN/HemF enzyme(s) that decarboxylate coproporphyrinogen III to protoporphyrinogen IX, ii) emergence of HemY variants that can oxidise both coproporphyrinogen III *and* protoporphyrinogen IX, iii) emergence of HemH ferrochelatases that can catalyse iron insertion into coproporphyrin III *and* protoporphyrin IX, and finally iv) loss of Fe-coproporphyrin III decarboxylases (HemQ/AhbD). Since there is a requirement for haem (or a significant growth advantage to synthesising it) in most organisms that have a functional haem biosynthetic pathway, it is plausible that the protoporphyrin- and coproporphyrin-dependent pathways co-existed before the protoporphyrin-dependent pathway came to predominate in proteobacteria and eukaryotes. Following this branching event, major clades have some interesting characteristics: HemQ/AhbD enzymes are largely absent from proteobacterial species that oxidise protoporphyrinogen via the classical pathway, and Firmicutes/Actinobacteria possess HemQ/AhbD enzymes yet do not oxidise protoporphyrinogen IX to protoporphyrin IX. This exclusive presence of a classical *or* a coproprophyrin-dependent haem pathway is particularly intriguing in light of demonstrations that HemQ stimulates protoporphyrinogen oxidation by *Propionibacterium acnes* HemY (Dailey et al. 2010). Since HemQ of *S. aureus* decarboxylates Fe-coproporphyrin III via a peroxide-dependent mechanism (Celis et al. 2015), it was hypothesised that that radical generation by HemQ has a greater impact upon protoporphyrinogen oxidation compared to coproporphyrinogen oxidation (Figure 3.1), resulting in the generation of reactive oxygen species that are toxic to the cell. It was therefore of interest to re-evaluate substrate specificity in *S. aureus* HemY and to examine how the likely co-existence of HemY and HemQ influenced flux through the protoporphyrin IX (classical) and coproporphyrin III pathways. Herein, we investigate this ancestral process in terms of how a combination of metalloporphyrin-bound HemQ and hydrogen peroxide influences the oxidation of porphyrinogen intermediates in both pathways (Figure 3.1).

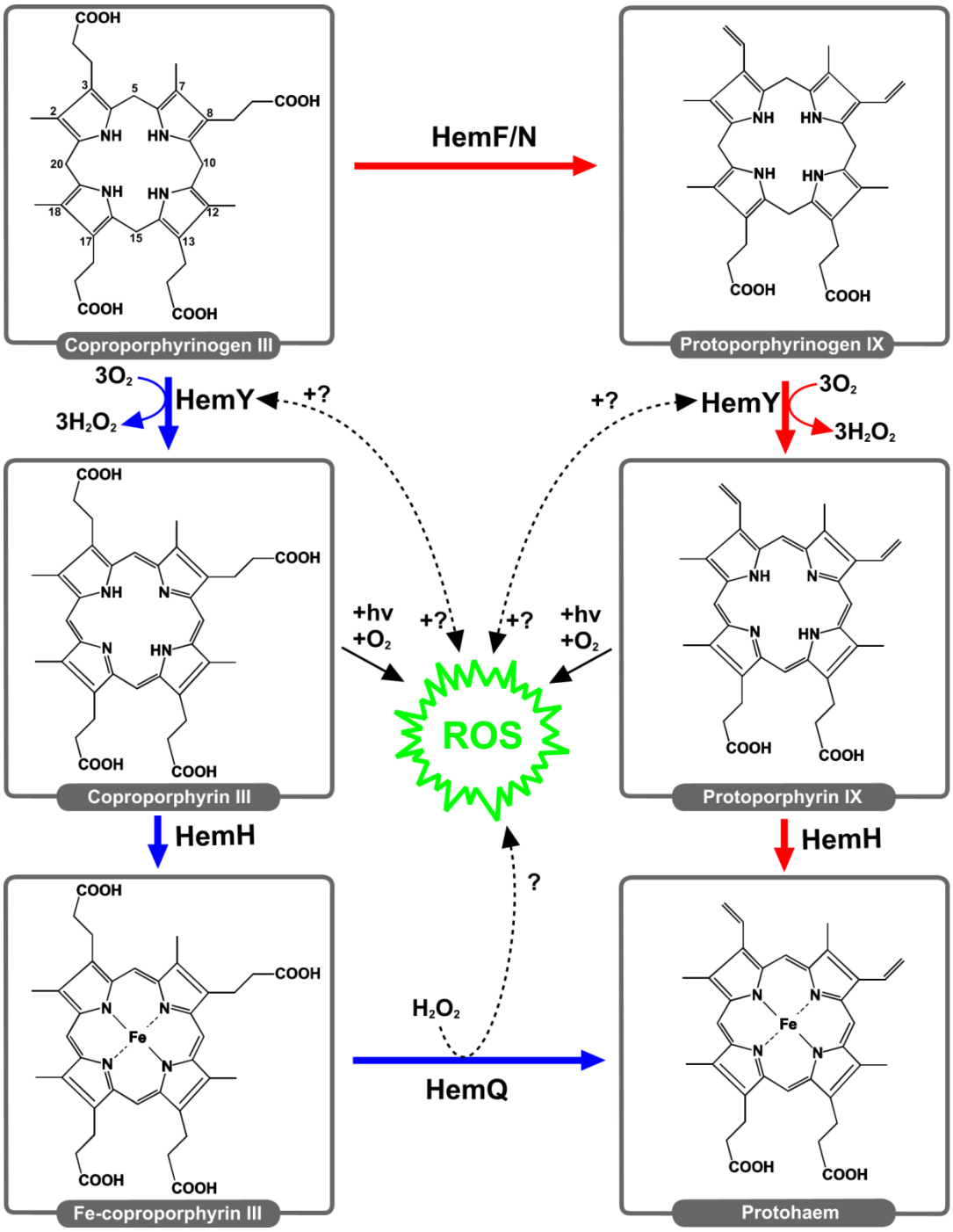


**Figure 3.1.** - The classical and coproporphyrin-dependent pathways of haem synthesis. This figure depicts haem synthesis in a hypothetical ancestral organism where the oxidation of coproporphyrinogen III to coproporphyrin III (blue) and the classical route involving a protoporphyrin IX intermediate (red) both take place. HemQ is hypothesised to generate reactive oxygen species (ROS), which in turn are hypothesised to impact upon protoporphyrinogen IX oxidation to a greater extent than coproporphyrinogen III.

### 3.1.1 - Spectroscopic and kinetic properties of HemY proteins

Spectral analysis of HemY proteins from other organisms highlights a few common characteristics of the purified protein. Besides the protein absorbance peak at roughly 280nm, absorption peaks at approximately 410nm have been reported for human HemY (Dailey & Dailey 1996) and *Saccharomyces cerevisiae* HemY (Poulson & Polglase 1975), and it has been proposed that these features result from bound protoporphyrin IX. Human HemY was also shown to have absorbance at 375nm and a broader absorbance peak at 450nm, a characteristic of oxidised FAD.

Kinetic data for HemY can vary greatly across different organisms and a selection of the published $K_m$ and $k_{cat}$ values can be found in Table 3.1. Various protoporphyrinogen oxidases have been shown to be inhibited by a variety of molecules, including diphenyl ethers such as acifluorfen, and the linear tetrapyrrole bilirubin (Ferreira & Dailey 1988; T. A. Dailey et al. 1994). Both of these are believed to be competitive inhibitors of protoporphyrinogen oxidases, with acifluorfen confirmed as an active site inhibitor via crystallisation studies with *B. subtilis* HemY (Qin et al. 2010).

Acifluorfen is not a planar molecule and is smaller than protoporphyrinogen IX, although was shown to occupy the active site cleft with part of the molecule in the tetrapyrrole-binding site adjacent to the FAD cofactor. It has been suggested that acifluorfen mimics half of a protoporphyrinogen IX molecule, as can be seen in Figure 3.2, with structural comparisons of the two molecules showing that the torsion angles at either oxygen in acifluorfen are comparable to the methylene bridges between pyrrole rings in protoporphyrinogen IX (Corradi et al. 2006). In addition, mouse HemY has been shown to be inhibited by haem breakdown products such as bilirubin, a linear tetrapyrrole that exhibits competitive inhibition patterns with respect to protoporphyrinogen IX, with a $K_I$ of 25 μM (Ferreira & Dailey 1988).

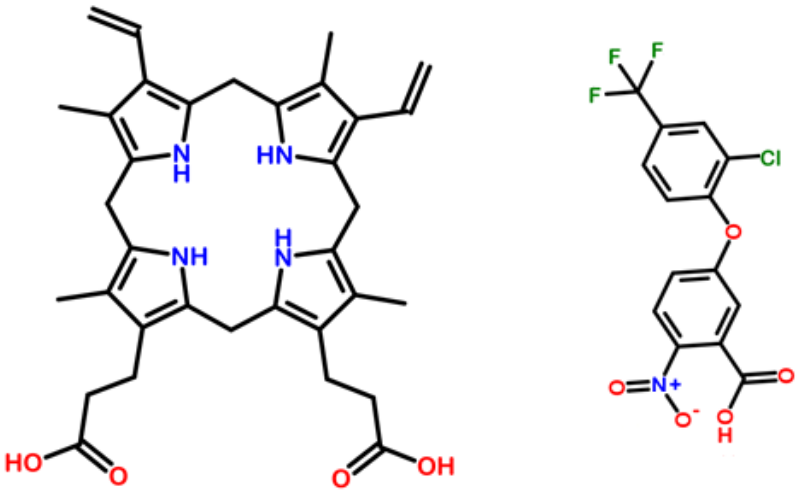


**Figure 3.2 –** Comparison of protoporphyrinogen IX (left) and its commonly used inhibitor Acifluorfen (right). Whilst the ring structures making up the individual sections of the molecule are different, the overall shape of the two molecules follow a similar pattern and presence of –COOH groups, allowing for acifluorfen to reside in the HemY active site.

It has previously been shown that haem-binding proteins can have an effect on the activity of HemY proteins from *Drosophila melanogaster* and *Propionibacterium acnes*, increasing the observed maximal rate (Shepherd & Dailey 2009; Dailey et al. 2010). According to studies performed using cytochrome *c*, stimulation of the protoporphyrinogen oxidase activity appears to require the hydrogen peroxide that is produced during the reaction. It has been hypothesised that this stimulation is due to radicals produced during peroxidase breakdown of hydrogen peroxide. It has been noted that the redox state of the iron in the bound haem becomes reduced during the reaction (Shepherd & Dailey 2009), a process that also happens during the breakdown of hydrogen peroxide by a peroxidase mechanism. Addition of superoxide dismutase to the assays appears to abolish the stimulatory effect, further supporting the theory of radical stimulation (Shepherd & Dailey 2009). Studies on the HemY from *P. acnes* utilised the haem-bound HemHQ as a stimulant to the reaction. These assays suggested that the presence of the haem-bound form of this protein can increase the maximal rate by a factor of over 6-fold (from 3.0 $min^{-1}$ to 19.8 $min^{-1}$), whilst the $K_m$ decreases by almost half (19µM to 10.1µM) (Dailey et al. 2010). Since cytochrome *c* and HemQ are found in the same subcellular compartments in eukaryotes (mitochondrial intermembrane space) and certain prokaryotes (cytoplasm), respectively, these observations have implications for the rate of HemY catalysis *in vivo*.

**Table 3.1 –** Kinetic data for previously characterised HemY proteins from various organisms.

| Organism | $K_m$ (μM) | $k_{cat}$ ($min^{-1}$) | Assay type | Substrate | Reference |
|---|---|---|---|---|---|
| Human | 1.7 | 10.5 | Discontinuous | P'gen IX | (Shepherd & Dailey 2005) |
| *Myxococcus xanthus* | 1.6 | 5.2 | Discontinuous | P'gen IX | (Shepherd & Dailey 2005) |
| *Aquifex aeolicus* | 2.8 | - | Discontinuous | P'gen IX | (Shepherd & Dailey 2005) |
| Human | 3.8 ± 0.3 | 5.7 ± 0.2 | Continuous | P'gen IX | (Shepherd & Dailey 2005) |
| *Myxococcus xanthus* | 3.6 ± 0.5 | 3.1 ± 0.2 | Continuous | P'gen IX | (Shepherd & Dailey 2005) |
| *Aquifex aeolicus* | 1.0 ± 0.1 | 0.4 ± 0.009 | Continuous | P'gen IX | (Shepherd & Dailey 2005) |
| *Saccharomyces* | 4.8 | - | Discontinuous | P'gen IX | (Poulson & Polglase 1975) |
| *Bacillus subtilis* | 1.0 ± 0.09 | 0.784 ± 0.011 | Continuous | P'gen IX | (Qin et al. 2010) |
| *Propionibacterium* | 19 | 3.0 | Continuous | P'gen IX | (Dailey et al. 2010) |
| *Bacillus subtilis* | 1.0 ± 0.15 | 0.19 ± 0.03 | Discontinuous | P'gen IX | (Corrigall et al. 1998) |
| *Bacillus subtilis* | 5.29 ± 0.36 | 0.05 ± 0.005 | Discontinuous | C'gen III | (Corrigall et al. 1998) |
| *Bacillus subtilis* | 4.92 ± 0.75 | 2.69 ± 0.6 | Discontinuous | Meso'gen IX | (Corrigall et al. 1998) |
| *Staphylococcus aureus* | 0.31 ± 0.01 | 1.33 ± 0.04 | Continuous | C'gen III | (Lobo et al. 2015) |
| Mouse | 6.5 | $450h^{-1}$($7.5min^{-1}$) | Discontinuous | P'gen IX | (Ferreira & Dailey 1988) |
| *Drosophila* | 3.8 ± 0.6 | 5.0 ± 0.3 | Continuous | P'gen IX | (Shepherd & Dailey 2009) |

## 3.1.2 – Crystal structures of HemY enzymes

Published crystal structures exist for HemY proteins from three different organisms: *Bacillus subtilis*, *Nicotiana tabacum* and *Myxococcus xanthus*. The structures for *N. tabacum* and *B. subtilis* were resolved to a resolution of 2.9 Å, with the structure for *M. xanthus* being resolved at 2.3 Å with acifluorfen bound and 2.7 Å with acifluorfen absent (Qin et al. 2010; Koch et al. 2004; Corradi et al. 2006). These structures possess a substrate binding domain, an FAD binding domain and a third domain that is associated with membrane binding in *N. tabacum* and *M. xanthus*. The latter domain is different in *B. subtilis* HemY, which is a soluble isoform. These modifications to the membrane binding domain consist mainly of a deletion of roughly 40% of the amino acids in this region, making it noticeably smaller and is thought to explain why the *B. subtilis* HemY enzyme is soluble (Qin et al. 2010).

The general secondary structure of each domain appears to be conserved across all three proteins. One domain is mostly made up of α-helices, and is referred to as the membrane binding domain (this domain is much smaller in *B. subtilis* HemY). The second domain is primarily made up of β-sheets and contains one α-helix; this domain has been shown to bind the inhibitors acifluorfen (Corradi et al. 2006; Qin et al. 2010) and 4-bromo-3-(50-carboxy-40-chloro-20-fluoro-phenyl)-1-methyl-5-trifluoromethyl-pyrazo (INH) (Koch et al. 2004) and is therefore regarded to be the substrate binding domain. Modelled structures for protoporphyrinogen IX and protoporphyrin IX (the substrate and product of the enzymes) have also been successfully docked into this domain in *N. tabacum*, which further supports the role for substrate binding (Koch et al. 2004). The final domain consists of a mixture of the two secondary structures and is shown in all three proteins to bind the FAD cofactor.

HemY from *N. tabacum* forms a loosely associated dimer structure, with the two monomers interacting at the membrane binding domain (Koch et al. 2004). The *M. xanthus* protein was proposed to also have a dimeric structure based on gel filtration data, although the crystal structure did not possess the interactions required to form a dimeric structure (Corradi et al. 2006). HemY from *B. subtilis* differs from these two membrane bound forms, as it exists as a monomer instead of a dimer (Qin et al. 2010). This may be due to the deletion in the membrane bound domain, as this is where the greatest interactions are found in the membrane bound isoforms.

The active site regions of the proteins exhibit subtle differences between the membrane-bound and soluble forms of HemY, as the inhibitor acifluorfen binds to different sites on the two proteins' forms. In *M. xanthus* HemY, the inhibitor binds deep into the active site cleft, with the 2-nitrobenzoic acid part of the molecule being held tightly in place by the residues: Arg-95, Phe-329 and Leu-332. The 2-chloro-4-trifluoromethylphenoxy part of the molecule resides in a larger space between residues Met-365 and Gly-167, and also sits at an angle of 45$^{o}$ relative to the active site plane and the FAD cofactor (Corradi et al. 2006). In contrast, HemY from *B. subtilis* (shown in Figure 3.3) has a set of amino acids at the analogous positions that have smaller sidechains (Ser-95, Thr-330 and Val-333). This appears to cause binding to a different region, with the 2-nitrobenzoic acid moiety sitting adjacent to the FAD cofactor (Qin et al. 2010). Binding in this region seems to weaken the affinity of the inhibitor, as it is a strong inhibitor of the membrane-bound HemY proteins and a weak inhibitor of the soluble HemY of *B. subtilis*.

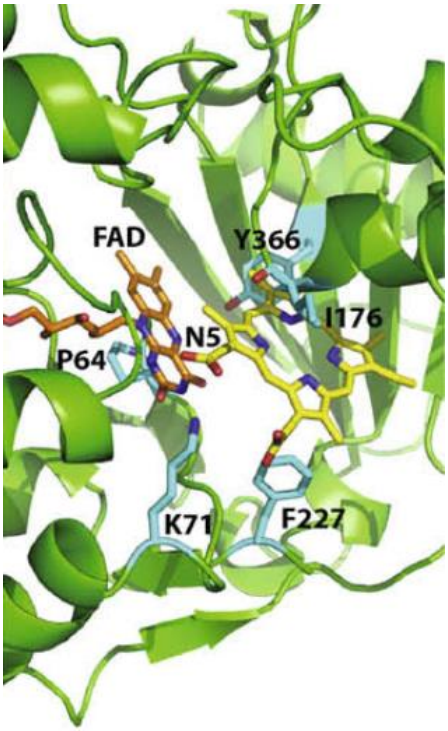


**Figure 3.3 –** A view of the *B. subtilis* HemY crystal structure active site with important residues visible (cyan). Protoporphyrin IX (yellow) has been modelled into the active site alongside the defined location of FAD (orange). Image originally published in the Journal of Structural Biology (Qin et al. 2010).

## 3.1.3 – Aims of the chapter

The initial research aim of this chapter was to investigate the HemY enzyme from *S. aureus*. Particular attention was made to these hypotheses:

- *S. aureus* HemY can oxidise both protoporphyrinogen IX and coproporphyrinogen III.
    - Determine kinetic parameters for these reactions.

- The presence of haem-loaded HemQ will stimulate the HemY-mediated oxidation of both substrates.
    - Stimulation will change the kinetic parameters of the reactions.

Once these points had been established, aims shifted to determine the mechanism of the HemQ-mediated stimulation of the HemY reaction, including the investigation of the hypotheses that:

- The presence of exogenous hydrogen peroxide will inhibit both reactions.

- Dedicated peroxidases/catalases will stimulate the HemY reaction.

- Superoxide dismutase will abolish the stimulatory effect of peroxidases/catalase,

# 3.2 – Results

## 3.2.1 – Analysis of the sequence and predicted structural model for *S. aureus* HemY

### 3.2.1.1 - Amino acid sequence comparisons

The HemY protein from *S. aureus* was subjected to a NCBI BLASTp search to check for amino acid sequence identity with other organisms. This enzyme was found to have a high sequence identity at the amino acid level to protoporphyrinogen oxidases from other *Staphylococcus* species (excluding *S. aureus*), with sequence identities in the 80%-95% range. However, it has a rather low sequence identity with protoporphyrinogen oxidases from other genera, with the closest match being *Macrococcus caseolyticus* at 61% followed by protoporphyrinogen oxidases from a variety of *Bacillus* species (including *B. subtilis*), which all range in the high 40% amino acid sequence identity range. Surprisingly, some organisms that are known to possess the coproporphyrin-dependent pathway (*P. acnes* and *M. tuberculosis*) have a very low sequence identity, with scores in the 20%-30% range. Output from the NCBI BLASTp search can be found in Table 3.2, whilst a multiple sequence alignment of these HemY enzymes is shown in Figure 3.4.

**Table 3.2 -** Results of a NCBI BLASTp search of HemY protein similarity from various organisms. All organisms have been confirmed to utilise the coproporphyrin-dependent pathway with the exception of *M. caseolyticus.* HemY protein amino acid sequences do not appear to be highly conserved throughout organisms that use this branch of the haem biosynthetic pathway.

| Organism | Protein | Max Score | Total Score | Query Cover (%) | E Value | Identity (%) | Accession Number |
|---|---|---|---|---|---|---|---|
| *S. aureus* (USA300) | PPO | 958 | 598 | 100 | 0 | 100 | EES92498.1 |
| *S. epidermidis* | PPO | 806 | 806 | 100 | 0 | 82 | WP_002476967.1 |
| *M. caseolyticus* | PPO | 584 | 584 | 99 | 0 | 61 | WP_041636144.1 |
| *B. subtilis* | PPO | 434 | 464 | 99 | 3.00x E-153 | 47 | WP_015483036.1 |
| *P. acnes* | PPO | 159 | 159 | 99 | 3.00x E-47 | 27 | EFD07069.1 |
| *M. tuberculosis* | PPO | 119 | 119 | 99 | 6.00x E-33 | 22 | WP_055357086.1 |

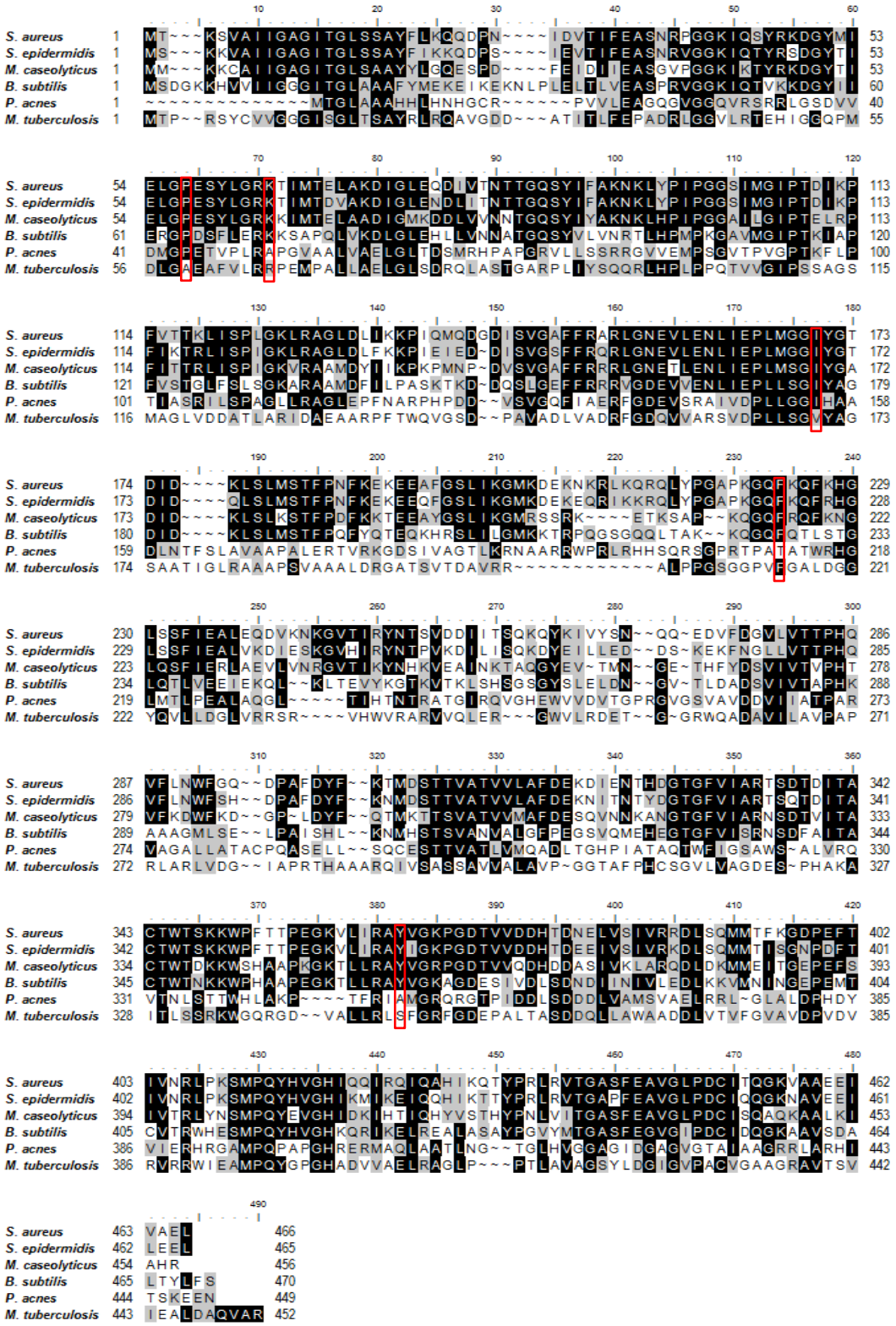


**Figure 3.4** – Multiple sequence alignment of HemY protoporphyrinogen oxidases from: *S. aureus*, *Staphylococcus epidermidis*, *Macrococcus caseolyticus*, *B. subtilis*, *P. acnes* and *M. tuberculosis*. Background colours represent sequence identity (black) similar amino acids (grey) and no identity (white). Residues highlighted in red are mentioned in more detail in subsequent modelling sections.

### 3.2.1.2 – Structural modelling of *S. aureus* HemY

A predicted structure of *S. aureus* HemY was obtained using the RaptorX structure prediction program, which uses the protein sequence to generate 3D models based on structural homology protein structures in the Protein Databank (PDB) (Peng & Xu 2011). The HemY protein from *B. subtilis* (PDBid = 3I6D (Qin et al. 2010)) was one of the top hits that the predicted structure was based on. The structural model was then analysed in CCP4MG (McNicholas et al. 2011), a molecular graphics program, which can be used to directly compare and superimpose proteins based on the similarity of their secondary structures. The predicted model of the *S. aureus* HemY was directly compared with the *B. subtilis* model, which contained the FAD cofactor and the inhibitor acifluorfen (Figure 3.5A). Superposition of the Cα atoms demonstrates very similar overall tertiary structures, with the exception of an extra set of helices in the *S. aureus* protein that is not present in the *B. subtilis* HemY (bottom left corner of panel A). Using the positions for the FAD and acifluorfen from *B. subtilis* with the superimposed *S. aureus* model (Figure 3.5B), it is possible to see that the *S. aureus* model can accommodate these molecules with minimal steric clashes, suggesting that these active site probes could bind to similar locations on the *S. aureus* enzyme.

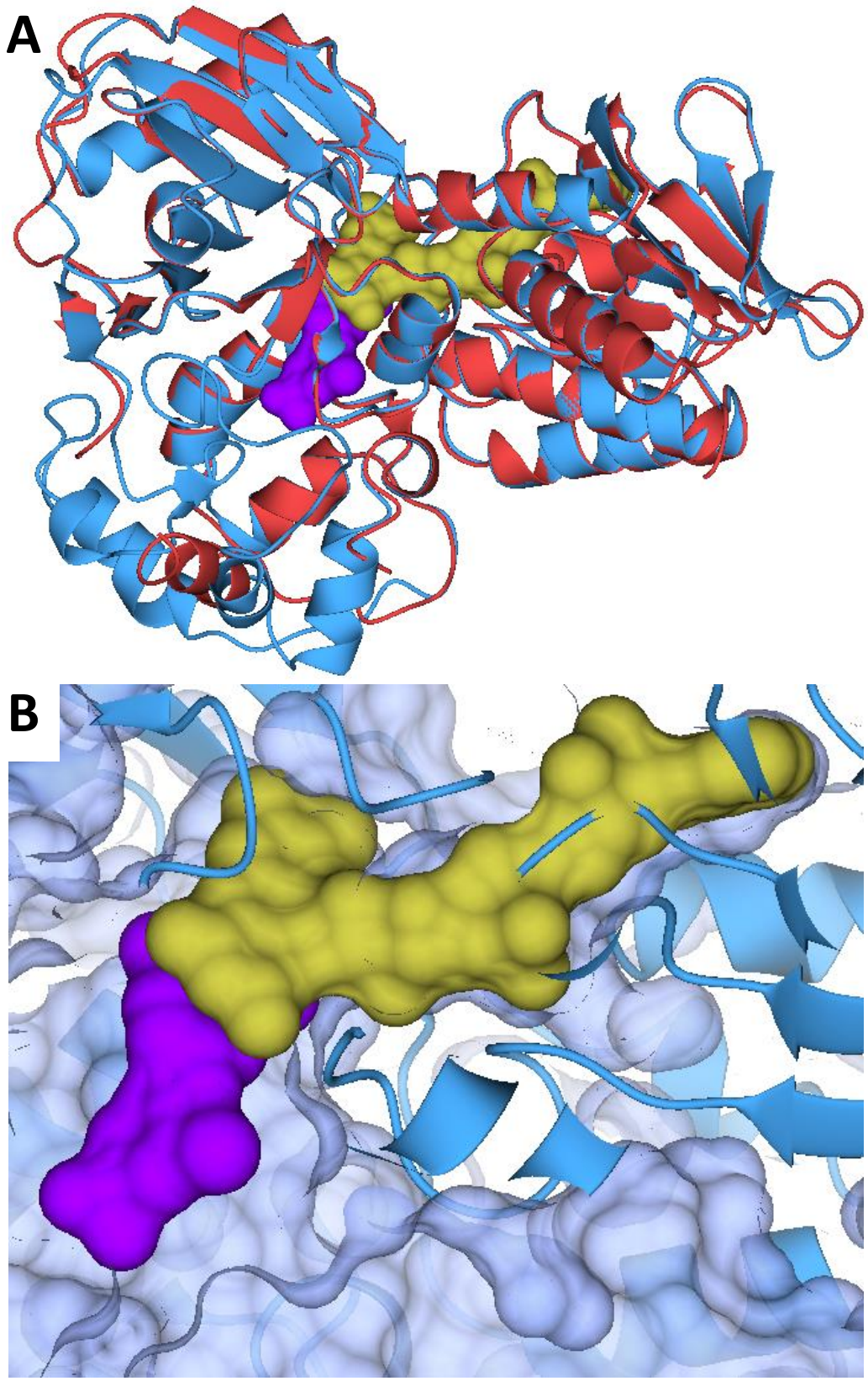


**Figure 3.5 –** Structural images of: **(A)** *B. subtilis* HemY, (PDBid = 3I6D (Red)), with bound FAD and acifluorfen (gold and purple respectively) superimposed with the *S. aureus* HemY structural model (Blue). **(B)** Close up surface representation of the *S. aureus* HemY FAD binding site with FAD (gold) and acifluorfen (purple) from *B. subtilis* HemY superimposed.

Work on the *B. subtilis* protein has shown that the binding site cavity appears to be much larger in this organism than other forms of HemY that have been crystalized, with a volume of 1,173Å$^3$ compared with 440Å$^3$ and 627Å$^3$ for *N. tabacum* and *M. xanthus* respectively. This cavity is also more positively charged in *B. subtilis* than in the other mentioned HemY proteins. Together these factors support the ability for coproporphyrinogen III, which has two extra negatively charged side chains and is a larger molecule compared to protoporphyrinogen IX, to bind in this area (Qin et al. 2010).

The acifluorfen molecule that was bound to the *B. subtilis* HemY was used as a template to superimpose both protoporphyrin IX and coproporphyrin III, products of the HemY reaction, into the active site of the predicted *S. aureus* HemY structure (Figure 3.6). The modelled porphyrins (of which only coproporphyrin III is shown) appear to fit into the site with very few steric clashes with the surfaces of the proteins or the FAD cofactor, which could be overcome in vivo due to the flexibility of both the protein and the porphyrin molecules. The negatively charged carboxylate groups on the coproporphyrin molecule appear to be positioned close to the blue regions of the electrostatic surface model of HemY, which are representing positively charged areas of the protein. This matches predictions by Qin et al. (2010) that the larger and more positively charged pocket allows for the binding of coproporphyrinogen III, which is held in place better by the increased positive charge on the surface.

To investigate whether *S. aureus* HemY has a tetrapyrrole-binding cleft that is well-suited to the oxidation of coproporphyrinogen III, the modelled acifluorfen in Figure 3.6 was overlaid with coproporphyrin III (Figure 3.6A). While there is only 48% sequence similarity in the primary sequence between the *S. aureus* and *B. subtilis* proteins, several residues that are important for catalysis in *B. subtilis* (including K71, P64, I176, F227 and Y366) are only conserved in their locations on the tertiary structure (Figure 3.6B), whilst being at sometimes vastly different locations on the amino acid chain. The conserved location of these residues appears to explain why these enzymes often lack sequence identity yet share a common function.

These amino acids interact with the substrate and FAD co-factor in different ways and many have a profound impact on the activity of the enzyme, with activity levels in mutant proteins ranging from slight decreases to almost a 100-fold decrease in activity when Y366 is mutated to a glutamine residue (Qin et al. 2010). K71 is believed to interact with the propionate side chains of the porphyrinogen molecule using charge-charge interactions. P64 is located behind (relative to the porphyrinogen substrate) and interacts with the FAD co-factor. I176, together with the FAD co-factor, aid in stabilising the "D" ring of the substrate, allowing it to be close enough to the accepting N5 atom of FAD for electron transfer to take place (Qin et al. 2010). Y366 and F227 are involved in stabilising the "A" and "C" rings respectively, with Y366 seemingly the most important residue for activity as mutations of this residue cause the greatest drops in activity levels (Qin et al. 2010).

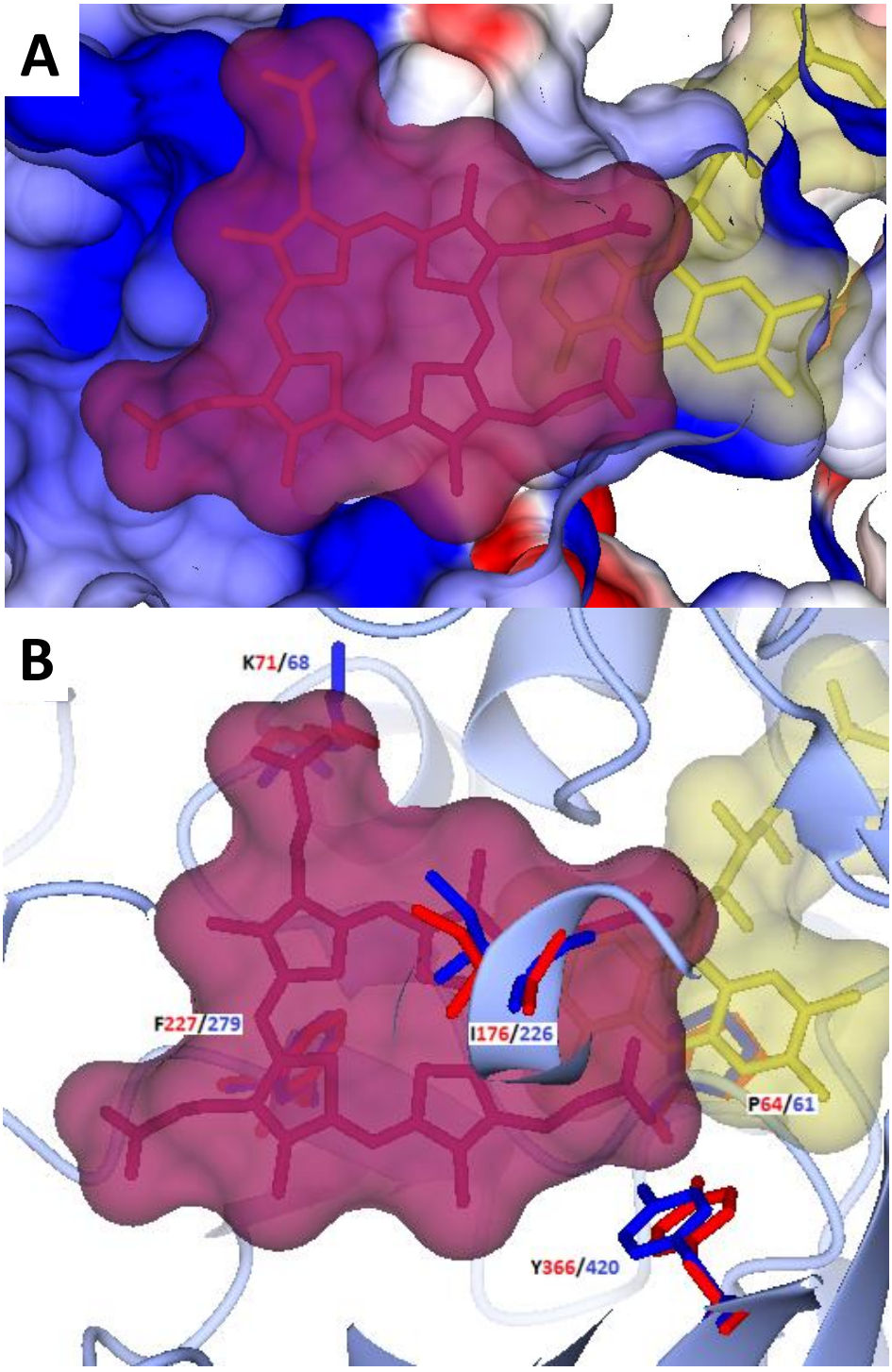


**Figure 3.6 –**Modelling of coproporphyrin III (purple) into the active site of the predicted *S. aureus* HemY model. Location of the porphyrin is based on the inhibitor acifluorfen from the *B. subtilis* crystal structure (with FAD present in gold). (A) Surface model of the protein, showing electrostatic potential (where blue = positive charge, red = negative and white = neutral for amino acids). Active site cavity gives no apparent steric inhibition to the presence of coproporphyrin III, with positive residues able to associate with –COOH side-chain groups (B) Comparative locations for proposed catalytic residues between *B. subtilis* (red) and *S. aureus* (blue). Amino acid location numbers are coloured to match organisms due to differing locations in the amino acid sequence.

## 3.2.2 – Biochemical analysis of purified HemY

### 3.2.2.1 – SDS-PAGE analysis of *S. aureus* HemY

*S. aureus* HemY was overexpressed in *E. coli* BL21 STAR cells and purified by affinity chromatography as described in Sections 2.3 and 2.4, with purity determined by SDS-PAGE as described in Section 2.5. Results from the resolved gels (example shown in Figure 3.7) show that a relatively pure protein that migrates at a rate corresponding to the predicted molecular mass of HemY (approximately 52 kDa) was present in the 15 mM imidazole wash or 300 mM imidazole elution fraction (sample analysed in Figure 3.7 only has protein in the 15 mM imidazole wash fraction).

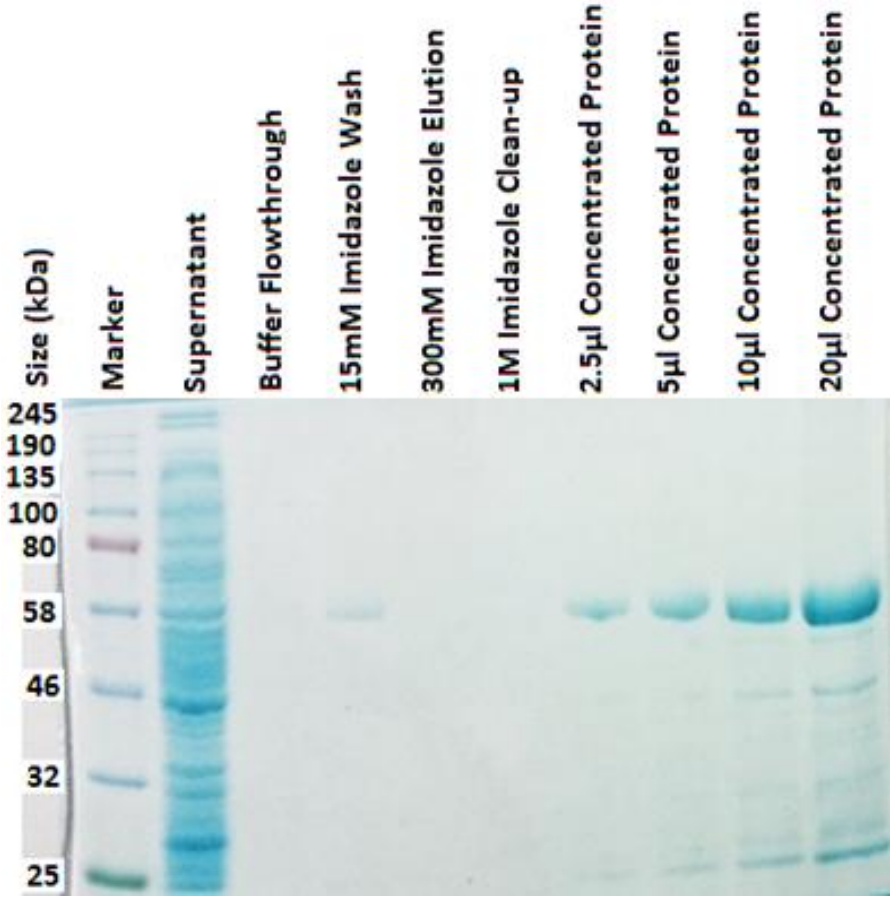


**Figure 3.7 –** SDS-PAGE analysis of the purification of *S. aureus* HemY. 5 µL of marker (NEB Colour Protein Standard, Broad Range) and 10 µL of labelled samples were used for the first six lanes. The final four lanes contained protein after spin concentration of the 15mM imidazole sample, and was added (left to right) in volumes of 2.5, 5, 10 and 20 µL.

### 3.2.2.2 – Spectroscopic analysis of purified HemY

Analysis of the purified *S. aureus* HemY via UV/Vis spectroscopy shows that the protein has porphyrin bound, with a sharp peak at 400 nm and two smaller peaks at 540 nm and 565 nm, typical of absorbance maxima for a porphyrin. There is also a broad absorbance feature from 450 nm – 520 nm, typical of an oxidised FAD cofactor. FAD has two characteristic peaks, one being a sharp peak at 375 nm and the other a broad peak around 450 nm. It is likely that the 375 nm peak of FAD is masked by the large porphyrin peak as a slight shoulder can be seen at 375 nm. These data strongly suggest that there is FAD bound to the protein, albeit at a sub-stoichiometric ratio. An example spectrum can be seen in Figure 3.8 below.

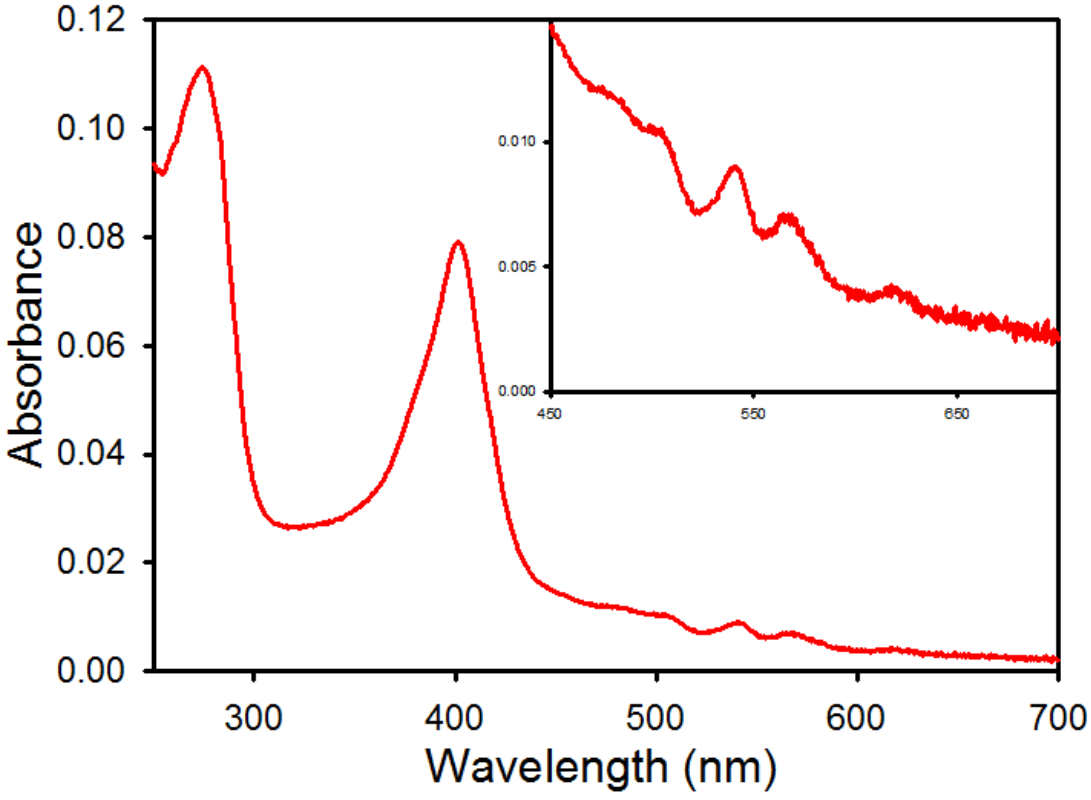


**Figure 3.8 –** Absorption spectrum of purified *S. aureus* HemY in its storage buffer (50mM Tris/MOPS pH 8.0, 100mM KCl, 0.2% (v/v) Tween 20). The inset shows a magnified view of the spectrum from 450nm to 700nm. A porphyrin peak can be seen at 400nm, with a slight shoulder at 375 nm indicating the presence of FAD.

## 3.2.3 – Optimisation and analysis of HemY assays

### 3.2.3.1 - Optimisation of the kinetic assay for protoporphyrinogen oxidase and coproporphyrinogen oxidase activities

HemY enzymes from *B. subtilis* (a Firmicute), *P. acnes,* and *M. tuberculosis* (both Actinobacteria) have previously been shown to catalyse the oxidation of both protoporphyrinogen IX and coproporphyrinogen III (Hansson et al. 1997; Dailey et al. 2010), supporting the hypothesis that the classical haem pathway evolved from the coproporphyrin-dependent route. Hence, it was hypothesized that HemY from *S. aureus* (a Firmicute) could oxidise both protoporphyrinogen IX and coproporphyrinogen III. To test this hypothesis it was necessary to optimise a continuous fluorescence assay to detect the fluorescent products protoporphyrin IX and coproporphyrin III. Neither protoporphyrinogen IX nor coproporphyrinogen III absorb light in the visible spectrum and appear colourless in solution; however protoporphyrin IX and coproporphyrin III do absorb light in the visible spectrum and are also fluorescent. Protoporphyrin IX has an absorbance maximum at 408 nm (Soret peak) with minor peaks at 558 nm and 600 nm plus minor spectral features between 600 nm and 700 nm (Smith 1975). When excited, this molecule emits light at 635 nm, and this property has been used during development of a continuous fluorescence assay for protoporphyrinogen oxidases (Shepherd & Dailey 2005).

Coproporphyrin III has a similar absorption spectrum to protoporphyrin IX (Figure 3.9), with the three peaks being shifted 10nm towards the UV end of the spectrum. Coproporphyrin III has an absorbance maximum at 399.5nm (Soret peak) with two minor peaks at 548 nm and 590 nm. There are also some minor spectral features between 600 nm and 700 nm, as previously observed (Smith 1975). Like protoporphyrin IX, coproporphyrin III is a fluorescent molecule with an emission wavelength in the same range as protoporphyrin IX (~620-635nm). The excitation wavelength has previously been reported to have a dramatic effect upon the auto-oxidation rate (Shepherd & Dailey 2005), presumably due to radical generation through photo-oxidation of porphyrin products. Hence it was necessary to optimise the optical parameters for this assay.

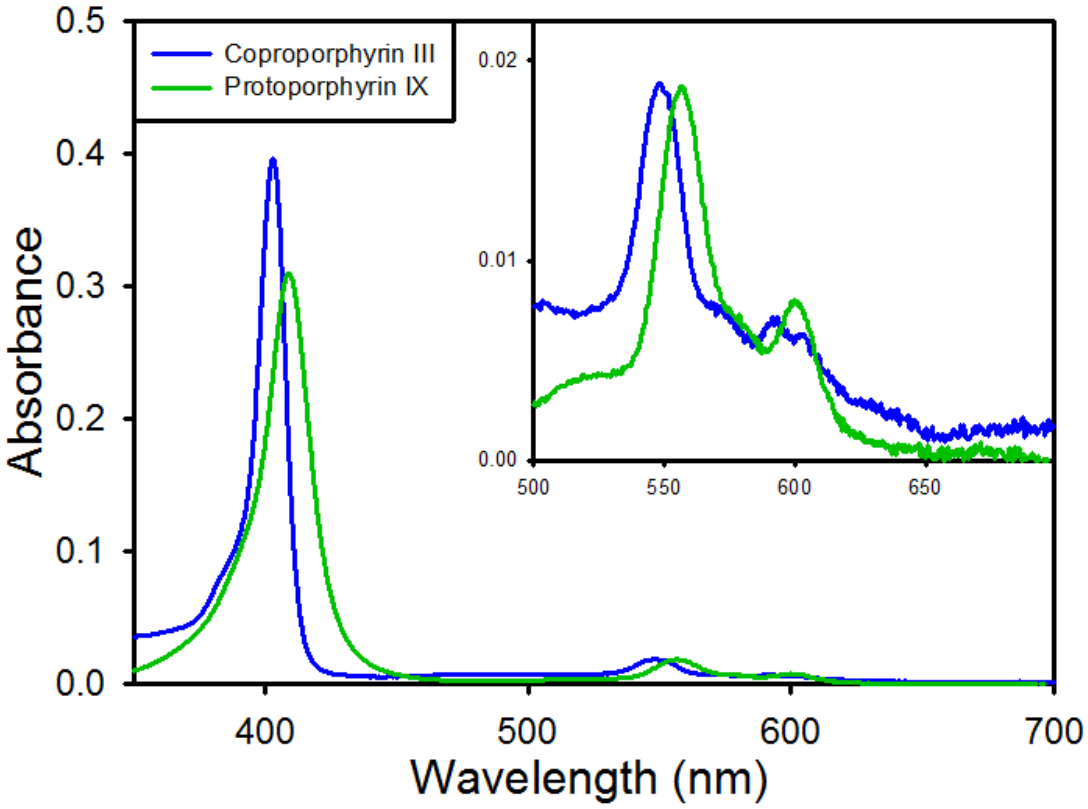


**Figure 3.9 –** Absorption spectra of protoporphyrin IX (green) and coproporphyrin III (blue). Inset shows a magnified view of the spectrum between 500 nm and 700 nm where smaller absorption peaks are located.

Optimisation of the HemY kinetic assay mainly involved minimising the rate of auto-oxidation. Of all of the excitation filters available in the plate reader used for the assays, only two were compatible with the absorption properties of protoporphyrin IX and coproporphyrin III: 400 nm and 520 nm band pass filters. Initial experiments were performed using protoporphyrinogen IX and the 400 nm filter, which produced variable levels of data quality, with a high and variable background oxidation rate detected. Trials testing the effect of using a 520 nm filter, as opposed to a 400 nm showed that the background oxidation rate was much lower with the 520 nm filter when comparable porphyrinogen concentrations were used (1.15µM and 1.5µM for the 400 and 520 nm filters respectively), as shown in Figure 3.10. The amount of protoporphyrin IX that is produced per minute when the 520 nm filter is used is 80% less than the amount produced when the 400 nm filter was used (1.19 µmol/min produced compared with 5.75 µmol/min). The datasets obtained using the 520 nm filter were less scattered, showing that the substrate was less prone to auto-oxidation using this filter, leading to cleaner sets of results.

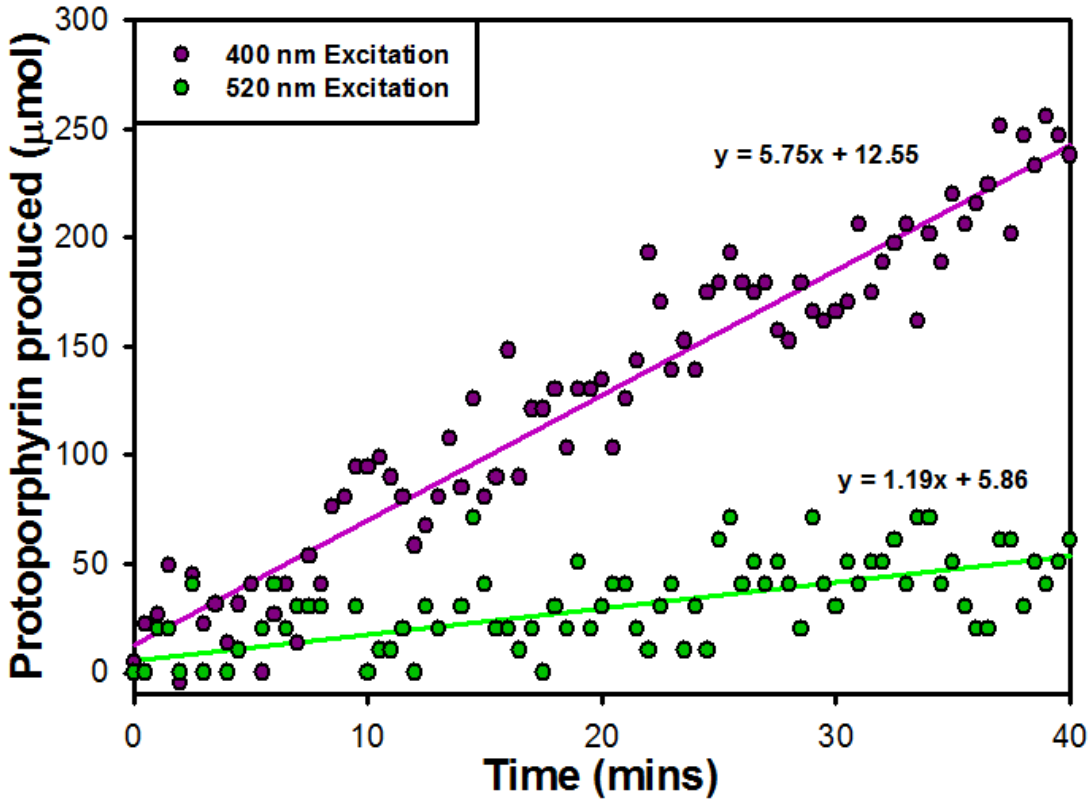


**Figure 3.10** – Comparison of auto-oxidation rates of protoporphyrinogen IX when excited using either a 400 nm or 520 nm wavelength (purple and green respectively). A 5-fold higher auto-oxidation rate can be observed when the 400 nm filter was used when compared with the 520 nm filter. Equations represent the parameters for the linear regression lines plotted.

Based on the above comparison, the 520 nm filter was chosen to be used as the excitation filter used throughout the HemY activity assays as it would reduce the energy of the excitation light, and to diminish the amount of light absorbed by the photolabile porphyrins, therefore making the substrate more stable in the assays. This had the effect of not only slowing the auto-oxidation (compared to the 400 nm filter), but also diminishing the fluorescence signal. The lower signal was compensated for by adjusting the signal gain on the plate reader and was therefore determined to be an acceptable consequence of using the 520 nm filter. A 620 nm band pass filter was placed at the emission side for detection of fluorescence from protoporphyrin IX and coproporphyrin III.

### 3.2.3.2 Kinetic analysis of *S. aureus* HemY

Purified recombinant HemY from *S. aureus* was assayed as described in Section 2.8 for oxidase activity with protoporphyrinogen IX and coproporphyrinogen III as substrates. Figure 3.11 shows typical traces from these assays alongside their respective auto-oxidation controls and corrected data with a linear regression over the first 5 minutes of the reaction. This raw data shows that *S. aureus* HemY does oxidise both substrates, as the change in magnitude for the HemY reaction data (in red) is greater than that of the auto-oxidation reaction data (shown in grey). These results had three additional repeats done using the same stocks of protein and substrate and performed in the same 96-well plate, giving a total of four results for the same concentration of substrate.

A total of seven different substrate concentrations were measured at the same time to provide data to determine $K_m$ and $k_{cat}$ values using the Michaelis-Menten equation. Coproporphyrinogen oxidase assays had better signal:noise compared with protoporphyrinogen oxidase assays, and the auto-oxidation levels were generally higher for protoporphyrinogen compared to coproporphyrinogen.

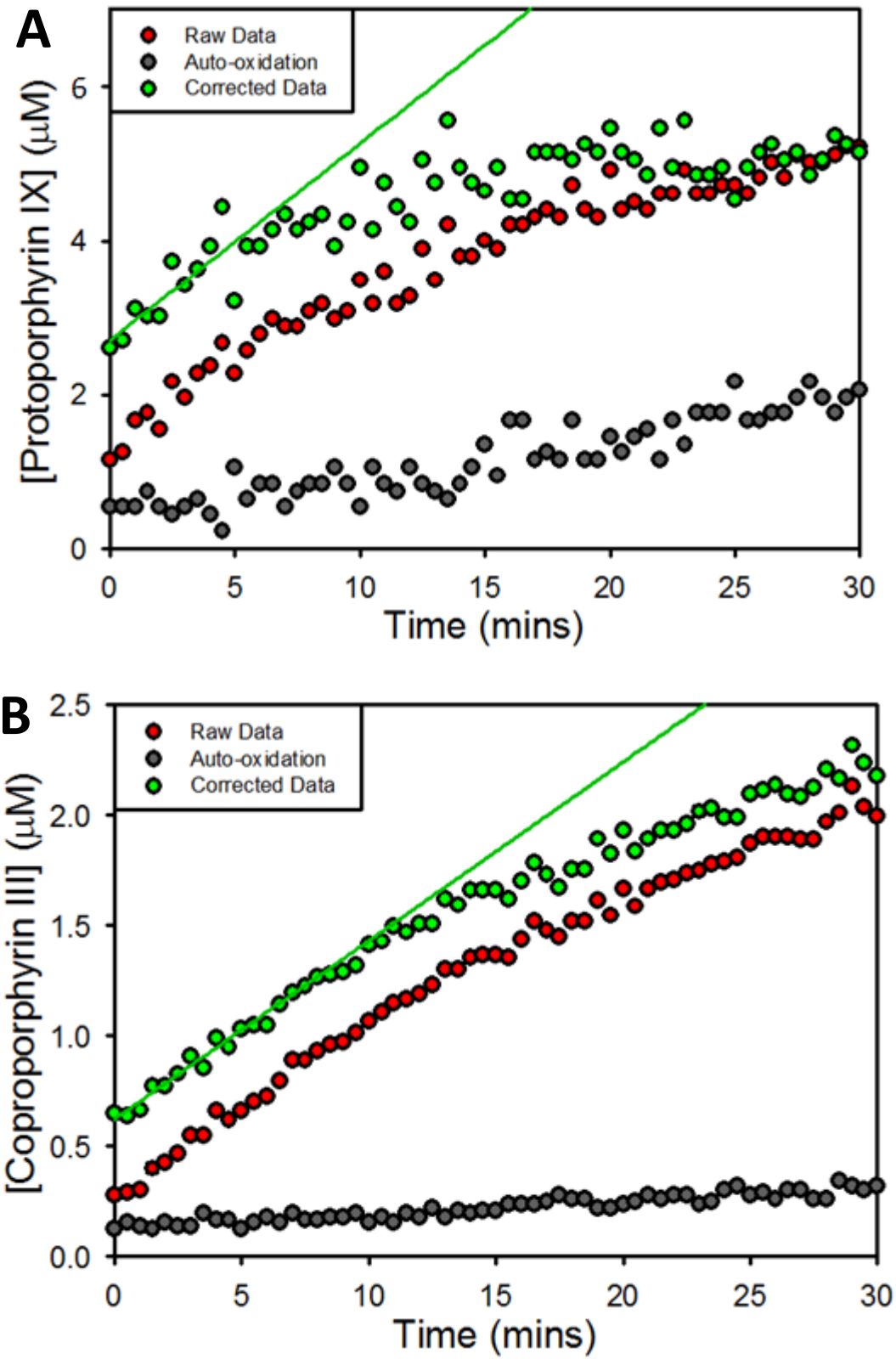


**Figure 3.11 –** Oxidase activities of purified *S. aureus* HemY. Assays using protoporphyrinogen IX **(A)** and coproporphyrinogen III **(B)** substrates are shown as raw unprocessed HemY data (red) with auto-oxidation controls (grey), and background subtracted data (corrected) with linear regressions of the maximal reaction rates (green).

## 3.2.4 – Kinetic analysis of *S. aureus* HemY

### 3.2.4.1 – *S. aureus* HemY exhibits similar maximal rates for the oxidation of protoporphyrinogen IX and coproporphyrinogen III

Kinetic analyses revealed $k_{cat}$ values of 0.44 ± 0.03 and 0.46 ± 0.02 $min^{-1}$ for protoporphyrinogen IX and coproporphyrinogen III, respectively (Figure 3.12). The $K_m$ for coproporphyrinogen III was determined to be 6.7 ± 0.8 µM, whereas the $K_m$ for protoporphyrinogen IX is likely to be lower than this, based on Lineweaver-Burke plots (Figure 3.14), but could not be accurately determined due to detection constraints at low substrate concentrations.

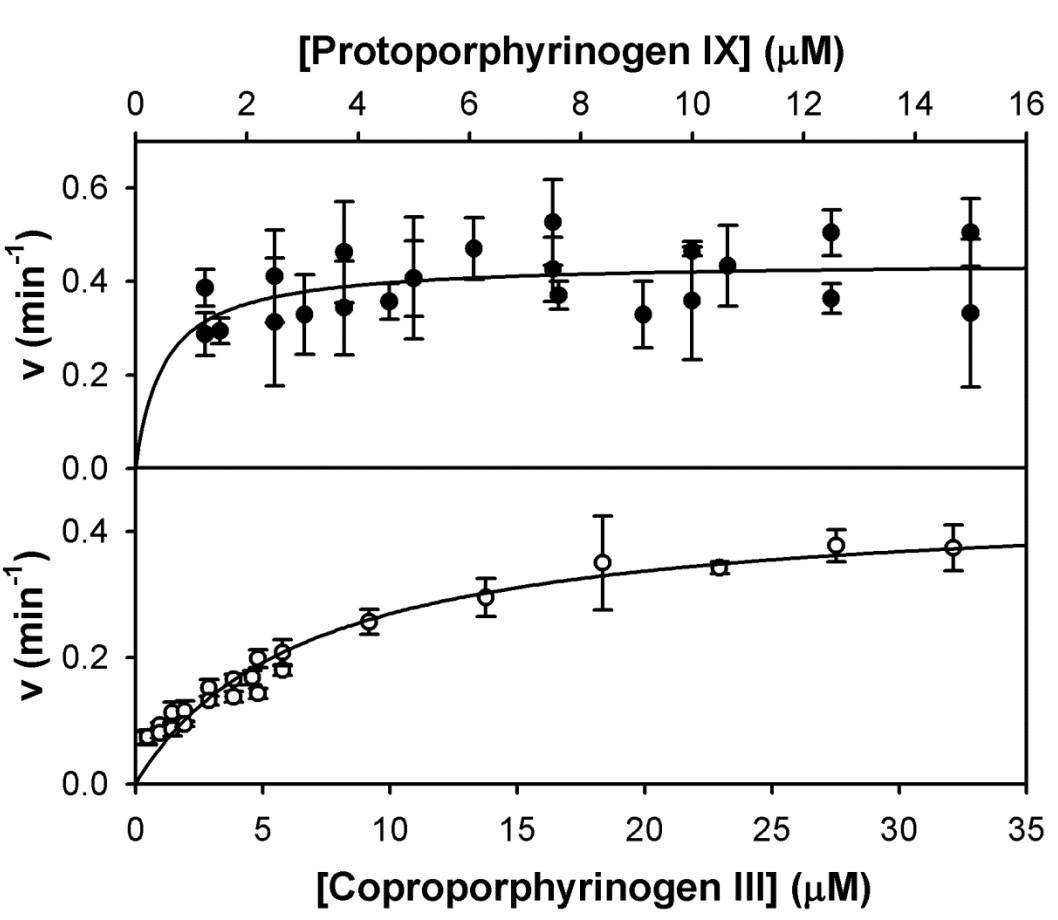


**Figure 3.12 -** Kinetic analysis of the HemY protoporphyrinogen oxidase utilising protoporphyrinogen IX and coproporphyrinogen III substrates. Nonlinear regression analysis reveals $k_{cat}$ values of 0.44 ± 0.03 and 0.46 ± 0.02 $min^{-1}$ for protoporphyrinogen IX and coproporphyrinogen III, respectively. The $K_m$ for coproporphyrinogen III is 6.7 ± 0.8 µM.

### 3.2.4.2 - Haem-bound HemQ stimulates HemY-mediated oxidation of protoporphyrinogen but not coproporphyrinogen III

A major focus of this study was to investigate why the classical pathway and coproprophyrin-dependent pathways have not yet been shown to co-exist. One hypothesis was that haem-bound HemQ produces toxic free radicals in the presence of protoporphyrin IX and peroxide, whereas the less reactive coproporphyrin III product will not support this radical generation. There has been a precedent for this, as the generation of superoxide by cytochrome *c* has previously been shown to stimulate the oxidation of protoporphyrinogen IX by an eukaryotic HemY enzyme (Shepherd & Dailey 2009). We therefore aimed to test the hypothesis that any stimulation of HemY-catalysed protoporphyrinogen oxidation by haem-loaded HemQ, as observed previously for *P. acnes* HemY/HemQ (Dailey et al. 2010), could only be observed when protoporphyrin IX is a reaction product (and not coproporphyrin III) and HemQ is specifically binding its haem product. This data has demonstrated that the presence of haem-loaded HemQ increased the $k_{cat}$ for protoporphyrinogen oxidation by 2.6-fold (Figures 3.13/3.14), whereas the same experiment when coproporphyrinogen III was used as a substrate yielded no significant increase in activity in the presence of HemQ. To support the hypothesis that peroxidase type chemistry of HemQ was contributing to this rate stimulation, HemY was assayed in the presence of HemQ that was loaded with bound haem, protoporphyrin IX, and coproporphyrin III (Figure 3.15). These data demonstrate that only haem-bound HemQ stimulates the HemY reaction, suggesting the involvement of peroxidase-like chemistry in this rate stimulation.

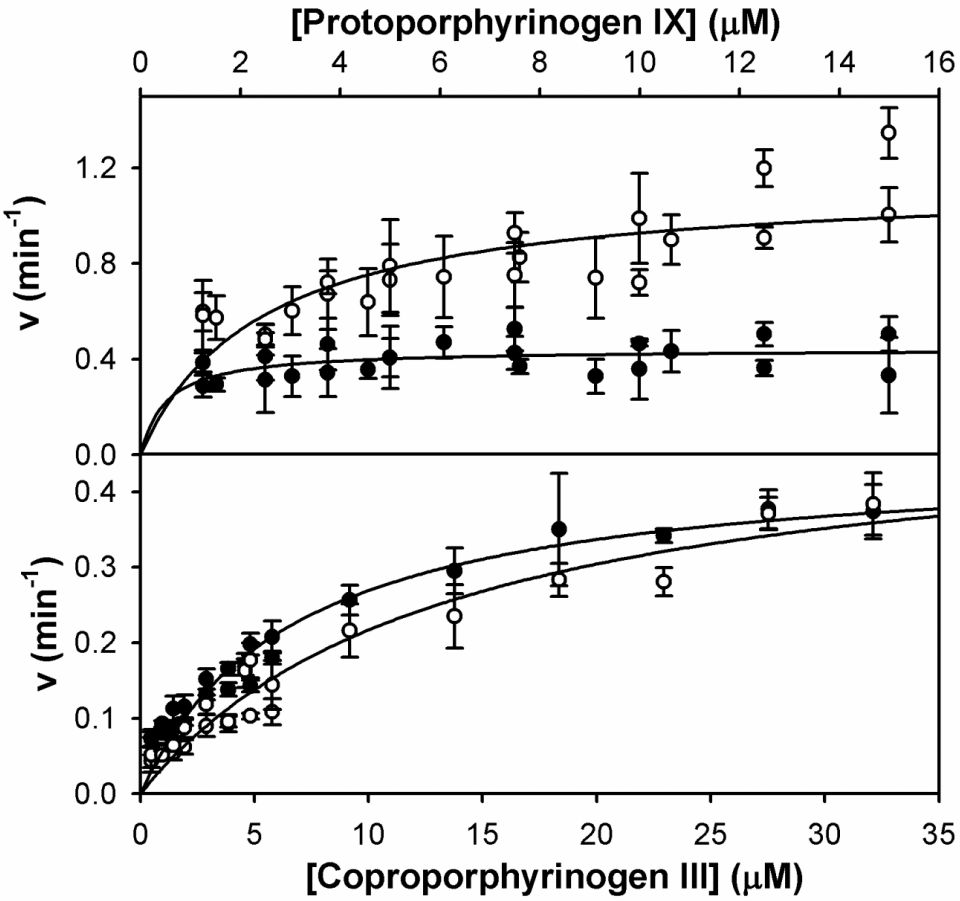


**Figure 3.13 –** Haem-loaded HemQ stimulates HemY-mediated oxidation of protoporphyrinogen but not coproporphyrinogen III. Steady state kinetics showing the effect of 1μM haem-loaded HemQ (white) on the activity of HemY using protoporphyrinogen IX and coproporphyrinogen III substrates compared to HemY only controls (black). Nonlinear regression analysis reveals HemQ-mediated 2.6-fold increase in $k_{cat}$ when protoporphyrinogen IX is used as a substrate, and a HemQ-mediated 1.1-fold increase in $k_{cat}$ when coproporphyrinogen III is used as a substrate.

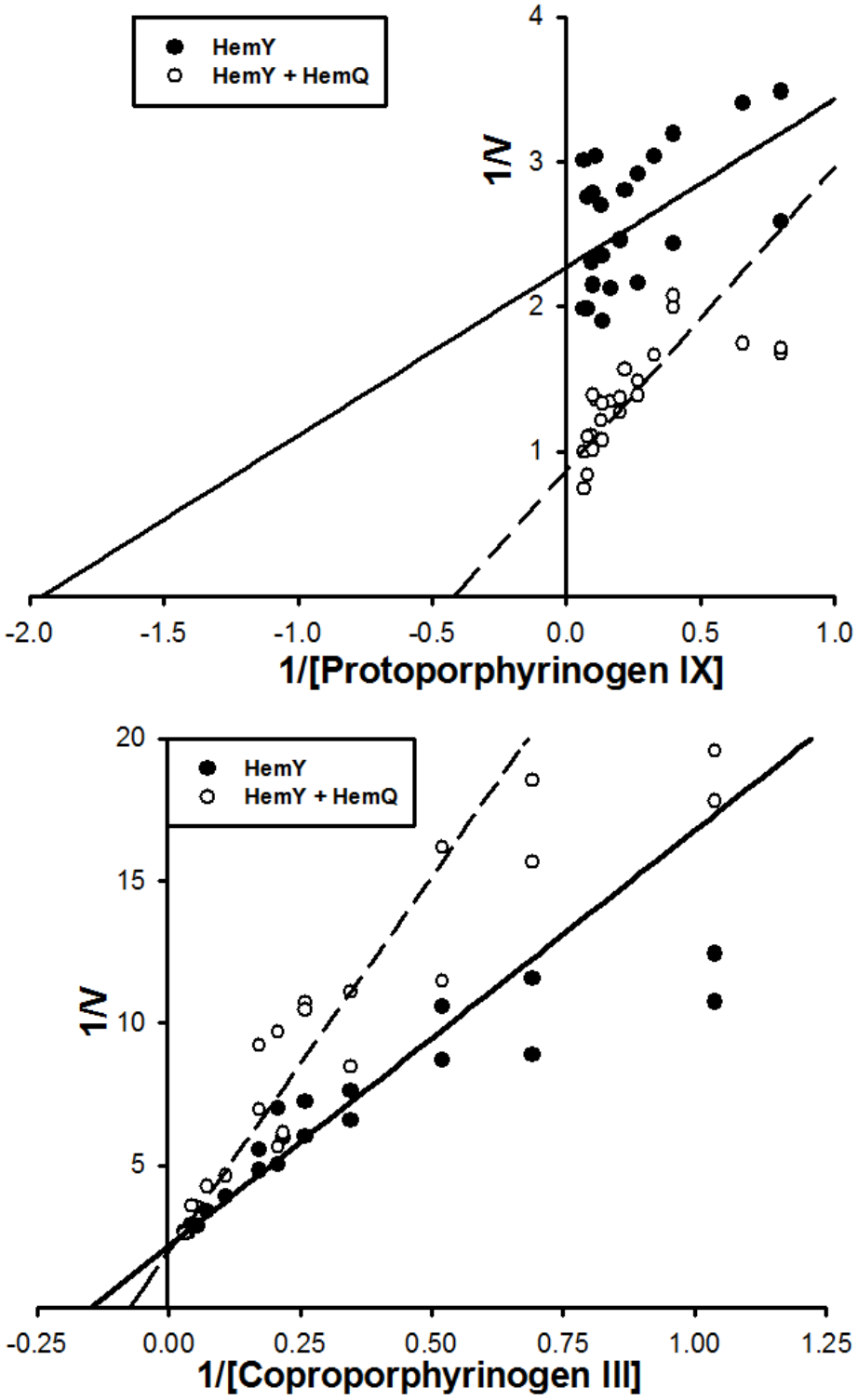


**Figure 3.14** – Lineweaver-Burke plots of HemY activity data. Top plot shows data for protoporphyrinogen IX assays, with the bottom plot showing data for coproporphyrinogen III assays coproporphyrinogen III both in the presence (white) or absence (black) of haem-loaded HemQ. Plots show a big difference in kinetic parameters for protoporphyrinogen IX oxidation in the presence of HemQ, whilst only a change in $K_m$ can be observed for coproporphyrinogen III oxidation.

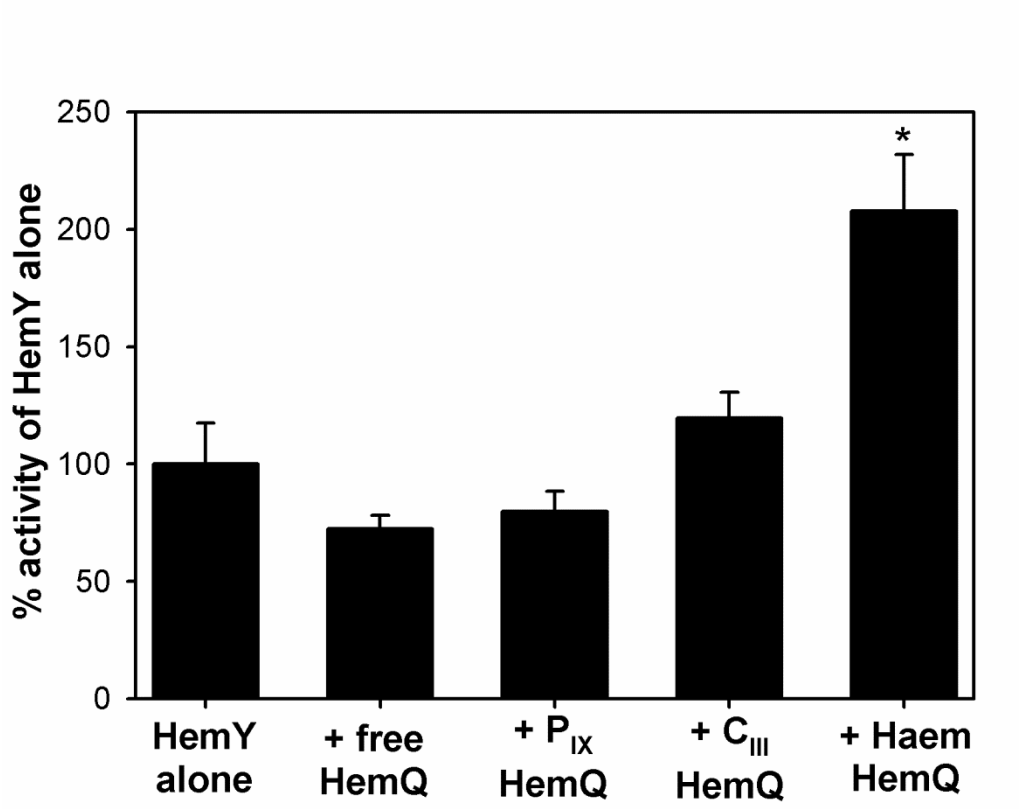


**Figure 3.15 –** HemQ must bind haem for stimulation of protoporphyrinogen oxidase activity. Protoporphyrinogen oxidase activity of HemY was assayed in the presence of HemQ (1 μM) and protoporphyrinogen IX (10 μM) with different tetrapyrroles bound. Error bars represent SD values based on four repeats. (Student's t-test, *P<0.05).

### 3.2.4.3 – Hydrogen peroxide participates in the HemQ-mediated stimulation of protoporphyrinogen IX oxidation via the generation of superoxide

It was hypothesised that hydrogen peroxide produced during HemY catalysis was participating in the HemQ-mediated rate stimulation. To confirm the involvement of hydrogen peroxide, HemY-catalysed protoporphyrinogen IX oxidation was assayed in the presence and absence of haem-loaded HemQ at various concentrations of peroxide (Fig. 3.16). In the absence of HemQ, peroxide elicited a gradual decrease in activity, whereas in the presence of HemQ the peroxide caused a significant stimulation of protoporphyrinogen IX oxidation. The same experiment was performed with coproporphyrinogen III as a substrate, and peroxide did not elicit any changes in HemY catalysis in the presence or absence of HemQ (Figure 3.16). Background rates for these reactions (Figure 3.17) were also measured to assess the effect of extra $H_2O_2$ on the substrates. These show an increased level of auto-oxidation of for protoporphyrinogen IX compared with coproporphyrinogen III, but also showed that extra $H_2O_2$ increased the amount of non-enzymatic protoporphyrinogen IX oxidation but not coproporphyrinogen. Background rates measured with HemQ present displayed an increase in the amount of porphyrin formed for both substrates, compared to rates without HemQ present, with a larger increase consistently seen for protoporphyrinogen IX.

To test the hypothesis that peroxidase chemistry was involved in the HemQ-mediated stimulation of HemY, protoporphyrinogen IX oxidation was measured in the presence of horseradish peroxidase (HRP, Figure 3.18), which demonstrated the same pattern of rate stimulation as haem-loaded HemQ (i.e. only when protoporphyrinogen IX was used as a substrate). To confirm that superoxide generation was involved in the HemQ-mediated stimulation of HemY, protoporphyrinogen IX oxidation was measured in the presence of superoxide dismutase (SOD) (Figure 3.18), which completely abrogated the stimulatory effect of HRP. Since exogenous peroxide caused some inhibition of HemY in the absence of HemQ (Figure 3.16), it was necessary to verify that the HRP stimulatory affect was not due to *removal* of peroxide. The presence of catalase in HemY assays did not elicit a stimulatory effect (Figure 3.18), confirming that peroxide removal was not responsible for the stimulation of HemY-catalysed protoporphyrinogen IX oxidation.

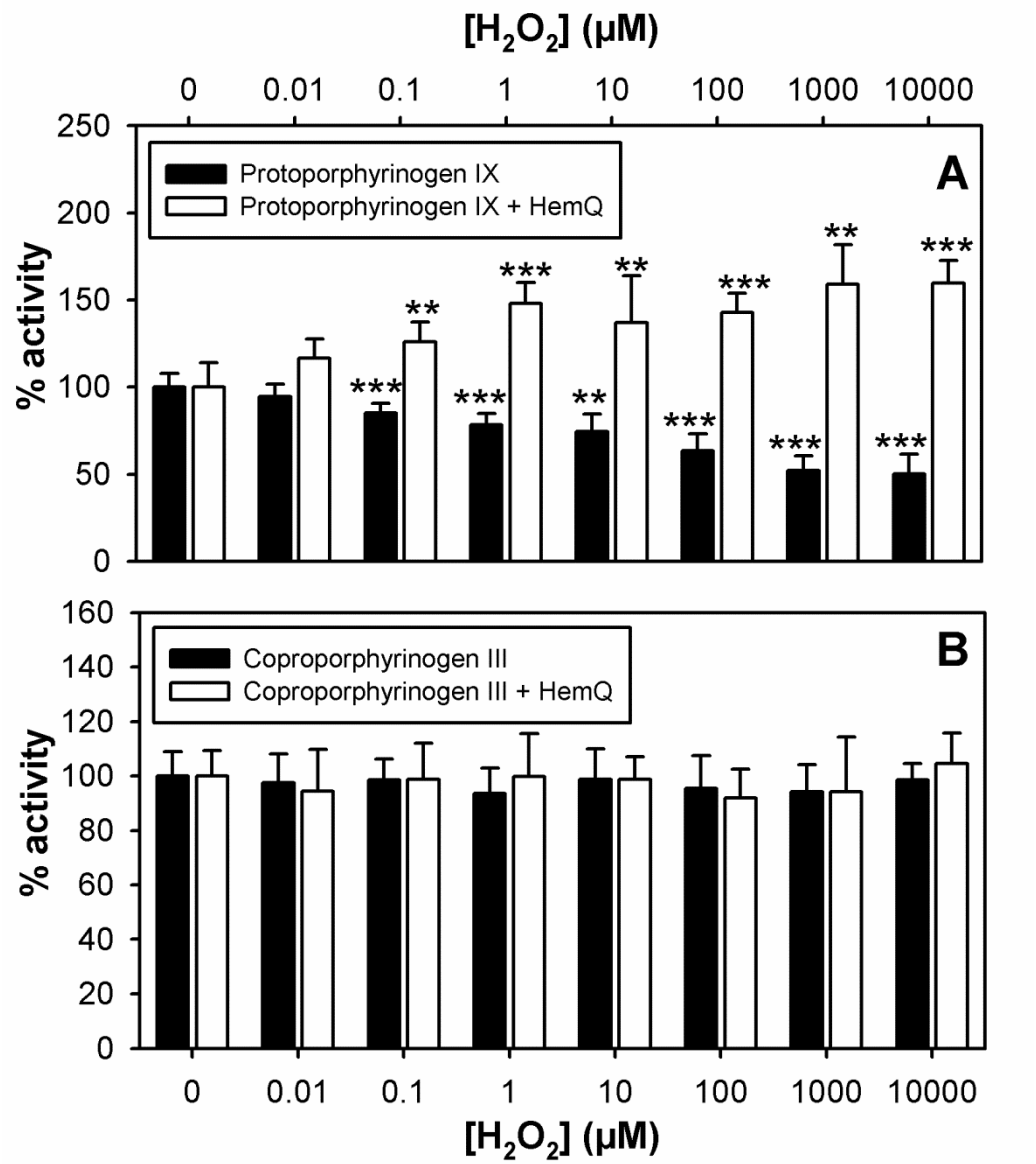


**Figure 3.16 –** Hydrogen peroxide stimulates protoporphyrinogen oxidase activity in the presence of HemQ. Protoporphyrinogen oxidase activity of HemY was assayed in the presence (1 μM) and absence of HemQ at various [hydrogen peroxide] using (A) 9.5 μM protoporphyrinogen IX and (B) 5.8 μM coproporphyrinogen III as substrates. Error bars represent SD values based on four repeats. Data has been normalised to the activities of HemY (either with or without HemQ) without hydrogen peroxide present for each corresponding dataset. (Student's t-test, *P<0.05, **P<0.01, ***P<0.001)

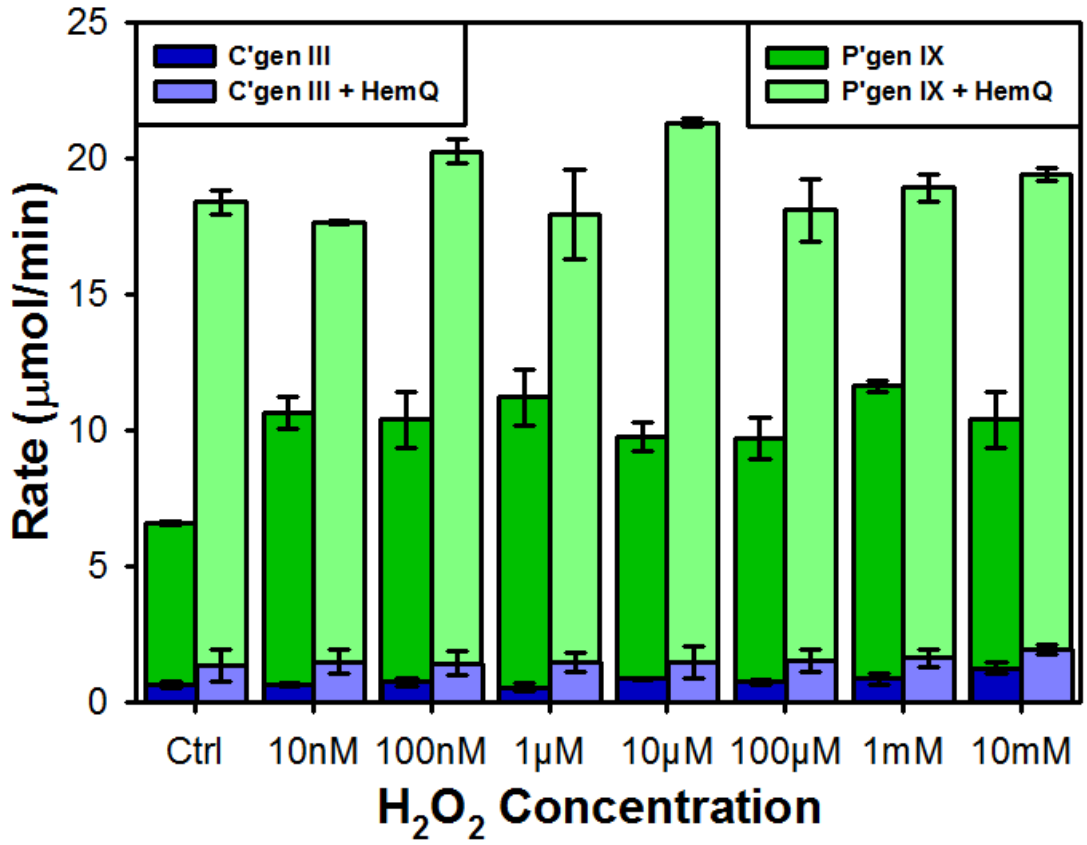


**Figure 3.17** – Auto-oxidation rates of protoporphyrinogen IX (9.48 µM - green) and coproporphyrinogen III (5.78 µM - blue). Assays performed with various [hydrogen peroxide] and in the presence (light colours) and absense (dark colours) of haem-loaded HemQ. Overall porphyrinogen oxidation increases with addition of haem-loaded HemQ, whilst background P'gen$_{IX}$ oxidation also increases with the presence of hydrogen peroxide.

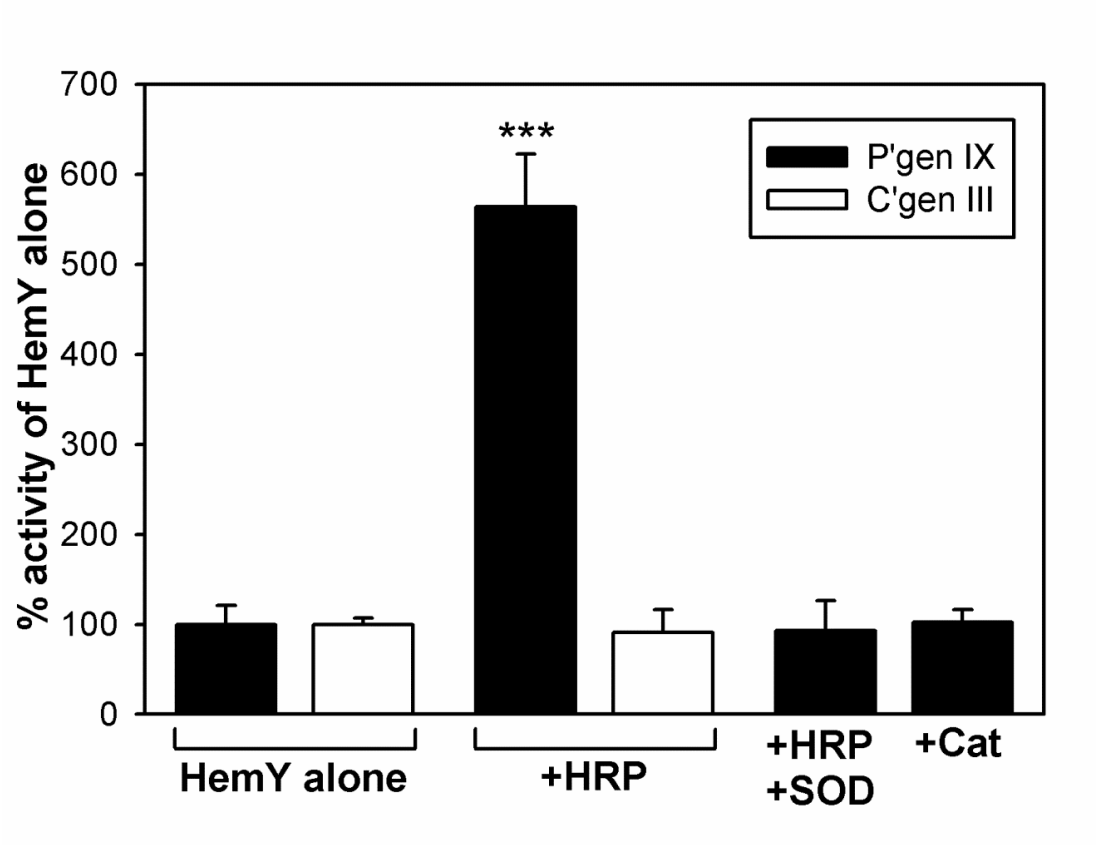


**Figure 3.18 –** Peroxidase-derived superoxide stimulates HemY-mediated oxidation of protoporphyrinogen IX. Kinetic assays showing the effect of HRP (1 µM), superoxide dismutase (1 µM) and catalase (1 µM) upon the activity of HemY (0.5 µM) using protoporphyrinogen IX (8.6 µM) and coproporphyrinogen III (8.2 µM) substrates. Data has been normalised to HemY only controls to compare between datasets. Error bars represent SD values based on four repeats. (Student's t-test, ***P<0.001).

## 3.3 – Discussion

This work examines the hypotheses that *S. aureus* HemY can participate in both the coproporphyrin-dependent and classical pathways and that the generation of ROS by the HemQ enzyme has a more profound effect upon macrocycle oxidation in the classical pathway compared to the coproporphyrin-dependent pathway. These investigations will aid our understanding of how the classical pathway evolved from the more ancient coproporphyrin-dependent pathway (Dailey et al. 2015).

Kinetic analysis of *S. aureus* HemY (Figure 3.12) revealed $k_{cat}$ and $K_m$ values of 0.46 ± 0.02 $min^{-1}$ and 6.7 ± 0.8 µM for coproporphyrinogen III oxidation compared to previous measurements of 1.33 ± 0.04 $min^{-1}$ and 0.31 ± 0.01 µM (Lobo et al. 2015), respectively. Previously, the oxidation of protoporphyrinogen IX for *S. aureus* HemY could not be detected (Lobo et al. 2015), so this reaction was re-examined. Structural modeling supports the hypothesis that *S. aureus* HemY can accommodate coproporphyrinogen (Figure 3.6), and the kinetic data described herein clearly show activity for the protoporphyrinogen IX substrate ($k_{cat}$ = 0.44 ± 0.03 $min^{-1}$). However, the background rate and signal:noise was significantly higher for the protoporphyrinogen IX reaction (Figure 3.10), which initially led to optimizing the assay to use an excitation wavelength of 520 nm as opposed to 400 nm. This use of the 520 nm excitation filter dropped the levels of auto-oxidation to 20% of the level observed when the 400 nm filter was used (Figure 3.10). This difference in the assay procedure may provide some insight into why enzymatic activity could not be detected in previous studies (Lobo et al. 2015).

The pattern of substrate specificity is consistent with previous observations for HemY enzymes from numerous Actinobacteria/Firmicutes (Dailey et al. 2015; Hansson & Hederstedt 1994; Dailey et al. 2010), and supports the hypothesis that evolutionary precursors to these HemY enzymes may once have also oxidized protoporphyrinogen IX *in vivo* in ancestral organisms. This is also supported by previous observations that the HemH ferrochelatases from Gram-positives can insert iron into both coproporphyrin III and protoporphyrin IX (Dailey et al. 2015).

If we accept the compelling evidence that the classical pathway evolved from the coproporphyrin-dependent pathway, an important question presents itself: why do the majority of Actinobacteria/Firmicutes now lack a functional coproporphyrinogen oxidase that prevents the formation of protoporphyrinogen IX and protoporphyrin IX? One potential explanation would be that the peroxide-dependent mechanism of HemQ can generate free radicals, which will have a greater cytotoxic effect in combination with protoporphyrin IX compared to the less reactive coproporphyrin III. This is consistent with a previous report that the more reactive protoporphyrin IX causes greater cellular damage (Aravind Menon et al. 1989). Hence, it was hypothesised that stimulation of HemY-mediated protoporphyrinogen IX oxidation by HemQ (Dailey et al. 2010) was due to the evolution of ROS, as previously reported for cytochrome *c* and eukaryotic HemY (Shepherd & Dailey 2009), and that this stimulation would be exacerbated when protoporphyrin IX is a reaction product (compared to the less reactive coproporphyrin III). HemY assays with both substrates in the presence and absence of HemQ were consistent with this hypothesis (Figure 3.13), and yielded the surprising observation that HemQ did not stimulate the oxidation of coproporphyrin III at all. Further kinetic analysis with haem/porphyrin loaded ligands confirm that haem, the product of the HemQ reaction, must be present for the stimulation of HemY activity (Figure 3.15). Further assays with varying hydrogen peroxide demonstrate that this ROS-generator stimulates the HemY reaction only when HemQ is present, but causes inhibition in the absence of HemQ (Figure 3.16, top). The most simple explanation for the inhibition of HemY by peroxide in the absence of HemQ is due to classical product inhibition. However, it is not clear why this does not take place when coproporphyrinogen III is used as a substrate (Figure 3.16, bottom), although conformational differences in active site structure are likely to exist when additional propionates are present on the porphyrinogen substrate.

The stimulation of HemY activity by peroxide and HRP combined with the abrogation of this rate enhancement by SOD (Figure 3.18) provide clear confirmation that it is the peroxidase activity of HemQ that enhances HemY-mediated protoporphyrinogen IX oxidation. If we return to the model in Figure 3.1, the current data are consistent with ROS generation by HemQ stimulating the HemY-catalysed oxidation of protoporphyrinogen IX only (and not the HemY-

mediated stimulation of coproporphyrinogen III oxidation). However, one should not overlook the profound effect that HemQ has on the nonenzymatic oxidation of protoporphyrinogen IX (Figure 3.17). While HemQ does appear to also elevate the nonenzymatic oxidation of coproporphyrinogen III, the overall rates are an order of magnitude lower than those for protoporphyrinogen IX that are comparable to the HemY-catalyzed turnover rates in Figure 3.12. This additional nonenzymatic rate enhancement is very likely to involve superoxide (from HemQ and possibly porphyrin-derived), adding weight to the hypothesis that peroxidase activity by HemQ will enhance the production of ROS in combination with tetrapyrrole intermediates of the classical pathway. From an evolutionary perspective, this generation of toxic ROS would provide a selection pressure to retain either the coproporphyrin-dependent pathway *or* the classical pathway, but not both. This model is also consistent with observations that HemQ enzymes may utilise alternative electron acceptors such as FMN, negating the requirement for HemY-derived peroxide in the coproporphyrin-dependent pathway. This may also explain why in proteobacteria that commonly utilise the classical pathway, HemJ or HemG enzymes that do not require oxygen nor produce hydrogen peroxide are the most common forms of protoporphyrinogen oxidase (Kobayashi et al. 2014; Dailey et al. 2015).

Chapter IV

# Characterisation of *S. aureus* HemH coproporphyrin III ferrochelatase

# Summary

HemH enzymes are known to catalyse the final step of classical haem synthesis, inserting ferrous iron into a protoporphyrin IX. However, for the recently discovered coproporphyrin-dependent pathway, HemH catalyses the penultimate reaction and inserts ferrous iron into coproporphyrin III instead of protoporphyrin IX. While many organisms have been tested in the past using classical pathway substrates or analogues (protoporphyrin based), only *M. tuberculosis*, *B. subtilis* and *S. aureus* have currently been tested for insertion of a divalent metal into coproporphyrin (Dailey et al. 2015; Lobo et al. 2015). This reaction has also been shown, in *B. subtilis* and *S. aureus*, to be partially inhibited by its own iron substrate.

The worked described herein provides a more detailed kinetic characterisation of *S. aureus* HemH. It has previously been reported that the HemH enzyme of *S. aureus* can utilise several divalent metals ($Fe^{2+}$, $Zn^{2+}$, $Co^{2+}$, $Cu^{2+}$ and $Ni^{2+}$) and the current work confirms that metal insertion occurs only with coproporphyrin III, not protoporphyrin IX. This enzyme works at a similar rate to other ferrochelatases when assayed with an iron concentration below 0.8 µM, above which substrate inhibition occurs. A more detailed look at the kinetics of the reaction revealed that while HemH catalysis occurs irrespective of which substrate binds first, the $K_m$ for iron is lower when the porphyrin binds first. Structural modelling of *S. aureus* HemH suggests the existence of multiple binding sites for metals around the active site, based on comparisons with the close structural homologue from *B. subtilis* (Lecerof et al. 2000; Lecerof et al. 2003). These data are consistent with a model whereby inhibition by iron is due to the occupation of multiple metals sites resulting in a diminished ability to bind coproporphyrin.

# 4.1 – Introduction

The HemH enzyme, or ferrochelatase as it is commonly known, is responsible for the insertion of a ferrous iron ion ($Fe^{2+}$) into the centre of porphyrin rings. It has always been thought that this protein was the final step in the classical haem synthesis pathway, where the $Fe^{2+}$ was inserted into a protoporphyrin IX molecule (Figure 4.1). While this is the case for the majority of organisms that express this enzyme, some organisms which utilise the coproporphyrin-dependent pathway have been shown to insert $Fe^{2+}$ into coproporphyrin III instead, making metal insertion the penultimate reaction in the pathway (Dailey et al. 2015). This class of HemH enzyme has been reported to exhibit broad substrate specificity, leading to a range of different combinations of substrates being used to study this protein, with the most common *in vitro* assays utilising zinc and deuteroporphyrin IX, both of which are not native substrates *in vivo* (Dailey et al. 2000): zinc is used as this enables the use of a fluorescence assay, and deuteroporphyrin IX is a water-soluble analogue of protoporphyrin IX.

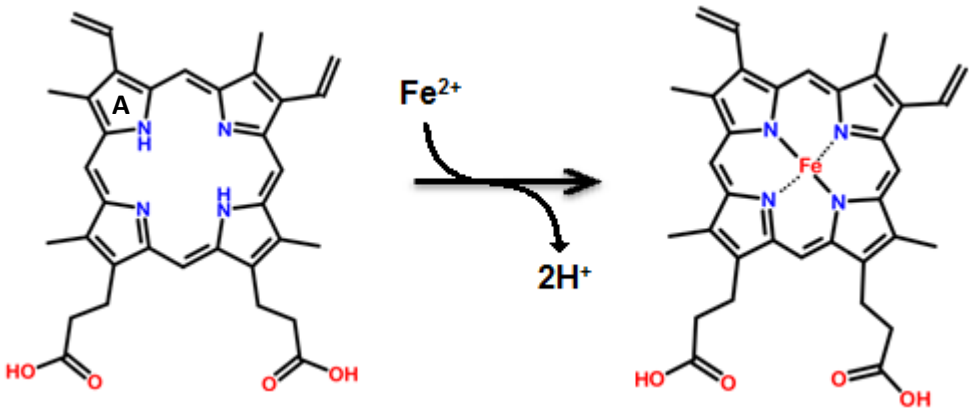


**Figure 4.1 –** Overview of the classical ferrochelatase reaction where $Fe^{2+}$ is inserted into the centre of protoporphyrin IX, releasing two protons.

## 4.1.1 – Kinetic parameters for HemH enzymes

As is the case with HemY, HemH is a membrane-bound protein in eukaryotes and many prokaryotes, but Gram-positive bacteria have been shown to encode a soluble form of the protein (Hansson & Hederstedt 1992; Dailey & Dailey 2002; Dailey et al. 1983; Wu et al. 2001). All of these forms of HemH have been shown to insert a variety of divalent metals into the centre of porphyrin molecules, with zinc being the most common metal used in *in vitro* assays due to being more stable in an aerobic environment than the natural $Fe^{2+}$ substrate (Camadro et al. 1984) and allows for fluorescence-based assays to be utilised. Other metals that have been shown to be inserted by HemH enzymes are cobalt, copper and nickel (Dailey et al. 2000; Dailey et al. 2015; Hansson et al. 2011; Dailey & Dailey 2002), although not all ferrochelatases can insert these ions. It has been reported that the soluble and membrane-associated forms of HemH can utilise different metals for insertion, with the *B. subtilis* protein being able to insert $Cu^{2+}$, but not $Co^{2+}$, which can be utilised by the majority of membrane associated ferrochelatases (Hansson et al. 2011). This is not always the case however, as it has been shown that the membrane-associated HemH from *Caulobacter crescentus* cannot utilise $Co^{2+}$, but instead uses $Ni^{2+}$ (Dailey & Dailey 2002). In addition, the soluble HemH from *M. tuberculosis* has the ability to insert $Cu^{2+}$, $Co^{2+}$ and $Ni^{2+}$ into its natural porphyrin substrate, coproporphyrin III (Dailey et al. 2015). Kinetic data available for ferrochelatases, summarised in Table 4.1, varies greatly due to the variety of substrates that have been used. This can make direct comparisons between organisms difficult as the enzymes may behave differently with different substrates. Maximal rates for ferrochelatases also appear to vary, with $k_{cat}$ values typically ranging from 0.11 $min^{-1}$ to 15.3 $min^{-1}$, with a surprisingly high rate recently reported for *S. aureus* HemH utilising coproporphyrin III and $Fe^{2+}$ which is reported to be 165 $min^{-1}$ (Lobo et al. 2015). This rate was not experimentally observed, but obtained after the data was fitted to a substrate inhibition curve, which also identified 0.8µM as the concentration where $Fe^{2+}$ inhibition occurs (Lobo et al. 2015). The fastest rate measured in this study was roughly 28 $min^{-1}$, which is one sixth of the value of the fitted $k_{cat}$. Parallel experiments performed for the *B. subtilis* HemH gave another high $k_{cat}$ value, 78 $min^{-1}$ (Lobo et al. 2015) compared with 0.11 $min^{-1}$ (Dailey et al. 2015) as previously reported.

**Table 4.1 –** Summary of available kinetic data for ferrochelatases from various organisms, including substrates used and other metal substrates that can be utilised. $M_{IX}$ represents Mesoporphyrin IX where it has been used as a porphyrin substrate

| Organism | $k_{cat}$ ($min^{-1}$) | Substrates | $K_m$ (µM) $P_{IX}$ | $K_m$ (µM) $C_{III}$ | $K_m$ (µM) $Fe^{2+}$ | $K_m$ (µM) Other | Other Metals | Reference |
|---|---|---|---|---|---|---|---|---|
| Human | 6.6 | $P_{IX}$ + Iron | 9.0 | - | 9.3 | - | $Co^{2+}$ | (Wu et al. 2001) |
| *M. tuberculosis* | 0.8 / 1.8 | $P_{IX}$ / $C_{III}$ + Iron | 720 | 10.5 | - | - | $Co^{2+}$, $Cu^{2+}$, $Ni^{2+}$ | (Dailey et al. 2015) |
| *B. subtilis* | 0.11 | $C_{III}$ + Iron | - | 7.8 | - | - | $Co^{2+}$, $Cu^{2+}$, $Ni^{2+}$ | (Dailey et al. 2015) |
| *B. subtilis* | 78 | $C_{III}$ + Iron | - | 0.15 | - | - | - | (Lobo et al. 2015) |
| *C. crecentus* | 14.5/16.0 | $P_{IX}$ / $M_{IX}$ + Iron | 6.2 | - | 30 | - | $Ni^{2+}$ | (Dailey & Dailey 2002; Shepherd et al. 2006) |
| *M. xanthus* | 4.9 | $M_{IX}$ + Iron | - | - | 6.5 | 9.6 ($M_{IX}$) | - | (Shepherd et al. 2006) |
| *P. putida* | 11.7 | $M_{IX}$ + Iron | - | - | 20 | 8.9 ($M_{IX}$) | - | (Shepherd et al. 2006) |
| *Bd. Bacteriovorus* | 4.4 | $M_{IX}$ + Iron | - | - | 28 | 8.0 ($M_{IX}$) | - | (Shepherd et al. 2006) |
| *S. aureus* | 15.3 / 165 | $P_{IX}$ / $C_{III}$ + Iron | - | - | 52 / 0.6 ($P_{IX}$ / $C_{III}$) | - | - | (Lobo et al. 2015) |

## 4.1.2 – Structural analysis of HemH crystal structures

While it appears that HemH proteins exhibit poor amino acid sequence identity (e.g. <10% between Human and *B. subtilis* ferrochelatases), the secondary and tertiary structures of these enzymes are quite similar in the core region (Wu et al. 2001). Comparisons between the three available ferrochelatases structures, *B. subtilis* (Lecerof et al. 2000), Human (Wu et al. 2001) and *S. cerevisiae* (Karlberg et al. 2002), suggest that the overall structures for all three ferrochelatases are very similar, with some small differences between them.

Structural differences between these proteins appear to be located towards the N- and C-termini, with Human and *S. cerevisiae* HemH having a helical region located close to the exterior of the active site which appears to be hydrophobic in nature and may be involved in association with the mitochondrial membrane, which points the active site towards the membrane (Karlberg et al. 2002; Wu et al. 2001). In comparison, *B. subtilis* HemH does not have this helix, giving it a more open active site. The lack of this membrane-associated helix could explain why this form of the protein is soluble rather than associated with a membrane (Lecerof et al. 2000).

Human and yeast ferrochelatases also have an extended C-terminal region when compared with the *B. subtilis* protein. The Human enzyme contains a [2Fe-2S] iron-sulphur cluster in this region, which is not present in the *S. cerevisiae* enzyme. This cluster is maintained by one residue in the core of the protein (Cys 196) and three in the extended C-terminal region (Cys 403, 406, 411), and at the time was thought to be responsible for anchoring the extended C-terminal to the rest of the monomer, and was also suggested to be indirectly involved in stabilising the dimer form of the protein (Wu et al. 2001). *S. cerevisiae* does not contain the necessary residues in the same location to form a cluster and the dimer stability is reportedly not affected (Karlberg et al. 2002). Other bacterial ferrochelatases have been found to ligate [2Fe-2S] clusters via an extra insertion, and are suggested to enhance $Fe^{2+}$ binding at low $Fe^{2+}$ concentrations (Shepherd et al. 2006). However, removal of these clusters does not result in a loss of activity, as has been seen with eukaryotic forms (Shepherd et al. 2006; Dailey et al. 1994a), and the *in vivo* role for these cofactors remains poorly understood.

There are also differences in the structure of the C-terminal region between the human and yeast ferrochelatases, with a coil and helix loop structure seemingly being reversed between the two proteins, which are in the area of the [2Fe-2S] cluster in the Human protein. It is proposed for both enzymes that the helix in this region is one of the secondary structures that forms the hydrogen bonds required for dimerisation to occur, which means that the [2Fe-2S] cluster would have another role in the protein (Karlberg et al. 2002; Wu et al. 2001). While the *B. subtilis* HemH does not possess this region on the C-terminus and is a monomeric protein, it is likely that this region is the main factor involved in dimerisation of the protein. The core structure, which appears to be structurally conserved, consists of two similar shaped domains each folded into a Rossmann-type fold, four parallel β-sheets with α-helices of each side, between which the porphyrin-binding cleft resides.

Many of the residues that are involved in the binding of the porphyrin substrate appear to be rather well conserved in their location and function (Medlock et al. 2008; Lecerof et al. 2000; Karlberg et al. 2002). One of the major conserved amino acid locations appears to be an invariant histidine residue that forms a hydrogen bond with a conserved glutamic acid residue, with this bond being broken upon porphyrin binding and the histidine forming an interaction with a protonated part of the pyrrole ring, supposedly ring B (Medlock et al. 2008). This histidine is also thought to be important for initiating secondary structure conformation change that initiates the distortion of the porphyrin ring (Medlock et al. 2008), although these residues are also reported to be involved in the binding of the metal substrate (Lecerof et al. 2003), with the mechanisms for how these residues are involved still to be completely determined. An invariant tryptophan residue is also present in all known ferrochelatases and has been suggested to be involved in stabilising the C ring of the porphyrin in the *B. subtilis* enzyme (Lecerof et al. 2000), although it is suggested that in the human enzyme that this tryptophan (along with L92, L98 and V305) is involved in the closing of the active site mouth via hydrophobic interactions (Medlock et al. 2008). These residues, also appear to be present in the *S. cerevisiae* protein, suggesting that the membrane-associated ferrochelatases act in a similar manner (Karlberg et al. 2002).

HemH structures exhibit a degree of variability with respect to the residues present on the opposite side of the porphyrin binding cleft to the metal binding sites. In the *B. subtilis* protein a series of residues reported to be involved in porphyrin binding are different when compared to the same locations in the human or *S. cerevisiae* structures. The leucine residues in the membrane-bound structures are not present in the *B. subtilis* protein as these appear to form part of the hydrophobic lip that covers the active site pocket. However, R30 and R31 (*B. subtilis*) appear to occupy a similar spatial location to the human L96 and L98, and both residues interact with the porphyrin substrate, with R30 interacting with the propionate group on ring D *via* a water molecule and R31 interacting with the propionate group on ring C along with K188. These residues also form a small enclosure over the porphyrin binding cleft, along with R33 and K188, although this not as large as the lid that covers the active site in the membrane-associated form (Lecerof et al. 2000; Wu et al. 2001).

The Y13 residue in *B. subtilis* HemH, which has been determined to aid the conserved histidine residue in stabilisation of the B ring of the porphyrin macrocycle, is not present in the membrane-associated ferrochelatases (Lecerof et al. 2000). The residue in this position in the other enzymes is a methionine whose role is not entirely understood (Wu et al. 2001; Karlberg et al. 2002). The presence of this methionine is further puzzling when it is considered that it and the histidine residue, on the opposite side of the porphyrin ring, are both ligands that can bind the haem iron and could therefore make product release difficult (Medlock et al. 2008). The tyrosine residue in *B. subtilis* has been implicated in a metal-binding function in the catalytic metal binding site along with the conserved histidine and glutamic acid residues (Lecerof et al. 2000; Lecerof et al. 2003) and it is possible that the methionine residue in this position aids in the insertion of metals into the porphyrin ring in a similar manner to the tyrosine residue found in the soluble form of ferrochelatase. The amino acid in this position has also been linked to the type of metal that can be inserted into the ring, with a Y13M mutation of the *B. subtilis* enzyme being able to insert $Co^{2+}$ at a much higher rate than the wild type but the ability to insert $Cu^{2+}$ drops to below detectable levels (Hansson et al. 2011). This would seem to suggest that the amino acid at this position is important for interactions with different metals, with a tyrosine residue seemingly important for $Cu^{2+}$ insertions and a methionine favouring $Co^{2+}$ insertion.

Soluble ferrochelatases have been crystalized with a variety of metals present in the metal binding cleft, and have been shown to have two separate sites in the same region where metals can bind; one close to the porphyrin binding site, held by the conserved histidine and glutamic acid residues and one closer to the surface of the protein, roughly 7Å from the H183 residue (Lecerof et al. 2003). This outer site has been shown to bind magnesium ions ($Mg^{2+}$), which are co-ordinated by the residues R46, D268 and E272. These residues are poorly conserved, although the human enzyme does contain residues that occupy the same space as those in *B. subtilis* ferrochelatase (Q122, E347 and E351) with the *S. cerevisiae* enzyme lacking an acidic sidechain (G322 instead of E272 and E351 in *B. subtilis* and human, respectively), but otherwise having the same overall structure as the human enzyme. This metal site has only been observed with a magnesium ion occupying it in *B. subtilis* and it has been reported that the presence of magnesium stimulates zinc insertion into deuteroporphyrin IX, with a mutation removing the ability to bind magnesium (E272S) showing no stimulation (Lecerof et al. 2003). The mechanism for this stimulation is not entirely understood, but it is proposed to be due to repulsion between metal ions present at both sites pushing the catalytic metal closer to the porphyrin ring (Lecerof et al. 2003). Studies on the human protein have not focussed on this potential metal site, and the *S. cerevisiae* enzyme does not seem able to bind metals in this site due to the glycine residue instead of a glutamate residue at position 322. It has been suggested that the *S. cerevisiae* ferrochelatase can bind the inhibitor $Cd^{2+}$ at two sites, with one site slightly further away from the active site than the proposed outer metal binding site, and is proposed to have a lesser effect on activity compared to the $Mg^{2+}$ binding site in *B. subtilis* (Karlberg et al. 2002). The inner binding site is suggested to bind and utilise several different divalent metals (see section 4.1.1), as well as metals such as $Cd^{2+}$ and $Pb^{2+}$ that have been shown to be inhibitors of ferrochelatases (Lecerof et al. 2003; Medlock et al. 2008). Residues that are predicted to be predominantly involved in metal binding in *B. subtilis*, where $Zn^{2+}$ and $Cd^{2+}$ have been observed, are the conserved residues H183 and E264 and the unique Y13 residue that resides on the other side of the porphyrin binding site (Lecerof et al. 2003). $Cd^{2+}$ has been shown to also bind to the nearby H262, which is located underneath the porphyrin substrate and is proposed to inhibit HemH by preventing binding of porphyrins due to this position (Lecerof et al. 2003).

## 4.1.3 – Aims of this chapter

The aims of this chapter were to address the following hypotheses:

- The HemH enzyme from *S. aureus* will insert $Fe^{2+}$ into both protoporphyrin IX and coproporphyrin III.
    - Determine kinetic parameters for these reactions.

- HemH will be able to insert zinc, cobalt, copper and nickel into the porphyrin ring.

Following the realisation that the insertion of iron into coproporphyrin can be inhibited at higher iron concentrations, research focus turned to determining the mechanism behind this inhibition using kinetic parameters from the following reaction conditions:

- Varying iron concentration at set coproporphyrin III concentrations.

- Varying coproporphyrin III concentration at set iron concentrations.

- Assaying in the presence of magnesium to simulate occupation of a metal binding site close to the active site.

# 4.2 – Results

## 4.2.1 – Sequence analysis and structure prediction for *S. aureus* HemH

### 4.2.1.1 – Multiple sequence alignment of HemH enzymes

As with the HemY protein, HemH from *S. aureus* displays high amino acid sequence identity with other members of the *Staphylococcus* genus when analysed in a NCBI BLASTP search, with identities typically >80%. Outside of this genus, the search gives a variety of ferrochelatases from a wide range of organisms with the top hits being between 60% and 70% identity, including *M. caseolyticus* (70%) and *B. subtilis* (63%), which is a higher degree of similarity than was seen for the HemY enzymes (Section 3.2.1.1). As with HemY, comparisons with *P. acnes* and *M. tuberculosis* yielded very poor sequence identities, with 27% identity for both *P. acnes* and *M. tuberculosis*.

A multiple sequence alignment of the protein sequences from *S. aureus*, *S. epidermidis*, *B. subtilis*, *P. acnes* and *M. tuberculosis* can be seen in Figure 4.2, which highlights fully conserved (black) and functionally conserved (grey) residues.

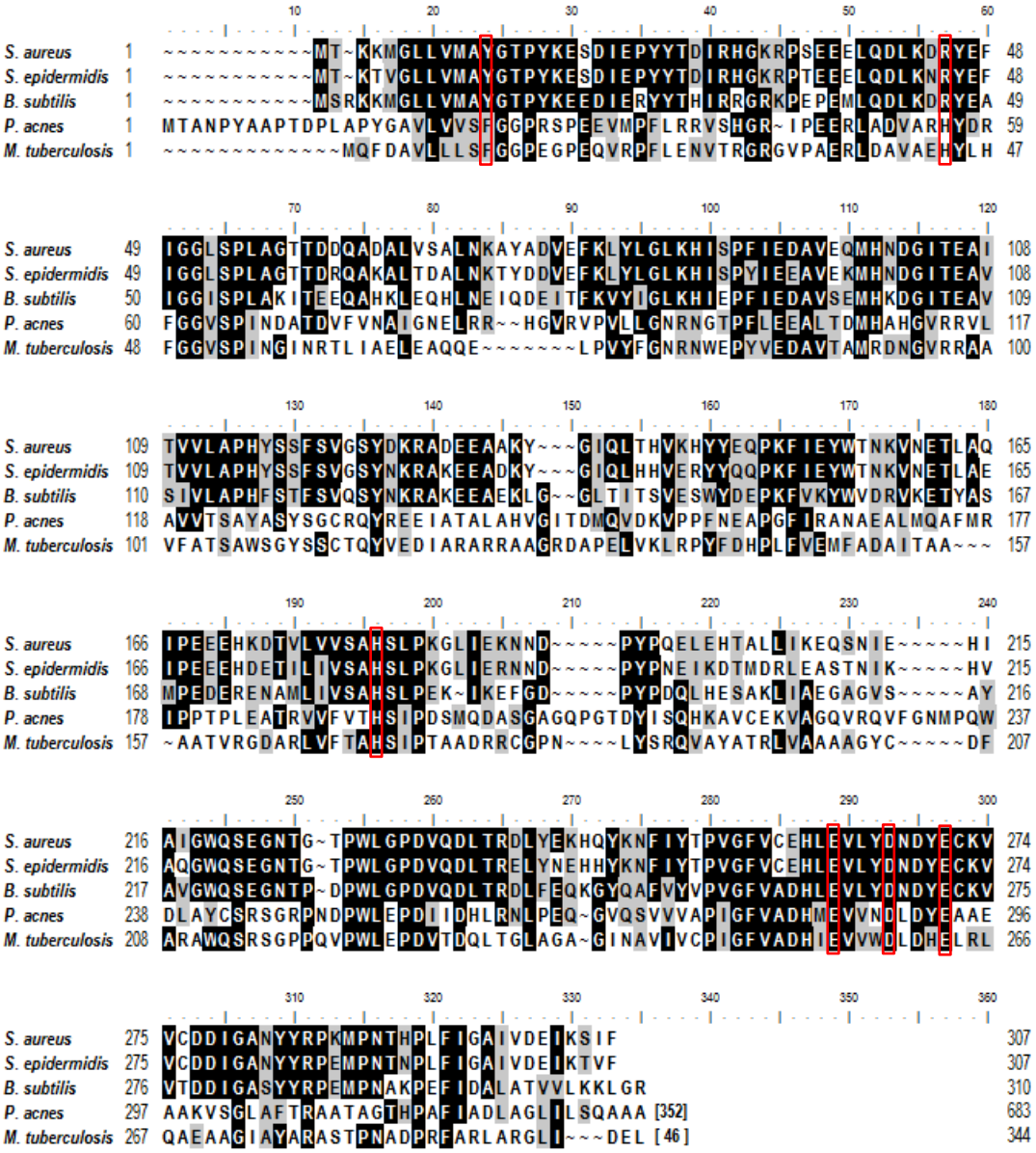


**Figure 4.2 –** Multiple sequence alignment of HemH proteins from *S. aureus*, *S. epidermidis*, *B. subtilis*, *P. acnes* and *M. tuberculosis*. Background colours represent fully conserved residues (black) and functionally conserved residues (grey). Residues highlighted in red are discussed in more detail in subsequent sections.

### 4.2.1.2 – Structural modelling of *S. aureus* HemH

A predicted structure for the *S. aureus* HemH protein was obtained using the RaptorX program (Peng & Xu 2011) using the existing *B. subtilis* ferrochelatase crystal structure (PDBid = 1DOZ, (Lecerof et al. 2000)) as a template. The resultant structural model was analysed using the CCP4 molecular graphics program (McNicholas et al. 2011) and was compared to the closest template, *B. subtilis* ferrochelatase (Lecerof et al. 2000). The solved structures for the *B. subtilis* enzyme include a variety of substrates including protoporphyrin IX, N-methylmesoporphyrin IX, and various metals. The presence of these ligands facilitated the modelling of coproporphyrin III, the natural substrate, into both the existing *B. subtilis* structure and the predicted *S. aureus* structure.

Preliminary analysis of the two structures (Figure 4.3 A) shows that the overall structure of the *S. aureus* ferrochelatase model is similar to the *B. subtilis* enzyme, with a very good overlay of Cα residues (RMS = 0.43/304) and no major differences in the size or number of secondary structural features between the two enzymes. Closer inspection of the binding sites for the two substrates (Figure 4.3 B) reveals that the amino acid residues that have been implicated in porphyrin binding in the *B. subtilis* structure (Lecerof et al. 2000) are largely conserved in both tertiary structures. Two of the residues that are involved in binding the porphyrin ring in *B. subtilis*, R31 and K188, are different in the *S. aureus* sequence: R31 in *B. subtilis* aligns to H30 in the *S. aureus* enzyme, whilst a glutamic acid residue just before K188 of *B. subtilis* (K185 in *S. aureus* HemH) that is absent in the *S. aureus* enzyme shifts these lysine residues to slightly different locations, with the sidechain of the *S. aureus* model predicted to be in a different orientation compared to the *B. subtilis* structure, as shown in Figure 4.3 B. These two residues are proposed to be involved in stabilising ring C of the porphyrin macrocycle by interacting with the propionic acid chain on the ring (Lecerof et al. 2000) and structural changes in this region are therefore likely to affect porphyrin binding.

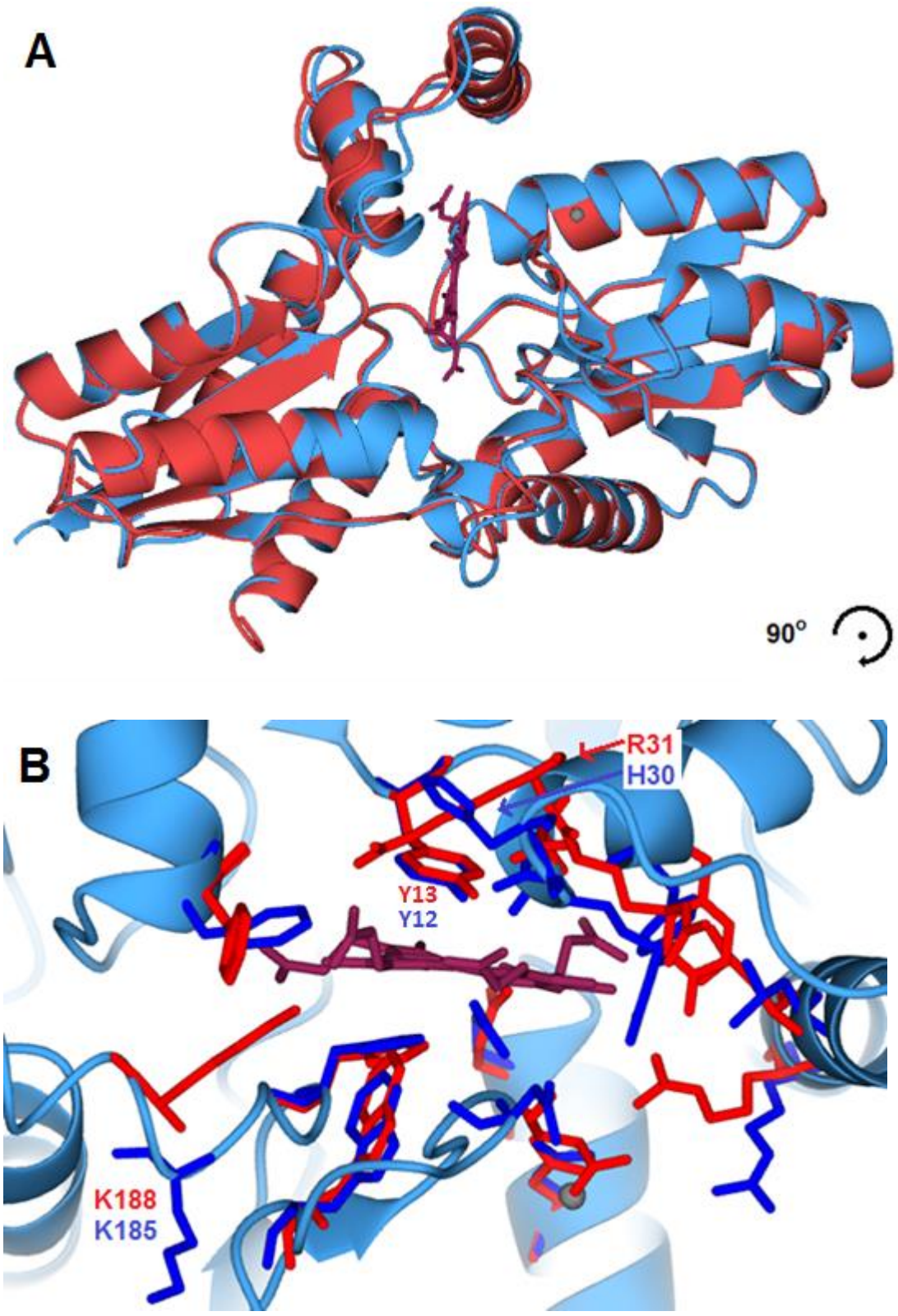


**Figure 4.3 – Analysis of a structural model for S. aureus ferrochelatase.** (A) Comparison of the structures of the HemH from *B. subtilis* (red) and *S. aureus* (blue) with coproporphyrin III (purple) and $Mg^{2+}$ (grey) modelled into their binding sites. (B) View of the binding sites, rotated 90° and magnified, with residues indicated to be involved in binding of substrates in *B. subtilis* (red, (Lecerof et al. 2000)) with the corresponding residues and from *S. aureus* (blue) for comparison.

Analysis of surface electrostatics for *S. aureus* HemH model, superimposed with the zinc and magnesium ions from the *B. subtilis* structure and a model of coproporphyrin III, shows that the binding sites for both the porphyrin and metal display significant negative charge, shown as red surface areas in Figure 4.4 A. The metal-binding sites were also compared between the *B. subtilis* and *S. aureus* organisms due to the difference in residues observed in various crystalized ferrochelatases, with the different residues present being linked to the substrate specificity, as shown in Section 4.1.2. There is also the observation in *B. subtilis* that presence of $Mg^{2+}$ ion in the outer metal binding site is required for crystals to form and is also able to increase the catalytic activity of the enzyme (Lecerof et al. 2003).

These metal binding sites, shown in Figure 4.4 A, are part of a large open cleft with the magnesium ion (black) located in the outer metal binding site, and the inner site occupied by a zinc ion (yellow) that is located much closer to the porphyrin ring (Lecerof et al. 2003). Given the high level of sequence identity with the *B. subtilis* HemH active site cleft, it is predicted that the H181 and E263 of the *S. aureus* HemH model will be involved in metal binding at the inner site with Y12 also being predicted to interact with the metal with the enzyme being likely to utilise the same metal substrates for insertion as *B. subtilis*. The magnesium ion in the outer site is held in place by residues R46, D268 and E272 in *B. subtilis* HemH, and it is therefore also likely that the corresponding residues in *S. aureus* (R45, D267 and E271) will have the same role in binding metals as in *B. subtilis* (Figure 4.4B).

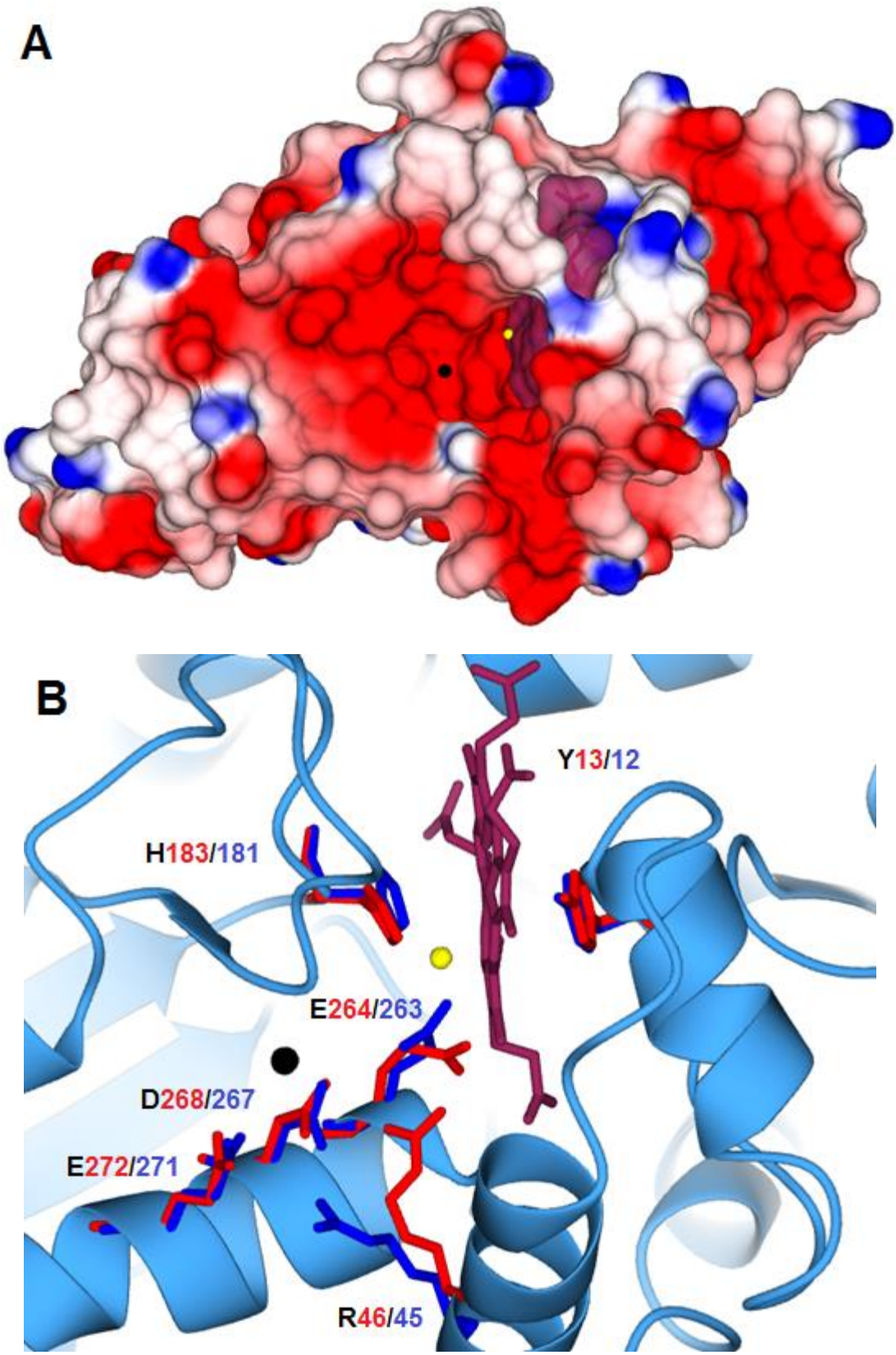


**Figure 4.4 –** (A) View of the electrostatic surface of the predicted *S. aureus* HemH model with $Mg^{2+}$ (black), $Zn^{2+}$ (yellow) and coproporphyrin III (purple) modelled into their binding sites based on the *B. subtilis* model. (B) Close up of the metal binding sites with the relevant residues for binding from both *B. subtilis* (red) and *S. aureus* (blue) with the same ligands as described for panel A.

## 4.2.2 – Engineering an expression plasmid for *S. aureus* HemH

The pTrcHis vector was used for *hemH* cloning as other recombinant HemH enzymes have successfully been overexpressed using this vector (Dailey et al. 2010). The *S. aureus hemH* gene was amplified from *S. aureus* USA300 genomic DNA via PCR as described in Section 2.10.1. A pTrcHis plasmid containing the *M. tuberculosis hemQ* gene, approximately 620 bp, was cut with NheI and HindIII and the *hemH* gene (950 bp) was ligated into NheI/HindIII-cut pTrcHis (Section 2.10.3) and transformed into chemically competent *E. coli* TOP10 cells (as described in Section 2.11).

As mentioned in Sections 2.10.2 and 2.10.3, the ligation step included the original *hemQ* gene fragment which could compete with the gene of interest and result in false positive colonies; therefore ampicillin-resistant colonies were screened via colony PCR using primers that anneal 200bp either side of the insertion site. Potential results from the colony PCR would include a 1000bp band for the presence of the original *hemQ* fragment, with the desired *hemH* fragment giving a band at 1300bp.

A PCR product at the expected size for a *hemH*-containing plasmid was found (highlighted in red in Figure 4.5), and this plasmid was extracted using a Qiagen spin miniprep kit and digested with NheI and HindIII to confirm the presence of a 900 bp *hemH* gene insert (Figure 4.6). The plasmid was confirmed to contain the correct insert (Appendix 2A-C) via Sanger sequencing (Beckman Coulter Genomics).

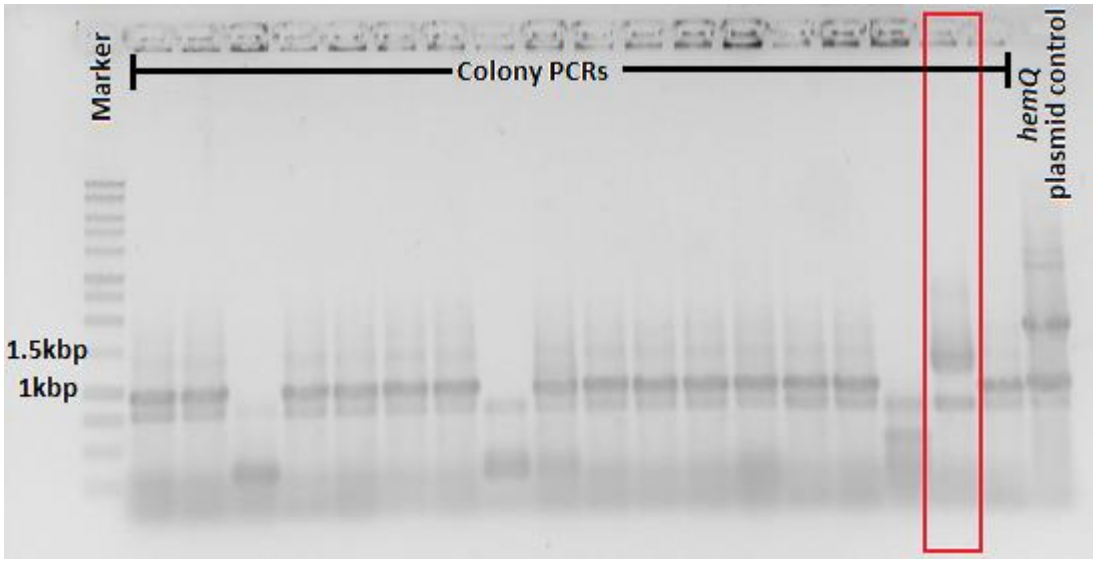


**Figure 4.5 –** Colony PCR of cells that have taken up a pTrcHis plasmid and were resistant to ampicillin. Highlighted lane shows a positive hit for a *hemH* gene fragment (1300bp). Other lanes contain either *M. tuberculosis hemQ* (band at roughly 950bp) or a lack of an insert (bands at roughly 400bp). All bands include plasmid DNA that has been amplified either side of the NheI and HindIII restriction sites (roughly 200bp each side).

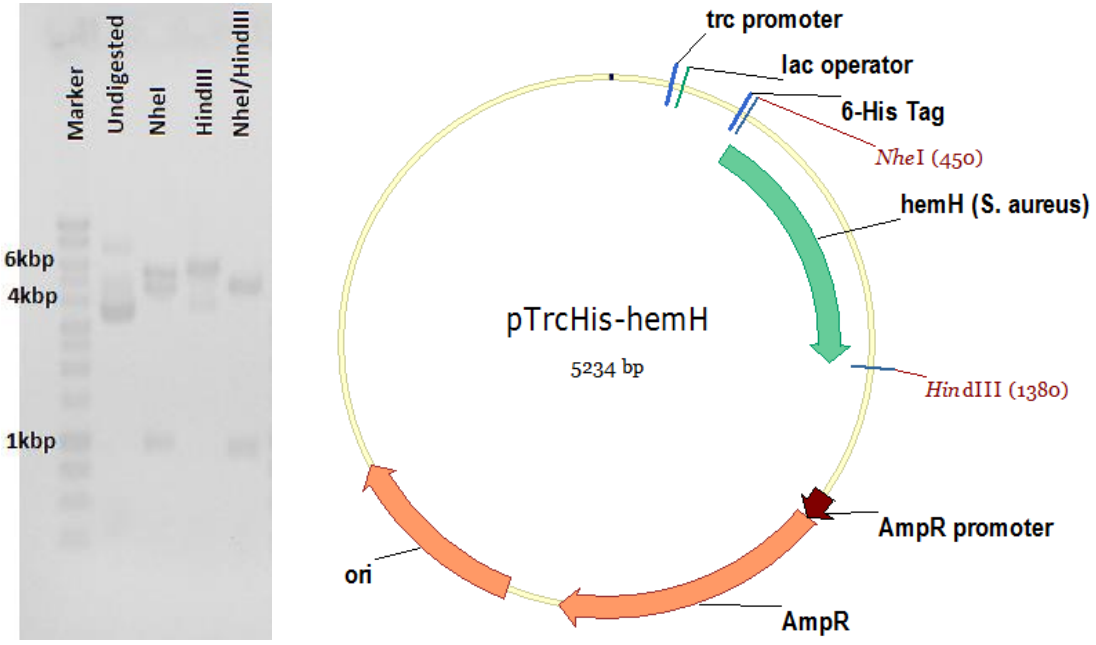


**Figure 4.6 – (Left)** Agarose gel showing the result of a restriction digest of miniprepped pTrcHis-*hemH* plasmid DNA. The desired fragment size of 924bp in the double digest lane confirms that the *hemH* gene is present. **(Right)** Plasmid map of the pTrcHis-*hemH* constructed plasmid showing restriction sites and important features of the plasmid

## 4.2.3 – Biochemical/spectroscopic analysis of purified HemH

*E. coli* JM109 cells containing the pTrcHis-*hemH* plasmid were harvested and the protein was purified via affinity chromatography as described in section 2.4. The purified protein was assessed for purity using SDS-PAGE and UV-Vis spectroscopy was used a preliminary assessment of porphyrin/haem binding. SDS-PAGE analysis (Figure 4.7) shows that a protein with a size of approximately 35kDa has been expressed and purified, which corresponds to the size of His-tagged *S. aureus* HemH protein (predicted size of 35.05 kDa). The purified HemH is very pure, with only very minor contamination in the concentrated elution samples. The HemH that was eluted with the 10 mM imidazole wash buffer exhibited the greatest purity, and was the protein fraction used in subsequent spectroscopic and kinetic studies.

The absorption spectra of the concentrated protein (Figure 4.8) does not appear to show any major spectral features other than the usual protein peak at 280nm. The lack of any significant spectral features other than this peak suggests that this protein is purified without bound tetrapyrroles or cofactors such as iron-sulphur clusters.

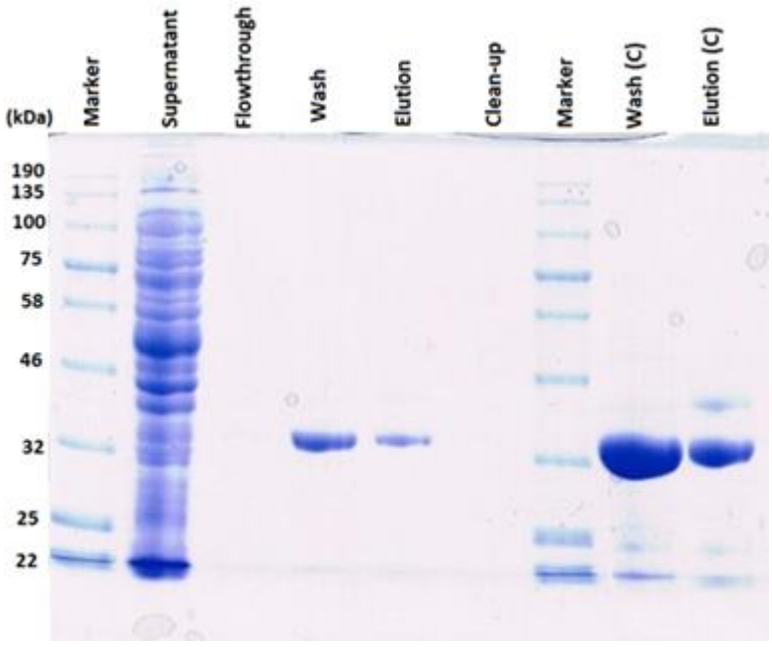


**Figure 4.7 –** SDS-PAGE of purified recombinant *S. aureus* HemH. Lanes marked with (C) are concentrated samples. 5 µl of un-concentrated samples and 10 µl of concentrated samples were loaded. A protein of roughly 35 kDa can be seen in both the Wash and Elution fractions, corresponding to the size of the HemH protein from *S. aureus.*

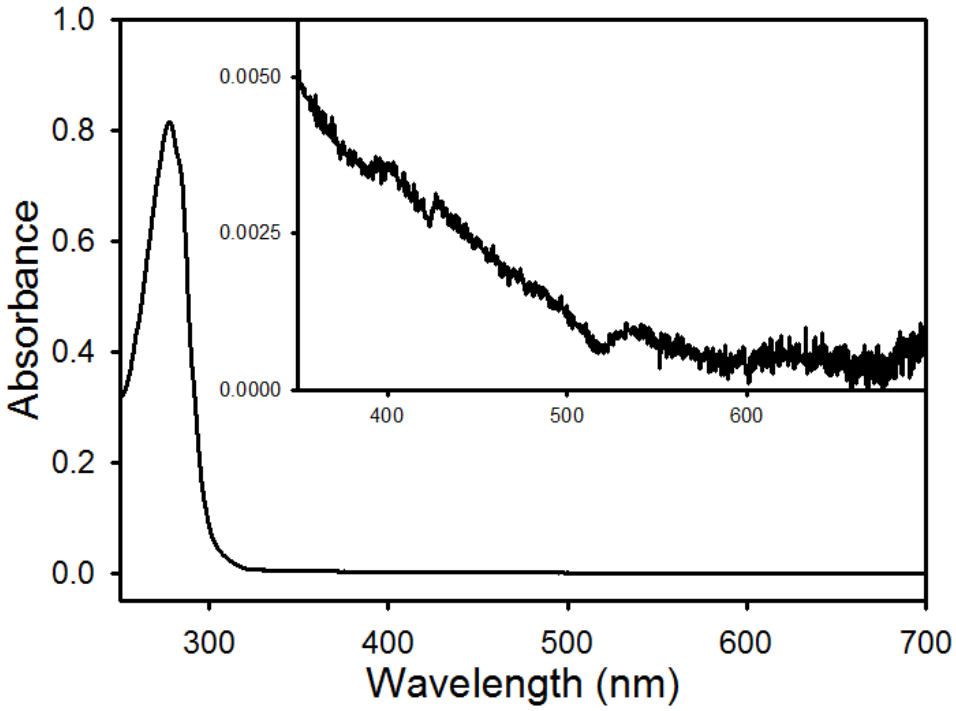


**Figure 4.8 –** UV/Vis absorption spectra of purified recombinant *S. aureus* HemH in its storage buffer (50 mM Tris/MOPS pH 8.0, 100 mM KCl, 0.1% sodium cholate). Inset shows a magnified view of the spectrum from 350-700nm.

## 4.2.4 – Substrate Specificity of *S. aureus* HemH

### 4.2.4.1 – Porphyrin Specificity

HemH was assayed for activity in the presence of coproporphyrin III and protoporphyrin IX to investigate substrate specificity and kinetic variations that result from different porphyrin substrates. Coproporphyrin was initially tested for iron insertion by HemH following the same protocol used in experiments on ferrochelatases by the Dailey lab (Sellers et al. 2001; Shepherd et al. 2006) as described in Section 2.13. This method observed changes in the three absorbance peaks in the 500-600 nm range, with a decrease in absorbance at 495 nm and an increase at 575 nm. Initial assays using high concentrations of iron did not produce enzymatic activity. However, a recent article reported that the HemH protein from *S. aureus* is inhibited by iron concentrations above 0.8μM (Lobo et al. 2015). When the iron concentration was dropped below this threshold, ferrochelatase activity was observable for *S. aureus* HemH, with the expected spectral changes being observed (Figure 4.9). HPLC analysis was also performed to detect coprohaem III evolution using a stopped assay (Section 2.13), with a quenched reaction mixture being compared to coproporphyrin III and coprohaem III commercial standards (Figure 4.10). The HPLC spectra show peaks at roughly the same positions as coproporphyrin III and coprohaem III, as well as a much larger unidentified peak between the two standards, detected at approximately 14 min.

*S. aureus* HemH was also assayed for iron chelatase activity using protoporphyrin IX, although no significant spectral changes could be observed to support the formation of proto-haem (Figure 4.11). This was consistent with HPLC analysis (Figure 4.12), which also demonstrated no activity with the protoporphyrin substrate: only a peak corresponding to protoporphyrin IX was observed when comparing assay reactions with commercial protoporphyrin IX and protohaem IX standards.

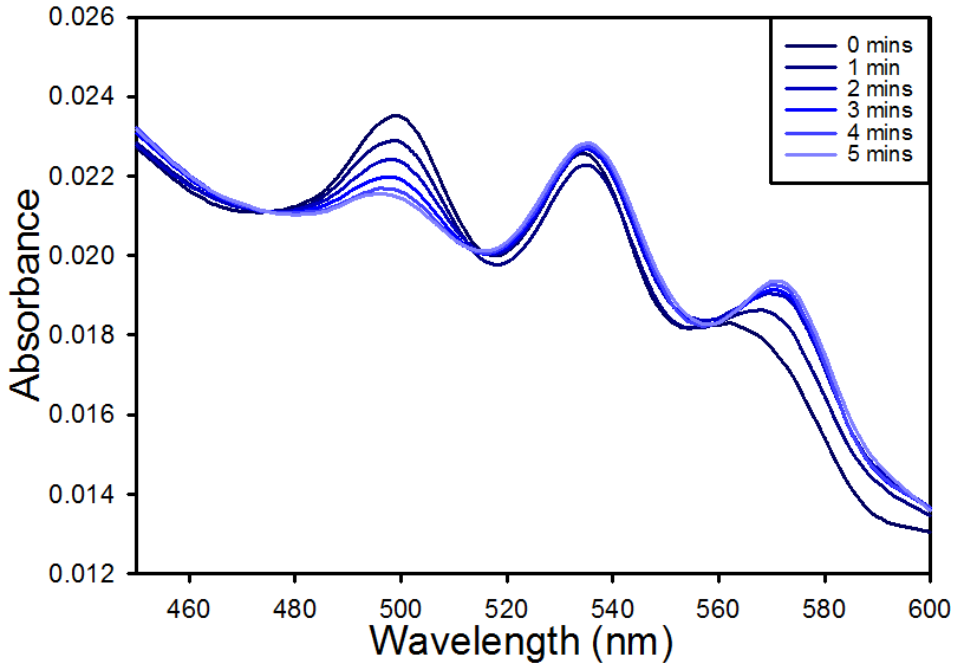


**Figure 4.9** - Spectral changes of minor coproporphyrin peaks during the first 5 minutes of the ferrochelatase assay. The peak at 495nm diminishes, whilst the peak at 565nm increases and shifts to approximately 570nm, indicating successful insertion of iron into coproporphyrin III.

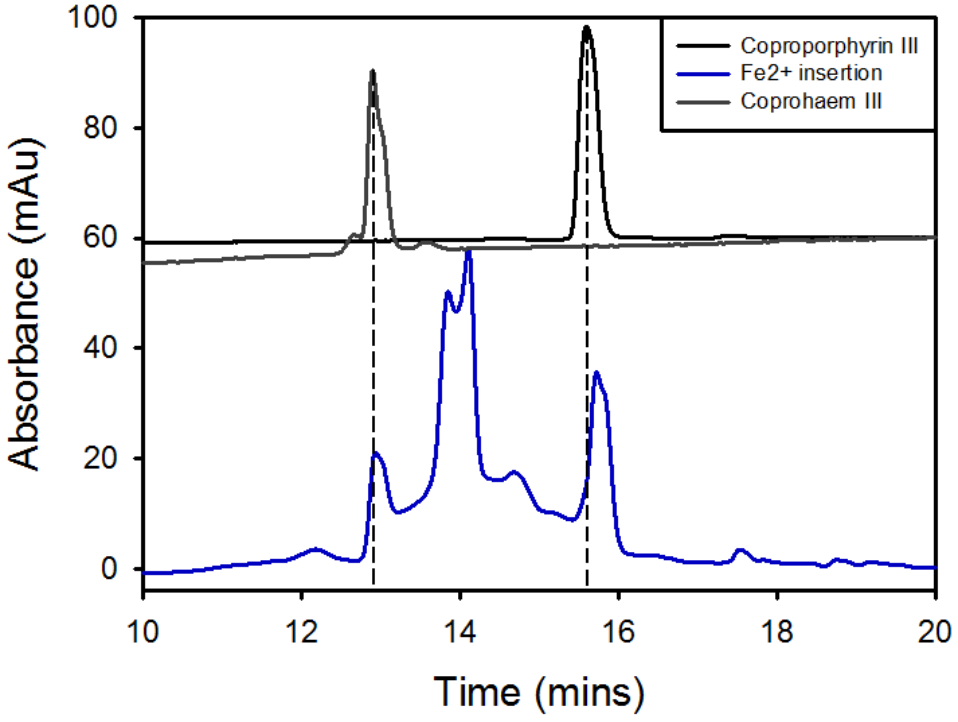


**Figure 4.10 –** HPLC analysis of iron insertion into coproporphyrin III by *S. aureus* HemH (blue). Assay has been compared with coproporphyrin III (black) and coprohaem III (grey) standards, which have been offset for clarity. HPLC conditions started with a solution containing 80% TFA (0.1% v/v) and 20% acetonitrile, rising to 100% acetonitrile in a linear gradient over 30 minutes with absorbance at 400 nm being detected.

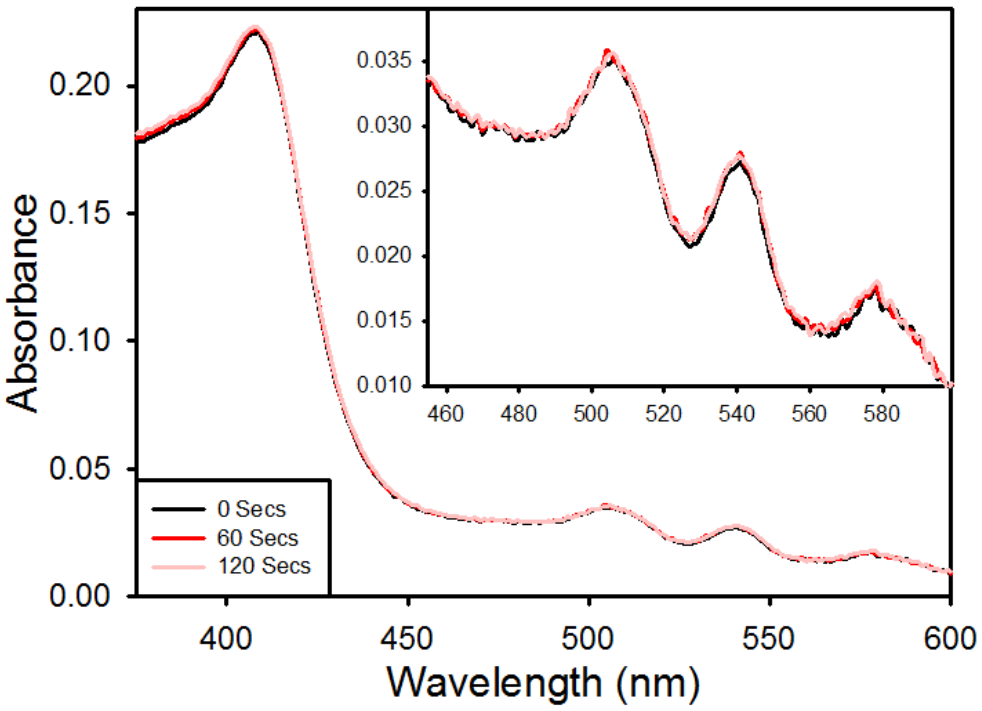


**Figure 4.11 –** Assay for iron insertion into protoporphyrin IX by *S. aureus* HemH. The lack of any noticeable change in spectral characteristics suggests that no reaction is taking place.

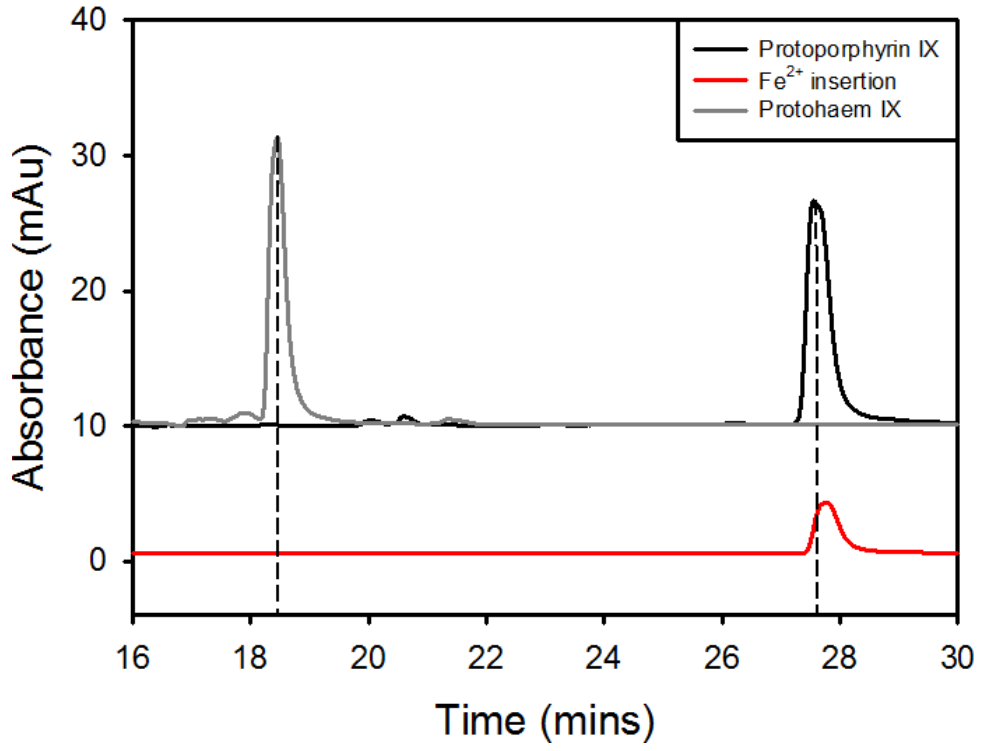


**Figure 4.12 –** HPLC analysis of iron insertion into protoporphyrin IX (red). Assay has been compared with protoporphyrin IX and protohaem IX standards (black and grey respectively, offset for clarity). No peak corresponding to protohaem IX can be observed in the reaction, suggesting that chelation is not occurring. HPLC conditions started with a solution containing 80% TFA (0.1% v/v) and 20% acetonitrile, rising to 100% acetonitrile in a linear gradient over 30 minutes with absorbance at 400 nm being detected.

### 4.2.4.2 – Metal Specificity

With other ferrochelatases being known to chelate a variety of metals, it was of interest to investigate the repertoire of metal chelation that is catalysed by *S. aureus* HemH. Many characterised ferrochelatases have been shown to catalyse the insertion of zinc and nickel, with copper and cobalt being inserted by some ferrochelatases. All metals that were tested appeared to be inserted into the coproporphyrin III molecule by *S. aureus* HemH, each reaction producing different spectral features for the different metalloporphyrins (described below).

Zinc insertion (Figure 4.13) produces a large increase and peak shift from 393 nm to 406 nm, as well as a decrease in the 500 nm peak, a large increase in the peak at 535 nm and a large increase and shift in the 562 nm peak to 572 nm. Cobalt insertion also produces a peak shift from 393 nm, this time to 413 nm, however with a decrease in absorbance (Figure 4.14). The minor peaks show a decrease in magnitude at 500 nm, a subtle increase at 535 nm and 562 nm, with a concomitant broadening of these peaks. Copper insertion elicited a decrease in the 393 nm peak (Figure 4.15), with a broadening of this peak due to a shoulder emerging at roughly 380 nm indicating an incomplete reaction. The 500 nm peak decreases, but is not fully diminished, suggesting that the reaction is slower than for the other metals mentioned so far. There is also a slight decrease in the 535 nm peak which is not seen in other metal insertions, and a slight increase in the 562 nm peak. Nickel insertion also elicited a decrease in the 393 nm peak with a shoulder forming at 401 nm, also indicating incomplete conversion to the metalloporphyrin and a slower reaction (Figure 4.16). In the minor peaks, the 500 nm peak decreased slightly, as with copper, and the two peaks at 535 nm and 562 nm increased in magnitude and moved closer together.

Whilst kinetic analyses of these extra metal substrates were not performed, a comparison of all four of the spectra shown in Figures 4.13-16 does give a clear indication that insertion of zinc and cobalt progresses much faster than that of copper and nickel. This can be seen in the complete shifting of the 393 nm peak in the zinc and cobalt spectra, whereas the peak still exists in the copper and nickel spectra although it is slightly smaller with a peak shoulder forming indicating that insertion is taking place.

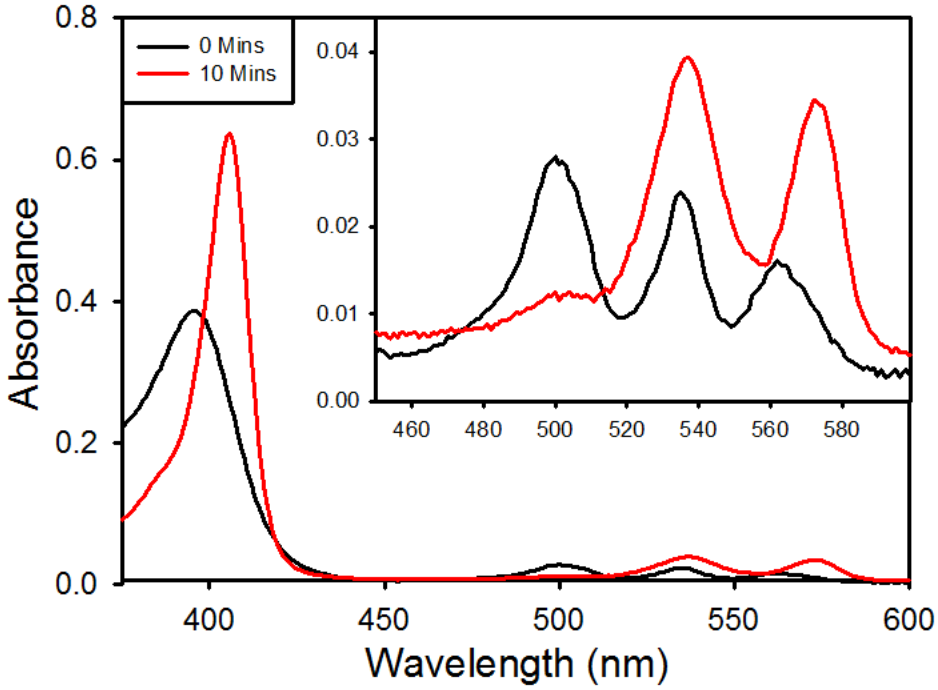


**Figure 4.13 -** Spectral changes during zinc insertion into coproporphyrin III by *S. aureus* HemH after 10 minutes of incubation. Inset shows and expanded view between 455 nm and 600 nm. Full conversion of peaks indicates complete insertion of zinc into the porphyrin.

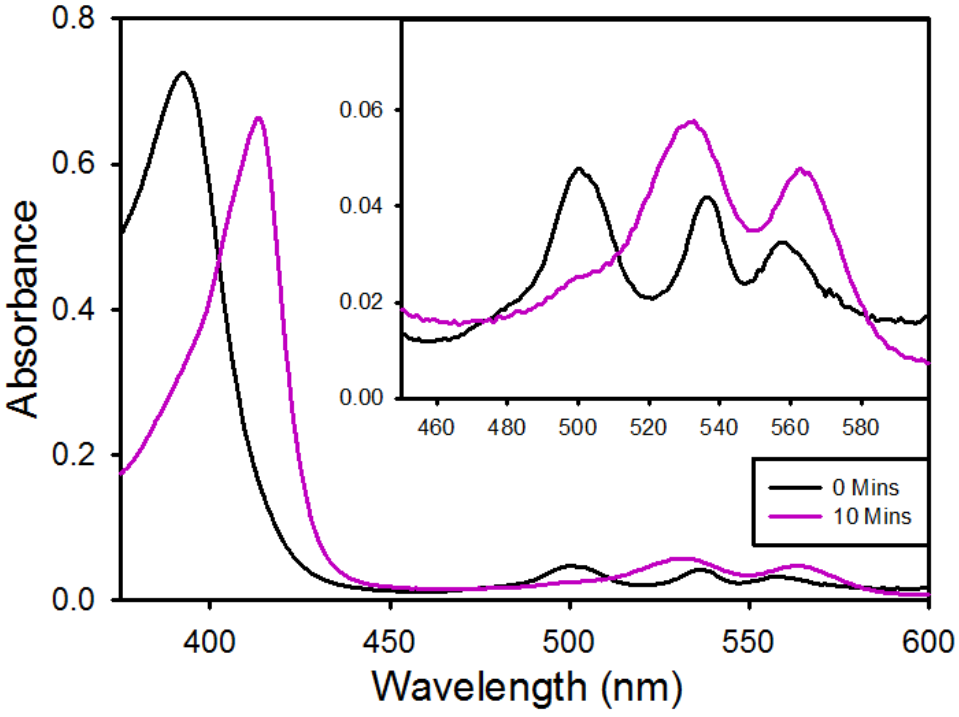


**Figure 4.14** – Spectral changes observed during insertion of cobalt into coproporphyrin III by *S. aureus* HemH over the course of 10 minutes. Inset shows an expanded view of the spectrum between 450 nm and 600 nm. Complete conversion of substrates can be inferred from the complete shifting of the absorption peaks

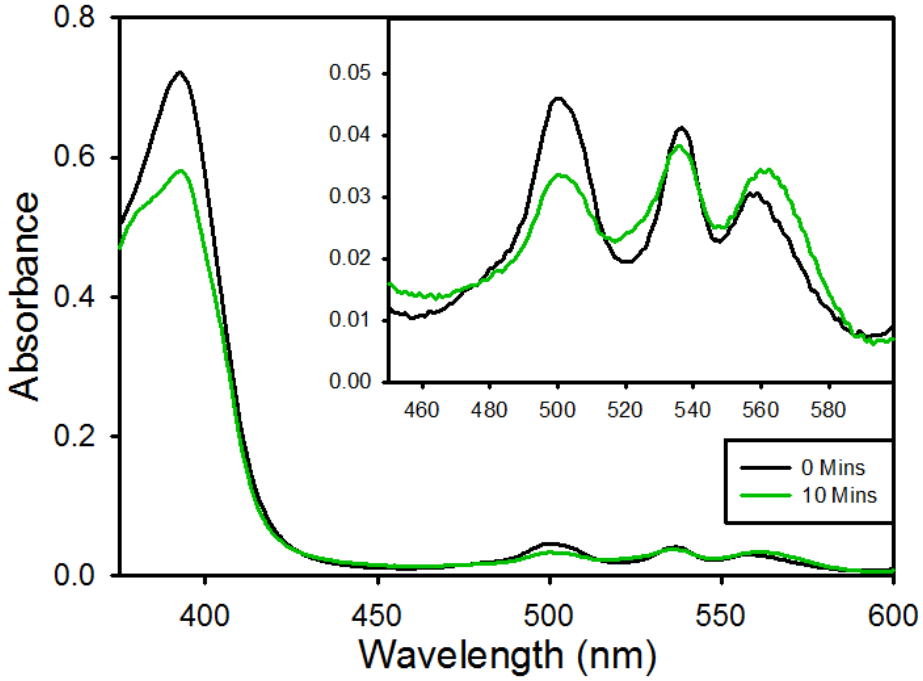


**Figure 4.15 –** Spectral changes observed during insertion of copper into coproporphyrin III by *S. aureus* HemH over the course of 10 minutes. Inset shows an expanded view of the spectrum between 450 nm and 600nm. Formation of a shoulder to the 393 nm peak indicates that there is incomplete conversion and therefore slower insertion has taken place (compared to $Zn^{2+}$ and $Co^{2+}$).

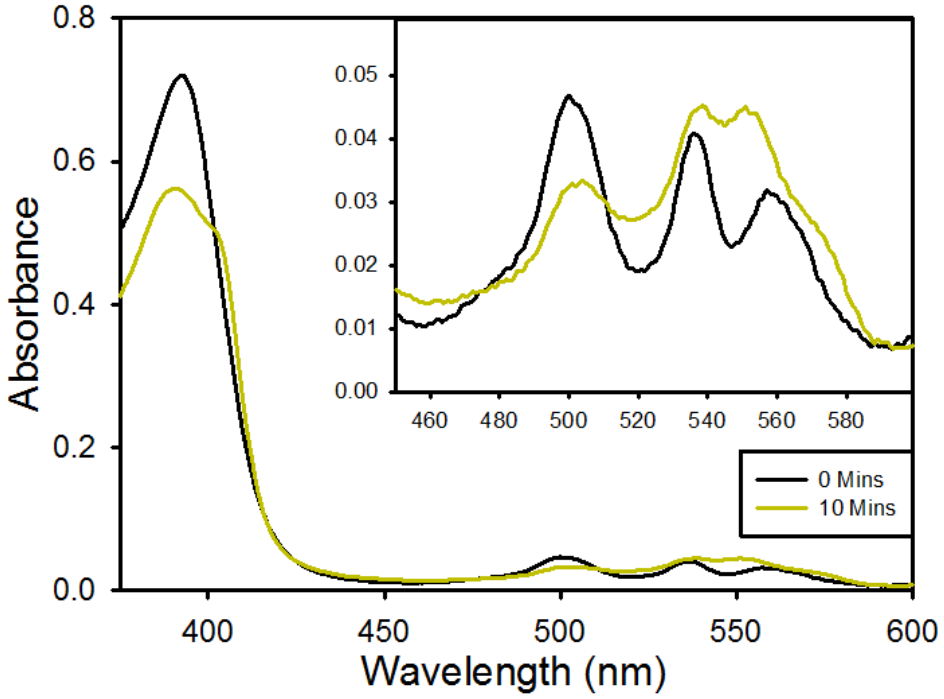


**Figure 4.16 –** Spectral changes observed during nickel insertion into coproporphyrin III by *S. aureus* HemH over 10 minutes. Inset shows an expanded view of the spectrum from 450 nm to 600 nm. Incomplete conversion of coproporphyrin III can be seen by the formation of a shoulder to the 393 nm peak indicating that this, like for copper, is a slow progressing insertion.

## 4.2.5 – Kinetic analysis of *S. aureus* HemH

Kinetic assays detected the formation of iron coproporphyrin by *S. aureus* HemH by measuring the decrease in absorbance at 392 nm using an extinction coefficient of 115 $mM^{-1}cm^{-1}$ (Lobo et al. 2015). This approach was adopted to further investigate the kinetic properties of *S. aureus* HemH.

### 4.2.5.1 – High iron concentrations inhibit HemH activity

Kinetic analyses confirmed the previously published observations that the HemH protein is partially inhibited at iron concentrations above 0.8µM (Figure 4.17). This inhibition does not completely abolish activity, with the rates dropping to between 1.5 and 2.5 $min^{-1}$, depending on the coproporphyrin concentration.

When the iron concentration was kept constant and coproporphyrin concentrations were varied, typical Michaelis-Menten kinetics were observed with no observable substrate inhibition (Figure 4.18). The reaction was performed using an iron concentration of 0.7 µM to maximise activity while ensuring that iron-mediated inhibition was kept to a minimum. These preliminary observations show that the enzyme has a $k_{cat}$ value of 10.5 ± 0.4 $min^{-1}$ with a $K_m$ of 1.5 ± 0.2 µM for coproporphyrin III.

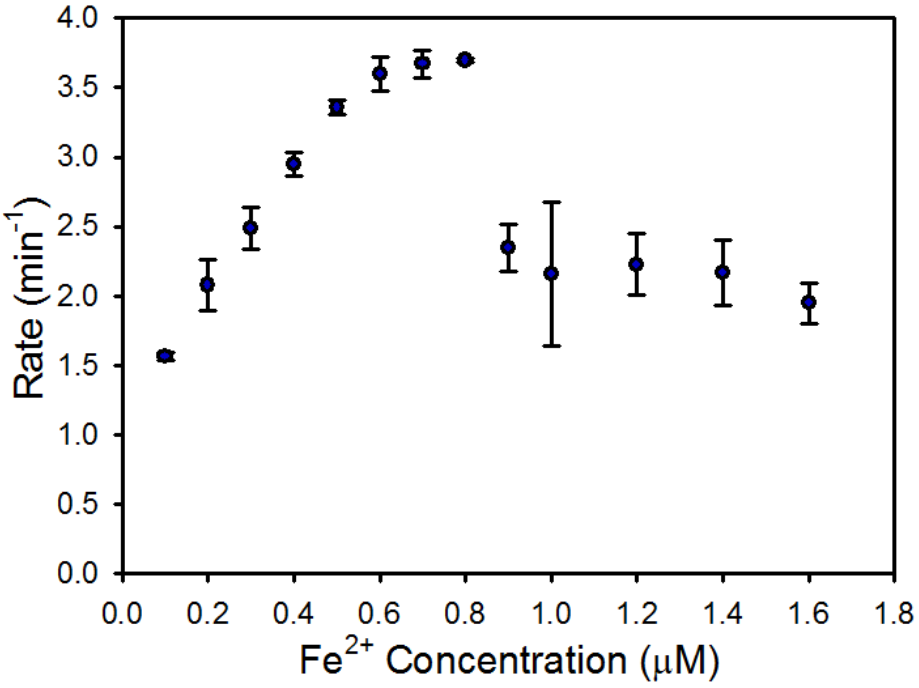


**Figure 4.17** – V *vs.* S kinetics for *S. aureus* HemH varying iron concentration in a constant coproporphyrin concentration. 1μM of coproporphyrin and 50nM of HemH protein was used during these assays. Iron concentrations above 0.8 μM appear to partially inhibit HemH activity. Error bars represent SD values based on 3 repeats.

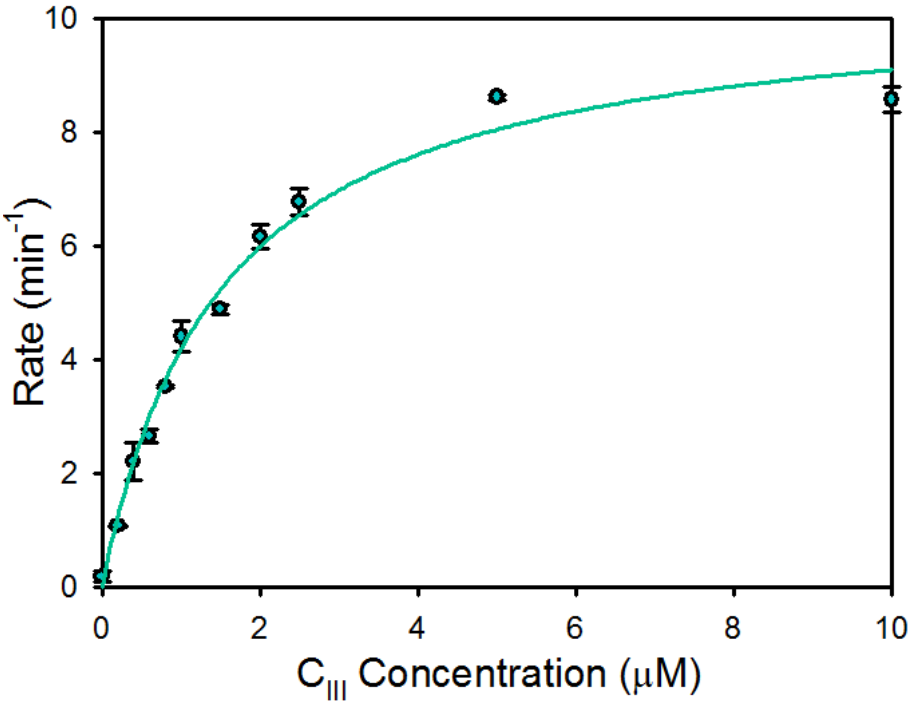


**Figure 4.18** – V *vs* S kinetics for the *S. aureus* HemH with varied coproporphyrin III concentrations and a fixed iron concentration. 0.7μM of iron was used, to keep under the 0.8μM inhibitory iron concentration, with 50 nM of HemH being used in all assays. $k_{cat}$ = 10.5 ± 0.4 $min^{-1}$, apparent $K_m$ = 1.5 ± 0.2 μM. Error bars represent SD values based on 3 repeats.

### 4.2.5.2 – *v vs.* [S] plots for *S. aureus* HemH provide a preliminary kinetic model

The HemH enzyme was assayed under various conditions to determine if the kinetic parameters could be used to provide information on the order of substrate binding. Using freshly purified protein, HemH was assayed across a range of substrate concentrations, whilst keeping the second substrate concentration constant, as performed in section 4.2.5.1. This was then repeated using the same protein, iron and coproporphyrin stocks at two different concentrations of the second substrate, e.g. if iron was the substrate being varied, this experiment would be repeated using three different coproporphyrin concentrations. The fixed concentrations tested for the second substrates were 0.3 µM, 0.5 µM and 0.7 µM. These were chosen so that they would be below the inhibitory iron concentration of 0.8 µM. When iron was varied (Figure 4.19) using fixed coproporphyrin concentrations, the $V_{max}$ values did not vary significantly (5.0 ± 0.26 $min^{-1}$, 5.7 ± 0.37 $min^{-1}$ and 5.5 ± 0.22 $min^{-1}$ for 0.3µM, 0.5µM and 0.7µM respectively). However, as the coproporphyrin concentration increases, the apparent $K_m$ value for iron decreases. When the coproporphyrin concentration was varied at three fixed iron concentrations (Figure 4.20), the $V_{max}$ values did not vary significantly, whilst the $K_m$ values for coproporphyrin *increase* as the iron concentration increases.

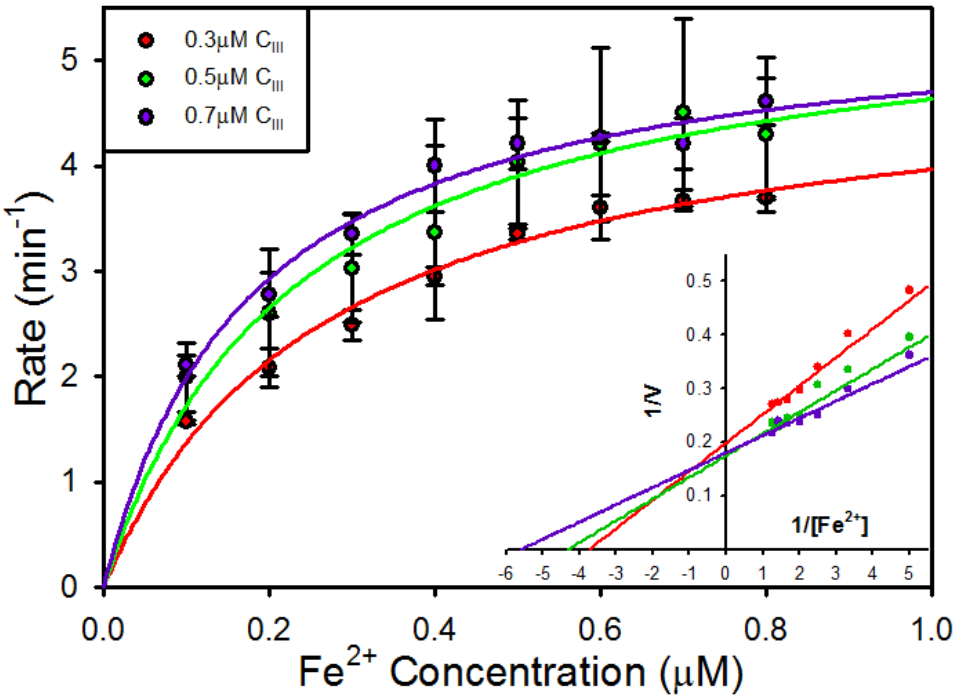


**Figure 4.19** – *v vs.* [$Fe^{2+}$] kinetics at three fixed coproporphyrin III concentrations. The maximal rates are similar for the different concentrations, but the $K_m$ decreases as more coproporphyrin III is present. Inset shows a Lineweaver-Burk plot for these datasets, further highlighting the changes in $K_m$ during these assays. To avoid common problems associated with Lineweaver-Burk plots, regression lines are defined by the kinetic parameters obtained using nonlinear regression analysis in the primary *v vs.* S plots.

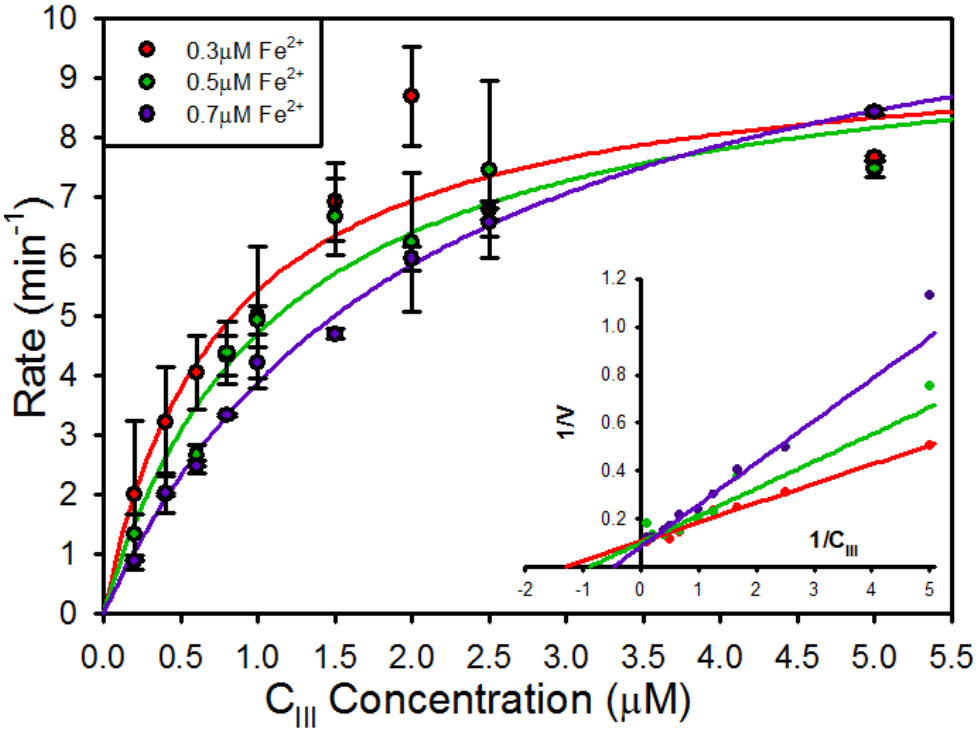


**Figure 4.20** – *v vs.* [$C_{III}$] kinetics at three different, set iron concentrations. Maximal rates appear to be similar with an increase in $K_m$ seen as the iron concentration rises. Inset shows a Lineweaver-Burk plot for the datasets, which further highlights the change in $K_m$. To avoid common problems associated with Lineweaver-Burk plots, regression lines are defined by the kinetic parameters obtained using nonlinear regression analysis in the primary V *vs.* S plots.

### 4.2.5.3 – Magnesium lowers the threshold for iron-mediated inhibition of HemH catalysis

It has previously been reported that magnesium can stimulate the activity of *B. subtilis* HemH when assayed with $Zn^{2+}$ and deuteroporphyrin IX substrates (Lecerof et al. 2003), so it was of interest to investigate the effect of magnesium upon *S. aureus* HemH catalysis. To determine whether magnesium affected iron binding, kinetic analyses were performed whereby the iron concentration was varied and the coproporphyrin concentration was kept constant (Figure 4.21). Surprisingly, rather than stimulating this reaction, iron-mediated substrate inhibition was observed at a lower iron concentration when magnesium was present: ~0.4 µM compared to 0.8 µM (Figure 4.21).

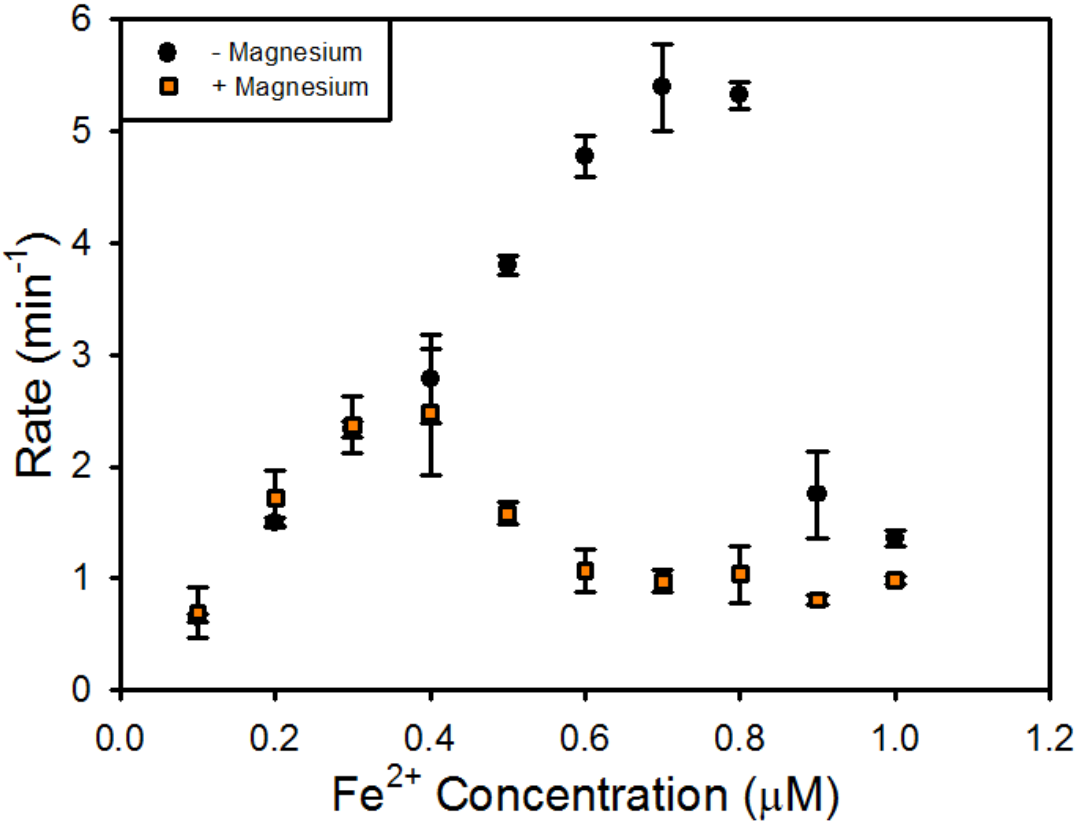


**Figure 4.21** – *v vs.* [$Fe^{2+}$] kinetics of the HemH reaction in the presence (orange) and absence (black) of 4mM $Mg^{2+}$. 50nM of HemH and 2µM of coproporphyrin III were used, with the $Fe^{2+}$ concentration being varied. Presence of magnesium in the assay appears to lower the concentration of $Fe^{2+}$ required for inhibition to 0.4 µM instead of 0.8 µM.

# 4.3 - Discussion

As with other ferrochelatases, the HemH protein from *S. aureus* was shown to catalyse the insertion of metals other than iron into the coproporphyrin ring. With a similar structure to *B. subtilis*, including a tyrosine at residue 13 that appears to be unique to soluble ferrochelatases, it is likely that *S. aureus* would be able to utilise the same metals as this well-studied protein. Spectroscopic analysis of the insertion of $Co^{2+}$, $Cu^{2+}$ and $Ni^{2+}$ into coproporphyrin III by the *S. aureus* protein showed similar patterns for modifications of the three peaks between 475 nm and 575 nm as was seen previously, although the magnitude change of the 560 nm peak did not increase as much as expected for $Co^{2+}$ and $Ni^{2+}$ (Figs 4.14, 4.16). Shifts in peaks could be seen as expected, which suggests that insertion of the metal has occurred. These data demonstrate that as well as iron insertion, *S. aureus* HemH can catalyse the insertion of zinc and cobalt, as well as catalysing less common chelatase reactions with copper and nickel.

It has previously been shown that the HemH from *S. aureus* inserts iron into coproporphyrin III (Lobo et al. 2015), supporting the existence of the coprohaem pathway that was first proposed by the Dailey group (Dailey et al. 2015). This reaction is inhibited by the primary metal substrate in concentrations higher than 0.8 µM, which causes a sharp decrease in activity, but does not totally abolish enzyme activity (Lobo et al. 2015). This inhibition could possibly explain the low levels of activity previously reported for the *B. subtilis* protein (Dailey et al. 2015), which has also been shown to be inhibited by high iron concentrations (Lobo et al. 2015), and may have masked the true maximal rate for the *M. tuberculosis* protein if it is also inhibited by the iron concentrations in the assays. An intriguing observation is that iron-mediated substrate inhibition has only been shown to occur when coproporphyrin III is used as a substrate, with successful assays utilising protoporphyrin seemingly unaffected by changes in iron concentration and producing classic Michaelis-Menten kinetics (Lecerof et al. 2003; Lobo et al. 2015). A similar pattern to previous work was seen in the reaction utilising coproporphyrin III during this work, with a sharp decrease in activity with an iron concentration above 0.8 µM (Figure 4.17). In our hands however, activity with protoporphyrin could not be measured (Figures 4.11 and 4.12). With coproporphyrin III as the

porphyrin substrate, our data reveal a $k_{cat}$ value of 10.5 ± 0.4 $min^{-1}$ that is similar to published constants for other ferrochelatases, with slightly higher values being observed for *C. crescentus* and *P. putida* (see Table 4.1). Intriguingly, significant activity ($k_{cat}$ = 15.3 $min^{-1}$) has been reported for *S. aureus* with protoporphyrin IX (Lobo et al. 2015), although activity with this porphyrin could not be detected in our hands.

Further kinetic analysis was performed, aimed at determining the optimal substrate binding order and an overall mechanism for the reaction. These assays (Section 4.2.5.2) show that the $V_{max}$ values remain unchanged across several datasets but the $K_m$ values for both iron and porphyrin substrate change as the concentration of the accompanying substrate varies. When iron was varied (Figure 4.19) using fixed coproporphyrin concentrations, the $V_{max}$ values did not vary significantly (5.0 ± 0.26 $min^{-1}$, 5.7 ± 0.37 $min^{-1}$ and 5.5 ± 0.22 $min^{-1}$ for 0.3 µM, 0.5 µM and 0.7 µM iron respectively). However, as the coproporphyrin concentration was increased, the $K_m$ value for iron decreased. This suggests that as the coproporphyrin levels increase, HemH can more readily utilise the iron substrate. When the coproporphyrin concentration was varied at three fixed iron concentrations (Figure 4.20), the $V_{max}$ values did not vary significantly, whilst the $K_m$ values for coproporphyrin *increased* as the iron concentration increased. This suggests that coproporphyrin binding is less efficient at higher iron concentrations.

Overall it appears that the most efficient way for the reaction to take place is for the porphyrin substrate to bind to HemH first, with the iron binding second. Whilst this is unlikely to affect the overall maximal rate, at lower concentrations of iron, a higher proportion of HemH molecules will have bound iron resulting in a higher steady state rate. This kinetic model, which only applies for iron concentrations below the 0.8 µM inhibitory concentration, can be seen in Figure 4.22.

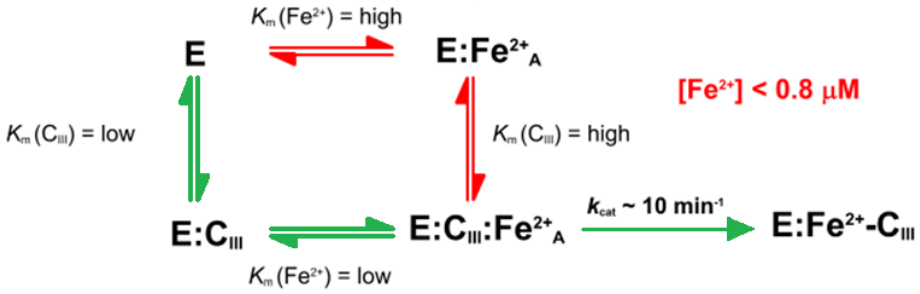


**Figure 4.22 –** Kinetic model for *S. aureus* HemH at [$Fe^{2+}$] < 0.8 µM. The green pathway represents the favourable route where coproporphyrin binds first. The red arrows show a less efficient mechanism where iron binds first. This mechanism would only apply to iron concentrations below 0.8µM.

At higher iron conditions (above 0.8 µM), it is hypothesised that bound iron at a second site may be acting as a noncompetitive inhibitor whereby saturation of this metal site results in a lower rate of metal chelation but does not completely abolish enzyme activity (Figure 4.22). This would explain the pattern of substrate inhibition that has been observed for both the *S. aureus* and *B. subtilis* HemH enzymes (Lobo et al. 2015). One possible molecular explanation for this phenomenon could be iron binding to an inhibitory metal site underneath the porphyrin which has been observed in studies with *B. subtilis* HemH using the inhibitor $Cd^{2+}$ (Lecerof et al. 2003). $Cd^{2+}$ was shown to bind to H262 in the *B. subtilis* enzyme, which corresponds to H261 in *S. aureus* HemH.

Another explanation for this phenomenon could be linked to the stimulation effect of $Mg^{2+}$ binding, where previously hypothesised repulsion between metal ions could stimulate the insertion of metal (zinc in this case) into the porphyrin (Lecerof et al. 2003). Attempts to recreate this result using the natural substrates coproporphyrin III and iron with magnesium as a molecular probe for the outer metal site have shown that rather than stimulating the reaction, iron-mediated inhibition is exacerbated by magnesium: the inhibition occurred at approximately 0.4µM iron rather than 0.8 µM (shown in Figure 4.21). This could be explained by the presence of a metal at the outer binding site influencing binding at the catalytic metal binding site via potential conformational changes in the porphyrin binding cleft. This change may hinder the ability of coproporphyrin III to bind efficiently enough to allow for iron insertion to occur. This explanation seems plausible when it is assumed that the presence of magnesium in a saturating concentration will only occupy the outer metal binding

site, and therefore remove one of two potential iron binding sites. When this occurs, the concentration of iron needed for inhibition to occur drops to half of the concentration required when iron is the only metal present and two metal binding sites are available for iron to bind to. This would seem to suggest that the partial inhibition is due to the occupancy of both metal sites before coproporphyrin can bind, which causes a conformational change that slows down the ability of coproporphyrin III to bind deep enough in the active site for iron insertion to occur.

Overall, the data in this chapter are consistent with iron being able to bind to more than one site on *S. aureus* HemH when it is present in high levels, resulting in partial inhibition of iron insertion into coproporphyrin III. This model (Figure 4.23) dictates that when ferrous iron levels elevate beyond 0.8 µM, iron would bind first to the inner metal binding site (labelled as A in Figure 4.23) with a second iron atom binding to the second binding site (either the inhibitory H261 or the $Mg^{2+}$ binding site, labelled as B in Figure 4.23), resulting in a lower affinity for coproporphyrin and therefore a lower $k_{cat}$ value of 2 $min^{-1}$.

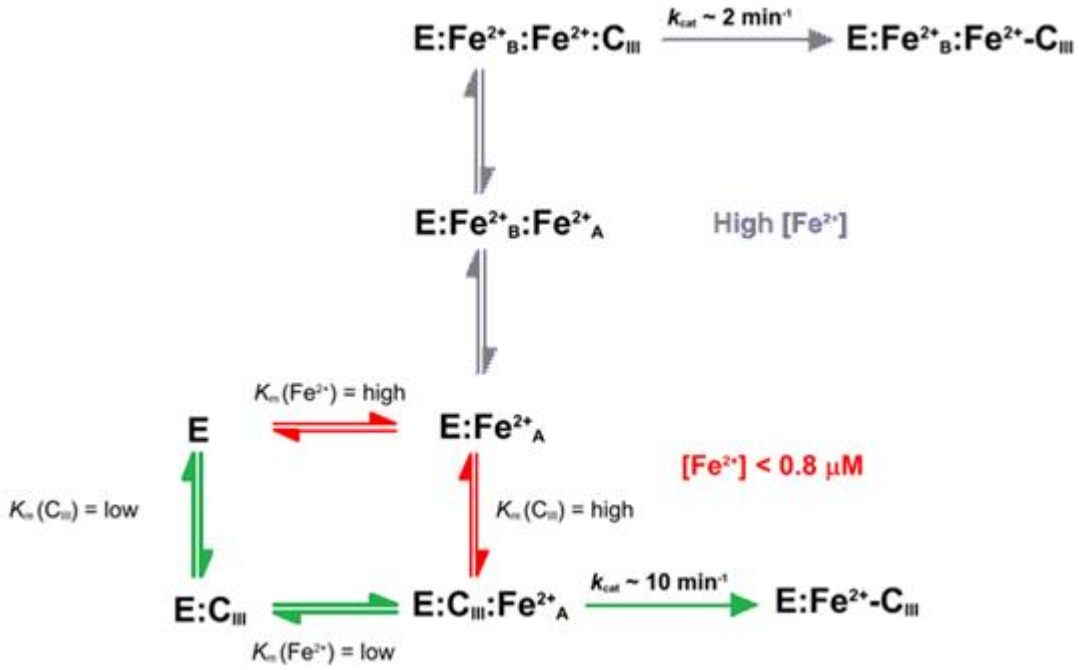


**Figure 4.23–** Kinetic model of the *S. aureus* ferrochelatase reaction and the proposed mechanism for the iron-dependent inhibition based on kinetic data. The green route represents the most efficient route, binding coproporphyrin III first, red represents a slightly less efficient route with iron binding first. The grey route represents the iron-mediated inhibition at high iron concentrations.

Chapter V

# Structural modelling and biochemical/ kinetic analysis of the HemQ coprohaem III decarboxylase

# Summary

HemQ is an enzyme that is essential for haem synthesis in certain Gram-positive bacteria, and has recently been shown to catalyse the final step in the coproporphyrin-dependent pathway converting coprohaem III to protohaem IX (Dailey et al. 2015). HemQ has previously been shown to bind both protoporphyrin IX and protohaem IX (Mayfield et al. 2013) in addition to the presumed binding of its native substrate, coprohaem III. The coprohaem decarboxylase reaction has been shown to require the presence of either flavin mononucleotide (FMN) or hydrogen peroxide ($H_2O_2$) for activity (Dailey et al. 2015), with $H_2O_2$ being required at a five-fold excess over coprohaem for complete conversion (Lobo et al. 2015). In addition, a harderohaem intermediate has been shown to form during conversion of coprohaem III to protohaem IX (Celis et al. 2015).

In the current work, further investigations into the HemQ enzyme provide functional insights beyond the published work described above. Fluorescence titrations were used to quantify binding affinities of protoporphyrin IX, protohaem IX, coproporphyrin III and coprohaem III. These data indicate that HemQ can bind non-metallated porphyrins with a higher affinity than metalloporphyrins, with the surprising observation that coprohaem III has the weakest affinity out of the four tetrapyrroles tested. Subsequent kinetic analyses using discontinuous assays revealed that the reaction follows a Michaelis-Menten kinetic profile, with a $V_{app}$ of 1.74 ± 0.12 $min^{-1}$ and a $K_m$(peroxide) of 90.4 ± 18.0 µM in the presence of 10 µM coprohaem. When the coprohaem concentration was varied it was not possible to estimate $V_{max}$ or $K_m$, although the maximum measured rate was 2.5 $min^{-1}$ which is comparable to maximal rates measured for HemY and HemH.

# 5.1 – Introduction

HemQ is a protein that has only been discovered recently (Dailey et al. 2010) and has been determined to be a coprohaem decarboxylase, converting the propionate groups on rings A and B of coprohaem III to vinyl groups and forming protohaem IX (Dailey et al. 2015). This reaction is the final step in haem synthesis in organisms that utilise the coproporphyrin-dependent pathway, i.e. HemQ is the final protein in these organisms. Biochemical characterisation of this protein is at an early stage, and a crystal structure of HemQ is not yet available.

## 5.1.1 – Discovery and importance of HemQ

HemQ was first discovered as a protein that was essential for haem synthesis in Gram-positive organisms, but with an unknown function. Initial studies on haem synthesis mutants of *E. coli* (Δ*hemG* or Δ*hemH*) showed that supplementing the haem defective strains with a plasmid encoding either *hemY* or *hemH* from Gram-positive organisms did not restore the synthesis of haem (Dailey et al. 2010). From here it was deduced that either membrane associated HemY and HemH proteins were required, or an extra protein was required. Subsequent genomic analysis of Actinobacteria showed that an open reading frame for a protein, annotated as a chlorite dismutase-like hypothetical protein and now referred to as *hemQ*, was often found adjacent to either *hemY* or *hemH*. This gene was also found to be fused in frame with *HemH* in *P. acnes*, leading to speculation that this hypothetical protein is involved in haem synthesis in some way.

A BLAST search of the amino acid sequence for this open reading frame identified chlorite dismutase-like hypothetical proteins as homologues, and formed a cluster of the orthologous proteins named group COG3253 (Dailey et al. 2010). This group was shown to have three sub-groups: proteins that have been shown to have chlorite dismutase activity, proteins without a defined function, yet are not chlorite dismutases, and proteins that are only present in Actinobacteria and had a completely unknown function at the time. Expression of this protein in a Δ*hemG* or Δ*hemH E. coli* mutant along with the Gram-positive *hemY* and *hemH* resulted in restoration of haem synthesis, but would not complement the mutants if expressed with just one of these proteins.

The deletion of *hemQ* from *S. aureus*, which is remote from other haem synthesis genes on the chromosome, has been shown to produce a small colony growth variant which is typical of a poorly respiring strain. A similar phenotype has also been observed for strains with defective tetrapyrrole synthesis, by way of a deleted *hemB* gene (Von Eiff et al. 1997; Mayfield et al. 2013). This phenotype can be alleviated if the cells are grown with exogenous haem present, further strengthening the link between HemQ and haem synthesis (Mayfield et al. 2013). Furthermore, these studies revealed that Δ*hemQ* mutants accumulate coproporphyrin III, with cellular levels of this porphyrin being five times higher than observed in wildtype *S. aureus* cells.

## 5.1.2 – Characterisation of recombinant HemQs

Recombinant HemQs that have been studied have been shown to exist as multimeric proteins that have the ability to bind haem, with the *S. aureus* HemQ shown to be a homohexamer when haem is bound (Dailey et al. 2010; Mayfield et al. 2013). HemQ monomers appear to vary in size, but have been described as migrating on SDS-PAGE at rates corresponding to proteins of 26 kDa and 30 kDa.

Due to the similarities with haem-binding chlorite dismutases, initial studies focussed on the haem-bound form of HemQ rather than the native protein. Addition of haemin to the protein prior to purification resulted in a bright red protein and a vast increase in the amount of haem detected by UV/Vis spectroscopy when compared to the protein purified without haemin (Dailey et al. 2010). Initial attempts to determine the haem-binding affinity of *M. tuberculosis* HemQ via UV-vis spectroscopy suggested that haem bound poorly, with a $K_d$ of 30-40μM, although the binding constant could not be accurately determined (Dailey et al. 2010). Subsequent analysis of the *S. aureus* HemQ using a fluorescence titration method revealed that haem binds with a $K_d$ of 1.70 μM (Mayfield et al. 2013). This value is much lower than the estimated $K_d$ for the *M. tuberculosis* HemQ but is still high when compared with some other haem binding proteins, which can reach as low as 0.88 $x10^{-4}$ nM for sperm whale myoglobin (Culbertson & Olson 2010). Interestingly it was also discovered that HemQ can bind protoporphyrin IX as well, with a higher $K_d$ of 2.21μM (Mayfield et al. 2013).

The haem-bound form of HemQ has also been shown to have low levels of peroxidase and catalase activities, as has been seen with other members of the COG3253 family, with activities reported to be between 3 and 4 orders of magnitude lower than those for typical peroxidases and catalases (Dailey et al. 2010; Mayfield et al. 2013). The low affinity for haem and peroxidase/catalase activity has led to speculation that a catalytic role with $H_2O_2$ was unlikely for HemQ *in vivo* (Mayfield et al. 2013), although the use of $H_2O_2$ as an electron acceptor for coprohaem decarboxylation does now seem like a possibility. Chlorite dismutase activity was also assessed for *S. aureus* HemQ, although no activity could be detected with chlorite concentrations up to 20mM (Mayfield et al. 2013). Another interesting observation for the haem-bound form of HemQ was that addition of this protein to a *P. acnes* HemY protoporphyrinogen oxidase assay caused a stimulation of the reaction, as mentioned in Chapter III, which did not occur when unbound HemQ was added (Dailey et al. 2010). The lack of chlorite dismutase activity and low peroxidase/catalase activity, combined with the amount of evidence linking this protein with the final stages of haem synthesis, suggested that the true role of this protein was in the terminal steps of haem synthesis.

## 5.1.3 – HemQ catalyses the final reaction of the coprohaem pathway

Further studies on HemQ were undertaken to elucidate a role in the haem biosynthetic pathway. Deletion of *hemQ* from *S. aureus* resulted in accumulation of coproporphyrin III (Mayfield et al. 2013) rather than protoporphyrin IX, which would have been expected should the other proteins of the classical haem synthesis pathway be working effectively. As mentioned in section 1.2.4, it appears that the gene annotated as *hemN* from Gram-positive organisms does not encode for an active coproporphyrinogen oxidase, and coproporphyrin III rather than protoporphyrin IX has been identified as an intermediate in these organisms (Dailey et al. 2015; Jacobs et al. 1971). This, along with the well-known observation that the *B. subtilis* HemY can oxidise coproporphyrinogen III (Hansson et al. 1997), suggested that other pathways that synthesise haem exist, bypassing protoporphyrin IX as a pathway intermediate.

HemH proteins from Gram-positive organisms had been shown to catalyse insertion of iron into coproporphyrin (see chapter 5), and HemY, HemH and HemQ were all required for haem synthesis to occur in *E. coli* Δ*hemG* or Δ*hemH* mutants (Dailey et al. 2010; Lobo et al. 2015). This led to the assertion that HemQ must be involved in converting coprohaem III into protohaem IX. This reaction had been observed in the alternative haem biosynthesis pathway, also as the final reaction, where the protein AhbD converts coprohaem to protohaem (Palmer et al. 2014). Assays involving HemY, HemH and HemQ, starting with coproporphyrinogen III and iron, were analysed by mass spectrometry and it was found that the products formed were protohaem and a monovinyl, monopropionyl haem intermediate (Dailey et al. 2015; Lobo et al. 2015), which was later revealed to be harderohaem isomers III and IV, with the main intermediate likely to be isomer III (Celis et al. 2015). The reaction only produced small amounts of protohaem when assayed without HemY and was determined to require the electron acceptors $H_2O_2$ or FMN to allow for full conversion of coprohaem to protohaem (Dailey et al. 2015). In assays containing HemY, HemH and HemQ, $H_2O_2$ could be produced by the HemY reaction and would likely be utilised by HemQ for the decarboxylation reaction. No differences to this reaction could be detected when FMN was present (Dailey et al. 2015).

## 5.1.4 – Model for the HemQ mechanism

HemQ is one of two enzymes that have been shown to convert the propionates of coprohaem to the vinyl groups found in protohaem, with the other enzyme being AhbD in the alternative haem biosynthetic pathway (Bali et al. 2011). AhbD is a radical *S*-adenosylmethionine (SAM) enzyme and the cleavage of SAM by a [4Fe-4S] cluster creates 5'-deoxyadenosyl (dAdo) radicals that are used by the enzyme to sequentially cleave the propionate side chains on rings A and B to form vinyl groups (Lobo et al. 2014). This mechanism is similar to the process employed by HemN, the classical oxygen-independent coproporphyrinogen oxidase, which is also a radical SAM protein and cleaves the same propionate side chains in the same sequential manner, forming harderoporphyrinogen as an intermediate (Layer et al. 2002). The absorption spectrum of HemQ lacks spectral features that are characteristic of iron-sulphur clusters, suggesting that HemQ enzymes do not have these clusters and therefore catalyse the reaction via a different mechanism (Dailey et al. 2010;

Mayfield et al. 2013; Celis et al. 2015). It has also been noted that the HemQ reaction does not occur when iron is absent from the porphyrin, as assays with Ni-coproporphyrin III did not result in conversion to Ni-protoporphyrin IX, strongly suggesting that the central iron is vital for activity (Dailey et al. 2015). Considering the peroxidase activity and the requirement for $H_2O_2$, it was hypothesised that a radical mechanism was responsible for the decarboxylation, resulting from the breakdown of Compound 0 (a $Fe^{III}$-OOH complex), although the precise nature of this reaction is not entirely clear (Celis et al. 2015). The breakdown of Compound 0 is predicted to follow one of three paths: The first being a heterolytic breakdown following the input of a proton to form Compound I ($Fe^{IV}$=O) and a water molecule, with the second and third paths being either a homolytic or concerted breakdown of this compound to form $Fe^{IV}$=O, water and a β-carbon radical. It has been predicted that the Compound I path may not be used, as HemQ seems to lack the amino acid residues required for formation of this compound (a distal His-Arg and proximal His-Glu/Arg motif) that are usually found in peroxidases, and therefore the reaction may proceed via the homolytic or concerted breakdown of Compound 0, although the exact mechanism is not entirely clear (Celis et al. 2015). The overall mechanism for the decarboxylation of coprohaem seems to require a free radical, formed either as part of a peroxidase reaction by HemQ or as a dAdo radical produced in the AhbD radical-SAM based reaction. The existence of two enzymes that catalyse the same reaction in different ways is not unheard of in haem synthesis, as both coproporphyrinogen oxidase and protoporphyrinogen oxidase reactions have multiple enzymes catalysing the same reactions (see section 1.2.2). The coprohaem decarboxylases AhbD and HemQ seem to follow the same pattern as other branches in tetrapyrrole synthesis pathways, with AhbD catalysing a reaction that is anaerobic, due to being a radical-SAM protein (Lobo et al. 2014), and HemQ being able to function in the presence of oxygen (Dailey et al. 2015). Studies looking at the co-occurrence of proteins that are involved in the decarboxylation of coproporphyrin-based molecules (i.e. HemF, HemN, HemQ and AhbD) showed that HemQ and AhbD are almost always found in organisms that lack either HemF or HemN (Dailey et al. 2015). A comparison between organisms containing HemQ and AhbD shows that 62.7% of organisms that contain AhbD also contain HemQ, which represents 27.6% of the 152 HemQ-containing organisms. It was also found that over 90% of both of these organisms also contain a HemY protein (Dailey et al. 2015).

## 5.1.5 – Aims of this chapter

The aims of this chapter were to investigate the ability of HemQ to bind different porphyrin ligands, determining binding characteristics by fluorescence titration. The hypotheses tested, based on the ability of HemQ to be purified with a variety of porphyrins bound, were:

- HemQ can bind protohaem IX, protoporphyrin IX, coproporphyrin III and coprohaem III.

- Metalloporphyrins will bind tighter than metal-free porphyrins.

A kinetic assays, both continuous and stopped assays, were also devised and trialled to determine preliminary kinetic parameters for the HemQ decarboxylation reaction, with the hypothesis that HemQ operates within a kinetic range similar to the ferrochelatase reaction.

# 5.2 – Results

## 5.2.1 – Structural analysis of *S. aureus* HemQ

### 5.2.1.1 – Analysis of the primary structure of HemQ

A NCBI protein BLAST search was performed using the protein sequence of *S. aureus* HemQ and it was found that there is high level of conservation between HemQ proteins within the *Staphylococcus* genus, with an average sequence identity of 82%. The BLAST search also showed that *B. subtilis* has a similar protein that has a 64% identity to the *S. aureus* HemQ. HemQ proteins from *M. tuberculosis* and *P. acnes* were also analysed, as they have been experimentally verified to decarboxylate coprohaem: *S. aureus* HemQ exhibits 22% and 24% sequence identity to the *M. tuberculosis* and *P. acnes* proteins, respectively. With the exception of the *M. tuberculosis* and *P. acnes* proteins, all other putative HemQ proteins are annotated as haem binding proteins in the NCBI protein database. The protein from *M. tuberculosis* is annotated as a chlorite dismutase and the protein from *P. acnes* is listed as a ferrochelatase, due to being fused with the HemH protein. *S. aureus* HemQ exhibits 44% identity with a haem-binding protein from the bacterium *Thermus thermophilus*, for which a crystal structure exists (Ebihara et al. 2005). This structure, listed as 1DVH in the protein databank, was originally annotated as a putative chlorite dismutase but has recently been changed to a novel haem binding protein and predicted to be a HemQ (Dailey et al. 2015).

A multiple sequence alignment for these sequences is shown in Figure 5.1. The conserved residues appear to mainly be located in the C- terminal half of the protein across the *S. aureus, S. epidermidis, B. subtilis* and *T. thermophilus* proteins. This region contains the residues that are responsible for haem binding when the 3D structures of the *T. thermophilus* and the predicted *S. aureus* HemQ were analysed (see section 5.2.1.2). This region is well-conserved, including a series of residues (Y145, P146, H172, Q185 and W198 in *S. aureus*) that are highly conserved in all HemQ proteins that have been experimentally investigated.

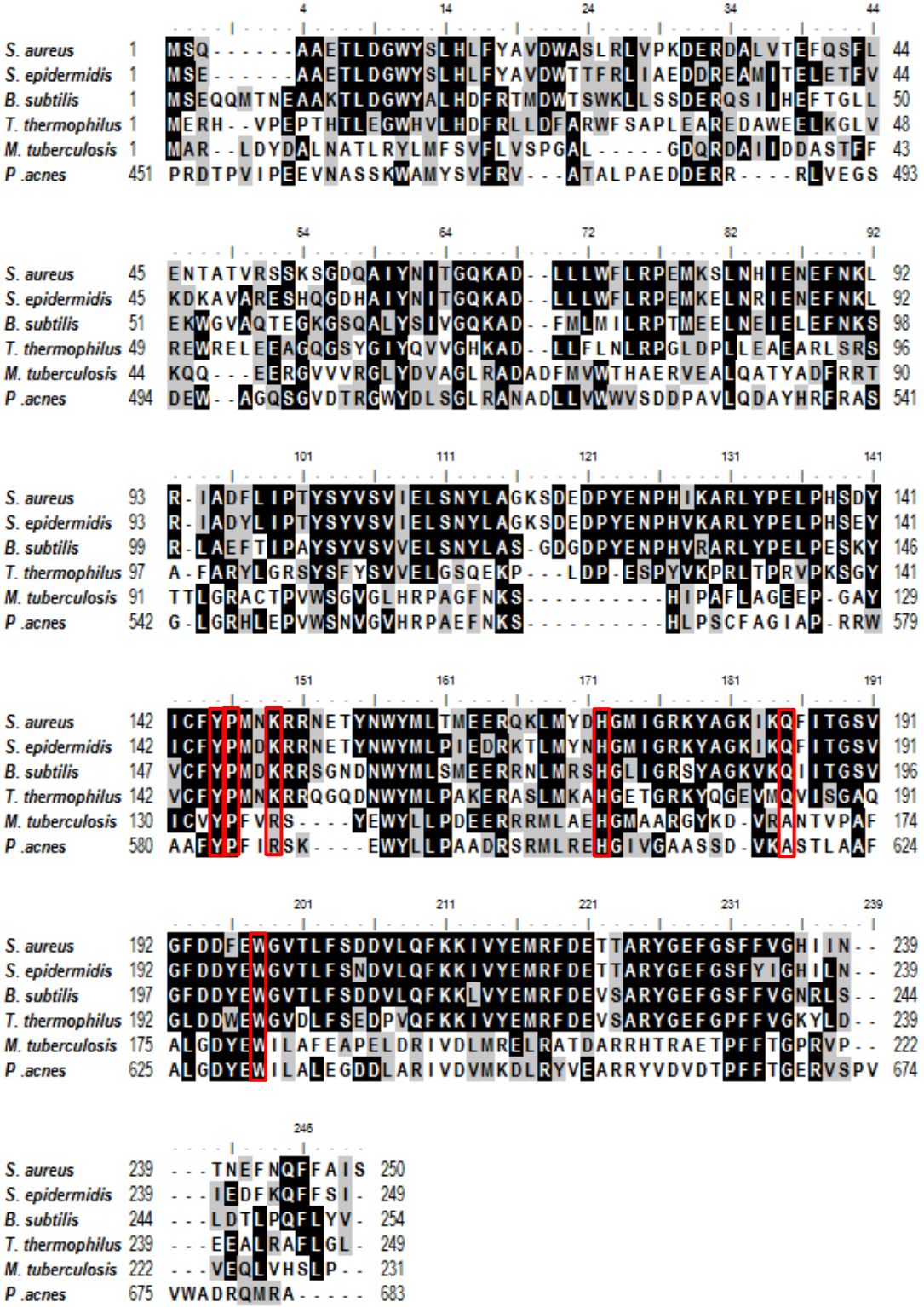


**Figure 5.1 –** Multiple sequence alignment of HemQ proteins from various organisms. Black shading represents identical residues whereas grey denotes functional similarity. The *P. acnes* sequence starts at residue 451 due to the native protein existing as a fusion with HemH, which is located at the N-terminus. Highlighted in red are conserved residues that are thought to be important for the decarboxylase reaction.

### 5.2.1.2 – Analysis of a structural model for HemQ

A predicted structural model for the HemQ from *S. aureus* was obtained using the amino acid sequence and the RaptorX software (Peng & Xu 2011), and was analysed using CCP4MG (McNicholas et al. 2011). The haem-binding protein from *T. thermophilus* (1VDH) was one of the structures selected by RaptorX as a template for the generation of a structural model for HemQ from *S. aureus*. This protein is predicted to be a HemQ (Dailey et al. 2015), and the crystal structure was solved without any ligands in the tetrapyrrole-binding cleft (Ebihara et al. 2005). A direct comparison of 1VDH and the *S. aureus* HemQ model is shown in Figure 5.2, which shows that the basic secondary and tertiary structures are very similar. The only obvious difference is the protein loop near the haem-binding site of the HemQ model, which has an extra helical structure and also a small insertion of three amino acids (bottom left of the structures in Figure 5.2). A coprohaem III molecule has also been modelled into the active site based on the position of a haem molecule in a similarly structured chlorite dismutase from *Dechloromonas aromatica* (Goblirsch et al. 2010), which has been used previously for comparison studies with the *T. thermophilus* HemQ structure (Celis et al. 2015).

The active site of the *T. thermophilus* model is proposed to be comprised of a series of residues between the α-helices α4 and α5 and the β-strands β5, β8, β9 and β10a (Ebihara et al. 2005). The main residues proposed to be involved in binding haem are H172, which is thought to co-ordinate the iron in the (copro)haem group, K149 and R218, which creates a positively charged environment, a typical feature of catalases and peroxidases, which stabilises the propionate groups on the haem molecule. Other residues that reside in this pocket are primarily hydrophobic in nature, which also supports the binding of a haem group (Ebihara et al. 2005). In addition to these residues, there is an aspartate residue that may form a hydrogen bond with H172, a common feature of peroxidase-like enzymes. Furthermore, the triad of hydrogen-bonding residues opposite the H172 residue (N185, Y145, W198) are typical of a peroxidase-like distal pocket. These identified residues can be seen in Figure 5.3, which shows the active site for both *S. aureus* and *T. thermophilus*.

**Figure 5.2 –** Comparison of the predicted HemQ structure from *S. aureus* (blue) and the crystal structure that the model was based on, HemQ from *T. thermophilus* (purple). Coprohaem III (green) has been modelled into the active site.

As mentioned in section 5.2.1.1, the active site is at the C-terminus of the protein, an area that is well-conserved between different HemQ proteins (Figure 5.1). The predicted model for *S. aureus* contains the majority of residues identified as being involved in haem binding in the *T. thermophilus* structure (Figure 5.3). These enzymes have been reported to lack a hydrogen bonding network that is normally present in the proximal haem-binding pocket of the closely related chlorite dismutase enzymes (Hofbauer et al. 2015; Hofbauer et al. 2016), although the 'HemQ' structures analysed did not appear to belong to any of those that had been experimentally verified. Initial comparisons between the HemQ proteins that have been experimentally verified and chlorite dismutases is the lack of a conserved arginine, which in most HemQs is replaced by a glutamine residue (Q185 in *S. aureus*) but is occasionally occupied by an alanine residue (in *M. tuberculosis* and *P. acnes*, see Figure 5.1).

Other conserved residues present in the haem binding pocket include a conserved tyrosine and proline doublet (Y145 and P146) and a tryptophan (W198) that is adjacent to the haem propionates. Aside from an adjacent glycine residue, there is a high level of variability close to the invariant axial histidine (H172). There is also a lysine/arginine residue (K149 in *S. aureus*) that could potentially stabilise the haem propionates and has the potential to contribute to a proximal hydrogen bonding network via water molecules. Other residues that are believed to be important to the HemQ proteins are W157, Y158, R165, E197 and R218, all of which are fully-conserved in the HemQs that are analysed herein. Several of these residues are shown in Figure 5.3 where they are compared to their locations in the *T. thermophilus* crystal structure, with coprohaem III having been modelled into the cleft. Residue locations between the two proteins appear to occupy very similar spaces, further highlighting the likely importance of these conserved residues.

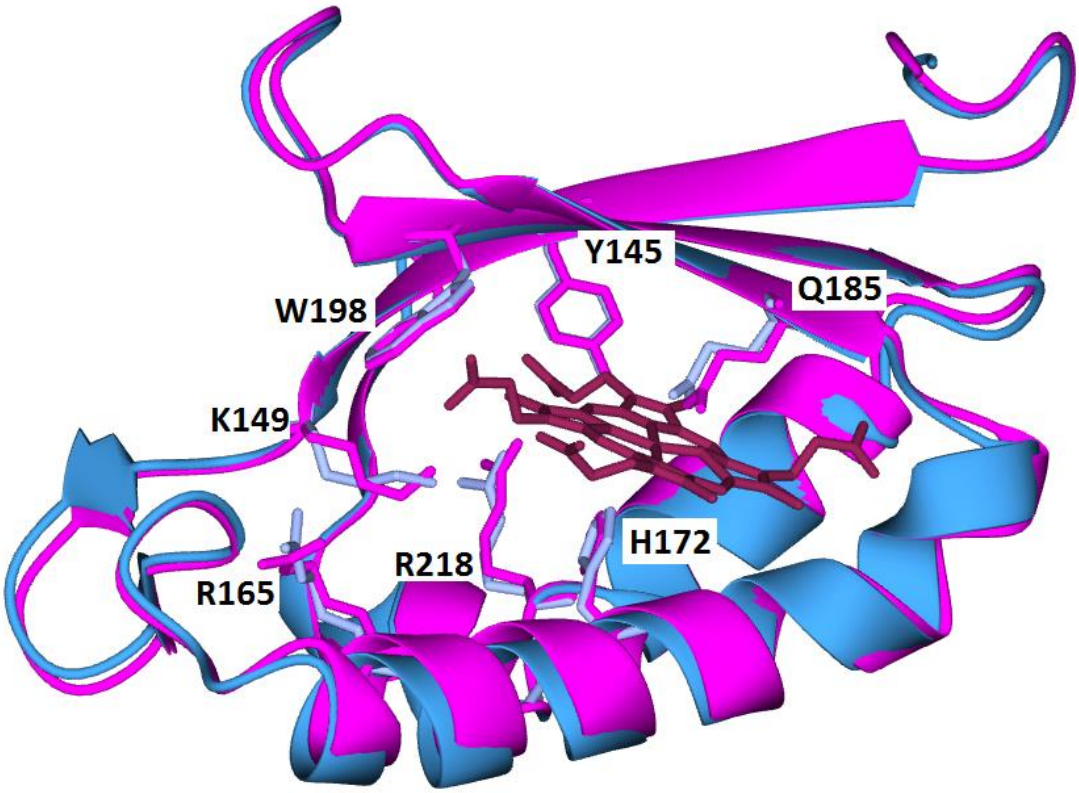


**Figure 5.3 –** The haem-binding sites of HemQ proteins from the *T. thermophilus* crystal structure (pink) and the *S. aureus* predicted model (blue) with coprohaem III modelled into the binding site (purple). Conserved residues believed to be important for binding the tetrapyrrole molecules are shown and numbered according to *S. aureus* residue locations.

Due to a lack of HemQ structures with bound tetrapyrroles, it has been difficult to accurately predict the shape of the *S. aureus* HemQ pocket when ligands are bound. Surface models for the HemQ structures appear to show a closing of the active site pocket between where rings A and B of the haem molecule are predicted to be located. It is anticipated that this section of the pocket opens up upon substrate binding, allowing for the coprohaem to move to a position deeper in the pocket. Whilst not a HemQ, the chlorite dismutase from *Dechloromonas aromatica* (PDBid = 3Q08) has a similar tertiary structure to both the *S. aureus* and *T. thermophilus* HemQs (Figure 5.4 – only *S. aureus* shown for clarity). This structure has also been solved with haem bound in the same location as the proposed active site for the HemQ protein, and was therefore used as a template for modelling coprohaem molecules into HemQ structures. The protohaem-bound 3Q08 structure has an α-helix that is not present in the HemQ structural model, which can be seen just above the ligand bound in Figure 5.4. It is possible that the movement of this helix, arises as the result of ligand binding, and may allow for the opening of the haem binding cleft. A multiple sequence alignment for *D. aromatica*, *T. thermophilus* and *S. aureus* can be seen in Appendix 3.

Superposition of coprohaem III into the active site of HemQ was performed using the location of protohaem IX in the *D. aromatica* crystal structure. Using this structure as a potential model for tetrapyrrole binding to HemQ, only minor steric clashes existed between the modelled HemQ structure and coprohaem (Figure 5.5).

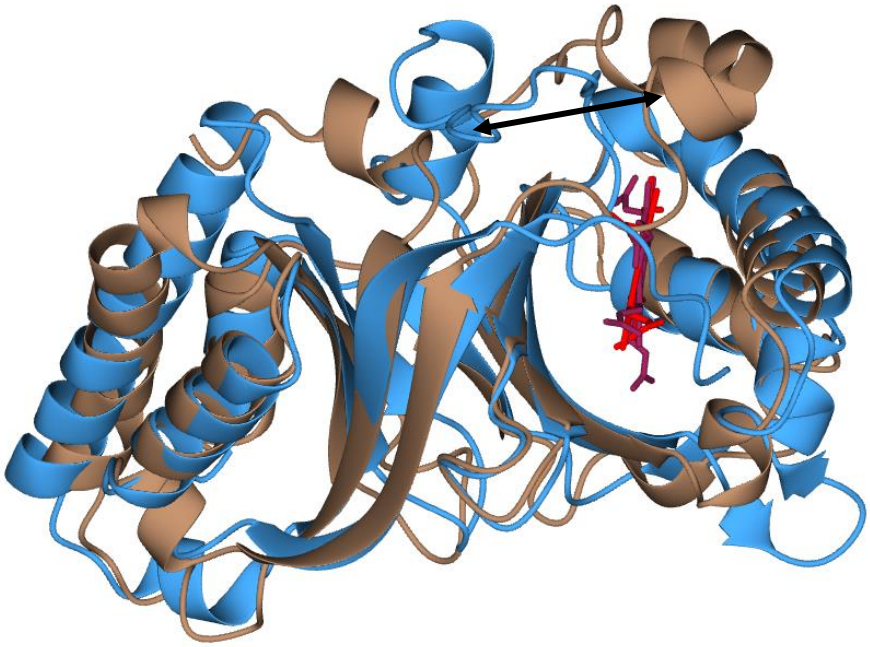

**Figure 5.4 –** Structural comparison of the chlorite dismutase from *D. aromatic*a (PDB 3Q08, brown) with protohaem IX bound (red) and the *S. aureus* HemQ structural model (blue). Coprohaem III (purple) has been modelled into the active site of *S. aureus* HemQ based on the location protohaem IX. The black arrow shows the change in location of an α-helix that may re-locate upon ligand binding.

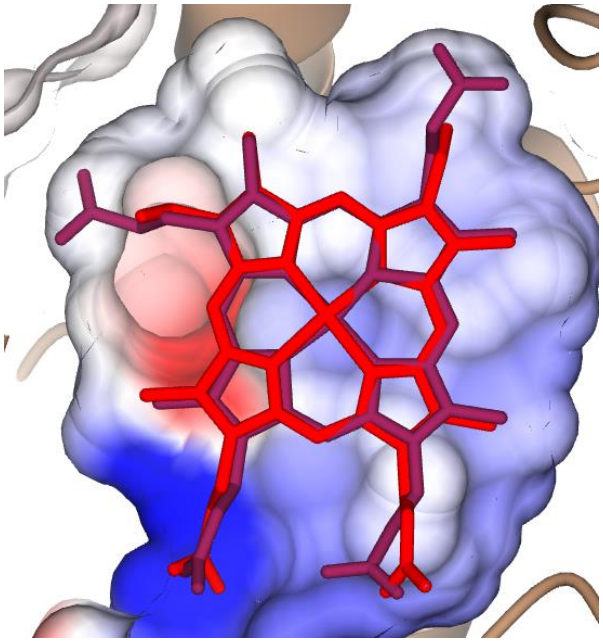

**Figure 5.5 –** Surface representation of the active site of HemQ from *S. aureus* with coprohaem III (purple) and protohaem IX (red) present in the active site based on the protohaem IX location in the chlorite dismutase from *D. aromatica*.

## 5.2.2 – Biochemical analysis of purified HemQ

*S. aureus* HemQ was overexpressed and purified as described in section 2.4 and SDS-PAGE was performed to assess purity. The protein expressed very well, as evidenced by a large band at the expected molecular mass in the soluble cell extract (Figure 5.6). This band migrates at a rate corresponding to a 30kDa protein, which agrees with the predicted molecular mass for HemQ (29.4kDa). There is another significant band at 140 kDa in the purified protein lane, which is roughly five times larger than the HemQ protein. This may be due to an aggregation of multiple peptide chains, as HemQ has previously been predicted to form homotetramers or homohexamers (Mayfield et al. 2013), with other HemQs shown to crystallise as homopentamers (Ebihara et al. 2005; Dailey et al. 2015). There is also a smaller impurity at a lower molecular weight, which may be a result of degradation of the HemQ protein, although this is a minor contaminant in comparison to the main band at 30 kDa.

A typical absorption spectrum of purified HemQ suggests that HemQ often purifies without a chromophoric cofactor, with the only absorbance peak being at 280 nm due to aromatic residues in the protein (Figure 5.7, grey trace). However, occasionally a minor peak at approximately 410nm is present (Figure 5.7, black trace). With the coproporphyrin-dependent pathway being absent in *E. coli*, it is likely that this peak is an artefact of the expression/purification system with HemQ binding to one of the native tetrapyrroles in *E. coli* such as protoporphyrin IX or protohaem.

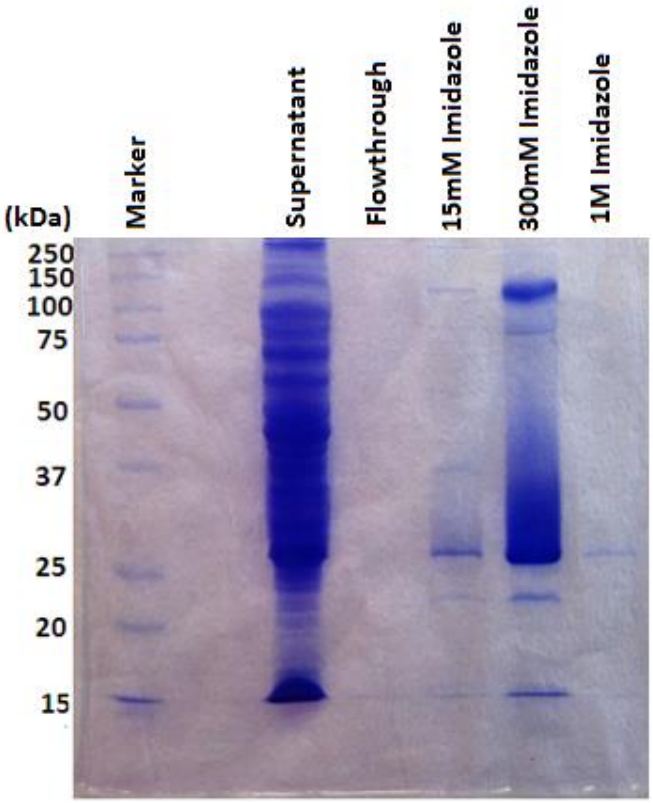


**Figure 5.6 –** SDS-PAGE analysis of HemQ following purification. A band corresponding to a protein of approximately 29kDa can be seen in all imidazole fractions, with the highest concentration being seen in the 300nM imidazole elution sample.

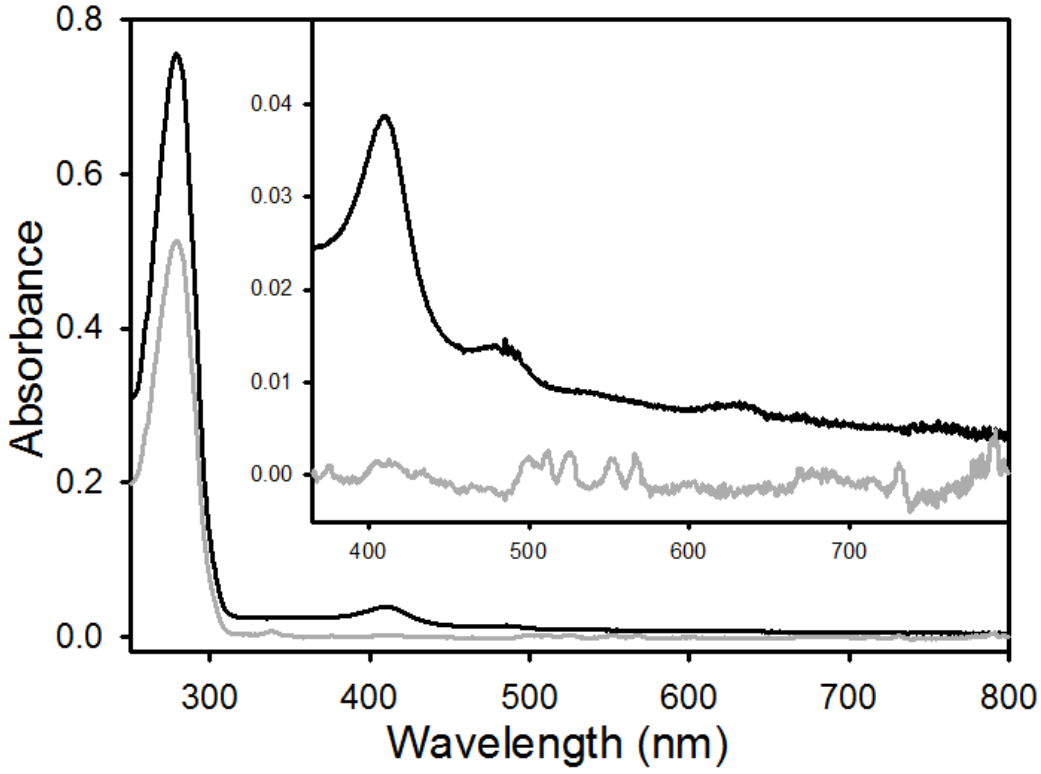


**Figure 5.7 –** UV/Vis spectra of two purified HemQ samples which have either a porphyrin bound (black) or nothing bound (grey). Inset shows a zoomed view between 375nm and 800nm.

HemQ that had been loaded with coproporphyrin III, protoporphyrin IX or protohaem IX was purified in the same way as the unloaded HemQ, the difference being that a concentrated porphyrin stock was added to the supernatant prior to being added to the purification column (Section 2.4). Any porphyrin that was not bound to HemQ was removed during the affinity chromatography and buffer exchange procedures. Absorption spectra were recorded for all of these proteins, which were subsequently used in HemY activity assays (Section 3.2.4.3). These spectra (Figure 5.8) exhibit large peaks at 392nm, 405nm and 411nm, which correspond to coproporphyrin, protoporphyrin and protohaem, respectively. This shows that as well as the substrate and product of the *in vivo* HemQ reaction (coprohaem III and protohaem IX), non-metallated forms of these porphyrins can bind to HemQ. This also suggests that axial coordination of a central metal by the H172 residue is not essential for HemQ to bind tetrapyrroles.

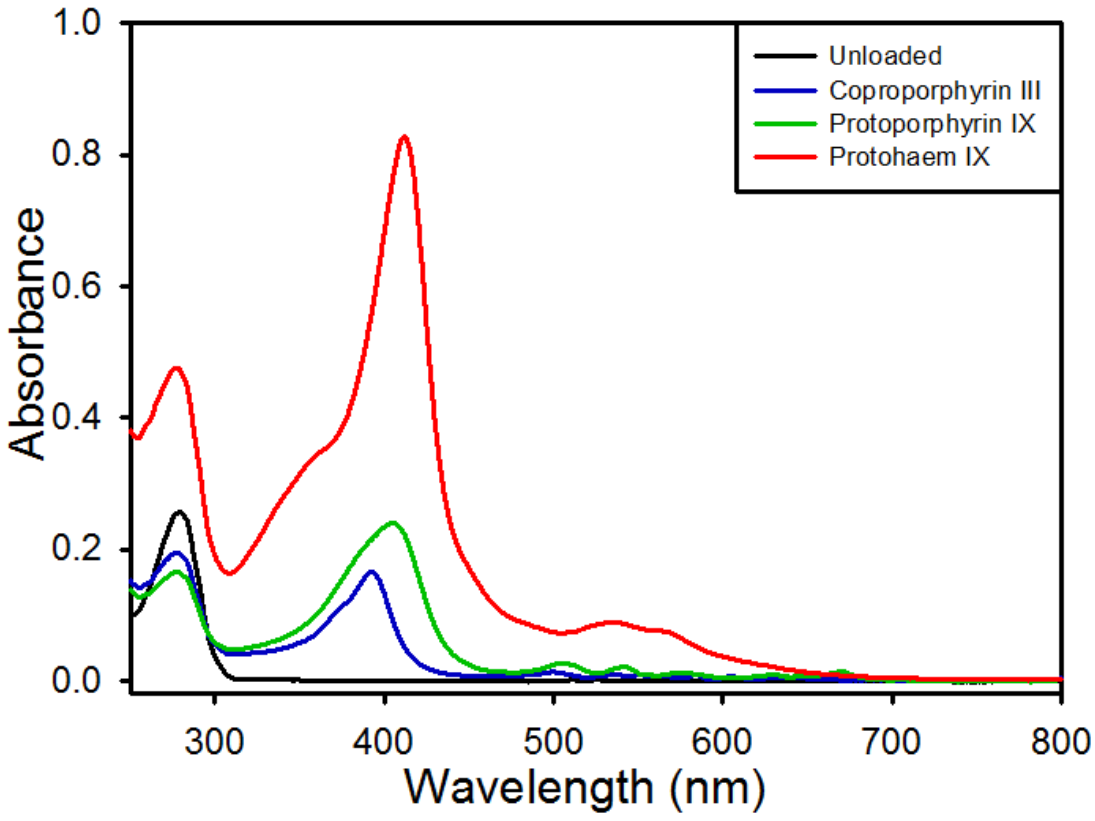


**Figure 5.8 –** Absorption spectra of HemQ either unloaded (black) or loaded with coproporphyrin III (blue), protoporphyrin IX (green) or protohaem IX (red). Porphyrins were added to the sonicated cell extract prior to being added to the purification column. Presence of spectral characteristics for the relevant porphyrins shows that porphyrins are being bound by HemQ and are remaining bound during the purification process.

## 5.2.3 – HemQ can bind porphyrins and metalloporphyrins

HemQ has the ability to bind porphyrins, but does not acquire a significant load of these molecules during purification (Figure 5.7). This would suggest that either HemQ expressed in *E. coli* does not have much opportunity to bind porphyrins that are produced in *E. coli*, or that it has a low affinity for these molecules. To investigate the affinity of HemQ for these ligands, *in vitro* fluorescence titrations were performed (Section 2.16) to analyse the binding of *S. aureus* HemQ with coprohaem III and protohaem IX as well as coproporphyrin III and protoporphyrin IX. The dissociation constants ($K_d$) for each tetrapyrrole was deduced from the change in fluorescence at 340nm (tryptophan fluorescence), which was fitted to the following equation:

$$F_{obs} = F_0 + F_{max}\frac{[L]_T + [E]_T + K_d - \sqrt{([L]_T + [E]_T + K_d)^2 - 4[L]_T[E]_T}}{2[E]_T}$$

Where $F_{obs}$ is the observed fluorescence (or observed change in fluorescence), $F_0$ is the initial fluorescence, $F_{max}$ is the maximum fluorescence (or maximum change in fluorescence), $[L]_T$ is the total ligand (porphyrin) concentration, $[E]_T$ is the total enzyme concentration and $K_d$ is the dissociation constant. Using this equation, the dissociation constants for coproporphyrin III, protoporphyrin IX, protohaem IX and coprohaem III were determined and are summarised in Table 5.1 with the fitted curves shown in Figure 5.9.

**Table 5.1 –** Summary of $K_d$ values for porphyrins binding to HemQ.

| Ligand | $K_d$ (nM) |
|---|---|
| Coproporphyrin III | 86 ± 10 |
| Protoporphyrin IX | 135 ± 24 |
| Protohaem IX | 216 ± 41 |
| Coprohaem III | 595 ± 127 |

The binding data suggests that metalloporphyrins bind with a lower affinity than non-metallated porphyrins, with the substrate for the *in vivo* reaction, coprohaem, binding with the lowest affinity of all ligands tested. There was no obvious pattern to which tetrapyrrole bound with greater affinity, as HemQ had a greater affinity for coproporphyrin III compared to protoporphyrin IX, although protohaem was bound with a greater affinity than coprohaem. These data suggest that the presence of a central iron and/or the presence of propionates on the A and B rings lower the binding affinity.

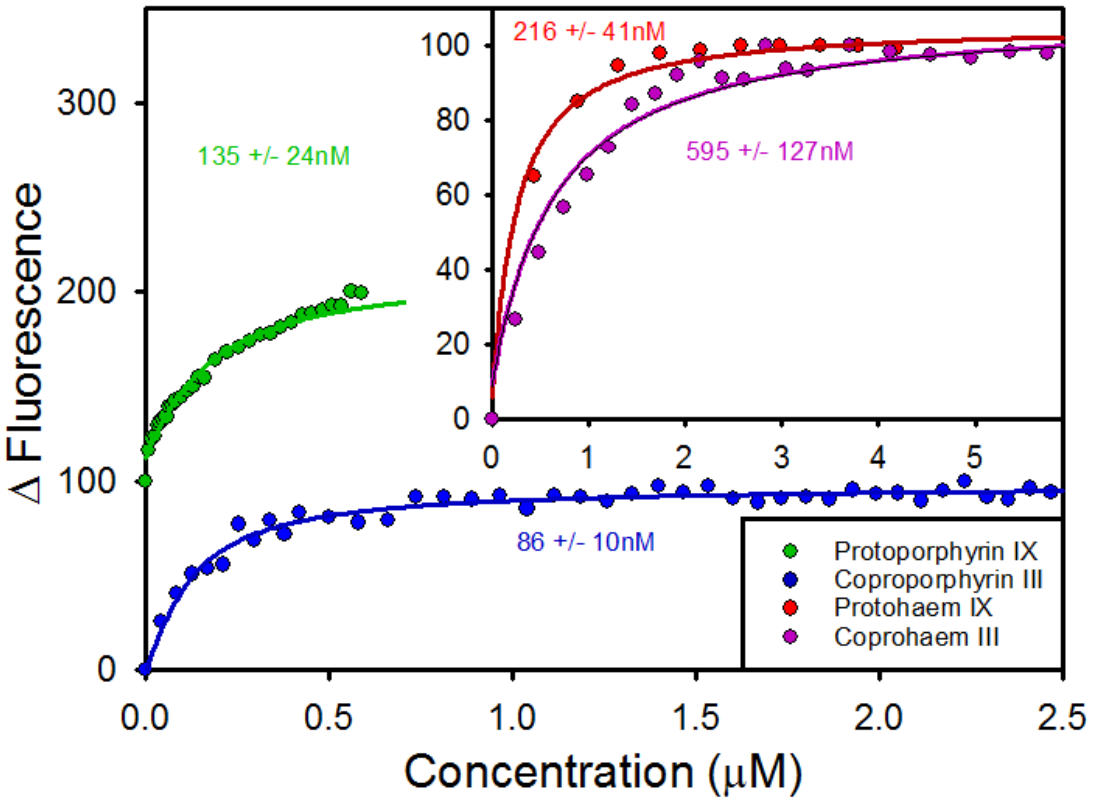


**Figure 5.9 –** Fluorescence titrations of HemQ with coproporphyrin III (blue), protoporphyrin IX (green), protohaem IX (red) and coprohaem III (purple) with their respective $K_d$ values. Data for protoporphyrin IX (green) was offset by 100 fluorescence units for clarity. 75 nM of HemQ was used in all titrations.

## 5.2.4 – Coprohaem decarboxylase activity of HemQ

With the discovery of a role for HemQ in the coprohaem branch of the haem synthesis pathway (Dailey et al. 2015) and the report of coprohaem decarboxylase activity for *S. aureus* HemQ (Lobo et al. 2015), it was of interest to characterise the steady state kinetics of this reaction for *S. aureus* HemQ. Initial attempts to determine activity using a continuous method, looking for absorption changes that could be monitored, showed some promising results for future development of a continuous assay (Figure 5.10), yet due to time constraints a more simple assay detection system was required. Hence, a discontinuous method using HPLC was developed to track protohaem formation over time (see section 2.15). The chromatograms revealed three distinct peaks present in samples from HemQ reactions (Figure 5.11) which compare to single peaks observed for control reactions. These observations are consistent with previous work (Dailey et al. 2015; Lobo et al. 2015; Celis et al. 2015), with two of these peaks corresponding to coprohaem III and protohaem IX. The third peak is predicted to be a harderohaem isomer which is reported to be an intermediate formed during the reaction (Celis et al. 2015).

The HemQ reaction, as mentioned earlier, requires either $H_2O_2$ or FMN to function (Dailey et al. 2015) as an electron sink during the oxidative decarboxylation of coprohaem. With the HemY reaction producing hydrogen peroxide, it was decided that this electron acceptor would be used in experiments, as this is an obvious and readily available electron acceptor for the *in vivo* reaction. Basic kinetics constants were determined by varying each substrate independently whilst keeping the other at a constant initial concentration. It was anticipated that this approach might also reveal whether each substrate can influence the binding of the other, as was seen for HemH in Chapter IV.

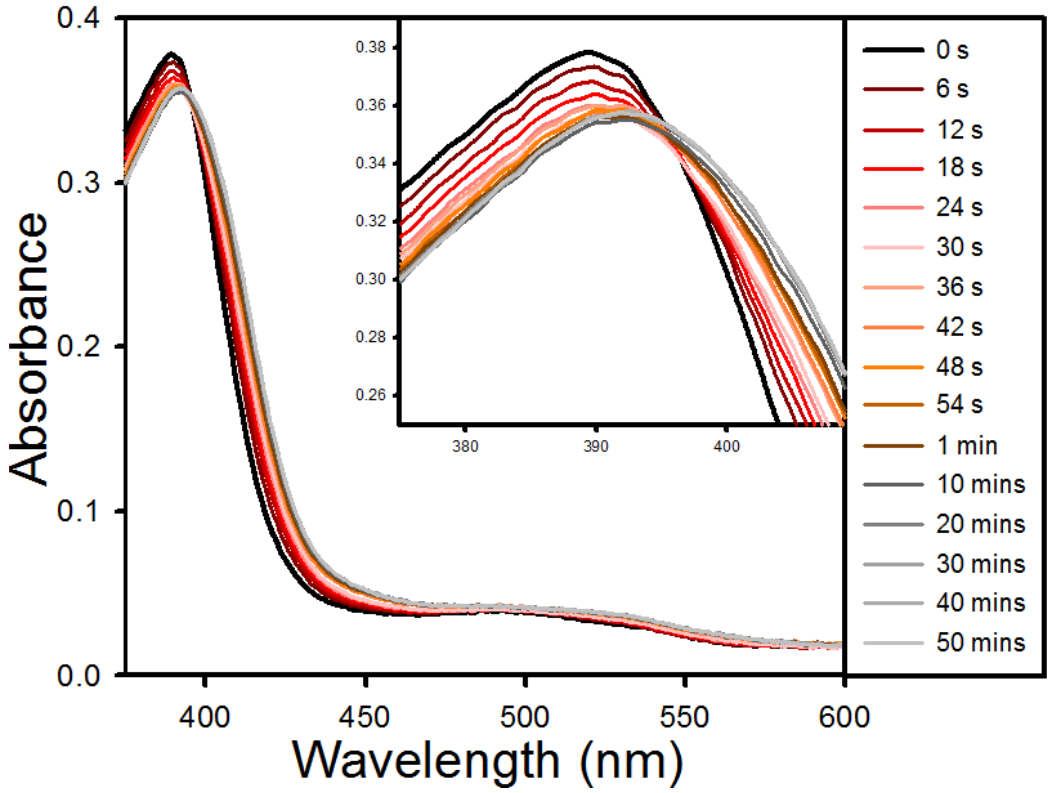


**Figure 5.10 –** Spectral kinetics of the coprohaem decarboxylase reaction catalysed by HemQ. The coprohaem III peak (at 390 nm) can be seen to decrease and red-shift. Inset shows an expanded view of the spectral changes between 375 nm and 410 nm. The changes in wavelength demonstrated here have potential for the development of a continuous spectroscopic assay for this reaction, following the change in absorbance at a particular wavelength. Further work would require identification of a suitable wavelength and reliable determination for an extinction co-efficient for this absorbance change.

Preliminary kinetic analysis revealed two distinct concentration dependencies for the different substrates (Figure 5.12). When hydrogen peroxide was varied, using 10 µM of coprohaem III, the reaction kinetics for the tested range shows classical hyperbolic Michaelis-Menten kinetics, yielding an apparent $K_{m(peroxide)}$ of 90.4 ± 18.0 µM and an apparent $V_{max}$ of 1.74 ± 0.12 $min^{-1}$. However, when the coprohaem concentration was varied using $H_2O_2$ fixed at 250 µM, there appears to be a more linear relationship at concentrations up to 20 µM coprohaem, or perhaps a low affinity Michaelis-Menten relationship. The data were fitted to the Michaelis-Menten equation to provide an estimated $V_{max}$ of 6.6 ± 3.4 $min^{-1}$ and an estimated $K_{m(coprohaem\ III)}$ of 37.4 ± 26.5 µM. Since the measured $K_d$ for coprohaem is approximately 0.6 µM (Table 5.1), these data perhaps suggest that the binding affinity of HemQ for the metalloporphyrin substrate is not the limiting step.

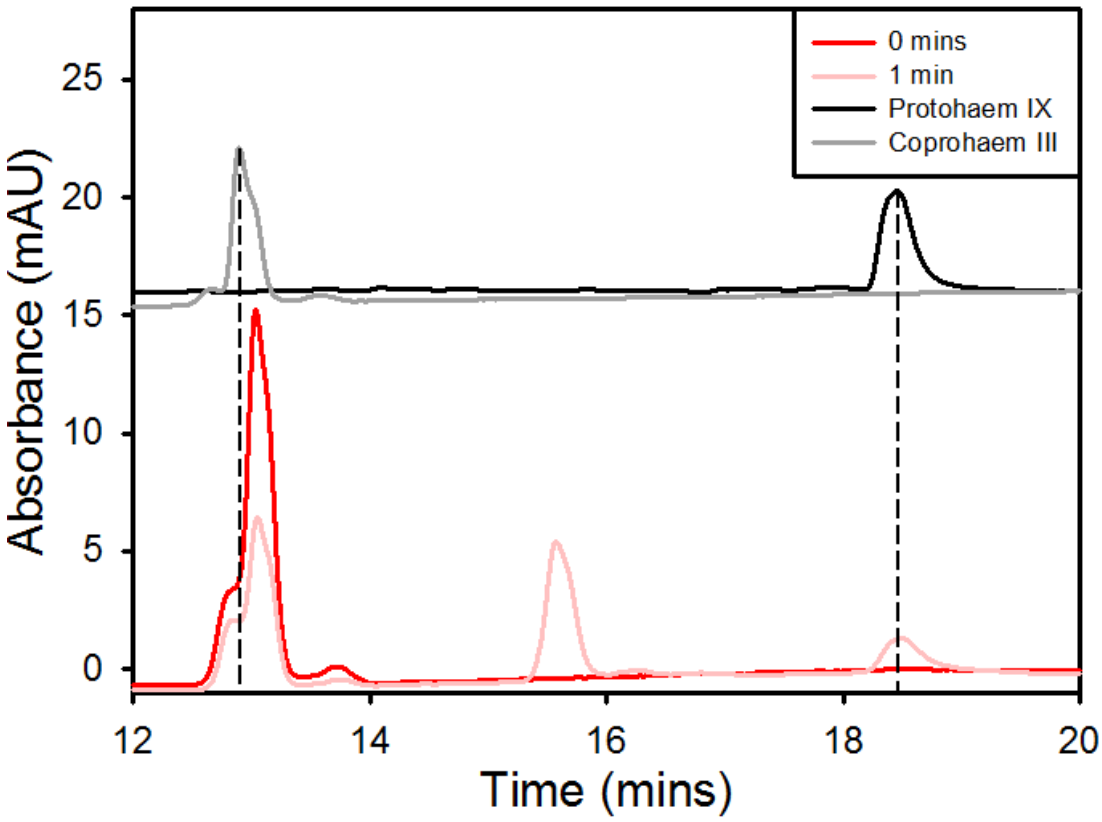


**Figure 5.11 –** HPLC chromatograms of the HemQ reaction at t = 0 (red) and t = 1 min (pink). Chromatograms at these time points show the production of coprohaem III, a harderohaem isomer and protohaem IX at 13, 15.5 and 18.5 minutes respectively. Standards for coprohaem III (grey) and protohaem IX (black) have been offset for clarity with droplines showing the maximal point of the absorbance peaks. HPLC conditions started with a solution containing 80% TFA (0.1% v/v) and 20% acetonitrile, rising to 100% acetonitrile in a linear gradient over 30 minutes with absorbance at 400 nm being detected.

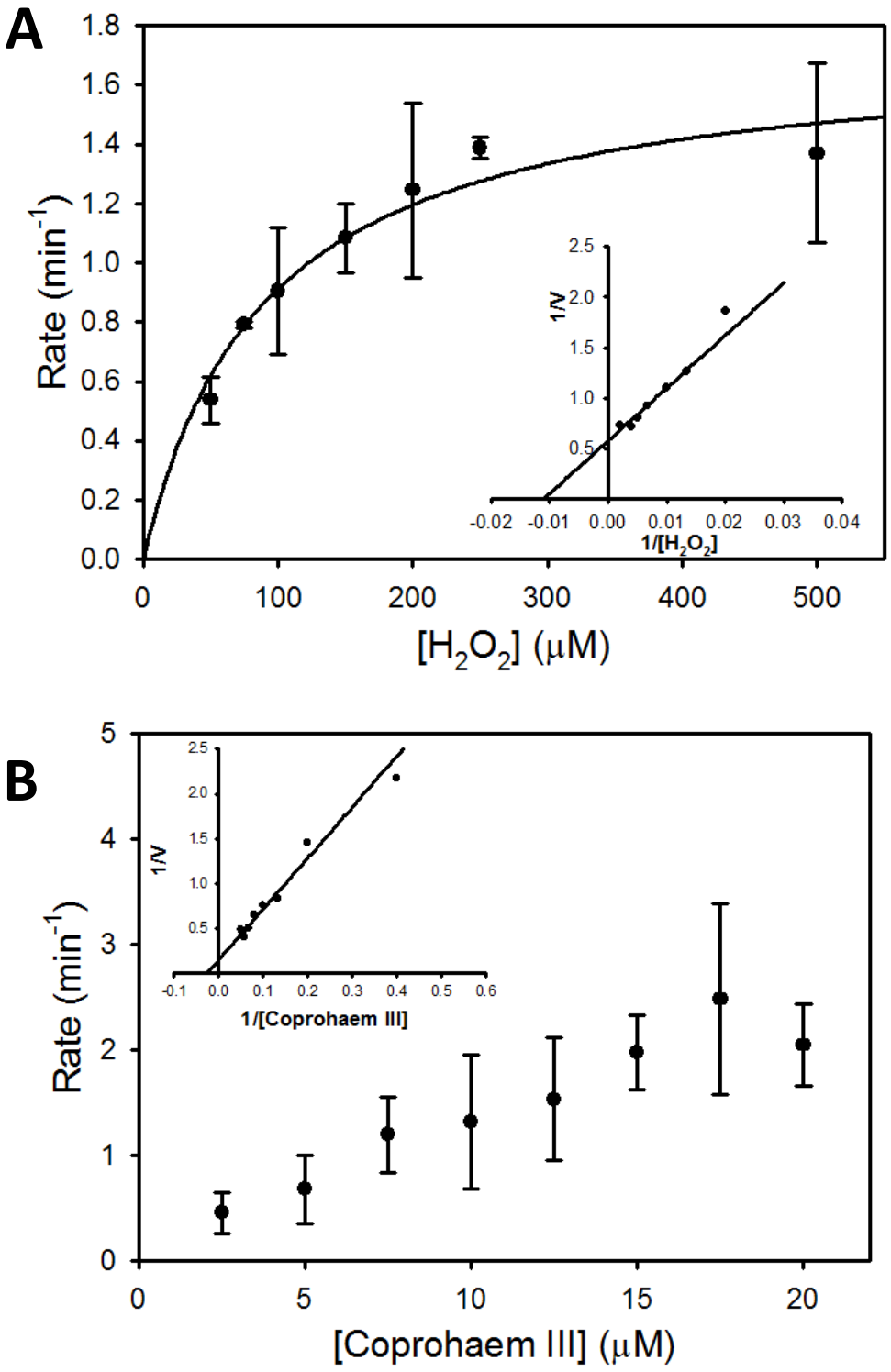


**Figure 5.12** – Kinetic analyses of the HemQ reaction varying either hydrogen peroxide (A) or the coprohaem III substrate (B). Stopped assays performed with samples of the reaction quenched, in a buffer containing 80% (v/v) Acetone and 0.02% (v/v) TFA, after 5, 10 and 15 seconds. Samples were analysed by HPLC, with sample peaks heights at 18.5 mins compared to a standard curve for known protohaem IX concentrations. Error bars represent SD values based on three repeats. Inset graphs show Lineweaver-Burke plots of kinetic data with linear regressions plotted based on Michaelis-Menten parameters.

# 5.3 – Discussion

Research into the HemQ protein has accelerated in recent years, culminating in the discovery that this enzyme is a coprohaem decarboxylase that catalyses the final step in coproporphyrin-dependent haem biosynthesis (Dailey et al. 2015; Lobo et al. 2015; Celis et al. 2015). The HemQ protein from *S. aureus* has been suggested to be made up of five identical subunits of 29.4kDa and when overexpressed and purified can bind tetrapyrroles. However, only binding studies with non-native porphyrin substrates had been performed, and there was a notable lack of steady state kinetics to describe this enzyme-catalysed step. Hence, ligand binding and kinetic analyses of HemQ were undertaken.

## 5.3.1 – HemQ binds metalloporphyrins with a lower affinity than non-metallated porphyrins

Binding experiments on *S. aureus* HemQ have been published before, although only protoporphyrin IX and protohaem IX were studied (Mayfield et al. 2013). This work reported a different pattern to the data presented herein, with protohaem binding with a greater affinity than protoporphyrin IX. However, these differences might be explained by variations in the experimental approach, as the pH of the samples was different to those used herein (pH 6.5 in Mayfield et al. (2013) compared with pH 8.0 here). Measurement of cellular pHs have been difficult to accurately determine, yet values between 7.0 and 8.0 have been noticed for various mammalian cells types, and bacteria such as *E. coli* (Roos & Boron 1981; Booth 1985; Bright et al. 1987) although value ranges for *S. aureus* are currently not readily available. The above mentioned range would suggest that the data contained in this thesis is slightly more physiologically relevant, however it is more likely that they are equally distant from the physiological cytoplasmic pH and therefore neither dataset is physiologically relevant.

Also, the published data do not appear to account for the absorption of the porphyrin, which has a significant affect upon fluorescence emission. In the experiments described herein, the fluorescent small molecule N-acetyltryptophanamide (NATA) was used in control experiments to account for loss of fluorescence resulting from ligand absorption: NATA will not bind the ligands so any decrease in fluorescence

can be attributed to absorbance of the ligand. Subtraction of this control gives a more specific change in fluorescence due to ligand binding. The current work suggests that HemQ binds non-metallated porphyrins with greater affinity than metalloporphyrins, an unexpected observation considering that the product and substrate for this enzyme are both metalloporphyrins. Another interesting observation is that the substrate for HemQ (coprohaem III) has a lower binding affinity than the product (protohaem IX). However, since free haem in the cell may react with hydrogen peroxide to produce reactive oxygen species, HemQ may have evolved to bind with moderate affinity to haem. In addition, it could be speculated that interaction of HemQ with a target protein may facilitate the release of this product.

There is no obvious pattern that describes how the tested tetrapyrroles can bind to HemQ. When the central iron is absent, $K_d$ values differ by only 49 nM (86 ± 10 and 135 ± 24 for coproporphyrin III and protoporphyrin IX, respectively), although when a central iron is present the $K_d$ values differ by 379 nM (216 ± 41 and 595 ± 127 for coproporphyrin III and protoporphyrin IX, respectively). Without structural data for ligand-bound HemQ, it is difficult to reconcile these variations, although one might speculate that the presence of iron and the interactions with the protein that arise from this may affect the tertiary structure of the protein deeper in the active site pocket (i.e. closer to the substituents on rings A and B).

## 5.3.2 – HemQ kinetic analysis

The most significant advancements in HemQ research are the identification of this protein as a coprohaem decarboxylase and identification of intermediates produced in the reaction (Dailey et al. 2015; Lobo et al. 2015; Celis et al. 2015). The current work provides additional insights into HemQ kinetics using coprohaem as the metalloporphyrin substrate and hydrogen peroxide as an electron acceptor. Kinetic parameters for the HemQ reaction were investigated using a discontinuous method with the substrates/products being detected by HPLC. Following the demonstration of coprohaem decarboxylase activity (Figure 5.11), a more detailed kinetic analysis was carried out varying each of the two substrates independently. Varying the hydrogen peroxide concentration with 10μM coprohaem present yielded classical Michaelis-Menten kinetics with an apparent $V_{app}$ of 1.7 ± 0.1 $min^{-1}$ and an apparent

$K_{m(peroxide)}$ of 90.4 ± 18.0 μM. When coprohaem is varied in a constant initial hydrogen peroxide concentration (250μM) the data indicated a more linear depdendence upon this substrate. During these assays, concentrations of coprohaem up to 20 μM were used due to solubility issues anticipated for higher porphyrin concentrations. The data in the range tested shows a relationship that could be linear or would follow low-affinity Michaelis-Menten kinetics. Nonlinear regression analysis using the Michaelis-Menten equation yields poor estimations of apparent kinetic constants of $V_{max}$ of 6.6 ± 3.4 $min^{-1}$ and an estimated $K_{m(coprohaem\ III)}$ of 37.4 ± 26.5 μM due to non-saturating concentrations of coprohaem. However, increasing the concentration did not seem sensible both due to solubility issues and avoiding concentrations that are not physiologically relevent: porphyrins are present in low (nmole/ng) levels in cells (Jacobs et al. 1971; Quintanilla-Vega et al. 1995).

Whilst more precise estimations of the maximum enzymatic rate will require further experimental investigation, the rates obtained herein are comparable to those observed for the HemH and HemY proteins (see Chapters III and IV). The highest rate observed for HemQ during this work is 2.48 $min^{-1}$ which is below the maximal rates observed for HemH and is higher than the values seen for the *S. aureus* HemY, which may indicate that oxidation of coproporhyrinogen is the limiting step in the terminal steps of haem synthesis in *S. aureus*.

Chapter VI

# Final Discussion

The aim of this work was to contribute to the pool of knowledge on the enzymes of the coproporphyrin-dependent pathway, which branches from the classical pathway at coproporphyrinogen III and does not form a protoporphyrin IX intermediate. As well as confirming previous reports of reactions catalysed by the HemY, HemH and HemQ enzymes from *S. aureus* (Lobo et al. 2015), detailed investigations have revealed novel insights into the mechanisms for HemY and HemH, whilst preliminary kinetic and binding data for the HemQ-catalysed reaction have been determined.

## 6.1 – Substrate utilisation by HemY provides insights into haem biosynthesis pathway evolution

Both soluble and membrane-bound forms of HemY have previously been shown to be stimulated by haem-binding proteins (Dailey et al. 2010; Shepherd & Dailey 2009). However, the current data reveal that soluble HemY from *S. aureus*, which catalyses the first reaction in the coprohaem pathway, is not stimulated when assayed with coproporphyrinogen III. This stimulation, specific to the protoporphyrinogen reaction, is due to radicals produced in the breakdown of $H_2O_2$ *via* a peroxidase mechanism (Figures 3.13, 3.16, 3.18). Another interesting observation is that presence of $H_2O_2$ inhibits HemY-mediated oxidation of protoporphyrinogen IX, but has no effect on coproporphyrinogen III oxidation (Figures 3.16). A look at the auto oxidation control rates (Figure 3.17) for these reactions shows that protoporphyrinogen oxidises faster in the presence of peroxide, whereas coproporphyrinogen oxidation is not noticeably affected. This, combined with the much higher much higher nonenzymatic oxidation of protoporphyrinogen compared to coproporphyrinogen, may provide some insight into the evolution of classical and coproporphyrin-dependent pathways.

Since the HemQ component of the coproprophyrin pathway has been identified in evolutionarily early-branching (Acidobacteria and Planctomyces) and transitional (Deinococcus-Thermus group) diderm phyla (Dailey et al. 2015; Gupta 1998; Gupta 2011), it is highly likely that this pathway is an evolutionary precursor to the classical protoporphyrin IX pathway. It has been predicted that the ancient coproporphyrin-dependent pathway may pre-date the production of atmospheric

oxygen, raising the question of how the oxygen-dependent HemY-mediated oxidation of porphyrinogens could take place (Dailey et al. 2015). The proposed age of the coproporphyrin-dependent pathway, combined with the lack of protoporphyrin intermediates in Actinobacteria and Firmicutes (Jacobs et al. 1971), the presence of haem synthesis proteins that have potential to be used in both pathways (HemY and HemH) and the lack of a functional HemN coproporphyrinogen oxidase (Lobo et al. 2015; Dailey et al. 2015) raises the strong possibility that the ability to synthesise protoporphyrin intermediates was acquired after the coproporphyrin-dependent pathway was in common use. It is possible that a transitional period may have occurred whereby organisms may have utilised both pathway branches before selective pressures made it more advantageous to only use one pathway branch. These pressures may have influenced the usage of one intermediate over the other due to the apparent differences between the reactivity of the two porphyrin species. The higher reactivity of protoporphyrin intermediates, which has been shown to cause greater cellular damage than coproporphyrin (Aravind Menon et al. 1989), and the ability of peroxidase reactions to stimulate the protoporphyrinogen oxidase activity of HemY via a radical mechanism that does not appear to stimulate coproporphyrinogen oxidase reactions (see Sections 3.2.4.3) can all lead to the presence of cytotoxic compounds that could potentially damage the cell. The apparent inability of the HemY coproporphyrinogen oxidase to be stimulated by peroxidases (Figure 3.18) or to be affected by hydrogen peroxide (Figure 3.16) suggests that the coproporphyrin intermediates are more stable in harsh conditions, therefore less likely to break down and produce potentially toxic radicals. Obvious factors that could have influenced pathway evolution include the availability of oxygen and exposure to UV light, both of which potentiate the toxic effects of porphyrins: it seems likely that the coproporphyrin-dependent pathway would be better suited to exposure to these environmental factors.

A good example of the dangers that the protoporphyrin pathway can pose is the condition erythropoietic porphyria in humans, where a build-up of protoporphyrin in cells leads to extreme photosensitivity resulting from the reaction of ultraviolet light with protoporphyrin creating free oxygen radicals as the porphyrin is broken down (Henderson et al. 1995; Balwani & Desnick 2012). The increased stability and decreased reactivity of coproporphyrin, compared to protoporphyrin, would lower

the amount of radicals that are produced and could allow for a greater survival than similar organisms using the classical protoporphyrin pathway. This hypothesis would hold true for some organisms that use the pathway today, such as *S. aureus* and *P. acnes*, which are cutaneous pathogens and have the potential to be exposed to high quantities of UV light. *Staphylococcus* species in particular are examples of organisms that would be exposed to high levels of light as they have been known to colonise the skin of a wide range of organisms (Kloos 1980).

While it is unclear exactly how the pathways have evolved, the multi-functionality of the HemY coproporphyrinogen oxidase suggests that the classical pathway arose as an adaptation to use protoporphyrin IX instead of coproporphyrin III. HemY enzymes from organisms that use the coproporphyrin-dependent pathway were originally tested for activity with protoporphyrinogen IX, with coproporphyrinogen III often tested as an alternative substrate instead of the primary substrate (Hansson et al. 1997). The ability to accept either porphyrinogen as a substrate could be due to an adaptation to allow for either pathway to be used, with later modifications to promote the use of the single pathway. The real evolutionary divergence of the classical pathway over the coproporphyrin-dependent pathway would be the point at which HemF/N enzymes appear, as this is the point at which protoporphyrinogen is formed. However, it appears that identification of this point will be difficult as a large proportion of HemN enzymes are misannotated (Dailey et al. 2015).

## 6.2 – Inhibition of ferrochelatase may limit cellular concentration of free haem species

It has previously been reported that ferrochelatases from both *S. aureus* and *B. subtilis* are inhibited at iron concentrations above 0.8µM (Lobo et al. 2015), an observation that would have been missed using the higher iron concentrations that are conventionally used (Wu et al. 2001; Shepherd et al. 2006). This inhibition could explain the low enzymatic rates reported for HemY enzymes from *M. tuberculosis* and *B. subtilis* (Dailey et al. 2015). It is difficult to assess how this iron concentration compares to the amount of free iron present in the cell, as iron levels are tightly controlled due to high toxicity in an aerobic environment (Andrews et al. 2003). An approximate estimate of the total cellular iron concentrations, based on

$10^6$ atoms of iron per cell in *E. coli* (Andrews et al. 2003) and a volume of 0.6μm$^3$ (Kubitschek 1990), gives a concentration of 155 mM which includes iron present in proteins (such as in iron sulphur clusters or in ligands such as haem). Hence, it is conceivable that iron is available for ferrochelatase at concentrations above 0.8μM (probably associated with a delivery protein), making the inhibition effect potentially important for limiting the amount of free haem species (either coprohaem or protohaem) available in the cell.

Magnesium ions clearly influence HemH activity as the presence of $Mg^{2+}$ in the regulatory metal binding site reduces the inhibitory iron threshold concentration to 0.4μM, half of what is needed to cause inhibition without magnesium. With the magnesium concentrations used (4mM) being in the physiological range for many types of cell (Cowan 1991), it is conceivable that the regulatory metal site could be occupied by this metal *in vivo*, causing ferrochelatase to be inhibited at cellular free iron concentrations above 0.4μM. However, as is the case with iron, magnesium is seldom found as a free ion in biological systems (e.g. $Mg^{2+}$ is often complexed with adenosine triphosphate (ATP)), so the potential interaction with HemH would be dependent upon complex dissociation as well as removal of the hydration shell. Furthermore, the relative affinity for magnesium and iron at low metal concentrations will also dictate which ion will occupy the HemH regulatory metal site *in vivo*.

The HemH kinetics described herein that were conducted below the inhibitory iron concentration threshold suggest that the reaction proceeds most efficiently if coproporphyrin III is the first substrate to bind as this appears to facilitate iron binding to the catalytic metal binding site (Fig. 4.22). Conversely, when iron is more abundant and presumably binds first to HemH, coproporphyrin binding is slightly hindered (Fig 4.23). A potential explanation for this hindrance is a conformational change in the porphyrin binding cleft as a result of iron binding, perhaps constricting the site and preventing the bulky propionate side chains on rings A and B of coproporphyrin III from accessing the active site. This model is consistent with previous observations that high iron concentrations do not cause inhibition when protoporphyrin IX is used as a substrate (Lobo et al. 2015).

While there is reduction in coproporphyrin III chelatase activity caused by the presence of the metals in the regulatory binding site, the residual activity of HemH (≈ 2 $min^{-1}$) is still at a level that is comparable to HemY (≈ 0.5 $min^{-1}$) and HemQ (max observed = 2.48 $min^{-1}$). This suggests that elevated iron would not necessarily result in a build-up of coproporphyrin III. In fact the rate limiting step in the pathway at this point, assuming for an equal amount of each enzyme *in vitro*, would appear to be the HemY reaction, which may limit the supply of coproporphyrin for HemH and potentially restrict the supply of $H_2O_2$ as an electron acceptor for HemQ. However, *in vivo*, other factors will arise that will also affect the amounts of the pathway intermediates, highest among these being the relative amounts of each pathway enzyme that is present in the cell and the actual substrate concentrations present in the cell at any particular time. Further research into the relative native expression levels of all of the haem synthesis enzymes would be needed to give insights into the rate limiting steps of haem synthesis for this newly discovered pathway branch. Porphyrin levels could also be analysed, however with the reactivity of certain pathway intermediates (mainly $C'gen_{III}$ which would oxidise to $C_{III}$) it may be hard to gain true readings for each enzymes substrate.

The regulation of HemH by the occupancy of the regulatory metal site by $Mg^{2+}$, $Fe^{2+}$ or other ions that are able to occupy this site, could serve to control the amount of coprohaem produced to limit the potential for ROS generation by metalloporphyrin-mediated Fenton chemistry (this hypothesis assumes that excess free iron is complexed to bacterioferritin whereas excess metalloporphyrins remain free). However, the lack of iron-mediated inhibition when protoporphyrin IX is used as a substrate (Lobo et al. 2015) indicates that during the evolution of the classical pathway, the lack of this regulation may render the cell susceptible to protohaem accumulation and subsequent ROS generation. This may provide an explanation why organisms such as *S. aureus* have evolved steps of the classical pathway (presumably adapted from the ancient coproporphyrin-dependent pathway) yet no longer utilise the classical pathway: elevated ROS produced by pathway intermediates have exerted a selection pressure to dispense with the classical pathway.

# 6.3 – The coprohaem decarboxylase: HemQ

Characterisation of coprohaem decarboxylase activity for HemQ provides the final piece of the puzzle for the elucidation of the coproporphyrin-dependent pathway for haem biosynthesis (Dailey et al. 2015). As a recently characterised protein, limited kinetic/binding data exists for HemQ enzymes and this work is ongoing. Recent investigations have reported that the decarboxylation of coprohaem III to protohaem IX occurs via a two-step radical-based mechanism producing one of two possible intermediates, harderohaem III or IV (Celis et al. 2015). It has also been noted that this protein is able to bind protoporphyrin IX and haem (Dailey et al. 2010; Mayfield et al. 2013), with the haem-bound form able to influence the HemY protoporphyrinogen oxidase reaction (Dailey et al. 2010). A novel kinetic analysis reported herein reveals the stimulation of HemY by haem-bound HemQ is due to a peroxidase activity of HemQ resulting in superoxide generation that aids in the oxidation of protoporphyrinogen IX (see Chapter III). This data demonstrates that the maximal rate for the enzyme when $H_2O_2$ is used with 10 µM coprohaem is 1.74 $min^{-1}$, with evidence to suggest that the reaction could progress more rapidly at higher coprohaem concentrations. The highest observed rate of 2.48 $min^{-1}$, obtained at concentrations of 17.5µM coprohaem and 250µM $H_2O_2$, suggests that this reaction can operate at similar rates to the HemH enzyme, with an estimated maximal rate of 6.6 $min^{-1}$. However, the maximal rate of *S. aureus* HemY coproporphyrinogen oxidase activity (≈ 0.5 $min^{-1}$) may limit the amount of coproporphyrin III (and therefore coprohaem) available to the terminal enzymes in this pathway, assuming for a equal amount of each protein *in vitro*. The concentrations of these enzymes in the cell will have a large role in the amount of substrate available, and would be a big indication into the rates that HemH and HemQ operate at *in vivo*.

As well as binding coprohaem, protohaem and the harderohaem intermediates, it has been shown through fluorescence titrations and by reconstitution during purification that HemQ is also able to bind the metal-free porphyrins coproporphyrin and protoporphyrin. Interestingly, the binding affinities for these porphyrins are tighter than for the metalloporphyrins that serve as the substrate and product, with coprohaem III itself having the lowest affinity out of these four ligands. It is a little surprising that HemQ is often purified from *E. coli* without bound ligand, although

the lack of coproporphyrin and coprohaem in *E. coli* and the tight regulation of classical haem synthesis is likely to limit the amount of tetrapyrrole ligands available. In *S. aureus*, the potential for protohaem to be retained by HemQ following the coprohaem decarboxylase reaction could serve to control the amount of free haem species in the cell. The tight binding of protoporphyrin and coproporphyrin to HemQ is unexpected, although since HemY catalysis is a likely limiting step in the coproporphyrin-dependent pathway, HemQ is unlikely to encounter copropophyrin *in vivo* and *S. aureus* does not make protoporphyrin IX at all (Jacobs et al. 1971).

## 6.4 – Conclusions and Future Work

This work provides new insights into the coproporphyrin-dependent pathway in *S. aureus*. Firstly, the radical-mediated stimulation of HemY activity by HemQ may explain why an organism ancestral to *S. aureus* once evolved the classical pathway and subsequently dispensed with it. Futher insights into how the radicals are interacting directly with the protoporphyrinogen substrate may provide crucial insights into why these organisms retained the coproporphyrin-dependent pathway instead of the classical route. Introduction of a functional HemN/HemF enzyme into *S. aureus* would be exciting approach to engineer a bacterium with both pathways that could be used to investigate how environmental conditions (e.g. light intensity, oxygen tension) could have influenced pathway evolution.

The HemH kinetics herein provide a working hypothesis for how iron and other metals could influence flux through the haem pathway *in vivo*. Future investigations would include site-directed mutagenesis of the metal binding residue (i.e. E272S mutation previously used (Lecerof et al. 2003)) and introduction of this protein in a *hemH* strain of *S. aureus*. It would be very interesting to use this mutation as a tool to investigate how extracellular and intracellular metals affect the accumulation of coprohaem *in vivo*. In addition, HemH from *S. aureus* was shown to catalyse the insertion of a variety of divalent metals ($Zn^{2+}$, $Co^{2+}$, $Ni^{2+}$ and $Cu^{2+}$), and further *in vitro* kinetic characterisation will be necessary to contribute to an *in vivo* model for metal chelation. Furthermore, crystallographic and NMR studies on coproporphyrin-bound HemH would provide further insights into how metals affect coproporphyrin binding.

This thesis reports for the first time the basic kinetic parameters for the HemQ enzyme from *S. aureus*, and these data demonstrate that HemQ has comparable $k_{cat}$ and $K_m$ values to the HemY and HemQ enzymes of *S. aureus*. The true *in vivo* electron acceptor has not yet been confidently assigned as the enzyme can reportedly utilise both $H_2O_2$ and FMN (Dailey et al. 2015), although the possibility that $H_2O_2$ is utilised is an attractive hypothesis considering that the HemY reaction produces this molecule. The process for obtaining kinetic parameters can be optimised in the future, as current techniques rely upon stopped assays and analysis *via* HPLC. In future, a continuous spectroscopic assay may be possible due to the differences in spectroscopic properties of coprohaem and protohaem (the beginnings of which can be seen in Figure 5.10). A potential problem with this method would be how the spectral characteristics of the harderohaem III and IV intermediates interfere with the spectral transitions between coprohaem and protohaem. Complexes of HemQ with all four of these isomers (Celis et al. 2015) suggest that harderohaem III and IV have very similar absorption spectra, so careful consideration of this would have to be made during the development of an absorbance-based assay.

Crystal structures of HemQ proteins currently do not contain bound ligands. Future co-crystallisation studies will provide insights into the positioning of aromatic residues in the active site that could participate in radical formation during the decarboxylase reaction, which combined with electron paramagnetic resonance (EPR) could provide detailed mechanistic insights into this unique reaction.

Detailed research into the evolution of the coproprophyrin-depdendent pathway is still in its infancy. Research so far has focussed upon the individual reactions in the pathway *in vitro*, and there has been a limited focus upon pathway analysis in whole cells. While there is plenty more work to be done on purified enzymes (e.g. investigating substrate channeling), some evolutionary aspects such as phototoxicity of pathway intermediates should be investigated further using genetic tools. The characterisation of coproporphyrin-dependent haem biosynthesis has revolutionised the central dogma on how haem is synthesised in nature. It is an exciting time to work in this area, and with the emergence of large bioinformatics/phylogenetics datasets on haem pathway enzymes (Dailey et al. 2015), there will be a need for more reductive studies on individual enzymes.

# References:


Andrews, S.C., Robinson, A.K. & Rodríguez-Quiñones, F., 2003. Bacterial iron homeostasis. *FEMS Microbiology Reviews*, 27(2–3), pp.215–237.

Aravind Menon, I., Persad, S.D. & Haberman, H.F., 1989. A comparison of the phototoxicity of protoporphyrin, coproporphyrin and uroporphyrin using a cellular system in vitro. *Clinical Biochemistry*, 22(3), pp.197–200.

Archer, G.L., 1998. *Staphylococcus aureus*: A well-armed pathogen. *Clinical Infectious Diseases*, 26(5), pp.1179–1181.

Bali, S. et al., 2011. Molecular hijacking of siroheme for the synthesis of heme and d1 heme. *Proceedings of the National Academy of Sciences of the United States of America*, 108(45), pp.18260–5.

Balwani, M. & Desnick, R.J., 2012. The porphyrias: Advances in diagnosis and treatment. *Blood*, 120(23), pp.4496–4504.

Barnard, G.F. & Akhtar, M., 1979. Stereochemical and mechanistic studies on the decarboxylation of uroporphyrinogen III in haem biosynthesis. *Journal of the Chemical Society, Perkin Transactions 1*, (3), pp.2354–2360.

Battersby, A.R., 2000. Tetrapyrroles: the pigments of life. *Nat. Prod. Rep.*, 17(6), pp.507–526.

Beale, S.I., 1990. Biosynthesis of the Tetrapyrrole Pigment Precursor, delta-Aminolevulinic Acid, from Glutamate. *Plant physiology*, 93(4), pp.1273–1279.

Beale, S.I., Gough, S.P. & Granick, S., 1975. The biosynthesis of delta-aminolevulinic acid from the intact carbon skeleton of glutamic acid in greening barley. *Proceedings of the National Academy of Sciences of the United States of America*, 72(7), pp.2719–2723.

van Belkum, A. et al., 2009. Co-evolutionary aspects of human colonisation and infection by *Staphylococcus aureus*. *Infection, Genetics and Evolution*, 9(1), pp.32–47.

Berlett, B.S. et al., 2001. Antioxidant activity of Ferrozine-iron-amino acid complexes. *Proceedings of the National Academy of Sciences of the United States of America*, 98(2), pp.451–6.

Booth, I.R., 1985. Regulation of cytoplasmic pH in bacteria. *Microbiological Reviews*, 49(4), pp.359–378.

Boynton, T.O. et al., 2011. Discovery of a gene involved in a third bacterial protoporphyrinogen oxidase activity through comparative genomic analysis and functional complementation. *Applied and Environmental Microbiology*, 77(14), pp.4795–801.

Boynton, T.O. et al., 2009. Identification of *E. coli* HemG as a novel, menadione-dependent flavodoxin with protoporphyrinogen oxidase activity. *Biochemistry*, 48(29), pp.6705–6711.

Bright, G.R. et al., 1987. Fluorescence ratio imaging microscopy: Temporal and spatial measurements of cytoplasmic pH. *Journal of Cell Biology*, 104(4), pp.1019–1033.

Brown, K.R. et al., 2002. Identification of novel hemes generated by heme A synthase: Evidence for two successive monooxygenase reactions. *Biochemistry*, 41(36), pp.10906–10913.

Buchenau, B. et al., 2006. Heme biosynthesis in *Methanosarcina barkeri* via a pathway involving two methylation reactions. *Journal of Bacteriology*, 188(24), pp.8666–8668.

Bulmer, A.C. et al., 2008. The anti-mutagenic properties of bile pigments. *Mutation Research - Reviews in Mutation Research*, 658(1–2), pp.28–41.

Bushnell, E.A.C. et al., 2011. The First Branching Point in Porphyrin Biosynthesis: A Systematic Docking, Molecular Dynamics and Quantum Mechanical/Molecular Mechanical Study of Substrate Binding and Mechanism of Uroporphyrinogen-III Decarboxylase. *Journal of Computational Chemistry*, 32(5), pp.822–834.

Camadro, J.M., Ibraham, N.G. & Levere, R.D., 1984. Kinetic studies of human liver ferrochelatase. Role of endogenous metals. *The Journal of Biological Chemistry*, 259(9), pp.5678–5682.

Casey, A.L., Lambert, P.A. & Elliott, T.S.J., 2007. *Staphylococci*. *International Journal of Antimicrobial Agents*, 29(SUPPL. 3), pp.S23–S32.

Cavallaro, G., Decaria, L. & Rosato, A., 2008. Genome-based analysis of heme biosynthesis and uptake in prokaryotic systems. *Journal of Proteome Research*, 7(11), pp.4946–4954.

Celis, A.I. et al., 2015. Unusual Peroxide-Dependent, Heme-Transforming Reaction Catalyzed by HemQ. *Biochemistry*, 54, pp.4022–4032.

Celis, A.I. & DuBois, J.L., 2015. Substrate, product, and cofactor: The extraordinarily flexible relationship between the CDE superfamily and heme. *Archives of Biochemistry and Biophysics*, 524, pp.3–17.

Charneski, C.A. et al., 2011. Atypical AT skew in Firmicute genomes results from selection and not from mutation. *PLoS Genetics*, 7(9), pp.1–14.

Corradi, H.R. et al., 2006. Crystal structure of protoporphyrinogen oxidase from *Myxococcus xanthus* and its complex with the inhibitor acifluorfen. *The Journal of Biological Chemistry*, 281(50), pp.38625–33.

Corrigall, A. V et al., 1998. Purification of and kinetic studies on a cloned protoporphyrinogen oxidase from the aerobic bacterium *Bacillus subtilis*. *Archives of Biochemistry and Biophysics*, 358(2), pp.251–256.

Cowan, J., 1991. *The Biological Chemistry of Magnesium*, New York: VCH Publishers.

Culbertson, D.S. & Olson, J.S., 2010. Role of Heme in the Unfolding and Assembly of Myoglobin. *Biochemistry*, 49(29), pp.6052–6063.

Dailey, H.A. et al., 1983. Bovine Ferrochelatase: Kinetic Analysis of Inhibition by N-Methylprotoporphyrin, Manganese, and Heme. *The Journal of Biological Chemistry*, 258, pp.11453–11459.

Dailey, H.A. et al., 2000. Ferrochelatase at the millennium: structures, mechanisms and [2Fe-2S] clusters. *Cellular and Molecular Life Sciences*, 57(13–14), pp.1909–26.

Dailey, H.A. et al., 2015. Noncanonical coproporphyrin-dependent bacterial heme biosynthesis pathway that does not use protoporphyrin. *Proceedings of the National Academy of Sciences of the United States of America*, 112(7), pp.2210–5.

Dailey, H.A. & Karr, S.W., 1987. Purification and characterization of murine protoporphyrinogen oxidase. *Biochemistry*, 26, pp.2697–2701.

Dailey, H.A. & Lascelles, J., 1974. Ferrochelatase activity in wild-type and mutant strains of *Spirillum itersonii*. *Archives of Biochemistry and Biophysics*, 160(2), pp.523–529.

Dailey, H.A., Sellers, V.M. & Dailey, T.A., 1994. Mammalian ferrochelatase. Expression and characterization of normal and two human protoporphyric ferrochelatases. *Journal of Biological Chemistry*, 269(1), pp.390–395.

Dailey, T.A. et al., 2010. Discovery and Characterization of HemQ: an essential heme biosynthetic pathway component. *The Journal of Biological Chemistry*, 285(34), pp.25978–86.

Dailey, T.A. & Dailey, H.A., 1996. Human protoporphyrinogen oxidase: expression, purification, and characterization of the cloned enzyme. *Protein Science*, 5(1), pp.98–105.

Dailey, T.A. & Dailey, H.A., 2002. Identification of [2Fe-2S] clusters in microbial ferrochelatases. *Journal of Bacteriology*, 184(9), pp.2460–2464.

Dailey, T.A., Meissner, P. & Dailey, H.A., 1994. Expression of a cloned protoporphyrinogen oxidase. *The Journal of Biological Chemistry*, 269(2), pp.813–5.

Deurenberg, R.H. & Stobberingh, E.E., 2008. The evolution of *Staphylococcus aureus*. *Infection, Genetics and Evolution*, 8(6), pp.747–763.

Ebihara, A. et al., 2005. Structure-based functional identification of a novel heme-binding protein from *Thermus thermophilus* HB8. *Journal of Structural and Functional Genomics*, 6(1), pp.21–32.

Von Eiff, C. et al., 1997. A site-directed *Staphylococcus aureus* hemB mutant is a small-colony variant which persists intracellularly. *Journal of Bacteriology*, 179(15), pp.4706–4712.

Ferreira, G.C. & Dailey, H.A., 1988. Mouse protoporphyrinogen oxidase. Kinetic parameters and demonstration of inhibition by bilirubin. *The Biochemical Journal*, 250(2), pp.597–603.

Franklin, K.A. et al., 2003. Misregulation of tetrapyrrole biosynthesis in transgenic tobacco seedlings expressing mammalian biliverdin reductase. *Plant Journal*, 35(6), pp.717–728.

Gherasim, C., Lofgren, M. & Banerjee, R., 2013. Navigating the B(12) road: assimilation, delivery, and disorders of cobalamin. *The Journal of Biological Chemistry*, 288(19), pp.13186–93.

Girvan, H.M. & Munro, A.W., 2013. Heme sensor proteins. *Journal of Biological Chemistry*, 288(19), pp.13194–13203.

Goblirsch, B.R. et al., 2010. Structural features promoting dioxygen production by *Dechloromonas aromatica* chlorite dismutase. *Journal of Biological Inorganic Chemistry*, 15(6), pp.879–888.

Grama, A. et al., 2016. Staphylococcal Scalded Skin Syndrome in Child. A Case Report and a Review from Literature. *The Journal of Critical Care Medicine*, 2(4), pp.192–197.

Grigg, J.C. et al., 2007. Haem recognition by a *Staphylococcus aureus* NEAT domain. *Molecular Microbiology*, 63(1), pp.139–149.

Guinan, M.E. et al., 1982. Vaginal Colonization with *Staphylococcus aureus* in Healthy Women: A Review of Four Studies. *Annals of Internal Medicine*, 96(Part 2), pp.944–947.

Gupta, R.S., 2011. Origin of diderm (Gram-negative) bacteria: Antibiotic selection pressure rather than endosymbiosis likely led to the evolution of bacterial cells with two membranes. *Antonie van Leeuwenhoek, International Journal of General and Molecular Microbiology*, 100(2), pp.171–182.

Gupta, R.S., 1998. Protein phylogenies and signature sequences: A reappraisal of evolutionary relationships among archaebacteria, eubacteria, and eukaryotes. *Microbiology and Molecular Biology Reviews*, 62(4), pp.1435–1491.

Han, Y.J. et al., 2010. Functional characterization of phytochrome autophosphorylation in plant light signaling. *Plant and Cell Physiology*, 51(4), pp.596–609.

Hansson, M. et al., 1997. Isolated *Bacillus subtilis* HemY has coproporphyrinogen III to coproporphyrin III oxidase activity. *Biochimica et Biophysica Acta*, 1340(1), pp.97–104.

Hansson, M. & Hederstedt, L., 1994. *Bacillus subtilis* HemY is a peripheral membrane protein essential for protoheme IX synthesis which can oxidize coproporphyrinogen III and protoporphyrinogen IX. *Journal of Bacteriology*, 176(19), pp.5962–70.

Hansson, M. & Hederstedt, L., 1992. Cloning and characterization of the *Bacillus subtilis hemEHY* gene cluster, which encodes protoheme IX biosynthetic enzymes. *Journal of Bacteriology*, 174(24), pp.8081–93.

Hansson, M.D. et al., 2011. Bacterial ferrochelatase turns human: Tyr13 determines the apparent metal specificity of *Bacillus subtilis* ferrochelatase. *Journal of Biological Inorganic Chemistry*, 16(2), pp.235–42.

Hansson, M.D., Lindstam, M. & Hansson, M., 2006. Crosstalk between metal ions in *Bacillus subtilis* ferrochelatase. *Journal of Biological Inorganic Chemistry*, 11(3), pp.325–33.

Heinemann, I.U., Jahn, M. & Jahn, D., 2008. The biochemistry of heme biosynthesis. *Archives of Biochemistry and Biophysics*, 474(2), pp.238–251.

Henderson, C.A. et al., 1995. Erythropoietic protoporphyria presenting in an adult. *Journal of the Royal Society of Medicine*, 88, pp.476–477.

Higgs, P.I., Larsen, R.A. & Postle, K., 2002. Quantification of known components of the *Escherichia coli* TonB energy transduction system: TonB, ExbB, ExbD and FepA. *Molecular Microbiology*, 44(1), pp.271–281.

Hofbauer, S. et al., 2016. From chlorite dismutase towards HemQ-the role of the proximal H-bonding network in haeme binding. *Bioscience Reports*, 36(2), p.e00312.

Hofbauer, S. et al., 2015. Structure and heme-binding properties of HemQ (chlorite dismutase-like protein) from *Listeria monocytogenes*. *Archives of Biochemistry and Biophysics*, 574, pp.36–48.

Jacobs, J.M. & Jacobs, N.J., 1987. Oxidation of protoporphyrinogen to protoporphyrin, a step in chlorophyll and haem biosynthesis. Purification and partial characterization of the enzyme from barley organelles. *The Biochemical Journal*, 244(1), pp.219–224.

Jacobs, N.J. & Jacobs, J.M., 1976. Nitrate, fumarate, and oxygen as electron acceptors for a late step in microbial heme synthesis. *Biochimica et Biophysica Acta (BBA) - Bioenergetics*, 449(1), pp.1–9.

Jacobs, N.J., Jacobs, J.M. & Brent, P., 1971. Characterization of the Late Steps of Microbial Heme Synthesis : Conversion of Coproporphyrinogen to Protoporphyrin. *Journal of Bacteriology*, 107(1), pp.203–209.

Jensen, P.E., Gibson, L.C. & Hunter, C.N., 1998. Determinants of catalytic activity with the use of purified I, D and H subunits of the magnesium protoporphyrin IX chelatase from *Synechocystis* PCC6803. *The Biochemical Journal*, 334 ( Pt 2, pp.335–44.

Jordan, P.., 1991. *Biosynthesis of Tetrapyrroles*, Amsterdam: Elsevier Science Publishings B.V.

Karlberg, T. et al., 2002. Metal binding to *Saccharomyces cerevisiae* ferrochelatase. *Biochemistry*, 41(46), pp.13499–13506.

Kato, K. et al., 2010. Identification of a gene essential for protoporphyrinogen IX oxidase activity in the cyanobacterium *Synechocystis sp.* PCC6803. *Proceedings of the National Academy of Sciences of the United States of America*, 107(38), pp.16649–54.

Kim, B.S. et al., 2014. Genome sequence of type strain of *Staphylococcus aureus* subsp. *aureus*. *Gut pathogens*, 6, pp.1–5.

Kloos, W.E., 1980. Natural Populations of the Genus *Staphylococcus*. *Ann. Rev. Microbiol*, 34, pp.559–592.

Kobayashi, K. et al., 2010. Catalysis and oxygen binding of Ec DOS: A haem-based oxygen-sensor enzyme from *Escherichia coli*. *Journal of Biochemistry*, 148(6), pp.693–703.

Kobayashi, K. et al., 2014. Molecular phylogeny and intricate evolutionary history of the three isofunctional enzymes involved in the oxidation of protoporphyrinogen IX. *Genome Biology and Evolution*, 6(8), pp.2141–2155.

Koch, M. et al., 2004. Crystal structure of protoporphyrinogen IX oxidase: a key enzyme in haem and chlorophyll biosynthesis. *The EMBO journal*, 23(8), pp.1720–8.

Koukos, G., Sakellari, D. & Arsenakis, M., 2015. Prevalence of *Staphylococcus aureus* and methicillin resistant *Staphylococcus aureus* (MRSA) in the oral cavity. *Archives of Oral Biology*, 60(9), pp.1410–1415.

Kranz, R.G. et al., 2009. Cytochrome *c* biogenesis: mechanisms for covalent modifications and trafficking of heme and for heme-iron redox control. *Microbiology and Molecular Biology Reviews : MMBR*, 73(3), p.510–528, Table of Contents.

Kresge, N. et al., 2006. A Pathway for Heme Biosynthesis : the Work of David Shemin. *The Journal of Biological Chemistry*, 281(34), pp.28–30.

Kubitschek, H.E., 1990. Cell Volume Increase in *Escherichia coli* after shiters to richer media. *J. Bacteriol.*, 172(1), pp.94–101.

Kuhner, M. et al., 2014. The alternative route to heme in the methanogenic archaeon *Methanosarcina barkeri*. *Archaea*, 2014.

Layer, G. et al., 2002. Oxygen-independent coproporphyrinogen-III oxidase HemN from *Escherichia coli*. *The Journal of Biological Chemistry*, 277(37), pp.34136–42.

Layer, G. et al., 2010. Structure and function of enzymes in heme biosynthesis. *Protein Science*, 19(6), pp.1137–61.

Lecerof, D. et al., 2003. Metal binding to *Bacillus subtilis* ferrochelatase and interaction between metal sites. *Journal of Biological Inorganic Chemistry*, 8(4), pp.452–8.

Lecerof, D. et al., 2000. Structural and mechanistic basis of porphyrin metallation by ferrochelatase. *Journal of Molecular Biology*, 297(1), pp.221–32.

Lobo, S.A.L. et al., 2014. Characterisation of *Desulfovibrio vulgaris* haem b synthase, a radical SAM family member. *Biochimica et Biophysica Acta*, 1844(7), pp.1238–47.

Lobo, S. Al et al., 2015. *Staphylococcus aureus* haem biosynthesis: characterisation of the enzymes involved in final steps of the pathway. *Molecular Microbiology*, p.n/a-n/a.

Lowy, F.D., 1998. *Staphylococcus aureus* Infections. *The New England Journal of Medicine*, 339, pp.520–532.

Maresso, A.W. & Schneewind, O., 2006. Iron acquisition and transport in *Staphylococcus aureus*. *BioMetals*, 19(2), pp.193–203.

Markwell, M.A.K. et al., 1978. A modification of the Lowry procedure to simplify protein determination in membrane and lipoprotein samples. *Analytical Biochemistry*, 87(1), pp.206–210.

Martins, B.M. et al., 2001. Crystal structure and substrate binding modeling of the uroporphyrinogen-III decarboxylase from *Nicotiana tabacum*: Implications for the catalytic mechanism. *Journal of Biological Chemistry*, 276(47), pp.44108–44116.

Masuda, T., 2008. Recent overview of the Mg branch of the tetrapyrrole biosynthesis leading to chlorophylls. *Photosynthesis Research*, 96(2), pp.121–143.

Mayfield, J.A. et al., 2013. The chlorite dismutase (HemQ) from *Staphylococcus aureus* has a redox-sensitive heme and is associated with the small colony variant phenotype. *The Journal of Biological Chemistry*, 288, pp.23488–504.

McNicholas, S. et al., 2011. Presenting your structures: the CCP4mg molecular-graphics software. *Acta Crystallographica Section D: Biological Crystallography*, 67(4), pp.386–394.

Medeiros, A. a, 1997. Evolution and Dissemination of β-Lactamases Accelerated by Generations of β -Lactam Antibiotics. *Clinical Infectious Diseases*, 24(Suppl 1), pp.19–45.

Medlock, A.E. et al., 2008. A π-Helix Switch Selective for Porphyrin Deprotonation and Product Release in Human Ferrochelatase. *Journal of Molecular Biology*, 373(4), pp.1006–1016.

Meunier, B., de Visser, S.P. & Shaik, S., 2004. Mechanism of oxidation reactions catalyzed by cytochrome P450 enzymes. *Chemical Reviews*, 104(9), pp.3947–3980.

Michael, C.A., Dominey-Howes, D. & Labbate, M., 2014. The antimicrobial resistance crisis: causes, consequences, and management. *Frontiers in public health*, 2(September), p.145.

Minetti, M. et al., 1998. Bilirubin is an Effective Antioxidant of Peroxynitrite-Mediated Protein Oxidation in Human Blood Plasma. *Archives of Biochemistry and Biophysics*, 352(2), pp.165–174.

Murphy, M.J. et al., 1974. Siroheme: a new prosthetic group participating in six-electron reduction reactions catalyzed by both sulfite and nitrite reductases. *Proceedings of the National Academy of Sciences of the United States of America*, 71(3), pp.612–6.

Nishimura, K., Nakayashiki, T. & Inokuchi, H., 1995. Cloning and identification of the *hemG* gene encoding protoporphyrinogen oxidase (PPO) of *Escherichia coli* K-12. *DNA research*, 2(1), pp.1–8.

Ogston, A., 1882. *Micrococcus* Poisoning. *Journal of Anatomy and Physiology*, 17(Pt 1), pp.24–58.

Palmer, D.J. et al., 2014. The structure, function and properties of sirohaem decarboxylase--an enzyme with structural homology to a transcription factor family that is part of the alternative haem biosynthesis pathway. *Molecular Microbiology*, 93(2), pp.247–61.

Panek, H. & O'Brian, M.R., 2002. A whole genome view of prokaryotic haem biosynthesis. *Microbiology*, 148, pp.2273–2282.

Peng, J. & Xu, J., 2011. RaptorX: Exploiting structure information for protein alignment by statistical inference. *Proteins: Structure, Function, and Bioinformatics*, 79(S10), pp.161–171.

Phillips, J.D. et al., 2009. Substrate Shuttling between Active Sites of Uroporphyrinogen Decarboxylase Is Not Required to Generate Coproporphyrinogen. *Journal of Molecular Biology*, 389(2), pp.306–314.

Pluym, M. et al., 2008. Heme binding in the NEAT domains of IsdA and IsdC of *Staphylococcus aureus*. *Journal of Inorganic Biochemistry*, 102(3), pp.480–488.

Poblete-Gutiérrez, P. et al., 2006. The porphyrias: clinical presentation, diagnosis and treatment. *European Journal of Dermatology*, 16(3), pp.230–40.

Poulson, R. & Polglase, W.J., 1975. The enzymic conversion of protoporphyrinogen IX to protoporphyrin IX. Protoporphyrinogen oxidase activity in mitochondrial extracts of *Saccharomyces cerevisiae*. *The Journal of Biological Chemistry*, 250(4), pp.1269–1274.

Qin, X. et al., 2010. Structural insight into unique properties of protoporphyrinogen oxidase from *Bacillus subtilis*. *Journal of Structural Biology*, 170(1), pp.76–82.

Quintanilla-Vega, B. et al., 1995. Porphyrin production and excretion by long-term cultures of adult rat hepatocytes and effect of lead exposure. *Toxicology*, 102(3), pp.275–283.

Ratledge, C. & Dover, L.G., 2000. Iron Metabolism in Pathogenic Bacteria. *Ann. Rev. Microbiol*, 54, pp.881–941.

Raux, E., Schubert, H.L. & Warren, M.J., 2000. Biosynthesis of cobalamin (vitamin B12): a bacterial conundrum. *Cellular and Molecular Life Sciences*, 57(13–14), pp.1880–93.

Rodgers, K.R., 1999. Heme-based sensors in biological systems. *Current Opinion in Chemical Biology*, 3(2), pp.158–167.

Roos, A. & Boron, W.F., 1981. Intracellular pH. *Physiological Reviews*, 61(2), pp.296–434.

Sellers, V.M. et al., 2001. Human ferrochelatase: Characterization of substrate - Iron binding and proton-abstracting residues. *Biochemistry*, 40(33), pp.9821–9827.

Shepherd, M. & Dailey, H.A., 2005. A continuous fluorimetric assay for protoporphyrinogen oxidase by monitoring porphyrin accumulation. *Analytical Biochemistry*, 344(1), pp.115–21.

Shepherd, M. & Dailey, H.A., 2009. Peroxidase Activity of Cytochrome *c* Facilitates the Protoporphyrinogen Oxidase Reaction. *Cellular and Molecular Biology*, 55(1), pp.3–11.

Shepherd, M., Dailey, T.A. & Dailey, H.A., 2006. A new class of [2Fe-2S]-cluster-containing protoporphyrin (IX) ferrochelatases. *The Biochemical Journal*, 397, pp.47–52.

Siepker, L.J. et al., 1987. Purification of bovine protoporphyrinogen oxidase: immunological cross-reactivity and structural relationship to ferrochelatase. *Biochimica et Biophysica Acta*, 913(3), pp.349–358.

Skaar, E.P., Humayun, M., et al., 2004. Iron-Source Preference of *Staphylococcus aureus* Infections. *Science*, 305(5690), pp.1626–1628.

Skaar, E.P., Gaspar, A.H. & Schneewind, O., 2004. IsdG and IsdI, Heme-degrading Enzymes in the Cytoplasm of *Staphylococcus aureus*. *Journal of Biological Chemistry*, 279(1), pp.436–443.

Smith, K.M., 1975. *Porphyrins and Metalloporphyrins*, Amsterdam: Elsevier Science Publishings B.V.

Smith, T.L. & Jarvis, W.R., 1999. Antimicrobial resistance in *Staphylococcus aureus*. *Microbes and Infection*, 1(4), pp.795–805.

Straka, J.G. & Kushner, J.P., 1983. Purification and Characterization of Bovine Hepatic Uroporphyrinogen Decarboxylase. *Biochemistry*, 22, pp.4664–4672.

Terry, M.J. & Lagariass, J.C., 1991. Holophytochrome Assembly. *The Journal of Biological Chemistry*, 266(33), pp.22215–22221.

Terry, M.J., Wahleithner, J.A. & Lagarias, J.C., 1993. Biosynthesis of the Plant Photoreceptor Phytochrome. *Archives of Biochemistry and Biophysics*, 306(1), pp.1–15.

Thauer, R.K., 1998. Biochemistry of methanogenesis : a tribute to Marjory Stephenson. *Microbiology*, 144, pp.2377–2406.

Thibodeau, E. et al., 2012. First report of a left ventricular assist device infection caused by *Staphylococcus schleiferi* subspecies *coagulans*: A coagulase-positive organism. *Diagnostic Microbiology and Infectious Disease*, 74(1), pp.68–69.

Turutoglu, H., Tasci, F. & Ercelik, S., 2005. Detection of *Staphylococcus aureus* in Milk By Tube Coagulase Test. *Bulletin of the Veterinary Institute in Pullway*, 49(4), pp.419–422.

Ventura, M. et al., 2007. Genomics of Actinobacteria: tracing the evolutionary history of an ancient phylum. *Microbiology and molecular biology reviews : MMBR*, 71(3), pp.495–548.

Vlasits, J. et al., 2010. Mechanisms of catalase activity of heme peroxidases. *Archives of Biochemistry and Biophysics*, 500(1), pp.74–81.

Walker, C.J. & Weinstein, J.D., 1991. In vitro assay of the chlorophyll biosynthetic enzyme Mg-chelatase: resolution of the activity into soluble and membrane-bound fractions. *Proceedings of the National Academy of Sciences of the United States of America*, 88(13), pp.5789–5793.

Wandersman, C. & Delepelaire, P., 2004. Bacterial Iron Sources: From Siderophores to Hemophores. *Annu. Rev. Microbiol*, 58, pp.611–47.

Wertheim, H.F.L. et al., 2005. The role of nasal carriage in *Staphylococcus aureus* infections. *The Lancet Infecitous Diseases*, 5(December), pp.751–762.

Whitby, F.G. et al., 1998. Crystal structure of human uroporphyrinogen decarboxylase. *EMBO Journal*, 17(9), pp.2463–2471.

Williams, R.E., 1963. Healthy carriage of *Staphylococcus aureus*: its prevalence and importance. *Bacteriological reviews*, 27(96), pp.56–71.

Wu, C.-K. et al., 2001. The 2.0 Å structure of human ferrochelatase, the terminal enzyme of heme biosynthesis. *Nature Structural Biology*, 8(2), pp.156–160.

Xu, K. & Elliott, T., 1993. An oxygen-dependent coproporphyrinogen oxidase encoded by the *hemF* gene of *Salmonella typhimurium*. *Journal of Bacteriology*, 175(16), pp.4990–4999.

Zeilstra-Ryalls, J.H. & Schornberg, K.L., 2006. Analysis of *hemF* Gene Function and Expression in *Rhodobacter sphaeroides* 2.4.1. *Journal of Bacteriology*, 188(2), pp.801–804.

# Appendix:

**Appendix 1 –** DNA primers used during the cloning of *S. aureus hemH*

| Primer Number | Name | Sequence (5' – 3') | Usage | Direction |
|---|---|---|---|---|
| 102 | hemH¬¬S-NheI | ATCATCATCATCATGGTATGGCTAGCATGACTAAAAAAATGGGATTATTA | Amplification of *hemH* from *S. aureus* genomic DNA | Forward |
| 103 | hemH-AS-HindIII | TCTCATCCGCCAAAACAGCCAAGCTTTTAAAATATAGACTTGATTTCATC | Amplification of *hemH* from *S. aureus* genomic DNA | Reverse |
| 104 | pTrcHis-FWD | GTGGGCACTCGACCGGAATT | Checking for *hemH* insertion / Sequencing of *hemH* | Forward |
| 105 | pTrcHis-RSE | TCAGGTGGGACCACCGCGCT | Checking for *hemH* insertion / Sequencing of *hemH* | Reverse |
| 116 | SAHemH66 | CCATATTATACAGATATTAG | Sequencing of *hemH* | Forward |
| 117 | SAHemH266 | ACCATTTATCGAAGATGCGG | Sequencing of *hemH* | Forward |
| 118 | SAHemH466 | CGAATAAAGTCAACGAAACA | Sequencing of *hemH* | Forward |
| 119 | SAHemH666 | GGTAATACAGGTACACCTTG | Sequencing of *hemH* | Forward |
| 120 | SAHemH866 | GAATACACATCCATTATTTA | Sequencing of *hemH* | Forward |

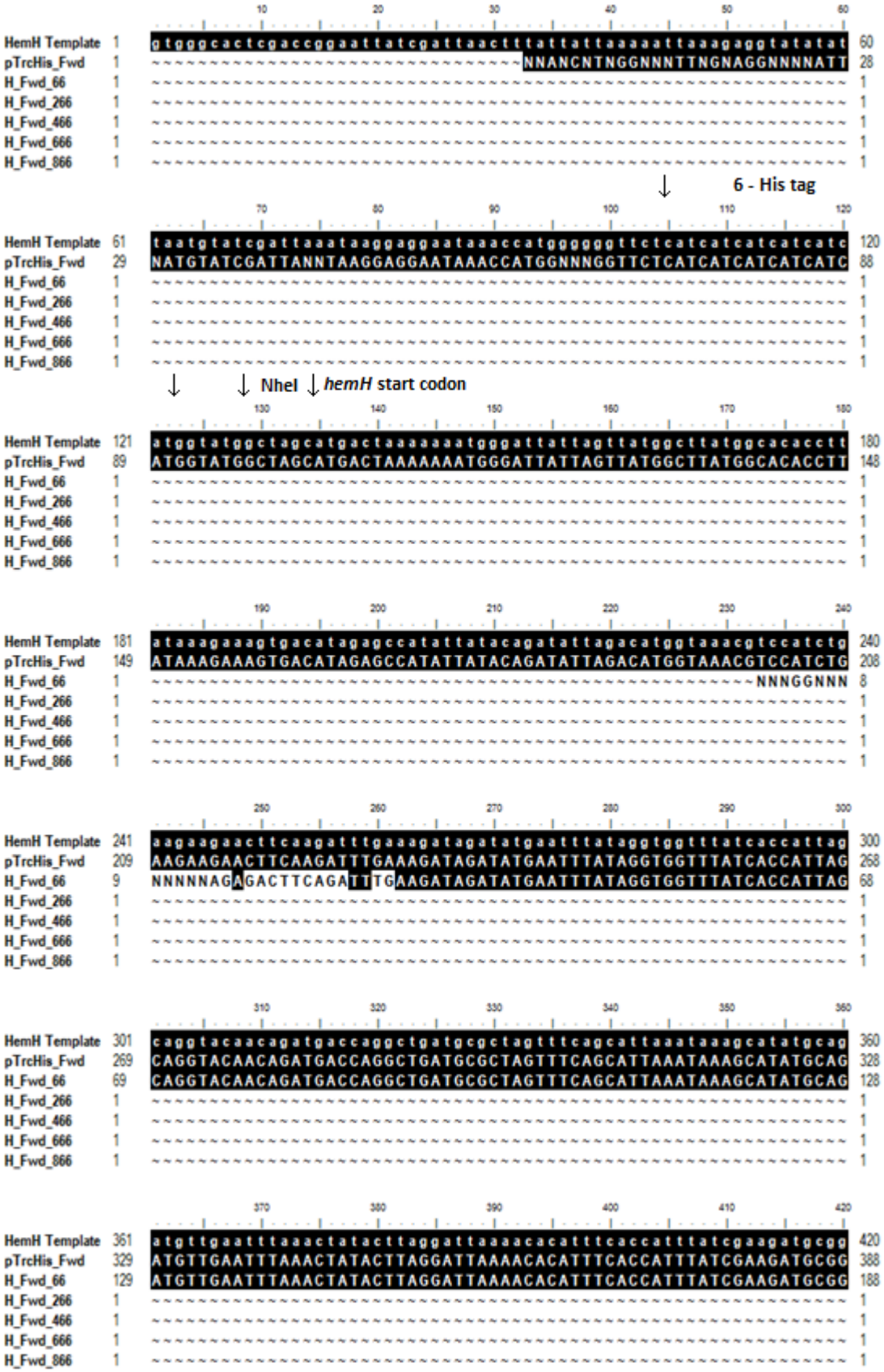


**Appendix 2A –** Alignment of *hemH* sequencing data (lines 2-7) against the desired plasmid sequence containing *S. aureus hemH* inserted into the NheI and HindIII sites of pTrcHis plasmid (start).

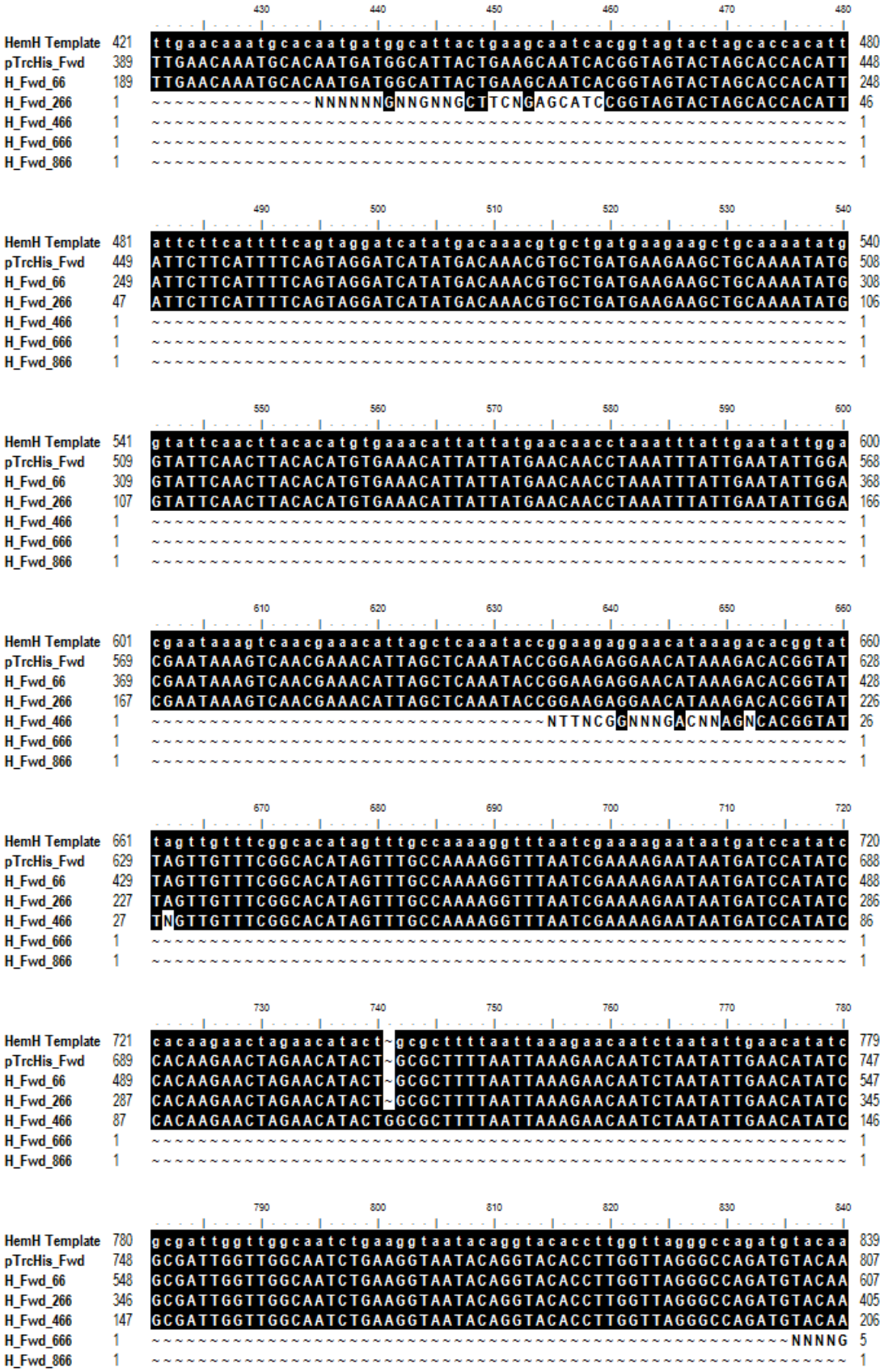


**Appendix 2B –** Alignment of *hemH* sequencing data (lines 2-7) against the desired plasmid sequence containing *S. aureus hemH* inserted into the NheI and HindIII sites of pTrcHis plasmid (middle).

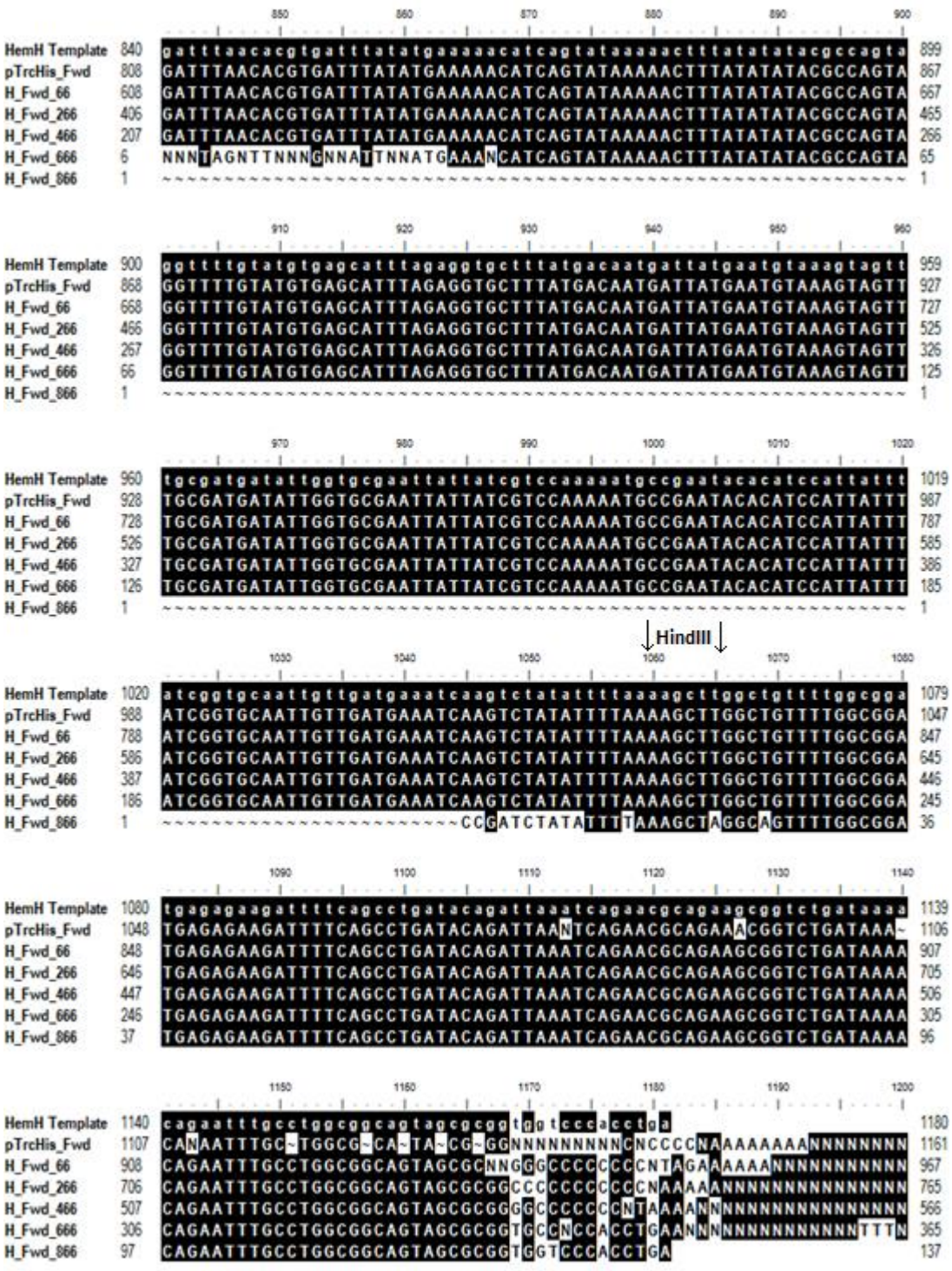


**Appendix 2C –** Alignment of *hemH* sequencing data (lines 2-7) against the desired plasmid sequence containing *S. aureus hemH* inserted into the NheI and HindIII sites of pTrcHis plasmid (end).

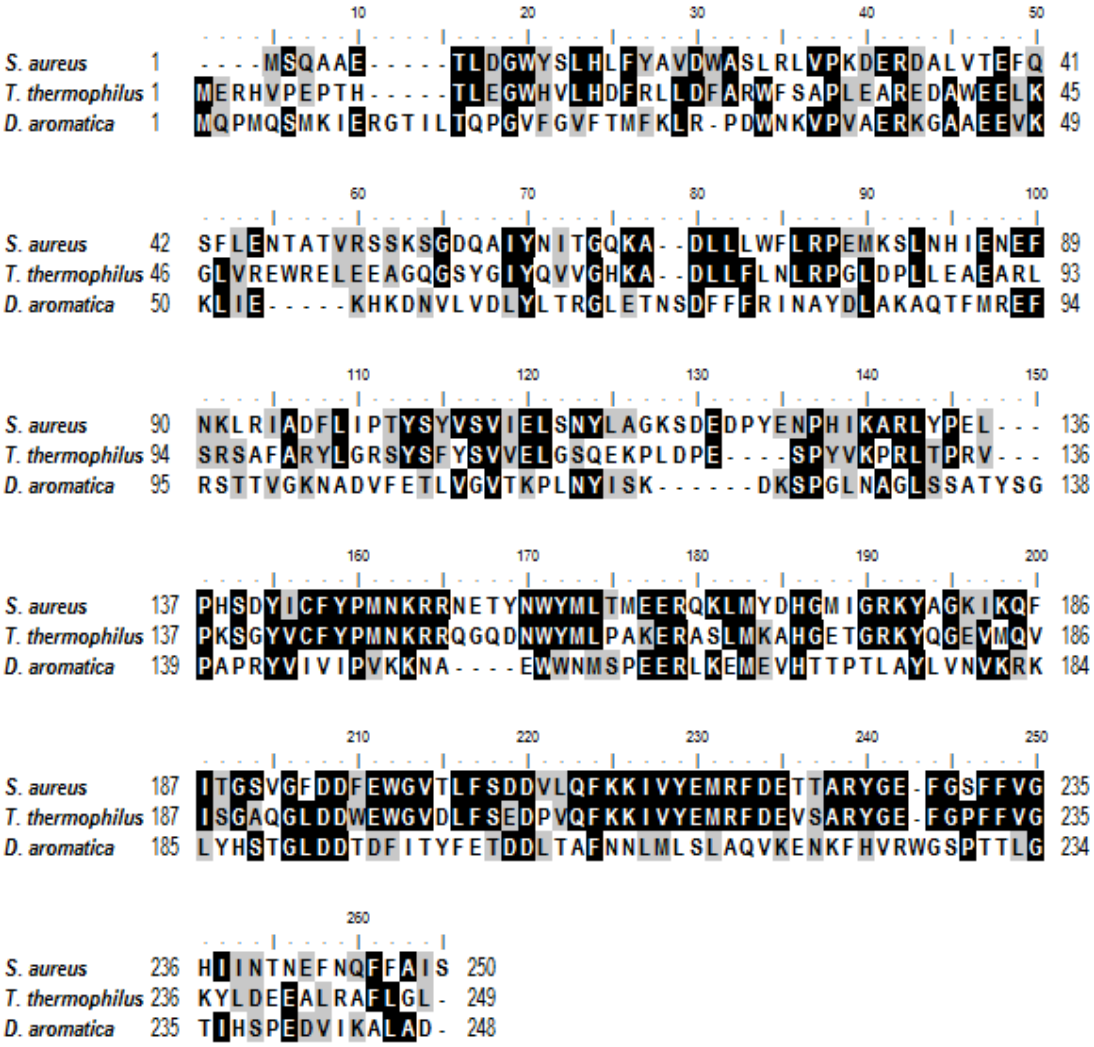


**Appendix 3 –** Sequence alignment of HemQ proteins from *S. aureus*, *T. thermophilus* and a chlorite dismutase from *D. aromatica*.

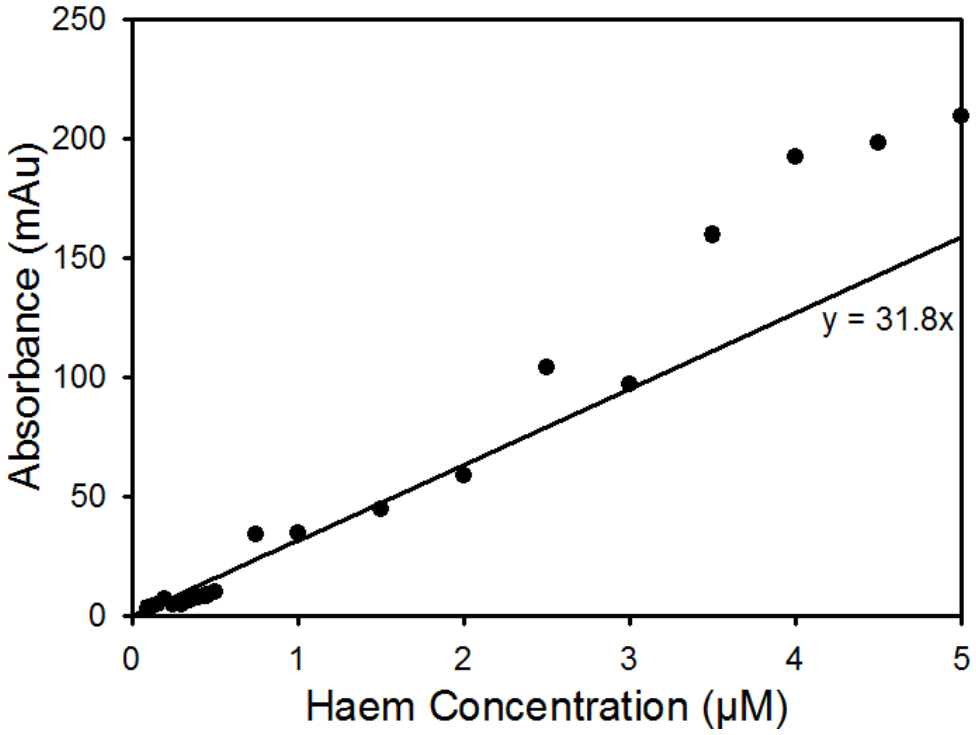


**Appendix 4 –** Haem standard curve for concentrations of haem between 0 and 5 µM analysed by HPLC. Data points represent the peak heights at the relevent concentrations.